Vigorous Star Formation In Galactic Nuclei

Philip John Puxley

Doctor of Philosophy

University of Edinburgh

1988

This thesis has been composed by me and consists entirely of my own work except where indicated in the text.

Philip John Puxley

December 1988

Abstract

This thesis presents a study of vigorous star formation in the nuclei of nearby galaxies. A variety of techniques have been employed to investigate several aspects of this phenomenon.

Analysis of mid– and far–infrared data, taken by the *Infrared Astronomical Satellite*, suggests that amongst nearby spiral galaxies the presence of a stellar bar is a necessary condition for the existence of vigorous star–formation activity. Such regions contribute, on average, one third of the luminosity of the host galaxy.

Medium–resolution radio continuum observations show that active star formation occurs in the central regions of galaxies, supporting the hypothesis that it is caused by a bar–driven inflow of disk material.

Near–infrared spectrophotometry has been used to study several of these highly dust–obscured regions in greater detail. Detection of the hydrogen recombination line Brγ, which arises in photoionized gas, is further evidence for the presence of a population of massive stars. Measurements of molecular hydrogen lines demonstrate that this gas is also photo–excited, in contrast with previous studies. Models of the gas excitation in star–forming regions are constructed and comparison of the predicted line intensities with observations yields information regarding the gas density and structure of the complexes.

The ionized gas in the archetypal starburst galaxy M82 is examined in greater detail through measurements made in mm–wavelength recombination lines (H40 and H53α). These observations avoid the problems which occur when shorter–wavelength lines are employed since they are unaffected by dust attenuation. The ionization state of the gas and the total luminosity are used to infer the range of stellar masses present in this galaxy. This range may be very narrow.

Acknowledgements

Throughout this work I have benefited greatly from interaction with my 'primary' supervisors, Tim Hawarden, Matt Mountain and Peter Brand. Of the original seven (or was it eight ?), these three survived the course and, along the way, shared with me their extensive collective knowledge of astronomy, physics and instrumentation, and their friendship too. I value all of these.

I am also indebted to many of the other staff of the Royal Observatory and Edinburgh University, who were (almost) always available for help and advice. I am also grateful to the SERC for financial support whilst undertaking my PhD, and generously supporting so many observing trips.

The happiness with which I shall remember the three–and–a–bit years spent in Edinburgh is undeniably due to the presence of a fine assortment of students, both past and present. Rather than offending anyone by leaving them out, I shall risk offending all by naming none. Having said that, however, I shall mention Toby Moore who suffered more than most by sharing an office with me for the duration but, despite this, was as good a mate as anyone could wish for. The atmosphere, both social and at work, which the students created, will be sorely missed. Thanks lads.

I also wish to thank my parents for the solid support they have always given me, and for allowing me to choose my own direction. Last, but certainly not least, I thank Mary for enduring so much; hopefully it will be less stressful in the years to come.

Table of Contents

Chapters :

Appendices :

Chapter 1

Introduction

This thesis is concerned with the global properties of star formation inferred from multi–frequency observations of spiral galaxies. Galaxies which exhibit signs of vigorous star formation, usually near their nuclei, are often referred to as "starburst galaxies", *i.e.* their star formation is thought so prolific that it must be short lived or episodic. This statement is open to conjecture however, since determination of the star–formation rate is usually based upon measurement of integrated properties, such as luminosity or ionization rate, and is thus dependent upon assumptions of the distribution of stellar masses and the star formation history. These quantities are poorly determined, especially in regions of active star formation, as is the amount of raw material available. Thus the lifetime of any 'burst' is rather uncertain. To avoid this quandary, the less precise definition of a starburst as a galaxy whose emission contains a sizeable contribution from regions of star formation activity, will be used here.

Interest in vigorous extragalactic star formation has increased dramatically in the decade since the speculation by Rieke & Lebofsky (1979) that infrared emission may be common in galaxies. This is undoubtedly due to major advances in mm and infrared instrumentation (few observations existed in 1979) and in the success of the Infrared Astronomical Satellite (*IRAS*) mission. Observations at wavelengths longer than the visible are crucial in investigating these sources because the sites of star formation are commonly heavily obscured by dust associated with the molecular material from which the stars formed. This dust is very efficient at converting ultraviolet and visible emission into longer wavelength (IR and mm) radiation. Thus the luminosity in the range 5–300 μm is a good approximation to the bolometric luminosity of the young stars (*e.g.* Thronson & Harper 1979). Moreover, since the attenuation of the radiation by dust is much less at longer wavelengths, these observations can probe deep into the star–forming complexes.

There are numerous ambitious questions which such measurements hope to provide answers to, many of which have much wider ramifications than just being restricted to starbursts. Amongst these problems are : What is the distribution of stellar types ? What is the state of the interstellar medium ? What is the star formation rate ? Do these global properties depend on the level of star formation activity ? What determines this level ? What triggers a starburst ? How do such systems evolve and over what timescale ? How does vigorous star formation affect the evolution of the galaxy as a whole ? Naturally, in such a young field these questions are still far from being answered satisfactorily, although many interesting results are emerging. In the bulk of this chapter, some of the relevant observations are reviewed and their implications discussed (§1.1). Where applicable, results from, or references to, other parts of the thesis are noted. The rest of this introduction briefly describes the various types of galaxy exhibiting unusual activity and examines the confusion concerning its nature (§1.2), a brief description of models of star–formation activity (§1.3), and a guide to the rest of this thesis (§1.4).

1.1 The Emission from Star–Forming Regions

There are two ways to approach a review of the emission from extragalactic star–forming complexes. The first is to describe these regions from the observers standpoint — to recount the observations made in each wavelength regime, see for example the summary of *"The IRAS View of the Extragalactic Sky"* (Soifer, Houck & Neugebauer 1987). The second course, that followed here, adopts the point of view of the source and involves a description of each component by consideration of its emission throughout the spectrum. The components considered are :

- Stars
- Ionized Gas
- Molecular Gas
- Neutral Atomic Gas
- Dust

This course was also chosen by Telesco (1988) in an important review of some aspects of enhanced star formation in the centres of galaxies. Enlightening accounts of the state of current research into this subject can also be found in the following conference proceedings : *Star Formation in Galaxies* (ed. Persson 1987), *Star Forming Regions* (eds. Peimbert & Jugaku 1987), *Starbursts and Galaxy Evolution* (eds. Thuan, Montmerle & Tran 1987), and *Galactic & Extragalactic Star Formation* (eds. Pudritz & Fich 1988).

1.1.1 Stars

As described above, much of the direct UV and visible emission from stellar photospheres is not measurable due to absorption by intervening dust grains. Nevertheless, a significant fraction of this radiation will escape from the starburst : from stars situated near the surface of the region, and from those to which there may be a fortuitous dust–free path due to patchy extinction. Since the level of star–formation activity can be very high, it is not unusual to observe strong blue continuum emission from these galaxies in addition to intense IR fluxes. Indeed, one of the first systematic searches for starburst nuclei utilized the former as the selection criterion (Balzano 1983). However, there exists a major problem with the interpretation of the blue luminosity (L_B) from starburst galaxies due to two different explanations as to its origin (Thronson & Telesco 1986, and references therein). Some authors take the source of L_B to be the newly formed massive stars which also account for the infrared luminosity (L_{IR}). In this case the ratio L_{IR}/L_B is a function of the amount and distribution of dust around the stars. In contrast, other workers assume that L_B includes a contribution from much less massive, and consequently older, stars. Thus, they regard L_{IR}/L_B as a measure of the current to past star–formation rates. The conflict between these two interpretations is not yet resolved. Fortunately, a more direct measure of the young, massive, stellar content than that inferred from L_B is available. These stars emit copiously at wavelengths $\lambda \leq 91.2$ nm and therefore ionize the interstellar hydrogen in their immediate vicinity, and in proportion to the ionizing flux. Line radiation from the recombination of protons and electrons is readily detectable (see §1.1.2).

Most of the photospheric emission from cooler, evolved, stars emerges in the near–infrared (1–5 μm). Much of this radiation can escape from the star–forming complex

unhindered due to the smaller extinction by dust at these wavelengths. There are two dominant populations of stars contributing to this emission : low–mass red giants and high–mass supergiants. These are at qualitatively similar evolutionary stages, though their timescales are difficult and thus they represent star formation at different epochs. As with the blue luminosity, however, it is different to separate the contributions of the two populations since their effective temperatures (*i.e.* their colours) are similar. This is particularly relevant to starburst galaxies since the relative fractions are expected to vary considerably. Due to insufficient time for their formation, the youngest starburst will contain no red supergiants or giants, besides any of the latter associated with previous episodes of star formation. At slightly later epochs, the more rapidly evolving supergiants may dominate the near–IR emission, whilst at later times still, red giants may contribute the major fraction of this emission. The latter phase will not be so prominent if the range of stellar masses formed (*i.e.* the initial mass function, IMF) does not extend to sufficiently low mass. There is a growing body of evidence that this may indeed be the case (see the review by Scalo 1987). Therefore the conventional assumption that the near–IR emission from galaxies can be attributed solely to the photospheric emission from red giants stars must be questioned, particularly in the case of starbursts. This is highlighted by recent observations of the starburst dwarf galaxy IIZw40 (Joy & Lester 1988) in which the 2-μm radiation arises entirely from free–free emission in ionized nebulae and from the black–body tails of the main sequence stars seen in blue light. An additional source of radiation which may complicate the interpretation of the near–IR emission from starbursts is that from hot small dust grains (see §1.1.5).

An observational way of detecting the presence of, and distinguishing between, red giants and supergiants does exist. This involves measurement of the broad photospheric CO absorption feature near 2.3 μm whose strength is sensitive to the stellar surface gravity (*i.e.* the stellar luminosity class). Until recently, only observations made through relatively broad filters have been available (*e.g.* Baldwin *et al.* 1973; Frogel *et al.* 1978) which are relatively insensitive to differences in the integrated stellar populations and whose use is hampered by the need to apply a K–correction because of the redshifts of the galaxies (Arnaud & Gilmore 1986). Databases of suitable infrared spectral standards are becoming available which will enable more detailed spectral

syntheses, based upon spectrophotometry, to be performed in the near future. In their seminal study of the starburst galaxy M82, Rieke *et al.* (1980) inferred a large population of giants from the strength of the CO bands in their 2-μm spectra. Together with other data, in particular the mass within the central regions, they concluded that the observed 2-μm luminosity could only be matched if the IMF was truncated at the lower end at about 3 $M_{\odot}$ (see also Chapter 6). Walker, Lebofsky & Rieke (1988) have analysed 2–2.5 μm spectra of a few nearby galaxies and suggest that the abnormally strong CO bands in NGC 4736 are the result of a very powerful, but old, starburst (since no other evidence for star–forming activity is seen). They also construct an evolutionary sequence for such systems on the basis of the CO depth and the hydrogen recombination line strength (§1.1.2). To conclude this discussion of the CO feature, a cautionary point made by Zinnecker (1987) is noted. The strength of this feature depends not only on surface gravity, but also on the metallicity of the star. It is possible to explain a given CO band depth by either lower metallicity supergiants or higher metallicity giants. Therefore the spectrum may reflect the pre–starburst and present composition in addition to the initial mass function and the current and past star formation rates.

Observations of starburst galaxies reveal other features, in addition to CO, originating directly from stars. Most notable are the ultraviolet absorption lines of CIV (λ155 nm) and SiIV (λ140 nm). These are characteristic of early–type stars (OB) and are thought to be formed in their winds (see the review by Kunth & Weedman 1987). These features have been observed in several galaxies (*e.g.* Weedman *et al.* 1981; Augarde & Lequeux 1985; Joseph, Wright & Prestwich 1986; Walsh *et al.* 1986). The absence of UV nebular emission lines such as CIV (λ155 nm), HeII (λ164 nm) and CIII (λ191 nm), which are indicative of Seyfert nuclei (*e.g.* Boksenberg *et al.* 1978), is taken as evidence that the energy source responsible for the strong IR emission is star formation. The non–appearance of the emission lines in starburst galaxies results from the overwhelmingly strong continua of the hot stars. Likewise, optical stellar absorption lines, primarily those of metals such as Na, Ca and Mg are weak, where detected, due to the dominance of the high mass stellar population.

Emission from ionized gas provides one of the major diagnostics of conditions within starburst galaxies. Most important is the radiation from protons and electrons : either due to their recombination, free–free (Bremsstrahlung) emission, or the synchrotron emission from relativistic particles gyrating in magnetic fields. The hydrogen recombination line emission may be either spontaneous (UV to mm wavelengths) or stimulated by background continuum sources (radio lines). Collisional excitation of the lower electronic levels may be significant in some galaxies (*e.g.* M82; Chapter 6) and ionization by the UV–precursors of fast shocks (Shull & Mckee 1979) has been suggested as a mechanism for the line emission from "Low Ionization Nuclear Emission–line Regions" (LINERs; Heckman 1980). In the majority of starburst galaxies, however, the primary source of hydrogen recombination line emission is believed to be the photoionized (HII) regions surrounding young hot stars, the input from planetary nebulae being negligible by comparison (Gallagher, Hunter & Tutukov 1984).

Observations of hydrogen recombination lines have two main applications : calculation of the total ionization rate, and thence inference of the high–mass stellar population, and determination of the extinction by dust. Their use involves a number of assumptions which are useful to note given the importance of these measurements, and since they are often ignored or only implicit in the literature.

The first assumption is that the lines originate from HII regions which are optically thick to Lyman photons : this is the Case B of Baker & Menzel (1938). Recombination directly into, or cascade down to, the ground electronic state produces a Lyman continuum, or line, photon which ionizes, or excites, another hydrogen atom close to the source of its emission. Thus, apart from Lyman emission by atoms at the edge of the ionized region, only the photons produced by transitions between higher n-levels can escape. This is a reasonable assumption since the electron temperatures and densities found in many HII regions ($T_e \sim 5 \times 10^3 - 10^4$ K; $n_e \sim 100 - 10^4$ cm^{-3}) imply that collisional excitation can be ignored and thus almost all bound electrons are in the ground state. Detailed numerical modelling of the electronic cascade yield relative line intensities for the transitions and relate these to the recombination rate. The most

recent, and comprehensive, work is that by Hummer & Storey (1987) who also discuss the temperature and density regimes at which Case B breaks down. Case B appears to hold in many cases, however there may be exceptions. An important observational result by Turner, Ho & Beck (1986) reveals that one location in the star–complex in M83 emits much less free–free radio emission than expected from its recombination line flux. They suggest that the emission is dominated by compact (*i.e.* young) HII regions in which the radio is optically thick. This result has implications not only for determination of the ionization rate, but also for the dust extinction since the intrinsic line ratios are altered. A slight variation on this model is that proposed by Thompson (1987) who notes the similarity between M83 and the "line excess" phenomena seen in a number of young stellar objects (*e.g.* Evans *et al.* 1987). The currently favoured explanation for these young, high mass loss, sources is that the line emission originates in ionized stellar winds in which ionization by Balmer, in addition to the usual Lyman, continuum photons occurs (Simon *et al.* 1983). Thus it appears that if the starburst is very young, the assumption of Case B may not be applicable.

The other two main assumptions, that of ionization bounded HII regions and of negligible dust content within the ionized zone, are difficult to examine observationally. Both of these can significantly affect determination of the total ionization rate, though not estimates of the extinction since the statistical level population is unchanged. For simplicity, it is usually assumed that the HII regions are ionization bounded and dust–free, *i.e.* all Lyman continuum photons result in an ionization. A more detailed examination of the effects of dust within HII regions, which competes for photons with hydrogen, can be found in the review by Mathis (1986), and references therein.

The principal observational effect of dust is attenuation of radiation from the starburst. The extinction is wavelength dependent and thus comparison of the observed hydrogen line strengths at two different wavelengths with their intrinsic (*e.g.* Case B) ratio yields the differential reddening between these lines. An empirically determined interstellar extinction curve, for example that by Rieke & Lebofsky (1985) which extends into the infrared, can then be consulted to determine the extinction at the wavelength of interest. This is

The presence of dust around, or within, an HII region will also reduce its size since dust removes UV photons. Consequently, the rate of emission of ionizing photons, inferred from recombination line or thermal continuum measurements, may be underestimated.

nation of two hydrogen lines can be used to determine A_V : the most common being the optical Hα and Hβ or the infrared Brγ and Brα lines. However, the situation is complicated if there exists a significant amount of dust between the HII regions, as may be expected in starburst galaxies. In this case, a line of wavelength λ will only probe to an optical depth of about $3A_\lambda$. Thus, longer wavelength lines, which suffer less extinction, will originate from all sources to a far greater physical depth, *i.e.* the number of emitting sources sampled by different lines is not the same. This scheme may account for the significant differences in the determinations of A_V performed using various lines and other techniques noted by a number of authors (see Skillman & Israel 1988, and references therein), though wavelength–dependent scattering by dust probably also plays a role (*e.g.* Mathis 1983). An analogous problem, that of dusty HII regions, has been discussed by Mathis (1970). As described in Appendix B (see also Chapter 4), measurement of at least three recombination lines allows evaluation of both foreground and internal extinction. The problems associated with an uncertain reddening correction are entirely circumvented if a line is of sufficiently long wavelength that it suffers no attenuation by dust, *e.g.* H53α at $\lambda \simeq 7$mm (see Chapter 6).

The other major goal of hydrogen line observations is determination of the recombination rate, equivalently the rate of emission of Lyman continuum photons (N_{LyC}) from hot stars. Comparison of N_{LyC} with the observed infrared luminosity can be used to test the assumption that both originate from a population of young stars. There are two main approaches. Empirically, many radio–selected Galactic HII regions (*e.g.* Jennings 1975) and star–forming galaxies (*e.g.* Telesco, Decher & Gatley 1986) display the same rough correlation $L_{IR} \propto N_{LyC}$ which extends over more than seven orders of magnitude (DePoy 1987). Galaxies containing active nuclei, *i.e.* those which exhibit broad emission lines (Δv $\sim$ 1000 km s^{-1}; Khachikian & Weedman 1974), display far larger values of this ratio (*e.g.* DePoy 1987). The alternative approach involves comparison of the Lyman continuum and infrared luminosities with theoretical values calculated from model stellar atmospheres for stars distributed according to some mass function (see also §1.4 and Appendix C). The result of these studies is that L_{IR} and N_{LyC} for many galaxies appear to be produced by young stars (*e.g.* Rieke *et al.* 1980; Beck, Beckwith & Gatley 1984; Telesco & Gatley 1984; Beck, Turner & Ho 1986). In a few cases, additional observational data (*e.g.* 2-μm luminosity, mass, line excitation

conditions) facilitates constraint of the range of stellar masses present. In the best-studied example, M82, this range may only be very narrow : approximately 20–30 $M_{\odot}$ (Chapter 6). A similar range was inferred for NGC 3690 by Augarde & Lequeux (1985). Depoy (1987) has employed the Brα recombination line width (*i.e.* the velocity dispersion) to derive an upper limit to the mass of the nuclear regions. This limit is comparable with the mass that must be contained within the OB stars responsible for the line emission, and thus also argues in favour of the dominance of massive stars. Additional observational evidence for a truncated mass function is reviewed by Scalo (1987).

Hydrogen recombination lines are also found at radio wavelengths, due to transitions between high n-levels. As demonstrated by Shaver,Churchwell & Walmsley (1978) and Bell & Seaquist (1978), they are generated by stimulated emission in foreground HII regions by non–thermal background radiation. Thus they cannot be applied in a straightforward way to determine the ionization rate, but do allow estimation of the electron density within the ionized regions. To date, the only galaxies with detected radio recombination line emission are the brightest starbursts: NGC 253 and M82. Seaquist, Bell & Bignell (1985) have utilized the high spatial resolution available at radio wavelengths using aperture synthesis techniques to map the distribution of ionized gas from emission in the H110α line in M82.

In addition to hydrogen, the lines from ionized species of various other elements have been observed. The well–known optical emission lines form the basis for discrimination between star formation and other types of activity in galaxies (*e.g.* Baldwin, Phillips & Terlevich 1981; Veilleux & Osterbrock 1986). These classification techniques exploit the different level populations resulting from excitation and ionization by stars, by the non–thermal (power–law) spectra of active galactic nuclei, and by shocks. The forbidden lines are extremely important diagnostics of the physical conditions (*i.e.* electron density and temperature) within the ionized regions. In [OIII], for example, the collisional excitation rates of the levels are strongly dependent on temperature due to their different threshold energies, but only weakly on density for most situations. Other species, like [OII], have two levels with nearly the same energy and thus the intensity ratio of forbidden lines emitted by these levels is a sensitive measure of the electron density. A review of these topics can be found in Osterbrock (1988). As with

all such experiments involving optical lines, however, they are insensitive to emission from below a depth of $A_V \simeq 3$. The infrared fine–structure lines of [OIII] at 52 and 88 μm and of [SIII] at 19 and 33 μm have been used as density diagnostics in the heavily extinguished star–forming nucleus of M82 (Lugten *et al.* 1986; Duffy *et al.* 1987). Mid–IR fine structure lines of nitrogen, argon and neon have also been detected from this galaxy and can be used to set limits on the elemental abundances and on the effective temperature of the ionizing UV field (*e.g.* Willner *et al.* 1977; Aitken *et al.* 1982). This, in turn, constrains the upper end of the initial mass function (see Chapter 6).

Along with the [OI]63 μm line and gas–grain collisions, emission in the [CII]158 μm line is one of the principal coolants of the warm gas found just outside HII regions. The ionization potential of neutral carbon is 11.3 eV and thus the CII line traces UV radiation in the range 91.2 – 110.1 nm (coincidentally, the same range as that responsible for fluorescent excitation of H_2; §1.1.3). [CII] emission has been detected from a handful of starburst galaxies and interpreted as originating in warm ($T \sim 300$ K) photodissociation zones lying between the HII regions and molecular clouds (Crawford *et al.* 1985; Tielens & Hollenbach 1985). It is estimated that more than 25% of the total interstellar gas mass in the central regions of M82 resides within the C^+ zones. The intimate association between molecular clouds and the C^+ emission has been demonstrated by the tight correlation between [CII]158 μm and ^{12}CO J = 1 $\rightarrow$ 0 line strengths observed in many different objects and by their similar spatial distributions (Crawford *et al.* 1985). Crawford *et al.* have also identified a dependence of the C^+ emission on the energy density of the UV radiation field, the latter being inferred from the infrared energy density assuming efficient dust reprocessing. This dependence is non–linear since attenuation by dust dominates the C^+ column density and its form is consistent with the predictions of the photodissociation zone models by Tielens & Hollenbach (1985). They conclude that since a higher UV intensity will increase not only the C^+ column density but also elevate the CO gas temperature, the standard conversion factor of CO : H_2 (derived from optically thick galactic clouds at about 10 K) may not be applicable to regions of large IR luminosity *e.g.* starburst galaxies (see also §1.1.3, and Maloney & Black 1988).

In addition to line radiation, the ionized gas in starburst galaxies is also a strong source of continuum emission. In most galaxies the non–thermal synchrotron emission from relativistic particles dominates the total radio flux, as deduced from analysis of

their radio spectral indices (*e.g.* Gioia, Gregorini & Klein 1982). Empirically there exists a tight correlation amongst star forming galaxies between the total radio and infrared fluxes which indicates that the non–thermal radio luminosity and the level of star formation activity are closely associated (*e.g.* Helou, Soifer & Rowan–Robinson 1985). This correlation is analysed in greater detail in Chapter 3. There is also good spatial correspondence between the radio and mid–IR (10 μm) distributions (*e.g.* Becklin *et al.* 1980; Telesco & Gatley 1984). It is believed that supernovae are ultimately responsible for the radiating electrons, but are not the direct source of the radio emission. VLBI observations of M82 and NGC 253 reveal many compact radio sources coincident with the IR–luminous regions (Unger *et al.* 1984; Kronberg, Biermann & Schwab 1985; Antonucci & Ulvestad 1988). The temporal variations of these point sources imply that they are supernova remnants. The close association between IR and radio emission can thus be understood if the time dependence of the star formation rate is not great, *i.e.* the birth rate of massive stars and the rate of supernovae are similar. Frequent use is made of these results to determine the spatial distribution of massive star formation in galaxies from high resolution radio synthesis maps (*e.g.* Chapter 3, and references therein). One problem with this interpretation is that the average radio flux integrated over the lifetime of a Galactic or extragalactic supernova remnant (*e.g.* Ulvestad 1982), multiplied by the expected supernova rate, is often an order of magnitude less than the observed flux (*e.g.* Duric 1986). The exact reasons for this discrepancy are not yet forthcoming, and the significance of the disagreement is unclear given our scant knowledge of the properties of supernovae in such active environments.

Multi–frequency radio continuum observations are often made in order to evaluate the contribution of the thermal component to the total emission. This is possible, in principle, since the thermal emission has a much flatter spectrum that does any optically thin non–thermal component. However, these estimates rely heavily on the assumed synchrotron spectral index, often taken to have a universally constant value, and may therefore be rather unreliable (*e.g.* Duric, Borneuf & Gregory 1988). In some galaxies there is no evidence for a non–thermal component, *e.g.* NGC 5253. Gonzáles–Riestra, Rego & Zamorano (1987) have modelled the UV and optical emission from this system and conclude that the star formation is exceptionally young; that is, there has been insufficient time for evolution of even the most massive stars to the supernova

phase. In other galaxies, there is clear evidence of significant spatial variations in the spectral indices over small scales (*e.g.* Seaquist & Bignell 1977; Turner & Ho 1983).

At high frequencies the emission may be solely due to thermal Bremsstrahlung. Comparison of this emission with that in a hydrogen recombination line allows estimation of the electron temperature through the dependence of the free–free flux on T_e (see Chapter 6). Bremsstrahlung emission may be significant at even higher frequencies : as noted in §1.1.1, it makes a major contribution to the 2-μm continuum flux density in IIZw40 (Joy & Lester 1988).

1.1.3 Molecular Gas

By far the most abundant molecule in the interstellar medium is H_2. This molecule is homopolar and thus its electric dipole transitions are forbidden. Only when excited by collisions or by absorption of ultraviolet photons is H_2 (quadrupole) emission observed (see Shull & Beckwith 1978, and Black & van Dishoeck 1987 for details of these mechanisms and reviews of Galactic observations). Discrimination between the two mechanisms is possible by determination of the rotational and vibrational excitation temperatures. In practice, this usually means comparison of the flux in the bright v=1–0 S(1) line at 2.122 μm with that in other transitions, *e.g.* v=1–0 S(0) at 2.223 μm and v=2–1 S(1) at 2.248 μm. (Use of these particular, relatively strong, emission lines minimizes the effects of reddening). If the gas density or UV intensity is large, collisional excitation or multiple photon pumping can mimic the (thermal) populations of the lower levels produced by shock excitation (Sternberg 1986). If these conditions are suspected, lines originating from higher vibrational levels must be observed.

The molecular hydrogen emission from extragalactic sources is discussed in detail in Chapters 4 and 5, and thus only a brief summary is given here. Eight of the nine nearby, and predominantly star–forming, galaxies for which the mechanism has been identified, have H_2 line ratios indicative of UV excitation (§4.3). This mechanism has also been suggested for two Seyfert galaxies : NGC 3227 on the basis of the line ratios, and NGC 4151 on the basis of the availability of UV photons, as inferred from the recombination line emission (Fischer *et al.* 1987). Evaluation of the UV field in the

star–forming systems from model calculations and scaled using their measured Brγ fluxes, also indicates that there are sufficient photons in the 91.2 – 110.8 nm band available to account for the observed 1–0 S(1) emission (§4.3.2; §5.3).

Interpretation of the molecular and atomic hydrogen line fluxes is complicated by the presence of dust within the photodissociation zones from which the (fluorescent) H_2 emission arises. The dust competes with H_2 for absorption of the non–ionizing UV photons. The intensity in a given transition of H_2 may therefore not be linearly proportional to the photon pumping rate, but depend on the gas density, UV intensity, and gas–to–dust ratio. Detailed numerical models can be found in Black & van Dishoeck (1987). Some starburst galaxies display very weak H_2 emission, relative to their Brγ fluxes (§5.4). This may be due to the intensity of the UV radiation incident on the molecular gas and consequent low H_2 excitation efficiency (see Chapter 5 for details).

An intriguing exception to the apparent predominance of radiatively excited H_2 in nearby galaxies is the starburst NGC 253. Observations of this galaxy by a number of workers, made through various apertures, indicate that the H_2 is shock excited (Rieke *et al.* 1988; G.S. Wright, personal communication; F.P. Israel, personal communication). The cause of the dissimilarity between NGC 253 and the other nearby systems is not currently understood. Shock–excited molecular hydrogen has also been detected in a number of other galaxies (see §4.1 for a review). In the most luminous examples, NGC 6240 and Arp 220, its origin may be due to shocks produced by the direct interaction of two gas rich galaxies, whereas in the Seyferts NGC 1068 and 1275, winds from the active nuclei may generate the shocks (§4.3.3 and references therein). Since NGC 253 falls into neither of these categories, the anomalous excitation of its H_2 needs to be examined in more detail.

The second most abundant molecule in galaxies is CO. It is readily detectable because it has a permanent dipole moment, a first rotationally–excited (J=1) level at an energy of 5.5 K, and because the Earth's atmosphere is relatively transparent at the wavelength of the $J = 1 \rightarrow 0$ transition ($\lambda = 2.6$ mm). The dissociation potential of CO is about 11 eV and consequently the assumption that almost all CO is contained within dusty molecular clouds, where dust– and self–shielding prevent photodissociation, is valid. Hence its primary application is as a tracer of the molecular gas (*i.e.* of H_2),

most of which is ordinarily not directly observable (see above).

Since molecular clouds in the Galaxy, and thus presumably in other galaxies, are usually very optically thick in the J = 1 → 0 ^{12}CO line, it is not possible to convert directly between CO intensity (I_{CO}) and H_2 column density, $N(H_2)$. Indirect arguments must therefore be used. The standard approach, developed by Young & Scoville (*e.g.* 1982), relies on three assumptions : (a) the excitation temperature is constant across the source; (b) the peak antenna temperature measures the beam filling factor, effectively the number of clouds in the beam; and (c) the clouds are in approximate virial equilibrium (*i.e.* the line width is directly related to the cloud mass). Over 200 galaxies have been observed in J = 1 → 0 ^{12}CO (*e.g.* the compilation by Verter 1985; Young 1986), and H_2 masses derived assuming a constant conversion factor. Differences in the CO emission between, and within, galaxies have been attributed solely to variations in their H_2 masses (see, for example, the review by Young 1987).

The assumption of a constant conversion factor between I_{CO} and $N(H_2)$ has been criticized recently, most forcefully by Maloney & Black (1988). These authors have analysed the conversion factor qualitatively, and find it sensitive to cloud parameters such as density, temperature and elemental abundance. They conclude that the molecular gas in starburst systems has probably been overestimated by up to a factor of 5, because the conditions under which the conversion factor will be constant are violated (see also Crawford *et al.* 1985). These criticisms may not be so damaging for less active galaxies. A small number of galaxies have been observed in higher CO lines and in transitions of different isotopes. The best–studied example is M82, in which the state of the CO component of the interstellar medium proves to be very complex. Measurements in J = 2 → 1 ^{12}CO and J = 1 → 0 and J = 2 → 1 ^{13}CO reveal variations in the optical depth, excitation temperature and filling factor both spatially and (from the velocity profiles) along the line–of–sight (Sofue 1988; N. Nakai, personal communication). Therefore, the properties of starburst galaxies inferred from J = 1 → 0 ^{12}CO measurements should be regarded with some caution until further observational data become available.

Apart from H_2, CO and OH (the first molecule discovered in external galaxies), emission from other molecular species has been observed in only a few extragalactic sources (Henkel & Bally 1985; Seaquist & Bell 1986; Martin & Ho

1986; Henkel *et al.* 1987; Henkel, Mauersberger & Schilke 1988). M82 has been mapped in transitions of HCN and HCO^+ using an aperture synthesis millimetre telescope by Carlstrom (1988). These molecules require much higher densities than CO for excitation; the critical densities are $n_{H_2} \sim$ few $\times 10^5$ cm^{-3} compared with $n_{H_2} = 10^3$ cm^{-3} for CO. Carlstrom concluded that a substantial fraction of the molecular gas in the central regions of M82 is contained in dense clouds ($n_{H_2} > 10^4$ cm^{-3}).

1.1.4 Neutral Atomic Gas

Neutral hydrogen (HI) emits at 21 cm, resulting from the magnetic dipole transition between the hyperfine levels of the ground state atom. This line radiation is most frequently used to trace the structure and dynamics of galaxies (*e.g.* the review by Giovanelli & Haynes 1988). In starbursts (and other systems containing powerful central radio continuum sources), HI is occasionally observed in absorption : 15% of the luminous *IRAS* galaxies surveyed by Mirabel & Sanders (1987) reveal HI absorption features up to 800 km s^{-1} wide. Interestingly, this absorption is often offset with respect to the nuclear optical line velocity (typically by 100 km s^{-1}), suggesting either inflow of HI into the nuclear region, or outflow of optical line–emitting gas. Supporting evidence for the latter comes from observations of blue wings in the emission lines in a number of instances (Heckman, Armus & Miley 1987). The relationship between the molecular and atomic hydrogen contents and with the star formation rate (SFR) in starbursts is not yet clear, although Young *et al.* (1986) suggest that SFR depends more on the total amount of molecular gas than on the atomic gas content, on the basis of a tighter correlation between L_{IR} and I_{CO} than with I_{HI}.

Far–infrared forbidden line emission in the low–level transitions of O^0 has been detected in M82, at 63 μm (Watson *et al.* 1984) and at 146 μm (Lugten *et al.* 1986). The ionization potential of neutral oxygen is 13.6 eV, very similar to that of hydrogen. Consequently, the [OI] lines are strongest in warm, neutral atomic matter, such as that close to HII regions. Emission in [OI]63 μm may dominate the cooling of this gas (Tielens & Hollenbach 1985). In M82, the line profiles of [OI]63 μm, and also of [OIII]88 μmwhich arises in the photoionized regions, are similar, supporting this interpretation. Furthermore, undersampled mapping of the far–IR lines [OI] and [CII]158 μm (see §1.1.2)

suggests comparable spatial distributions. The neutral oxygen lines require moderately high (neutral hydrogen) densities to excite their upper levels. In M82, Lugten *et al.* derive a neutral gas density of $n_H \simeq 10^4$ cm^{-3} and temperature of $T \sim 200$ K. Comparison with the ionized gas reveals that these two components are in approximate pressure equilibrium.

1.1.5 Dust

As has been noted several times in this introduction, dust plays an important role in characterizing the observed radiation from galaxies, primarily via the absorption of optical and UV light and the re–emission of this energy in the infrared and millimetre regimes ($1 < \lambda < 1000\,\mu$m). There exists a wide range in the fraction of the total luminosity that escapes in the infrared : 98% of the prodigious output of Arp 220 is emitted in the IR, compared with 84% for M82, 30% for the Galaxy, and only a few per cent for M31 (Telesco 1988, and references therein). These systems contain a variety of sources which contribute to the dust heating. In M82 this is principally young stars (Rieke *et al.* 1980; Chapter 6), and thus determination of L_{IR} effectively measures the bolometric luminosity, L_{BOL}. Along with the ionization rate, L_{BOL} provides one of the principal tools for investigating the high–mass stellar population (*e.g.* Chapter 6).

Studies of galaxies such as M31, in which much of the IR luminosity arises from dust heated by the interstellar radiation field from older stars (Walterbos & Schwering 1987), are important since observations of spirals made at low resolution (*e.g. IRAS*) can include a significant contribution from their (M31–like) disks. Likewise, detailed studies reveal 50% of the infrared luminosity from the Galaxy is generated in this way, the remainder being due to warm dust heated by OB stars (40%), and hot dust, 10% (Cox & Mezger 1987). The characteristic dust temperatures associated with these components are approximately 20, 40 and 400 K respectively (Walterbos 1988). The latter component is thought to arise from small grains (or large molecules) transiently heated by the absorption of single UV photons (Sellgren 1984) and may dominate the galaxian disk emission at wavelengths between 10 and 30 μm. In Arp 220, a significant fraction of the IR luminosity may be generated by a heavily obscured active nucleus (*e.g.* DePoy, Becklin & Geballe 1987). *IRAS* observations (at 12, 25, 60, and 100 μm)

are often employed to estimate the contribution of these various components to the total emission (*e.g.* Helou 1986; Rowan–Robinson 1987). However, since there are measurements at only four broad–band wavelengths, the model fits are sensitive to the intrinsic shapes of the component spectra.

Observations made at higher spatial resolutions, either using ground–based ($\lambda \lesssim 30\,\mu$m, $0.35 \lesssim \lambda \lesssim 1$ mm) or airborne (intermediate λ) telescopes, may resolve some of the individual components in nearby galaxies. The finest example is NGC 1068 which contains both a Seyfert nucleus and an adjacent 'disk' of young stars (*e.g.* Telesco & Decher 1988). These two components display very dissimilar IR energy distributions (*e.g.* Telesco 1988). The mid–IR spatial distribution has been examined in a number of other systems, ordinarily at $10\,\mu$m, and proves to be a respectable tracer of the IR luminosity within galaxies, provided that their emission is dominated by young stars (Telesco 1988, and references therein).

Sub–millimetre and millimetre wavelength continuum observations are effective in ascertaining the distribution of cold dust, and are necessary for determining its temperature since the longest wavelength *IRAS* band ($100\,\mu$m) often does not sample emission past the peak of the galaxian energy distribution. This long wavelength emission is invariably optically thin and thus the mass of dust can be calculated if the temperature, wavelength dependence of the emissivity, and dust grain properties are known (*e.g.* Hildebrand 1983). The grain emissivity law at these wavelengths is not known precisely, but can be determined from multi–wavelength measurements for the individual cases (*e.g.* Gear, Robson & Griffin 1988). Plausible estimates of the average grain properties (size and density) are available (see discussion by Hildebrand 1983). Furthermore, the cold dust may reside within molecular clouds and thus adoption of an appropriate dust–to–gas conversion factor enables the gas mass to be estimated (*e.g.* Hildebrand 1983; Gear *et al.* 1988; Thronson *et al.* 1987). The gas mass derived in this way is independent of that determined from observations of molecular tracers such as CO (§1.1.3) and promises to provide a valuable test of the assumptions involved in the latter, once sufficient data becomes available.

There are two principal sources of uncertainty associated with the mm–wavelength continuum method : the conversion factor between dust and gas masses (equivalently,

and more commonly, stated as the conversion factor between gas column density, $N(H_2)$, and dust optical depth, τ_λ), and the source of the dust emission. Dealing with the latter point first, this reflects concern that significant radiation may originate from cold grains associated not with molecular clouds, but with diffuse atomic gas, analogous to the far–IR "cirrus" in our Galaxy (*e.g.* Cox & Mezger 1987). This may be less of a problem in starburst regions where the interstellar radiation field is expected to be relatively intense and, consequently, the exposed dust grains warm. Few determinations of the conversion ratio $N(H_2)/\tau_\lambda$ exist. All have been derived from Galactic objects, although a fairly wide range of environments are included : dense star–forming clouds, reflection nebulae and diffuse cirrus (*e.g.* Whitcomb *et al.* 1981; Hildebrand 1983; Jaffe *et al.* 1984; Rengarajan 1984). Thronson (1988) reviews these studies and concludes that the ratio varies by less than a factor of 3. He further argues that, despite this ambiguity, gas masses derived from dust continuum measurements should be superior to those arrived at using the CO technique since the sources of uncertainty in the former are, at least, relatively obvious.

In addition to the continuum emission, there exist several characteristic features due to dust in the infrared spectra of many galaxies. Near 10 μm, a broad absorption attributed to cool silicate grains is often seen towards heavily extinguished sources. The depth of this feature has been related to the visual extinction (*e.g.* Roche & Aitken 1984). Thus, measurements of the silicate optical depth in galaxies provides an estimate of A_V. The accuracy of this technique is hampered by the possibility of reciprocal emission from warm grains along the line–of–sight, differences in grain composition (*e.g.* Roche & Aitken 1985), and the difficulty in determining the continuum level (*e.g.* Phillips, Aitken & Roche 1984). The latter problem arises due to the presence of several narrow adjacent emission features, in particular those at 8.6 and 11.3 μm. These features, along with others near 3.3, 6.2 and 7.7 μm are generally thought to be due to stretching and bending of the bonds in small grains/large molecules, *i.e.* polycyclic aromatic hydrocarbons (*e.g.* Leger & Puget 1984; Allamandola *et al.* 1987). An important empirical result is that galaxies dominated by star formation display different 8–13 μm spectra than those containing active nuclei (Aitken & Roche 1985; Roche & Aitken 1985). Specifically, the dust emission features are generally not observed in active galaxies. A plausible explanation is that the grains are destroyed by intense short

wavelength continuum emission; a suggestion consistent with the observation that the 11.3 μm feature peaks outside the ionized region in Orion and NGC 7027 (*e.g* Aitken *et al.* 1979; Aitken & Roche 1983). Thus the dust line emission provides a diagnostic of the environment in which it is heated.

1.1.6 What Does a Starburst Galaxy Look Like ?

To conclude this brief review of the emission from starburst galaxies, data taken from the literature for the nearby system M82 have been compiled to illustrate the overall spectral energy distribution and several of the other features described in the rest of Section 1.1. These data are shown in Figure 1.1. It is not claimed that this spectrum is typical of starburst galaxies — indeed, it can only to hope represent a particular system viewed at some unspecified epoch during its evolution and from a special vantage point. Moreover, various beam sizes were used for this work : the radio ($\lambda \geq$ 3mm), *IRAS*, and optical measurements generally refer to the whole galaxy, whereas apertures of 25–50$''$ were used for the other observations. The latter corresponds approximately to the extent of the star–forming complex. So as better to clarify the spectral regimes in which the energy is emitted, the ordinate of Figure 1.1 is given as νS_ν (where S_ν is the flux density in Jy at a frequency ν). Several magnified portions of the spectrum are shown, containing lines of particular interest, though primarily for decorative purposes. The data in Figure 1.1 are taken from the compilation by Klein, Wielebinski & Morsi (1988), and references therein, except for the 2.2–5 μm points (Willner *et al.* 1977), 1.25 & 1.65 μm points (Aaronson 1977), optical B & V points (DeVaucouleurs, Corwin & Bollinger 1977), and the X–ray measurement by Watson *et al.* (1984). The higher resolution measurements are : H110α (Shaver, Churchwell & Walmsley 1978), H53α (Chapter 6), [OIII]λ88 μm (Duffy *et al.* 1987), and 2–13 μm spectrum (Willner *et al.* 1977).

An alternative view of the central regions of this galaxy is presented in Figure 1.2, where the spatial distributions of a number of diverse radiations are shown. This diagram is taken from Telesco (1988). Note the good overall correlation between the molecular gas (CO), warm (40 and 100 μm) and hot (10 μm) dust, and the radio and 2-μm continuum emission.

Figure 1.1

Spectral energy disribution of the starburst galaxy M82 and several spectra of astrophysical interest : (a) H110α, (b) H53α, (c) [OIII]λ88 μm, and (d) the rich 2–13 μm region.

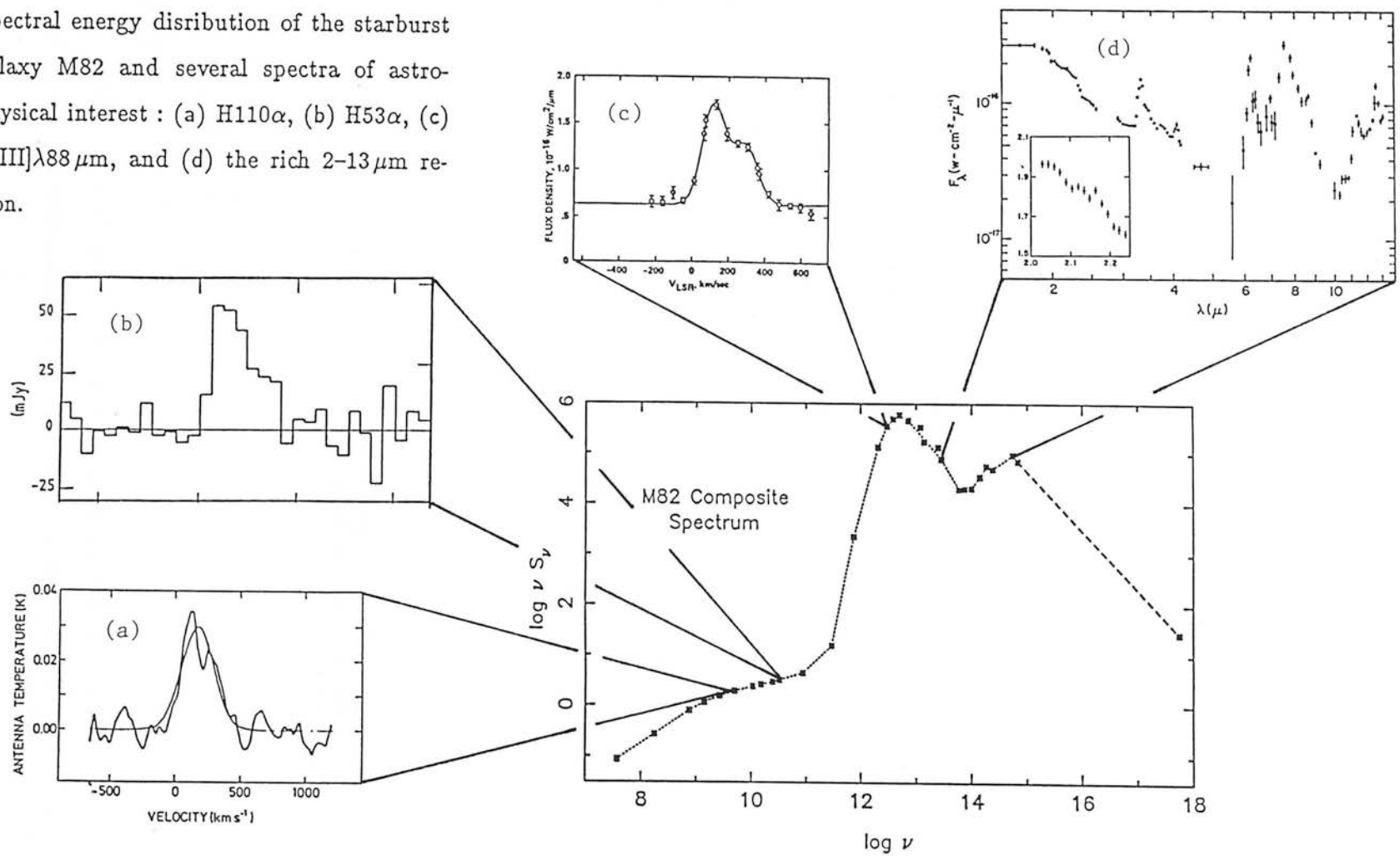

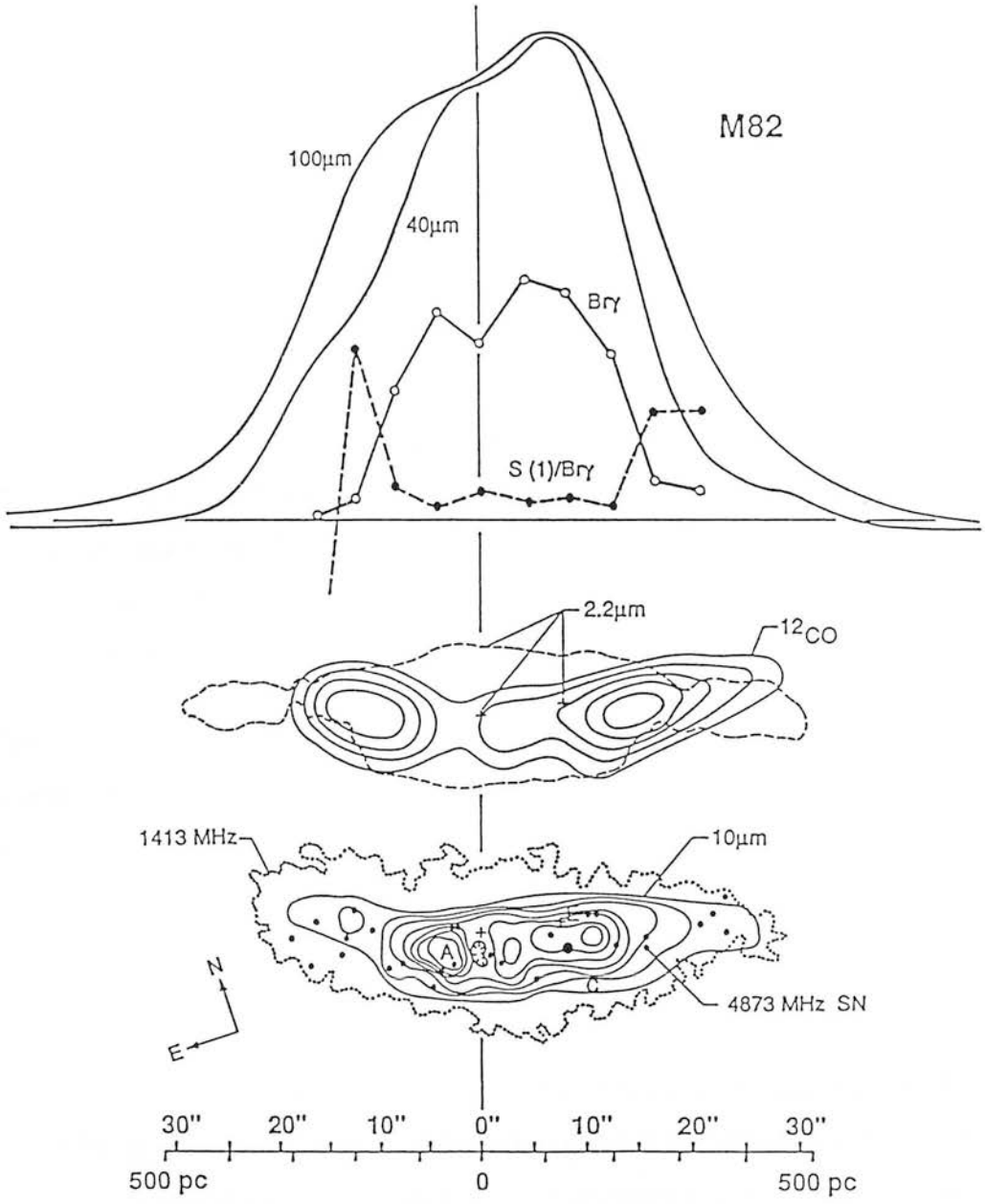

Figure 1.2

Spatial distributions of various line and continuum radiations in the central star-forming complex of M82 (from Telesco 1988, and references therein).

1.2 Activity in Galaxies

In this section, some of the various types of galaxy exhibiting star–formation, or other, activity are discussed. Examination of the latter is instructive since many of their observable properties (*e.g.* large IR luminosity, strong optical line and radio continuum sources) may be qualitatively similar to those of star–forming systems. It is helpful to consider these galaxies in terms of their infrared luminosity (L_{IR}).

At very high luminosities ($L_{IR} > 10^{12}$ $L_\odot$), infrared selected galaxies exceed in space density the only other known objects with comparable levels of emission, the quasars (Soifer *et al.* 1986). Even for $L_{IR} \gtrsim few \times 10^{11}$ $L_\odot$, their space density is approximately equal to that of optically selected Seyferts, and much larger than optically selected starburst galaxies (from Huchra 1977). There have been three suggestions as to the dominant source of this energy : a starburst (*e.g.* Joseph & Wright 1985; Rieke *et al.* 1985); a dust enshrouded active nucleus (*e.g.* Soifer *et al.* 1984); and the kinetic energy from the direct collision of two galaxies (Harwit *et al.* 1986).

There are several observations which are useful for discriminating between the various proposed energy sources. The galaxy–galaxy collision model predicts the existence of highly ionized species such as O^{3+} and Ne^{4+}, formed in 10^6 K gas at the impact front. These would not be produced in HII regions and thus measurement of their IR fine–structure lines ($\lambda \sim 25\,\mu$m) can discriminate against starburst models. Such data are not yet available.

For discrimination between star formation and dusty active nuclei, the width of an infrared hydrogen recombination line (generally large in AGNs) and comparison of the inferred ionization rate (N_{LyC}) and IR luminosity are the most common techniques (*e.g.* DePoy 1987; see also §1.1.2). There are two potential difficulties with this approach. Rieke *et al.* (1985) suggest that supernovae could generate the energy required to produce the broad line component in an exceptionally powerful starburst. However, as noted by DePoy (1987), such galaxies would be expected to exhibit greater than average ratios of N_{LyC}/L_{IR} since the high supernova rates demanded implies a large population of high–mass stars. This is contrary to observations. In fact, DePoy (1987) finds that galaxies with broad recombination lines have ratios which are smaller than average. In

itself, the ratio N_{LyC}/L_{IR} is not a good discriminant against star formation since a wide range of values can be reproduced in starburst models by suitable adjustment of the stellar initial mass function and starburst age (see Appendix C). Nevertheless, taken together with the recombination line width, active nuclei and vigorous star formation can be distinguished using this ratio.

As mentioned in Section 1.1.5, the narrow dust emission features are also useful diagnostics of the energy source. Examination of the optical line emission is another popular method (§1.1.2). However, as observed by Rieke, Lebofsky & Walker (1987), caution should be taken whenever the source is heavily extinguished. Rieke *et al.* cite the example of NGC 253 whose 'nuclear' spectrum resembles that of a LINER (*c.f.* Heckman 1980). Their interpretation of the optical line emission from this starburst galaxy is that of excitation of extranuclear low density gas by supernova shocks. The heavy obscuration surrounding the nuclear star–forming complex (typically, $A_V \sim 12$ from IR line observations) prevents optical measurements from probing the region of HII–type excitation. Terlevich & Melnick (1985) identify a further possible problem involving the use of optical spectra as a diagnostic. They have constructed models for regions of high–mass star formation taking the effects of mass–loss on the stellar evolution into account, and find that the presence of hot luminous stars, which spend much of their lifetime burning helium ("Warmers"), may alter the nebula emission from that of a normal HII region into a spectrum resembling that of a Seyfert. They further suggest that variability of the non–thermal radio emission may be caused by supernovae and their remnants (Terlevich & Melnick 1987).

In the case of Arp 220 ($L_{IR} \sim 10^{12}$), one of the best–studied ultra–luminous galaxies, Becklin & Wynn–Williams (1987) suggest that a dust–embedded AGN is the most likely explanation on the basis of (i) its compact size at 20 μm ($< 1.5\widehat{''}$; or 500 pc), (ii) a broad Brα recombination line ($\Delta v \sim 1300$ km s^{-1}; DePoy, Becklin & Geballe 1987), and (iii) an unresolved 2-μm source ($<0.2\widehat{''}$). DePoy (1987) has made a detailed optical and near–IR line and continuum study of another luminous galaxy (17138–1017; $L_{IR} \sim 2.5 \times 10^{11}$ L$_\odot$) and finds that the emission is consistent with that from an episode of massive star formation. DePoy has also analysed less complete data for a larger sample of galaxies having wider range in L_{IR} ($5 \times 10^{10} - 10^{12}$ L$_\odot$), and suggests that most have recombination line emission consistent with vigorous star

formation, although active nuclei appear to be required by several sources. Clearly, detailed observations such as those performed on 17138–1017 and Arp 220 are to be desired in order to ascertain the energy generation mechanism(s).

As in the extremely luminous systems (*e.g.* Houck *et al.* 1985), interactions and mergers appear to play an important role in galaxies of lower luminosity : $(L_{IR}/10^{11}\,L_{\odot}) \sim 1-5$ (*e.g.* Joseph & Wright 1985; Cutri & McAlary 1985). Within this luminosity range, there is evidence for both nuclear star formation and the presence of AGN. Indeed, the two co–exist in a number of cases, such as NGC 1068 & NGC 7469 (*e.g.* Wilson 1987). The common link is generally believed to be shown by numerical simulations which reveal that an interaction can drive gaseous material from the disk into the central regions where it may form stars, fuel a compact nuclear source, or do both (*e.g.* Combes 1987). The connection between vigorous star formation activity and galaxy interactions is now well established : from optical (Larson & Tinsley 1978), near–infrared (Joseph *et al.* 1984), and *IRAS* properties (Telesco, Wolstencroft & Done 1988).

At lower IR luminosities ($few \times 10^{10} - 10^{11}\ L_{\odot}$), there are two dominant classes of galaxy : barred spirals and luminous Sc systems. In the former, the same mechanism which produces gas–inflow in interacting galaxies (a rotating gravitational potential) is thought to apply, though in this case the driving force is the bar. The end results are qualitatively similar : vigorous star formation activity (Chapter 2), and a high incidence of Seyfert nuclei (Simkin, Su & Schwarz 1980). Evidence supporting the former hypothesis comes from the strong infrared and radio continuum sources observed near the nuclei of these galaxies (Chapter 3; Devereux 1987). In contrast to the centralised sources in barred spirals, the infrared emission from luminous Sc galaxies arises in the disk (*e.g.* Persson & Helou 1986).

To conclude this brief overview of the various types of star–forming galaxy, two other classes presently undergoing a high level of star formation must be mentioned : clumpy ("Magellanic") irregulars and blue dwarf (a.k.a. blue compact or extragalactic HII region) galaxies. There are several differences between these and the other starburst (*i.e.* interacting/merging and barred spiral) galaxies described above, and which are summarised here (Huchra 1987, and references therein). In general, the irregular and "starburst" galaxies have similar optical and UV spectra (although the latter are much

dustier), and thus their inferred stellar properties are similar. These galaxies are best modelled by a burst of star formation superposed on an old stellar population. In contrast, the blue dwarf systems appear to be almost pure starbursts — their optical spectra are completely dominated by emission from hot gas with only a weak continuum. Their low metallicity is consistent with their apparent youth. Morphologically, the star formation in blue dwarf galaxies is proceeding over the whole galaxy, whereas in the irregular and other starbursts it is localised; invariably near the nucleus in the latter. The luminosity of the clumpy irregular galaxies is greater than that of the blue dwarf systems but less than that of the barred spirals and interactors.

1.3 Starburst Models

One of the main objectives for studies of starburst galaxies is determination of the features that characterize star formation in different environments, namely : the star formation rate, the time dependence of this rate, the age of the star–forming episode, and the distribution of stellar masses (IMF). In general, observations can only measure their integrated action, *i.e.* summed over the present–day stellar population, and thus models are required to separate, and thereby examine, their properties. Essentially all models of star formation in galaxies have been based upon the technique developed by Tinsley (1968, 1972).

At its most complex, the model involves construction of a grid of either theoretically or observationally determined stellar spectra covering the required range of stellar masses and for various times during the main sequence and subsequent evolution. The stellar population at any epoch can be determined by defining the IMF and star formation history (*i.e.* rate, age, etc.), and thus the total emission at the wavelength, or band, of interest calculated by summing over that from all of the stars present. Comparison of the value of a given observable, such as bolometric or blue luminosity, with that predicted, thereby constrains the allowed ranges of the input parameters. An early important result from such modelling was that the blueness of some galaxies was most likely due to a recent burst of star formation (Searle, Sargent & Bagnuolo 1973, Huchra 1977), occurring particularly in interacting or otherwise peculiar galaxies (*e.g.* Larson & Tinsley 1978).

The original models were only concerned with reproducing the optical U–B and B–V colours. Subsequent refinements of importance to studies of starbursts have included prediction of : the emission from photo–ionized gas, in particular that in the hydrogen recombination lines (equivalently, the ionization rate), but also from other species such as O^{2+}; the total (bolometric) luminosity; the 2-μm continuum emission and CO index (§1.1.1); the UV spectrum; the total (thermal + non–thermal) radio luminosity; and the total mass (*e.g.* Biermann 1976; Rieke *et al.* 1980; Kennicutt 1983; Bruzual 1983; Gehrz,Sramek & Weedman 1983; Gallagher, Hunter & Tutukov 1984; Telesco 1985; Gonzáles–Riestra, Rego & Zamorano 1987; Belfort, Mochkovitch & Dennefeld 1987; Guiderdoni & Rocca–Volmerange 1987; Chapter 6). In this thesis a simplified form of the model, introduced by Gehrz, Sramek & Weedman (1983) and Telesco & Gatley (1984), is adopted. This involves the assumption that the stellar properties such as Lyman continuum and bolometric luminosity are constant throughout the stars lifetime in a particular evolutionary stage, usually the main sequence phase. Similar results are obtained using the two approaches. A full description of the model used in this thesis is given in Appendix C.

As alluded to in section 1.1.1, the emission at any given wavelength is dominated by stars in a particular mass range. This occurs not only because of the mass–dependence of the stellar emission at that wavelength, but also due to the number of stars of that mass present (the present–day mass function, PDMF). In a zero–age starburst (*i.e.* one in which the stars are distributed according to the IMF), for example, high–mass stars ($M_* > 15$ M$_\odot$) dominate the ionization rate, and thereby the recombination line emission, intermediate mass stars ($M_* \sim 5 - 15$ M$_\odot$) dominate the total luminosity, whilst low mass stars ($M_* < 5$ M$_\odot$) dominate the total mass. Thus, in principle, measurement of many such observables can determine the number of stars of each mass present (the PDMF). However, it is far from trivial to separate the effects of the IMF and star formation history on this distribution, and thus several simplifying assumptions are often made. The most common are that of a universal initial mass function slope, though not necessarily of the lower and upper bounds, and of constant star formation rate. Some justification for the former is provided by Scalo (1986) who reviews various determinations of the IMF and concludes that there is no compelling evidence for any systematic variations of the slope. The latter assumption is more dubious, but may

be applicable to starbursts in which the age and duration of a star–forming episode is expected to be much shorter than a Hubble time. Several of the important results obtained from starburst models have been noted, along with the relevant observations, in Section 1.1.

1.4 Thesis Guide

The substance of this thesis is divided into five parts. Each deals with a different observing technique for investigating the global properties of star formation in extragalactic environments. Chapter 2 describes the construction of a sample of nearby infrared–bright spiral galaxies by comparison of the *IRAS* database with various optical catalogues, and subsequent identification of barred spirals as sites of vigorous star formation. Chapter 3 examines the radio properties of this sample using medium resolution 20-cm continuum data. In particular, the detection rate, morphology, and the infrared–radio correlation are discussed. Chapter 4 presents the first results from a 2-μm spectrophotometric survey of IR–bright spirals. The excitation mechanism responsible for the molecular hydrogen emission is analysed. Chapter 5 expands on the discoveries of the previous section and describes a model of the molecular and atomic hydrogen line excitation. Variations in the relative levels of emission from these species are also examined. Chapter 6 focuses on a particular starburst galaxy : M82. Measurement of the H53α recombination line strength is used to infer a reddening–independent ionization rate. The implications of this rate on the stellar initial mass function are examined using a model which incorporates the emission from photo–ionized gas (H^+, O^{2+} and N^{2+}) as well as the total luminosity. The final chapter summarizes the thesis and suggests directions for future research.

With the exception of Chapter 5, the main chapters have all been published or submitted for publication. Where appropriate, a reference is given in the preface at the beginning of the chapter. With the sole exception of Chapter 2, which has been extensively re–written, their contents are essentially unchanged from the published or submitted versions. In this way, each chapter is self–contained, incorporating its own introduction and references. A brief explanatory paragraph prefacing every chapter describes the relevance of that particular section to the rest of the thesis. Much of

the work of this thesis comes from various collaborations which are noted in the preface to each chapter. Details of other assistance, where pertinent, are given in the acknowledgements found after the conclusions of each section.

Three appendices are also included after the final chapter : (A) reduction of the spectrophotometry data; (B) the effects of dust extinction in star–forming complexes; and (C) line and continuum modelling of starbursts. These sections present more detailed information than that contained within the papers.

References

Aaronson, M., 1977. *Ph.D. Thesis*, Harvard University.

Aitken, D.K. & Roche, P.F., 1983. *Mon. Not. R. astr. Soc.*, **202**, 1233.

Aitken, D.K. & Roche, P.F., 1985. *Mon. Not. R. astr. Soc.*, **213**, 777.

Aitken, D.K., Roche, P.F., Allen, M.C. & Phillips, M.M., 1982. *Mon. Not. R. astr. Soc.*, **199**, 31P.

Aitken, D.K., Roche, P.F., Spenser, P.M. & Jones, B., 1979. *Astr. Astrophys.*, **76**, 60.

Allamandola, L.J., Tielens, A.G.G.M. & Barker, J.R., 1987. In *Polycyclic Aromatic Hydrocarbons and Astrophysics*, p.255, eds. Léger, A., d'Hendecourt, L. & Boccara, N., Reidel.

Antonucci, R.J. & Ulvestad, J.S., 1988. Submitted to *Ap. J.*

Arnaud, K.A. & Gilmore, G., 1986. *Mon. Not. R. astr. Soc.*, **220**, 759.

Augarde, R. & Lequeux, J., 1985. *Astr. Astrophys.*, **147**, 273.

Baker, J.G. & Menzel, D.H., 1938. *Ap. J.*, **88**, 52.

Baldwin, J.R., Danziger, I.J., Frogel, J.A. & Persson, S.E., 1973. *Astrophys. Lett.*, **14**, 1.

Baldwin, J.A., Phillips, M.M. & Terlevich, R., 1981. *Pub. A.S.P.*, **93**, 5.

Balzano, V.A., 1983. *Ap. J.*, **268**, 602.

Beck, S.C., Beckwith, S. & Gatley, I., 1984. *Ap. J.*, **279**, 563.

Beck, S.C., Turner, J.L. & Ho, P.T.P., 1986. *Ap. J.*, **309**, 70.

Becklin, E.E., Gatley, I., Matthews, K., Neugebauer, G., Sellgren, K., Werner, M.W. & Wynn–Williams, C.G., 1980. *Ap. J.*, **236**, 441.

Becklin, E.E. & Wynn–Williams, C.G., 1987. In *Star Formation in Galaxies*, p.643, ed. Persson, C.J., US Govt. Print. Off., Washington, DC.

Belfort, P., Mochkovitch, R. & Dennefeld, M., 1987. *Astr. Astrophys.*, **176**, 1.

Bell, M.B. & Seaquist, E.R., 1978. *Ap. J.*, **223**, 378.

Biermann, P., 1976. *Astr. Astrophys.*, **53**, 295.

Black, J.H. & van Dishoeck, E.F., 1987. *Ap. J.*, **322**, 412.

Boksenberg, A. *et al.*, 1978. *Nature*, **275**, 404.

Bruzual, G., 1983. *Ap. J.*, **273**, 105.

Carlstrom, J.E., 1988. In *Galactic and Extragalactic Star Formation*, p.571, eds. Pu-

dritz, R.E. & Fich, M., Kluwer Acad. Publ., Dordrecht.

Combes, F., 1988. In *Galactic and Extragalactic Star Formation*, p.475, eds. Pudritz, R.E. & Fich, M., Kluwer Acad. Publ., Dordrecht.

Cox, P.N. & Mezger, P.G., 1987. In *Star Formation in Galaxies*, p.23, ed. Persson, C.J., US Govt. Print. Off., Washington, DC.

Crawford, M.K., Genzel, R., Townes, C.H. & Watson, D.M., 1985. *Ap. J.*, **291**, 755.

Cutri, R.M. & McAlary, C.W., 1985. *Ap. J.*, **296**, 90.

de Vaucouleurs, G., Corwin, H.G. & Bollinger, G., 1977. *Ap. J. Supp.*, **33**, 229.

DePoy, D.L., 1987. *Ph.D. Thesis*, University of Hawaii.

DePoy, D.L., Becklin, E.E & Geballe, T.R., 1987. *Ap. J.*, **316**, L63.

Devereux, N., 1987. In *Star Formation in Galaxies*, p.219, ed. Persson, C.J., US Govt. Print. Off., Washington, DC.

Duffy, P.B., Erickson, E.F., Haas, M.R. & Houck, J.R., 1987. *Ap. J.*, **315**, 68.

Duric, N., 1986. *Ap. J.*, **304**, 96.

Duric, N., Borneuf, E. & Gregory, P.C., 1988. *A.J.*, **96**, 81.

Evans, N.J., Levreault, R.M., Beckwith, S. & Skrutskie, M., 1987. *Ap. J.*, **320**, 364.

Fischer, J., Geballe, T.R., Smith, H.A., Simon, M. & Storey, J.W.V., 1987. *Ap. J.*, **320**, 667.

Frogel, J.A., Persson, S.E., Aaronson, M. & Matthews, K., 1978. *Ap. J.*, **220**, 75.

Gallagher, J.S., Hunter, D.A. & Tutukov, A.V., 1984. *Ap. J.*, **284**, 544.

Gear, W.K., Gee, G., Robson, E.I., Ade, P.A.R. & Duncan, W.D., 1986. *Mon. Not. R. astr. Soc.*, **219**, 19P.

Gear, W.K., Robson, E.I. & Griffin, M.J., 1988. *Mon. Not. R. astr. Soc.*, **231**, 55P.

Gehrz, R.D., Sramek, R.A. & Weedman, D.W., 1983. *Ap. J.*, **267**, 551.

Gioia, I.M., Gregorini, L. & Klein, U., 1982. *Astr. Astrophys.*, **116**, 164.

Giovanelli, R. & Haynes, M.P., 1988. in *Galactic and Extragalactic Radio Astronomy*, p.523, eds. Vershuur, G.L. & Kellerman, K.I., Springer–Verlag, Berlin.

González–Riestra, R., Rego, M. & Zamorano, J., 1987. *Astr. Astrophys.*, **186**, 64.

Guiderdoni, B. & Rocca–Volmerange, B., 1987. *Astr. Astrophys.*, **186**, 1.

Harwit, M., Houck, J.R., Soifer, B.T. & Palumbo, G.G.C., 1987. *Ap. J.*, **315**, 28.

Heckman, T.M., 1980. *Astr. Astrophys.*, **152**, 87.

Heckman, T.M., Armus, L. & Miley, G.K., 1987. *A.J.*, **93**, 276.

Helou, G., 1986. *Ap. J.*, **311**, L33.

Helou, G., Soifer, B.T. & Rowan–Robinson, M., 1985. *Ap. J.*, **298**, L7.

Henkel, C. & Bally, J., 1985. *Astr. Astrophys.*, **150**, L25.

Henkel, C., Jacq, T., Mauersberger, R., Mentan, K.M. & Steppe, H., 1987. *Astr. Astrophys.*, **188**, L1.

Henkel, C., Mauersberger, R. & Schilke, P., 1988. *Astr. Astrophys.*, in press.

Hildebrand, R.H., 1983. *Q. Jl. R. astr. Soc.*, **24**, 267.

Houck, J.R., Schneider, D.P., Danielson, G.E., Beichman, C.A., Lonsdale, C.J., Neugebauer, G. & Soifer, B.T., 1985. *Ap. J.*, **290**, L5.

Huchra, J.P., 1977a. *Ap. J.*, **217**, 928.

Huchra, J.P., 1977b. *Ap. J. Supp.*, **35**, 171.

Huchra, J.P., 1987. In *Starbursts and Galaxy Evolution*, p.199, eds. Thuan, T.X., Montmerle, T. & Tran, J.T.V., Editions Frontières, France.

Hummer, D.G. & Storey, P.J., 1987. *Mon. Not. R. astr. Soc.*, **224**, 801.

Jaffe, D.T., Hildebrand, R.H., Keene, J., Harper, D.A., Loewenstein, R.F. & Moran, J.M., 1984. *Ap. J.*, **281**, 225.

Jennings, R.E., 1975. In *HII Regions and Related Topics*, p.137, eds. Wilson, T.L. & Downes, D., Springer–Verlag, Berlin.

Joseph, R.D., Meikle, W.P.S., Robertson, N.A. & Wright, G.S., 1984. *Mon. Not. R. astr. Soc.*, **209**, 111.

Joseph, R.D. & Wright, G.S., 1985. *Mon. Not. R. astr. Soc.*, **214**, 87.

Joseph, R.D., Wright, G.S. & Prestwich, A.H., 1986. in *New Insights in Astrophysics*, p.597, ESA SP–263.

Joy, M. & Lester, D.F., 1988. *Ap. J.*, **331**, 145.

Kennicutt, R.C., 1983. *Ap. J.*, **272**, 54.

Klein, U., Wielebinski, R. & Morsi, H.W., 1988. *Astr. Astrophys.*, **190**, 41.

Kronberg, P.P., Biermann, P. & Schwab, F.R., 1985. *Ap. J.*, **291**, 693.

Kunth, D. & Weedman, D., 1987. In *Scientific Accomplishments of the IUE*, p.623, ed. Kondo, Y., Reidel, Dordrecht, Holland.

Larson, R.B. & Tinsley, B.M., 1978. *Ap. J.*, **219**, 46.

Leger, A. & Puget, J.L., 1984. *Astr. Astrophys.*, **137**, L5.

Lugten, J.B., Watson, D.M., Crawford, M.K. & Genzel, R., 1986. *Ap. J.*, **311**, L51.

Maloney, P. & Black, J.H., 1988. *Ap. J.*, **325**, 389.

Martin, R.N. & Ho, P.T.P., 1986. *Ap. J.*, **308**, L7.

Mathis, J.S., 1970. *Ap. J.*, **159**, 263.

Mathis, J.S., 1983. *Ap. J.*, **267**, 119.

Mathis, J.S., 1986. *Pub. A.S.P.*, **98**, 995.

Mirabel, I.F. & Sanders, D.B., 1988. In *Galactic and Extragalactic Star Formation*, p.551, eds. Pudritz, R.E. & Fich, M., Kluwer Acad. Publ., Dordrecht.

Osterbrock, D.E., 1988. *Pub. A.S.P.*, **100**, 412.

Peimbert, M. & Jugaku, J., 1987. Eds., *Star Forming Regions*, IAU 115, Reidel, Dordrecht, Holland.

Persson, C.J., 1987. Ed., *Star Formation in Galaxies*, US Govt. Print. Off., Washington DC.

Persson, C.J. & Helou, G., 1987. In *Star Formation in Galaxies*, p.153, ed. Persson, C.J., US Govt. Print. Off., Washington, DC.

Phillips, M.M., Aitken, D.K. & Roche, P.F., 1984. *Mon. Not. R. astr. Soc.*, **207**, 25.

Pudritz, R.E. & Fich, M., 1988. Eds., *Galactic and Extragalactic Star Formation*, Kluwer Acad. Publ., Dordrecht.

Rengarajan, T.N., 1984. *Astr. Astrophys.*, **140**, 213.

Rieke, G.H., Cutri, R.M., Black, J.H., Kailey, W.F., McAlary, C.W., Lebofsky, M.J. & Elston, R., 1985. *Ap. J.*, **290**, 116.

Rieke, G.H. & Lebofsky, M.J., 1979. *Ann. Rev. Astr. Astrophys.*, **17**, 477.

Rieke, G.H. & Lebofsky, M.J., 1985. *Ap. J.*, **288**, 618.

Rieke, G.H., Lebofsky, M.J., Thompson, R.I., Low, F.J. & Tokunaga, A.T., 1980. *Ap. J.*, **238**, 24.

Rieke, G.H., Lebofsky, M.J. & Walker, C.E., 1988. *Ap. J.*, **325**, 679.

Roche, P.F. & Aitken, D.K., 1984. *Mon. Not. R. astr. Soc.*, **208**, 481.

Roche, P.F. & Aitken, D.K., 1985a. *Mon. Not. R. astr. Soc.*, **213**, 789.

Roche, P.F. & Aitken, D.K., 1985b. *Mon. Not. R. astr. Soc.*, **215**, 425.

Rowan–Robinson, M., 1987. In *Star Formation in Galaxies*, p.133, ed. Persson, C.J., US Govt. Print. Off., Washington, DC.

Scalo, J.M., 1986. *Fund. Cosm. Phys.*, **11**, 1.

Scalo, J.M., 1987. In *Starbursts and Galaxy Evolution*, p.445, eds. Thuan, T.X., Montmerle, T. & Tran, J.T.V., Editions Frontières, France.

Seaquist, E.R. & Bell, M.B., 1986. *Ap. J.*, **303**, L67.

Seaquist, E.R., Bell, M.B. & Bignell, R.C., 1985. *Ap. J.*, **294**, 546.

Seaquist, E.R. & Bignell, R.C., 1977. *Astr. Astrophys.*, **55**, 163.

Searle, L., Sargent, W.L.W. & Bagnuolo, W.G., 1973. *Ap. J.*, **179**, 427.

Sellgren, K., 1984. *Ap. J.*, **277**, 623.

Shaver, P.A., Churchwell, E. & Walmsley, C.M., 1978. *Astr. Astrophys.*, **64**, 1.

Shull, J.M. & Beckwith, S., 1982. *Ann. Rev. Astr. Astrophys.*, **20**, 163.

Shull, J.M. & McKee, C.F., 1979. *Ap. J.*, **227**, 131.

Simkin, S.M., Su, H.J. & Schwarz, M.P., 1980. *Ap. J.*, **237**, 404.

Simon, M., Felli, M., Cassar, L., Fischer, J. & Massi, M., 1983. *Ap. J.*, **266**, 623.

Skillman, E.D. & Israel, F.P., 1988. *Astr. Astrophys.*, in press.

Sofue, Y., 1988. In *Galactic and Extragalactic Star Formation*, p.409, eds. Pudritz, R.E. & Fich, M., Kluwer Acad. Publ., Dordrecht.

Soifer, B.T., Helou, G., Lonsdale, C.J., Neugebauer, G., Hacking, P., Houck, J.R., Low, F.J., Rice, W. & Rowan-Robinson, M., 1984. *Ap. J.*, **283**, L1.

Soifer, B.T., Houck, J.R. & Neugebauer, G., 1987. *Ann. Rev. Astr. Astrophys.*, **25**, 187.

Soifer, B.T., Sanders, D.B., Neugebauer, G., Danielson, G.E. & Persson, C.J., 1986. *Ap. J.*, **303**, L41.

Sternberg, A., 1986. *Ph.D. Thesis*, Columbia University.

Telesco, C.M., 1985. In *Rutherford Appleton Laboratory Conference on Extragalactic IR Astronomy*, p.87, ed. Gondhalekar, P.M.

Telesco, C.M., 1988. *Ann. Rev. Astr. Astrophys.*, **26**, 343.

Telesco, C.M. & Decher, R., 1988. *Ap. J.*, in press.

Telesco, C.M., Decher, R. & Gatley, I., 1986. *Ap. J.*, **302**, 632.

Telesco, C.M. & Gatley, I., 1984. *Ap. J.*, **284**, 557.

Telesco, C.M., Wolstencroft, R.D. & Done, C., 1988. *Ap. J.*, **329**, 174.

Terlevich, R. & Melnick, 1985. *Mon. Not. R. astr. Soc.*, **213**, 841.

Terlevich, R. & Melnick, J., 1987. In *Starbursts and Galaxy Evolution*, p.393, eds. Thuan, T.X., Montmerle, T. & Tran, J.T.V., Editions Frontières, France.

Thompson, R.I., 1987. *Ap. J.*, **321**, 153.

Thronson, H.A., 1988. In *Galactic and Extragalactic Star Formation*, p.621, eds. Pudritz, R.E. & Fich, M., Kluwer Acad. Publ., Dordrecht.

Thronson, H.A. & Harper, D.A., 1979. *Ap. J.*, **230**, 133.

Thronson, H.A. & Telesco, C.M., 1986. *Ap. J.*, **311**, 98.

Thronson, H.A., Walker, C.K., Walker, C.E. & Maloney, P., 1987. *Ap. J.*, **318**, 645.

Thuan, T.X., Montmerle, T. & Tran, J.T.V., 1987. Eds. *Starbursts and Galaxy Evolution*, Editions Frontières, France.

Tielens, A.G.G.M. & Hollenbach, D., 1985. *Ap. J.*, **291**, 722.

Tinsley, B.M., 1968. *Ap. J.*, **151**, 547.

Tinsley, B.M., 1972. *Astr. Astrophys.*, **20**, 383.

Turner, J.L. & Ho, P.T.P., 1983. *Ap. J.*, **268**, L79.

Turner, J.L., Ho, P.T.P. & Beck, S.C., 1987. *Ap. J.*, **313**, 644.

Ulvestad, J.S., 1982. *Ap. J.*, **259**, 96.

Unger, S.W., Pedlar, A., Axon, D.J., Wilkinson, P.N. & Appleton, P.N., 1984. *Mon. Not. R. astr. Soc.*, **211**, 783.

Veilleux, S. & Osterbrock, D.E., 1987. *Ap. J. Supp.*, **63**, 295.

Verter, F., 1985. *Ap. J. Supp.*, **57**, 261.

Walker, C.E., Lebofsky, M.J. & Rieke, G.H., 1988. *Ap. J.*, **325**, 687.

Walsh, J.R., Nandy, K., Thompson, G.I. & Meaburn, J., 1986. *Mon. Not. R. astr. Soc.*, **220**, 453.

Walterbos, R.A.M., 1988. In *Galactic and Extragalactic Star Formation*, p.361, eds. Pudritz, R.E. & Fich, M., Kluwer Acad. Publ., Dordrecht.

Walterbos, R.A.M. & Schwering, P.B.W., 1987. *Astr. Astrophys.*, **180**, 27.

Watson, D.M., Genzel, R., Townes, C.H., Werner, M.W. & Storey, J.W.V., 1984. *Ap. J.*, **279**, L1.

Weedman, D.W., Feldman, F.R., Balzano, V.A., Ramsey, L.W., Sramek, R.A. & Wu, C., 1981. *Ap. J.*, **248**, 105.

Whitcomb, S.E., Gatley, I., Hildebrand, R.H., Keene, J., Sellgren, K. & Werner, M.W.,

1981. *Ap. J.*, **246**, 416.

Willner, S.P., Soifer, B.T., Russell, R.W., Joyce, R.R. & Gillett, F.C., 1977. *Ap. J.*, **217**, L121.

Wilson, A.S., 1987. In *Star Formation in Galaxies*, p.675, ed. Persson, C.J., US Govt. Print. Off., Washington, DC.

Young, J.S., 1987. In *Star Formation in Galaxies*, p.197, ed. Persson, C.J., US Govt. Print. Off., Washington, DC.

Young, J.S., 1987. In *Star Forming Regions*, p.557, eds. Peimbert, M. & Jugaku, J., Reidel, Dordrecht, Holland.

Young, J.S., Schloerb, F.P., Kenney, J.D. & Lord, S.D., 1986. *Ap. J.*, **304**, 443.

Young, J.S. & Scoville, N.Z., 1982. *Ap. J.*, **258**, 467.

Zinnecker, H., 1987. In *Starbursts and Galaxy Evolution*, p.165, eds. Thuan, T.X., Montmerle, T. & Tran, J.T.V., Editions Frontières, France.

Chapter 2

Enhanced Star Formation – The Importance of Bars in Spiral Galaxies

Preface : In this chapter, the presence of a bar in a spiral galaxy is identified as a necessary condition for vigorous star formation activity. This discovery initiated the radio and infrared spectrophotometric observational programmes which form a major part of this dissertation. The work for this section was carried out in collaboration with Tim Hawarden, Matt Mountain and Sandy Leggett, and a less well developed version was published in *Monthly Notices* (Hawarden, Mountain, Leggett & Puxley, 1986. *Mon. Not. R. astr. Soc.*, **221**, 41P).

Summary

Analysis of an *IRAS*–selected sample of nearby luminous spiral galaxies shows that more than one third of the barred systems, corresponding to 8% of all barred spirals in the Shapley–Ames catalogue, have an excess of flux at 25 μm. On average, the total infrared luminosity of these systems is more than 50% greater than that of other *IRAS*–selected spirals. These properties are probably attributable to an episode of vigorous star formation caused by a bar–driven inflow of material.

2.1 Introduction

Two characteristic features of barred spiral galaxies of early to intermediate type are the dust lanes which trace the hydrodynamic shocks in the bar, and the associated rings of HII regions around the nucleus. Observations of HI by Sancisi, Allen & Sullivan (1979),

and optical spectroscopy by Pence & Blackman (1984), for example, suggest that in such structures there is an inflow of material. Numerical simulations of barred spirals (*e.g.* Schwarz 1984; Combes & Gerin 1985) suggest that this inflow is driven by the bar and that the material swept inwards accumulates near one of the inner resonances, if such features are dynamically permitted. At least two of these rings (in NGC 1097 and 3310) are unambiguously the location of enhanced star formation (Telesco & Gatley 1981, 1984).

As much of the radiation from star–forming regions is absorbed by dust and re–radiated in the infrared (*e.g.* Thronson & Harper 1979), the unbiased all–sky survey provided by the *Infrared Astronomical Satellite (IRAS) Point Source Catalog* (see the *IRAS Explanatory Supplement* 1985) has been used to study this process in spiral galaxies from the *Revised Shapley–Ames Catalog* (Sandage & Tammann 1981, 'RSA'). The construction of the sample is described in Section 2.2 and galaxies selected in the process are examined. The *IRAS* properties of the sample are analysed in Section 2.3 and a simple model for their emission is developed. Section 2.4 briefly discusses some of the relevant results from numerical simulations of the dynamics and gas flow in barred spiral galaxies.

2.2 Sample Construction

The production of the infrared–selected sample of galaxies involved several steps which are summarized in Table 2.1. Firstly, the RSA and *IRAS Point Source Catalogs* (PSC2) were cross–correlated. The re–issued (version 2) of the *IRAS* PSC was used for this work since it contains a statistical correction for the flux overestimation of weak sources in the first edition of the catalogue. (Comparison between PSC1 and 2 reveals that differences between catalogued flux densities for the selected galaxies are small, however; only 17% have corrections greater than the quoted 1σ errors and all are less than 2σ). *IRAS* point sources within $90''$ of each RSA galaxy were selected, 863 sources in all (69% of the RSA). Examination of this subset showed that in all but a very few cases, only one *IRAS* source had been paired with each galaxy. The 'spurious' *IRAS* matches are invariably weak and were rejected at a later stage of the sample construction. To put this result on a firmer basis, the discrepancies between RSA and PSC2 positions were

examined. Fig 2.1 shows the (optical–*IRAS*) offsets in declination and right ascension (both in arcsec). Approximating the error distributions by Gaussians yields full widths at half–maxima of about $30\widehat{''}$. These values are consistent with that given in the *IRAS Explanatory Supplement* (1985) for the "cross–scan" difference ($31\widehat{''}$) between *IRAS* and Dressel & Condon (1976) optical positions.

Since this study is concerned with the morphology of the *IRAS*–detected galaxies, it is important to consider what biases in morphological type, if any, are introduced by the selection criteria. Fairclough (1985) examined this problem in detail and concluded (i) that virtually all (94%) RSA spirals were detected by *IRAS*, and (ii) that no important changes in the relative fractions of Hubble types amongst detected and undetected spirals occurs. Likewise, the apportionment of unbarred (SA), barred (SB) and "mixed–type" (weakly barred; SX) spirals remains constant between RSA and *IRAS*–selected samples (see Table 2.2). The optically bright galaxies *not* detected in at least one of the 4 infrared wavebands (12, 25, 60 & 100 μm) by *IRAS* are predominantly ellipticals and lenticulars due to their low dust contents (*e.g.* de Jong *et al.* 1984; Fairclough 1985).

The second stage in construction of the catalogue involved selection of spiral galaxies having Hubble types between SO/a and Scd (inclusive), *i.e.* those with some reliably identifiable trace of spiral structure. Morphological types taken from the *Second Reference Catalogue of Bright Galaxies* (de Vaucouleurs, de Vaucouleurs & Corwin 1976, 'RC2') were used throughout this work because of the homogeneity of their classification. This step removed a further 194 galaxies.

Thirdly, only those spirals detected by *IRAS* in all 4 wavebands (numbering 226 in all) were picked since one of the motivations for this work was to examine the infrared energy distributions particularly at the shorter wavelengths where the Planck function of warm dust intimately associated with young star–forming regions peaks (*e.g.* Adams & Shu 1985). The distributions of several observable properties for this sub–sample have been compared with those for spirals detected in only 1, 2 or 3 of the *IRAS* bands to examine possible selection effects (see Fig. 2.2–2.6).

To quantify the similarity or disparity of the distributions, the non–parametric

Table 2.1: Summary of the construction of the *IRAS*–selected galaxy sample.

Sample Code	Catalogue Description	Number of Objects
1	Shapley–Ames galaxies (RSA)	1246
2	RSA galaxies paired with *IRAS* sources ($90\widehat{''}$ search radius)	863
3	Spirals from #2 with Hubble types S0/a–Scd (inclusive)	669
4	Galaxies in #3 detected in all four *IRAS* wavebands	226
5	Previous sample after removal of known Seyferts and LINERs	194

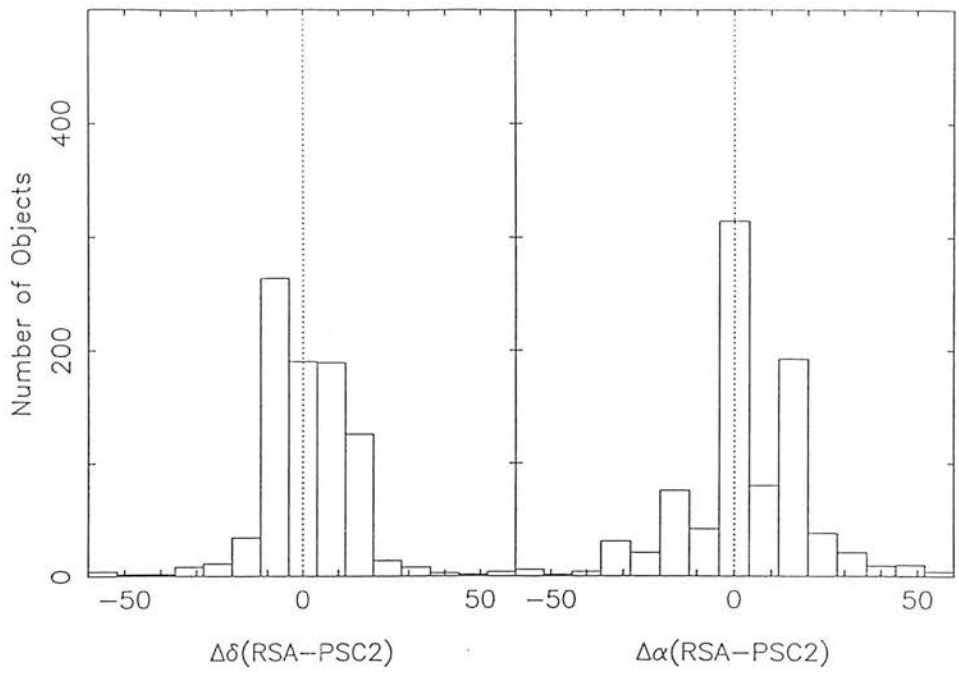

Figure 2.1: Offsets in arcsec of DEC and RA between optical (Shapley–Ames) and *IRAS* catalogued galaxy positions.

Table 2.2: Distribution of unbarred (SA), barred (SB) and mixed–type (SX) spirals in three of the galaxy samples : all Shapley–Ames spirals (# 782), Shapley–Ames spirals (SO/a–Scd) detected by *IRAS* in all 4 bands (# 226), Shapley–Ames spirals detected by *IRAS* but not in all wavebands (# 443).

Sample	Fraction of all Spirals		
	unbarred	barred	mixed
RSA	0.33	0.35	0.32
IRAS (all bands)	0.39	0.29	0.32
IRAS (detected)	0.32	0.34	0.34

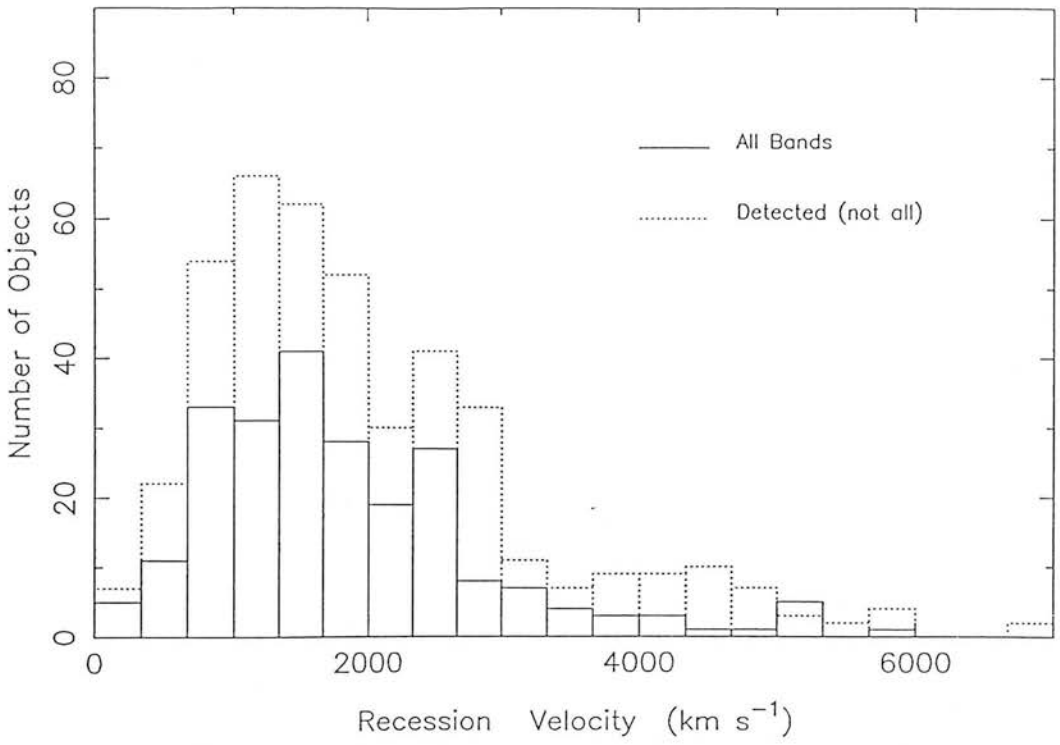

Figure 2.2: Recession velocity distributions for Shapley–Ames galaxies detected by *IRAS* in all four wavebands (solid line), and for those detected by *IRAS* but not in all bands (dotted line).

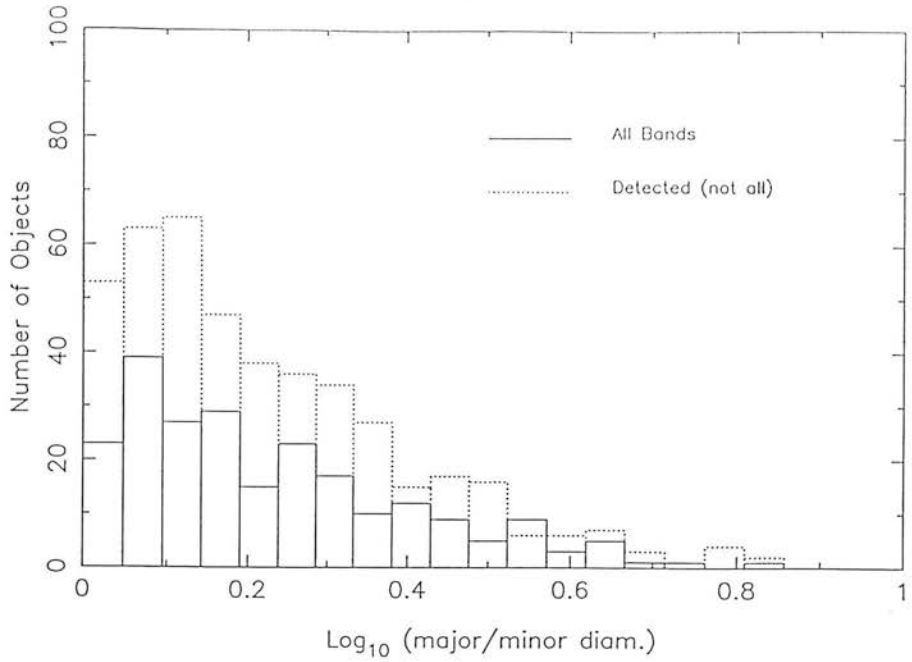

Figure 2.3: As Fig. 2.2 but for distributions of major/minor diameters.

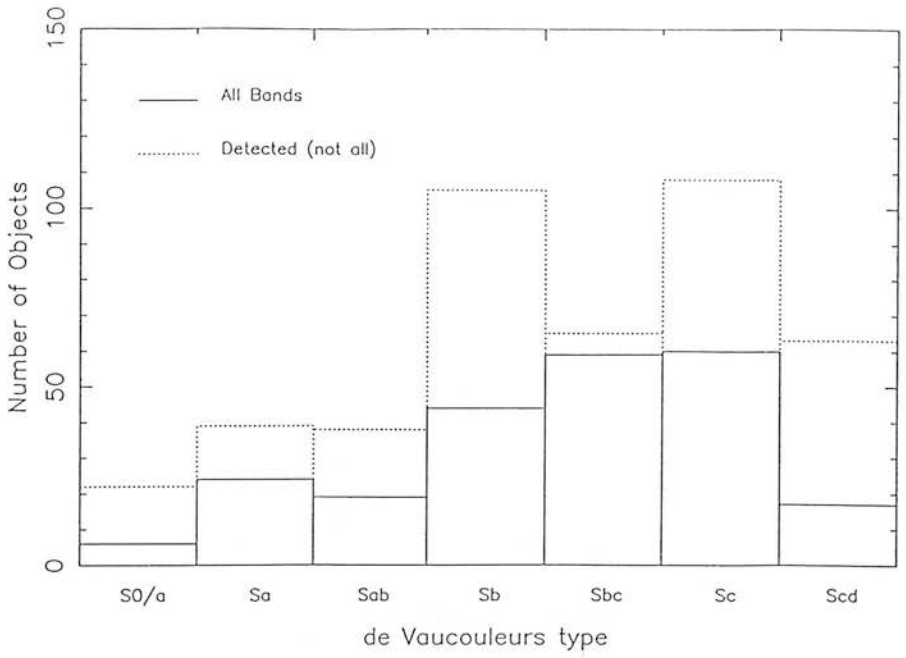

Figure 2.4: As Fig. 2.2 but for distributions of Hubble types as classified by de Vaucouleurs.

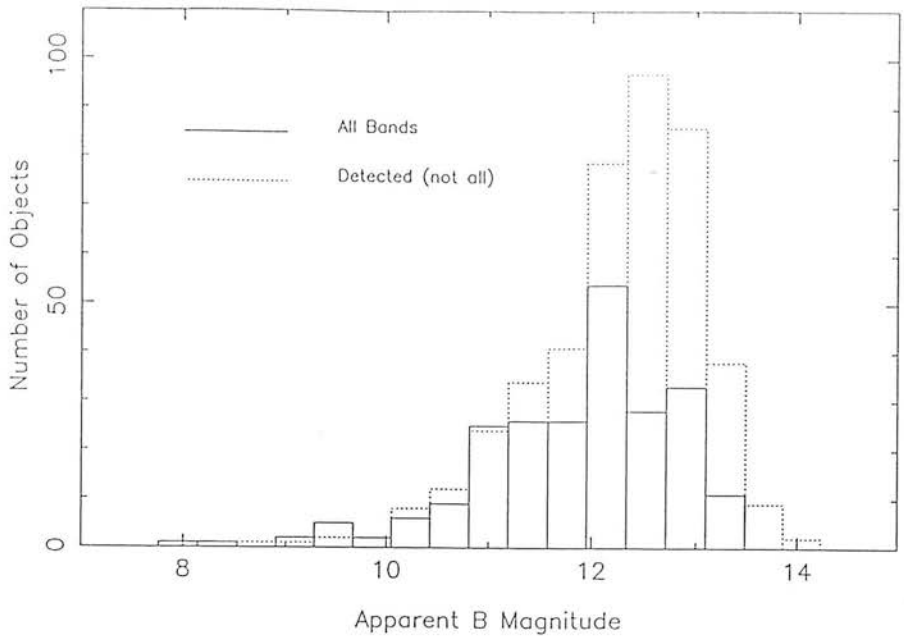

Figure 2.5: As Fig. 2.2 but for distributions of apparent integrated blue magnitude.

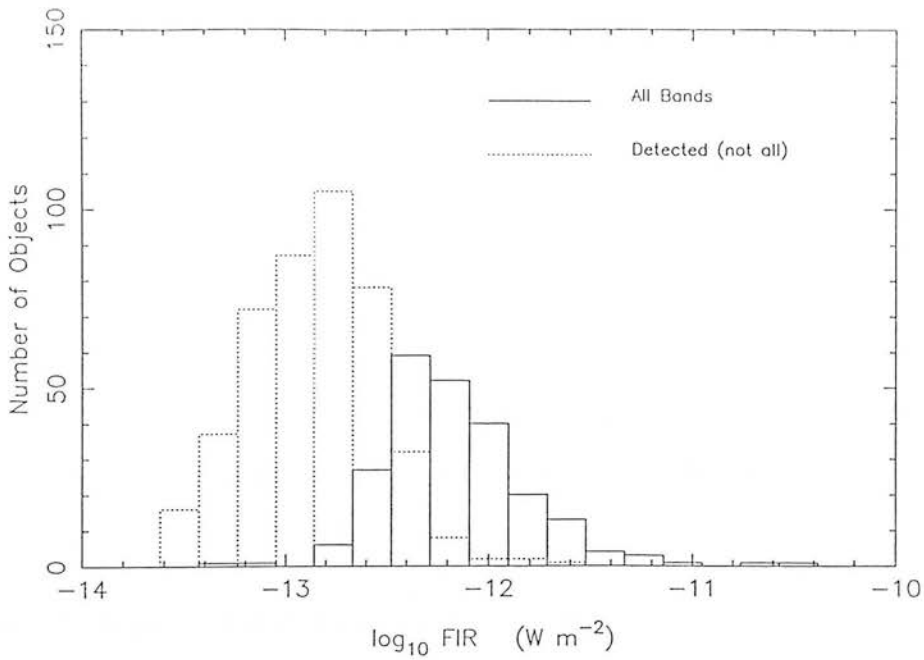

Figure 2.6: As Fig. 2.2 but for distributions of the *IRAS* FIR parameter defined in the text.

Kolmogorov–Smirnov (K–S) statistical test was employed (*e.g.* Siegel 1956). This test shows that there are no significant differences between the two samples in their recession velocity (taken from RSA and corrected for solar motion using the values in RC2; Fig. 2.2), axial ratio (ratio of major to minor diameter, from RC2, evaluated at a blue surface brightness of 25 mag (arcsec)$^{-2}$; Fig. 2.3) and Hubble type (Fig 2.4) distributions. The null hypothesis that the two datasets were drawn from the same population cannot be rejected (*i.e.* the probability that any difference in their cumulative frequency distributions is due to chance is 10% or greater). As with the distribution of Hubble types, Table 2.2 shows that the relative fractions of barred, unbarred, and mixed–type spirals in the two sub–samples are not significantly different.

Examination of Fig 2.5 suggests that the average apparent blue magnitude (taken from RSA, not corrected for extinction) of the galaxies detected by *IRAS* in all wavebands is slightly brighter than that of the comparison sample. This suggestion is confirmed by the K–S statistic (the null hypothesis being rejected at the 99.9% confidence level) and the median values of the two samples — 12.03 and 12.40 mag, respectively. This distinction is minor, however, compared with the distributions of the *IRAS* FIR parameter illustrated in Fig. 2.6. The FIR parameter, defined in the *Cataloged Galaxies and Quasars in the IRAS Survey* (1985) as :

$$\left(\frac{FIR}{\mathrm{W\ m^{-2}}}\right) = 3.25 \times 10^{-14} \left(\frac{S_{60}}{\mathrm{Jy}}\right) + 1.26 \times 10^{-14} \left(\frac{S_{100}}{\mathrm{Jy}}\right) \qquad (2.1)$$

is effectively the flux measured through an 80-μm wide filter centred at 80 μm, and is a widely–used representation of the far–infrared emission.

Figs 2.2–2.6 and Table 2.2 indicate that the spiral galaxies detected by *IRAS* in all 4 bands are primarily an infrared–luminous subset of those detected in at least one band, their other properties being similar.

Of the 226 galaxies detected by *IRAS* at 12–100 μm a further 32 systems listed as Seyferts of types 1 or 2 or as LINERs by Véron–Cetty & Véron (1985) were discarded (*i.e.* those whose infrared emission may be generated by an active nucleus). Although not all of the remaining 194 spirals have published optical spectra, the overwhelming majority of those which do display emission line strengths characteristic of HII regions

(see §1.1.2). These 194 galaxies constitute the infrared selected sample analysed in the following section.

2.3 Analysis of the *IRAS* Results for the Sample Galaxies

In Fig. 2.7 a scatter diagram showing the ratio of *IRAS* PSC2 25μm/12μm flux densities *vs* the ratio of 100μm/25μm flux densities is presented. The morphological families (A,B,X) are shown independently and it is immediately obvious that a major fraction of the barred galaxies exhibit enhanced emission at 25 μm. (In this context, the "barred" galaxies are taken to include spirals of types SB *and* SX). Furthermore it is clear that the superposition of at least two components is required to describe adequately the location of a galaxy in this *IRAS* 2–colour diagram. Consideration of the *IRAS* colours for several classes of object suggests that the contribution from regions of high–mass star formation to the total emission increases as one proceeds from the lower right–hand corner of Fig. 2.7 to the upper left–hand corner (*c.f.* Helou 1986). For example, spirals with a low level of star–formation activity such as M31 ($S_{25}/S_{12} \simeq 0.9$, $S_{100}/S_{25} \simeq 20$; Walterbos & Schwering 1987) and M81 ($S_{25}/S_{12} \simeq 1.1$, $S_{100}/S_{25} \simeq 35$) would fall in the lower right end of the distribution, whereas actively star–forming regions such as that in Cygnus ($S_{25}/S_{12} \simeq 4$, $S_{100}/S_{25} \simeq 13$; T. Moore, personal communication) and the "starburst" galaxy M82 ($S_{25}/S_{12} \simeq 5$, $S_{100}/S_{25} \simeq 4$) would occupy the upper left corner. Thus it may be concluded from Fig. 2.7 that the excess 25-μm emission noted above arises in regions of active star formation and that high levels of this activity, sufficient to dominate the infrared colours of galaxies, occur almost exclusively in barred systems. Similar conclusions were reached by Devereux (1987), from small–aperture 10-μm photometry of galactic nuclei.

To confirm that this result is not an artefact introduced due to sample selection, several of the galaxian observable properties were examined as in Section 2.2. Once again, no significant differences in the axial ratio or distance (corrected for Virgo cluster membership) distributions between (i) barred galaxies with $S_{25}/S_{12} \geq 2.22$ (chosen to exclude all but three of the unbarred systems, and hereafter referred to as 'h' spirals), (ii) barred galaxies with $S_{25}/S_{12} < 2.22$ (hereafter 'l' galaxies), and (iii) lSA galaxies, could be identified using the K–S statistic. The dependence of *IRAS* emission on Hubble

type amongst the sample galaxies is examined in Chapter 3.

To support the assertion that galaxies exhibiting 25-μm excesses have greatly enhanced rates of star formation, a simple model was constructed using the average observed *IRAS* fluxes of a group of 10 luminous ($\overline{L_{IR}} \simeq 3 \times 10^4$ L$_\odot$) unresolved HII regions in a field in Cygnus. The average mid–far infrared energy distribution for these HII regions is shown in Fig. 2.8 along with typical *IRAS* spectra for three subsets from the galaxy sample. The subsets are : (i) strongly barred spirals with 25-μm excesses (*i.e.* hSB galaxies; upper solid line), (ii) other strongly barred spirals (lSB; middle solid line), and (iii) unbarred systems (lSA; lower solid line). The points represent the mean emission in each *IRAS* waveband, in units of W Hz^{-1}, and all have 1σ uncertainties of about 0.5 dex. The latter reflects the scatter in the observed *IRAS* flux density ratios (Fig. 2.7). Nevertheless, it is noticeable that the average hSB galaxy is systematically more luminous in each band than the average lSB galaxy (and, of course, has a different spectral shape), which in turn is more luminous than the typical unbarred spiral. The mean luminosities for these three samples are $\overline{L_{IR}}/10^{10} = 4.14$, 2.61 and 1.71 L$_\odot$ respectively. The luminosity of each galaxy was calculated from :

$$\left(\frac{L_{IR}}{\mathrm{L}_\odot}\right) = \left[15.7\left(\frac{S_{12}}{Jy}\right) + 20\left(\frac{S_{25}}{Jy}\right) + 9\left(\frac{S_{60}}{Jy}\right) + 4.7\left(\frac{S_{100}}{Jy}\right)\right] \times 1.53 \times 10^5 \times \left(\frac{D_{75}}{Mpc}\right)^2 \qquad (2.2)$$

where D_{75} is the distance of the galaxy in Mpc (adopting a Hubble constant of 75 km s^{-1} Mpc^{-1}) and which incorporates a factor taking into account the emission longward of 100 μm (the 1 mm flux density is assumed, for computational convenience, to be the same as that at 12 μm).

The luminosity and spectral shape of the mean hSB galaxy may be approximately reproduced by the addition of about 5×10^5 luminous HII regions, such as those found in Cygnus, to the mean lSB galaxy. The agreement between the spectral shapes of the model and typical hSB galaxies is only approximate since this simple scheme omits the extended emission seen in *IRAS* SKYFLUX images across the whole Cygnus complex.

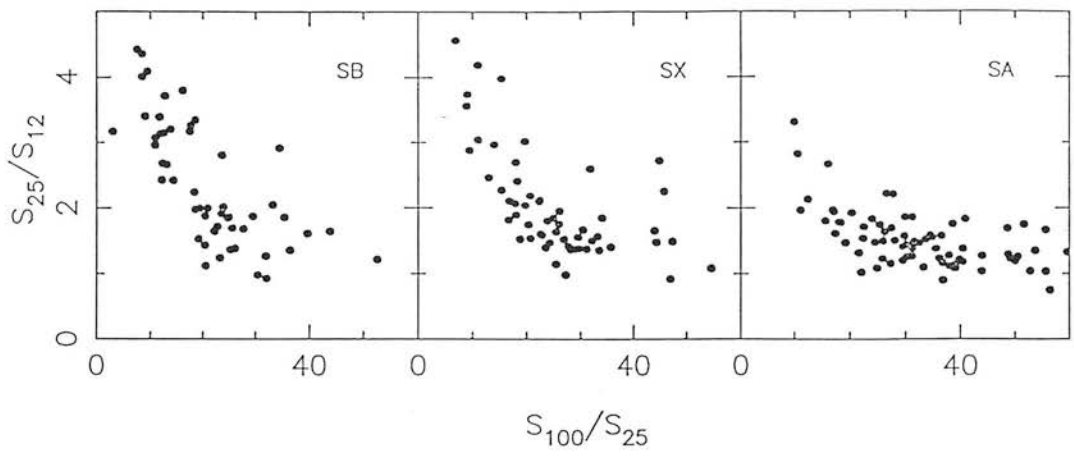

Figure 2.7: 2–colour diagram showing the ratios of *IRAS* flux densities S_{25}/S_{12} *vs* S_{100}/S_{25} for barred (SB), mixed–type (SX), and unbarred (SA) spiral galaxies.

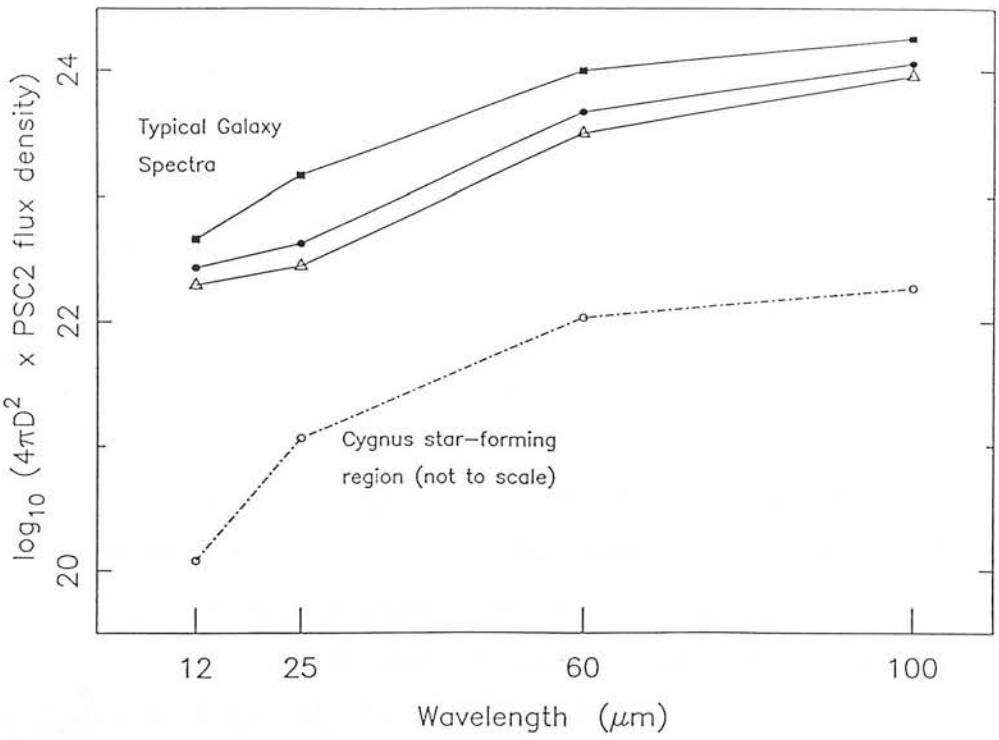

Figure 2.8: Typical *IRAS* galaxy spectra (solid lines; upper : hSB, middle : lSB, lower : lSA, where the 'h' prefix refers to galaxies having a flux density ratio $S_{25}/S_{12} \geq 2.22$, and the converse for those with an 'l' prefix), and the average *IRAS* spectra for luminous HII regions in the Cygnus star–forming complex.

2.4 The Effect of the Bar

In a barred spiral galaxy, the stellar bar produces a perturbation superposed on the general axisymmetric potential which varies as $\cos 2\theta$ (the same is true for a tidally interacting pair of galaxies). To examine the effect that this potential has on the motion of gas in the disk, consider a bar pattern which rotates at an angular frequency Ω_p. There exists a radius at which Ω_p equals the angular velocity of disk material ($\Omega_p = \Omega(r)$). This is called the co–rotation resonance. Gas interior to co–rotation moves faster than the bar pattern and the torque applied by the potential causes this gas to lose angular momentum and flow inwards. (The converse happens exterior to co–rotation).

If the angular velocity of the bar pattern is sufficiently slow and the run of mass with radius is appropriate, then several other resonances, in addition to that occurring at co–rotation, may exist (see Fig. 2.9, from Combes 1988). The most important of these are the inner and outer Lindblad resonances (ILR, OLR) which occur when $\Omega_p = \Omega - \kappa/2$ and $\Omega_p = \Omega + \kappa/2$, respectively, where κ is the natural frequency of oscillation of a particle in its orbit. Material at a Lindblad resonance follows a closed periodic orbit in the reference frame of the rotating perturbation and consequently the inwardly (outwardly) swept gas accumulates at the inner (outer) Lindblad resonance. If there is no ILR, then gas inflow from co–rotation will reach the nucleus.

The accumulation of gas, either at a resonance or in the nucleus, enables the clouds of molecular gas to collide, coalesce, and ultimately collapse, to form stars. Combes & Gerin (1985) and Schwarz (1984) have simulated the motion of these clouds in a bar potential. These simulations are more realistic than earlier models which treated the gas as a continuous fluid (*e.g.* Roberts 1969). Fig. 2.10 shows the results for one of the simulations run by Combes & Gerin. In Fig. 2.10a, the circles represent the location of molecular clouds after 10 rotations of the bar. The roughly circular gas annulus at the ILR can be seen clearly. Fig. 2.10b presents this information in another way; the contours show the energy dissipated in cloud–cloud collisions.

The numerical simulations compare favourably with the distribution of molecular gas shown in a CO map of the barred spiral galaxy NGC 1097 (Fig. 11a; Gerin, Nakai

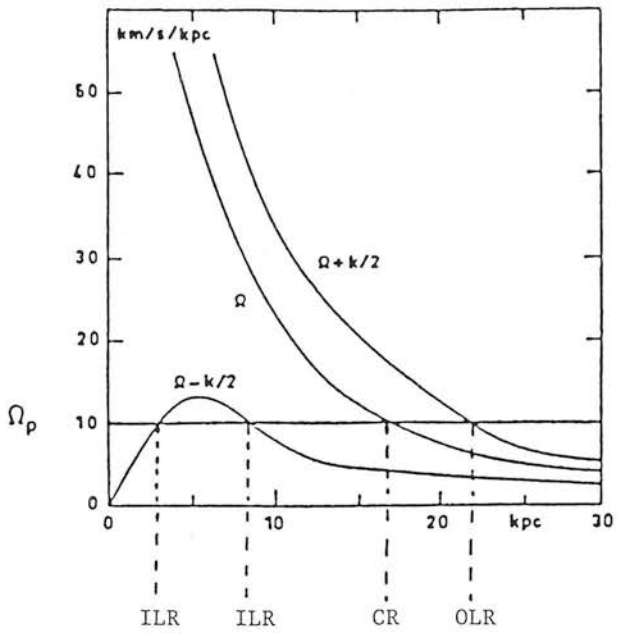

Figure 2.9: Radial dependences of the functions $\Omega - \kappa/2$, Ω, and $\Omega + \kappa/2$ for a model galaxy. Their intersection with the horizontal line, representing the angular velocity of the bar pattern (Ω_p), defines the inner Lindblad, co–rotation and outer Lindblad resonances, respectively.

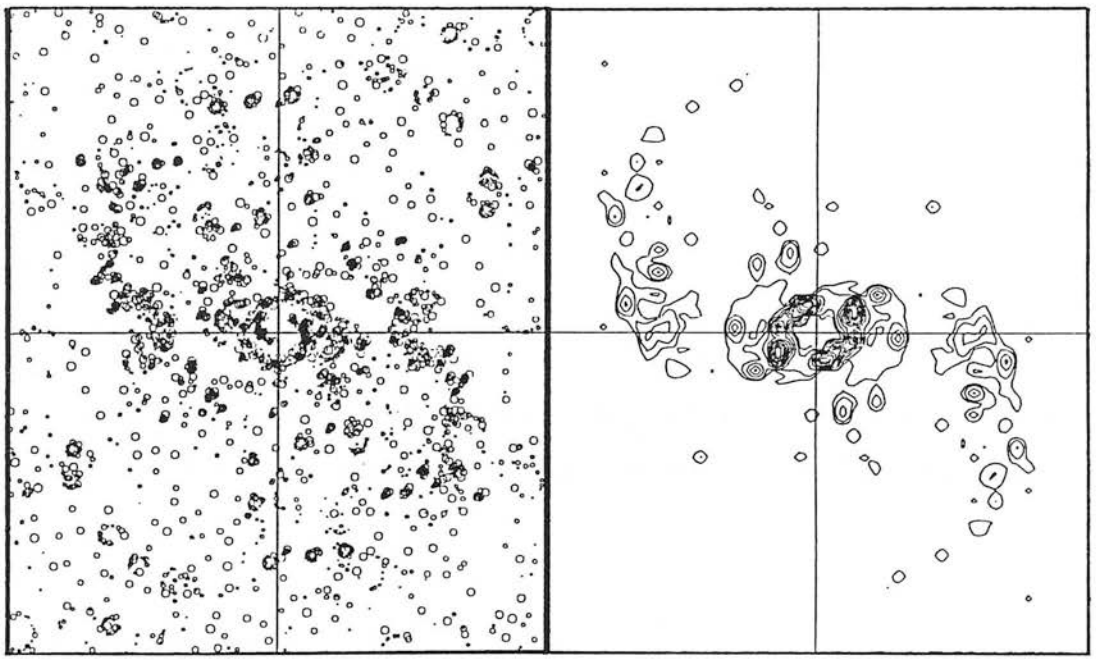

Figure 2.10: From numerical simulations of the motion of gas clouds in a bar potential (Combes & Gerin 1985), (a) the distribution of clouds after 10 rotations of the bar pattern (note the accumulation of material at the inner Lindblad resonance), and (b) contours of the energy dissipated in inelastic cloud–cloud collisions.

& Combes 1988). The contours of CO intensity are superimposed on an image of the central regions of this system taken in blue light which shows the ring of young stars formed from this material. This ring can be seen more clearly in Fig. 11b where contours of radio continuum emission (believe to trace recent supernova remnants) are presented (Hummel, van der Hulst & Keel 1987).

2.5 Conclusions

A sample of 194 nearby, infrared–bright, infrared–luminous spiral galaxies has been constructed. All were detected in the four *IRAS* wavebands (12, 25, 60 and 100 μm) and they have typical infrared luminosities in the range $(2-4)\times 10^{10}$ $L_{\odot}$. Investigation of the selection procedure shows that they are an IR–luminous subset of spiral galaxies detected by *IRAS*, their other properties (*i.e.* distance, blue magnitude, axial ratio and morphological type) being comparable.

Analysis of the *IRAS* properties of this sample reveals that the presence of a stellar bar is a necessary condition for the existence of enhanced 25-μm emission. This emission is interpreted as evidence for vigorous star formation activity, known AGNs having been excluded. Simple modelling of the active systems suggests that their extra luminosity and spectral shape can be reproduced by the addition of about 5×10^5 luminous embedded HII regions (each with $L_{IR} \sim 3 \times 10^4$ $L_{\odot}$) to a 'normal' galaxy.

The stellar bar is believed to play a fundamental role in the occurrence of vigorous star formation. Numerical simulations show that gas clouds are swept inwards towards the nucleus by the bar potential where they may accumulate and later form stars.

Acknowledgements

Thanks are due to Jon Fairclough and the IPMAF team at RAL for providing *IRAS* software, Eric Becklin and Nick Devereux for stimulating discussions, and to Bob Joseph for advice and contributions to the early stages of this work.

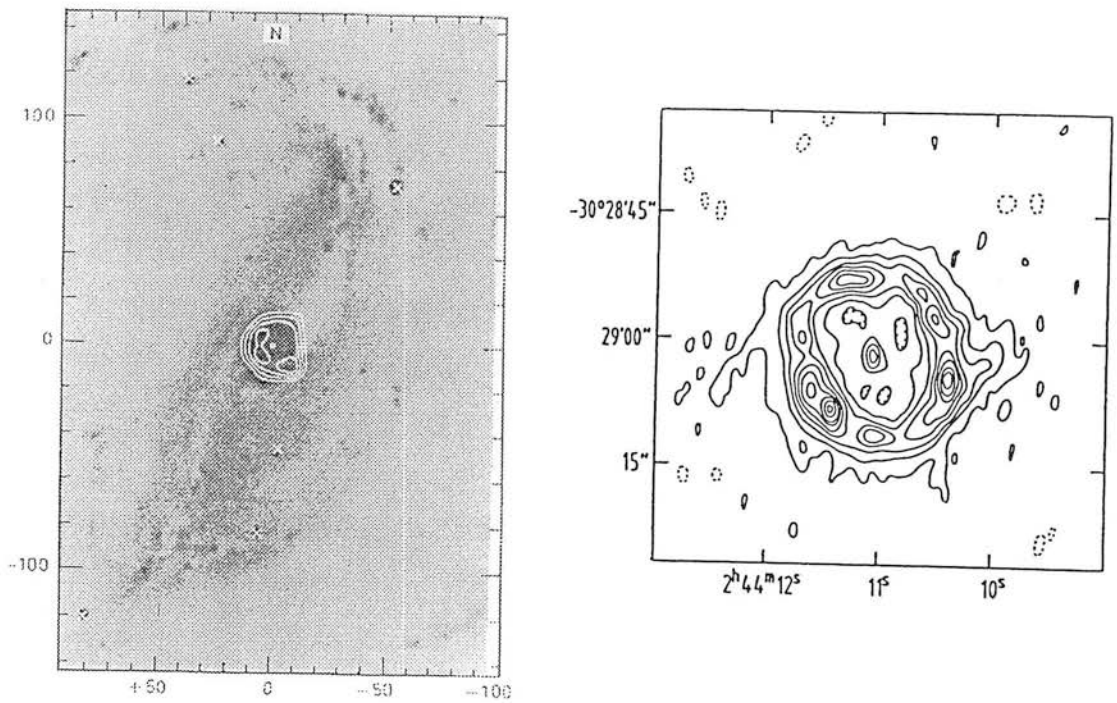

Figure 2.11: The barred spiral galaxy NGC 1097 : (a) contours of molecular gas (^{12}CO) superimposed on the blue light distribution (Gerin *et al.* 1988), and (b) contours of the radio continuum emission (Hummel *et al.* 1987).

References

Adams, F.C. & Shu, F.H., 1985. *Ap. J.*, **296**, 655.

Catalogued Galaxies and Quasars Observed in the IRAS Survey, 1985. Prepared by Lonsdale, C.J., Helou, G., Good, J.C. & Rice, W., Jet Propulsion Laboratory.

Combes, F., 1988. In *Galactic and Extragalactic Star Formation*, p.475, eds. Pudritz, R.E. & Fich, M., Kluwer Acad. Publ., Dordrecht.

Combes, F. & Gerin, M., 1985. *Astr. Astrophys.*, **150**, 327.

de Jong, T. *et al.* 1984. *Ap. J.*, **278**, L67.

de Vaucouleurs, G., de Vaucouleurs, A. & Corwin, H.C., 1976. *Second Reference Catalogue of Bright Galaxies*, University of Texas Press, Austin. 'RC2'

Devereux, N., 1987. *Ap. J.*, **323**, 91.

Dressel, L.L. & Condon, J.J., 1976. *Ap. J. Suppl. Ser.*, **31**, 187.

Fairclough, J.H., 1985. In : *Rutherford Appleton Laboratory Workshop on Extragalactic Infrared Astronomy*, p32, ed. Gondhalekar, P.M.

Gerin, M., Nakai, N. & Combes, F., 1988. *Astr. Astrophys.*, **203**, 44.

Helou, G., 1986. *Ap. J.*, **311**, L33.

Hummel, E., van der Hulst, J.M. & Keel, W.C., 1987. *Astr. Astrophys.*, **172**, 32.

IRAS Explanatory Supplement, 1985. Eds. Beichman, C.A., Neugebauer, G., Habing, H.J., Clegg, P.E. & Chester, T.J., US Government Printing Office, Washington DC.

Pence, W.D. & Blackman, C.P., 1984. *Mon. Not. R. astr. Soc.*, **210**, 547.

Roberts, W.W., 1969. *Ap. J.*, **158**, 123.

Sancisi, R., Allen, R.J. & Sullivan, W.T., 1979. *Astr. Astrophys.*, **78**, 217.

Sandage, A. & Tammann, G.A., 1981. *A Revised Shapley–Ames Catalog of Bright Galaxies*, Carnegie Institution of Washington Publication No. 635. 'RSA'

Schwarz, M.P., 1984. *Mon. Not. R. astr. Soc.*, **209**, 93.

Siegel, S., 1956. *Non–parametric Statistics for the Behavioral Sciences*, McGraw–Hill.

Telesco, C.M. & Gatley, I., 1981. *Ap. J.*, **247**, L11.

Telesco, C.M. & Gatley, I., 1984. *Ap. J.*, **284**, 557.

Thronson, H.A. & Harper, D.A., 1979. *Ap. J.*, **230**, 133.

Véron–Cetty, M.-P. & Véron, P., 1985. *ESO Scientific Report*, No. 4.

Walterbos, R.A.M. & Schwering, P.B.W., 1987. *Astr. Astrophys.*, **180**, 27.

Chapter 3

Enhanced Star Formation in Barred Spiral Galaxies : Radio Continuum Emission

Preface : Following the discovery of enhanced 25-μm emission by barred spiral galaxies, described in the previous chapter, the source of this radiation was investigated utilizing the higher spatial resolution available with radio interferometry; location of the emitting region being an important test of the bar–driven inflow hypothesis. This work was performed in collaboration with Tim Hawarden and Matt Mountain and has been published : Puxley, Hawarden & Mountain, 1988. *Mon. Not. R. astr. Soc.*, **231**, 461.

Summary

The radio properties of an *IRAS*–selected sample of nearby spiral galaxies have been investigated using new and published 20-cm continuum observations. Virtually all of the galaxies with steep 12–25 μm spectra are barred and possess a central radio source of linear extent less than 1–3 kpc. It is argued that the activity in these systems is due to enhanced star formation rather than a compact nucleus. The central sources contribute, on average, 35% to the total radio emission and their typical far-infrared luminosity is estimated to be a few $\times 10^9$ $L_\odot$. In contrast to the other *IRAS* wavebands, the 25 μm– radio correlation shows a marked dependence on the level of star–formation activity.

3.1 Introduction

During the last fifteen years there have been a number of surveys investigating the dependence of radio continuum emission on morphological type for optical– or radio–selected samples of bright spiral galaxies. Low resolution observations generally measure only the total flux and show no clear dependence of the radio emission on Hubble type or the existence of a bar (Cameron 1971; Dressel & Condon 1978; Dressel 1979). Surveys made with an angular resolution of better than about 20 arcsec are able to separate the central (< few kpc) and disk components in these nearby spirals (Condon & Dressel 1978; Hummel 1980, henceforth 'H80'; Hummel 1981, henceforth 'H81'). Several trends are apparent in the radio properties. The emission from the disk is indistinguishable for the de Vaucouleurs (1959) morphological families SA, SB and SX. This is consistent with the low resolution results since the disk contributes, on average, 90% to the total 1415 MHz flux. However, the central component is typically twice as powerful in those systems possessing a bar (H81). There is also a strong correlation with Hubble type; the contribution of the central component to the total flux is significantly greater in early type spirals.

Observations at even higher resolutions, typically 0.2 to 2 arcsec, probe the structure of the central regions and can suggest mechanisms for energy production in these sources (Condon 1980; van der Hulst, Crane & Keel 1981; Condon *et al.* 1982; Hummel, van der Hulst & Dickey 1984). Although the number of galaxies so far observed at high resolution is small, several interesting relations are emerging. Galaxies of type Sab or earlier generally have compact core sources with flat or inverted radio spectra and high brightness temperatures, whilst galaxies of type Sb and later preferentially have complex sources and steep, non–thermal spectra. These observations have been cited as evidence for the existence of two different energy sources in the central regions (*e.g.* Condon & Dressel 1978; Biermann 1980; Ulvestad 1982). Emission from an active nucleus may be responsible for the compact core sources, whereas numerous supernovae and HII regions produced in a burst of vigorous star formation are the most likely power source in those systems with a complex extended radio morphology. Some galaxies show an intermediate class of central radio structure in which both mechanisms may be operating.

In many spiral galaxies much of the luminosity is thermal emission from dust at wavelengths between 10 and 1000 μm. Hence the all–sky survey provided by the Infrared Astronomical Satellite (*IRAS*) at 12, 25, 60 and 100 μm is a valuable database in which to examine the infrared properties of galaxies and their dependence on optical morphology. Of dominant importance appears to be the presence of an interacting companion galaxy or the existence of a stellar bar (*e.g.* Chapter 2; Joseph *et al.* 1984; see also the reviews by Wynn–Williams 1987 & Becklin 1987).

Galaxy–galaxy interactions and mergers have been identified as causing strong infrared emission in some systems both from ground-based 1–10 μm photometry (Joseph *et al.* 1984; Cutri & McAlary 1985; Joseph & Wright 1985) and from *IRAS* observations (*e.g.* Lonsdale, Persson & Matthews 1984). Indeed, some of these galaxies are amongst the most luminous known having $L_{IR} = 10^{11} - 10^{13}$ $L_\odot$ ($H_0 = 75$ km s^{-1} Mpc^{-1}); in contrast, the infrared luminosity of nearby spirals varies between 10^9 and 10^{11} $L_\odot$ (de Jong *et al.* 1984; Fairclough 1985).

In Chapter 2, Shapley Ames galaxies (Sandage & Tammann 1981, 'RSA') in the *IRAS* Point Source Catalogue (1985) were analysed and it was found that most of the luminous non–Seyfert non–interacting spirals were barred (see also Devereux 1987). It was concluded that their extra luminosity and 'warm' 25 – 100 μm *IRAS* colours may be fitted by a burst of vigorous star formation, although a heavily obscured active nuclear source is not excluded in all cases; indeed it is possible that active nuclei and vigorous star formation coexist in a number of systems. For both interacting and barred galaxies it has been suggested that the non–axisymmetric perturbation in the gravitational potential induced by the companion or the bar causes an inflow of interstellar material towards the centre (*e.g.* Combes & Gerin 1985) capable both of feeding a compact nuclear source and of increasing the rate of star formation.

As a first step in testing this hypothesis for the barred spirals, it is necessary to identify the location of the source producing the excess infrared emission, since the resolution available with *IRAS* (typically 1–2 arcmin) is too poor to allow discrimination between central and disk infrared sources. Observation of continuum radio emission from the HII regions and supernova remnants associated with the starburst or compact nucleus is the simplest way of determining the source location.

In this chapter, the dependence of radio continuum emission on morphological type is investigated for an infrared selected sample of nearby galaxies, with particular emphasis on the barred systems. The sample is defined in Section 3.2 and new 20 cm continuum observations are presented. These are analysed together with data taken from H80 in Sections 3.3 and 3.4.

3.2 Sample, Observations and Results

The infrared selected sample comprises the 194 Shapley Ames spiral galaxies (Sandage & Tammann 1981) with morphological types in the Second Reference Catalogue of Bright Galaxies (de Vaucouleurs, de Vaucouleurs & Corwin 1976, 'RC2') between SO/a and Scd which were detected by *IRAS* in all four bands. The non–uniform *IRAS* limiting fluxes, particularly those at 12 and 25 microns, means that this sample is not flux limited. Approximate limiting flux densities are 0.5 Jy at 12, 25 and 60 μm, and 1.5 Jy at 100 μm (*IRAS Explanatory Supplement*, 1985). Seyfert and LINER galaxies in the catalogue by Véron-Cetty & Véron (1985) were excluded from the sample.

As in Chapter 2, galaxies with ratios of the *IRAS* 25-μm/12-μm point source flux density $S_{25}/S_{12} \geq 2.22$ are denoted by the prefix 'h' and it is these which are believed to contain regions of enhanced star formation. Galaxies with $S_{25}/S_{12} < 2.22$ are denoted by the prefix 'l'. The use of point source flux densities biases towards the central galaxy regions, however there is no evidence of any distance–related selection effects in this sample. For example, the 25-μm/12-μm colour temperature shows no correlation with distance as might be expected due to an increasing contribution from the 'cooler' disc for more distant objects. The lack of any such dependence is due to the major contribution of the central regions to the total infrared emission at these wavelengths.

H80 observed 280 optically bright spirals with the Westerbork Synthesis Radio Telescope (WSRT) at a resolution of about 20 arcsec. Of these, 97 are in common with the *IRAS* sample as are 8 of the Sbc spirals observed at 1465 MHz with the VLA by Hummel *et al.* (1985); these latter observations have resolution about 14 arcsec. No corrections have been applied to convert between 1465 MHz and 1415 MHz flux densities as such corrections would be smaller than the quoted errors. Both sets of

observations have sufficient resolution to be able to separate disk and central emission.

To increase the overlap between the radio and *IRAS* samples, observations were made during February 1986, using the WSRT at 1400 MHz, of a further 22 galaxies. Integration times were typically 10 minutes per object and the observations were performed, wherever possible, at an hour angle which maximised the ratio of projected optical major axis to resolution. The east–west linear array of telescopes resulted in a fan–shaped synthesized beam; to minimise confusion between sources close together in declination, most galaxies were therefore observed twice with an hour angle separation of about 2 hr. The two observations were combined and 'CLEANed' maps were produced in the usual way (Högbom 1974; Clark 1980). Calibration was performed by regular observation of 3C286, 3C147 and 3C48 which are unresolved at the longest baseline. These sources were assumed to have 20 cm flux densities of 14.30, 21.57 and 15.67 Jy respectively (Strom, van Someren Greve & Miley 1980).

Following Hummel (1980), the galaxies have been subdivided into four categories according to their radio morphology :

- C : small diameter ($\leq$ 20 arcsec) central source, unresolved in these observations, which is conspicuous above any extended emission;
- E : extended disk emission;
- CE : both disk and central components;
- ND : non–detections.

An uncertain classification is indicated with a question mark. To facilitate classification, slices through the galaxies were taken at a position angle corresponding to maximum resolution. Due to the fan–shaped beam this was commonly close to 90 degrees. Typical examples for each of the four categories (C, E, CE and ND) are illustrated in Fig. 3.1. Two methods were used to determine the 20 cm flux density: (i) the total flux density (S_{tot}) was calculated by summing over a box drawn around each source on the map; (ii) where appropriate, the flux density of the central component (S_{cen}) was determined by fitting the Gaussian 'CLEAN' beam to the map peak. To confirm it as unresolved, the value obtained in (ii) was compared with the peak flux estimated directly from the map. For many of the galaxies, lower resolution maps were also made by editing

out the data pertaining to the longest baselines. Total flux densities were estimated as above. Comparison between the low and high resolution results reveals no significant differences within the estimated error of 15%. However, it should be noted that our estimates of the total flux density may be less than values derived from single dish observations due to the low sensitivity to extended structure arising from missing short spacings.

Results for the 22 galaxies observed are given in Table 3.1. The columns are:

1. galaxy name (NGC number)
2. distance in Mpc, derived from the RC2 or RSA radial velocity (H_0 =75 km s^{-1} Mpc^{-1}).
3. flux density of central component (S_{cen}) in mJy
4. total flux density (S_{tot}) in mJy
5. radio morphology classification
6. IRAS (h,l) and RC2 morphological family classification (SA:unbarred, SB:barred).

Notes concerning individual galaxies are indicated in column (7) and given below :

NGC 1309 There is 7 mJy source 3 arcmin N of the field centre.

NGC 1832 Hummel *et al.* (1985) find S_{tot} = 58 mJy and S_{cen} = 2 mJy from VLA observations at 1465 MHz.

NGC 2280 The source consists of two components separated by about 2 arcmin. The source located at the field centre has S_{tot} = 18 mJy.

NGC 2748 Hummel *et al.* (1985) find S_{tot} = 55 mJy and $S_{cen} < 5$ mJy.

NGC 2967 A second source in the field has S_{tot} = 33 mJy, but the separation is very uncertain due to the low declination. It is not included in the flux quoted in Table 3.1.

NGC 3147 Hummel (1980) finds S_{tot} = 124 mJy using the WSRT and S_{cen} = 20 mJy from VLA observations (Hummel *et al.* 1985).

NGC 4419 A second source 2 arcmin NW of the galaxy is not included in the quoted flux density. If included, the total flux density becomes S_{tot} = 55 mJy.

Table 3.1: New observations at 20 cm of 22 *IRAS*–selected bright spiral galaxies.

NGC name	Distance (Mpc)	S_{cen} (mJy)	S_{tot} (mJy)	Radio class.	*IRAS*/RC2 class.	Notes
922	40.0	–	< 5 mJy/beam	ND	lSB	
1022	20.0	33	33	C	hSB	
1241	53.5	–	< 3 mJy/beam	ND	lSB	
1309	27.6	–	< 6 mJy/beam	ND	lSA	*
1832	23.7	<5	45	E	lSB	*
2280	22.1	<5	34	E	lSA	*
2748	22.1	–	< 3 mJy/beam	ND	lSA	*
2967	27.3	<7	39	E	lSA	*
2985	19.1	–	< 3 mJy/beam	ND	lSA	
3044	15.9	11	30	CE	hSB	
3147	38.4	12	130	CE	lSA	*
3177	16.1	20	34	CE	lSA	
3367	38.8	22	61	CE	hSB	
3611	19.6	13	30	CE	lSA	
3655	18.6	<8	55	E	lSA	
3885	20.9	32	64	CE?	hSA	
4419	13.7	33	33	C?	hSB	*
4900	11.7	–	< 7 mJy/beam	ND	lSB	
5775	21.1	–	< 6 mJy/beam	ND	lSB	
5792	26.3	15	30	CE	lSB	
5915	29.7	20	55	CE?	hSB	
5936	54.3	46	145	CE	hSB	*

NGC 5936 A second source 0.5 arcmin from the field centre is included in the total flux density. Otherwise, $S_{tot} = 46$ mJy and the radio classification becomes C.

For the non–detections, 3σ upper limits are quoted. There are three galaxies in common between these observations and those of H80 and Hummel *et al.* (1985). Estimates of the flux densities are consistent within the quoted errors.

3.3 Analysis of Sample — radio structure

By combining the observations with published results referred to above, a homogeneous data set for 124 of the 194 galaxies in the *IRAS* selected sample was constructed. To investigate the dependence of radio continuum morphology on optical morphology (specifically the presence of a bar), the incidence of central sources (classified either C or CE), extended sources and non–detections for the sub–classes (i) all h systems, (ii) lSB and l mixed–type (lSX) spirals, and (iii) lSA galaxies, are tabulated in Table 3.2. The relative fractions of galaxies in these sub–classes are shown in Fig. 3.2. There are several interesting results.

Virtually all of the h galaxies, those believed to possess enhanced star formation, contain central radio continuum sources. Less than one half of the l barred galaxies and only a quarter of the unbarred systems exhibit this feature. This effect is much clearer than that recently reported by Kalloglyan & Kandalyan (1986). If the interpretation of the *IRAS* data is correct, then this result strongly suggests that the enhanced star formation is contained within a region of angular diameter 15–20 arcsec located at the galactic nucleus. This corresponds to a region of linear extent between 1 and 3 kpc for typical distances to our galaxies of 10–30 Mpc. The three h galaxies which are not classified as possessing central sources are NGC 3310, NGC 4088 and NGC 4369. NGC 3310 possesses a central star-forming complex which is known from 10 μm mapping (Telesco & Gatley 1984) to be 25 arcsec across; subsequent VLA observations show that the radio emission is coextensive and therefore resolved in the Westerbork measurements. VLA images of NGC 4088 (Hummel et al 1985) show a knotted radio structure over about 90 arcsec which is therefore also resolved. The unbarred spiral NGC 4369 has only a moderate quality 12 μm flux density and is perhaps misclassified

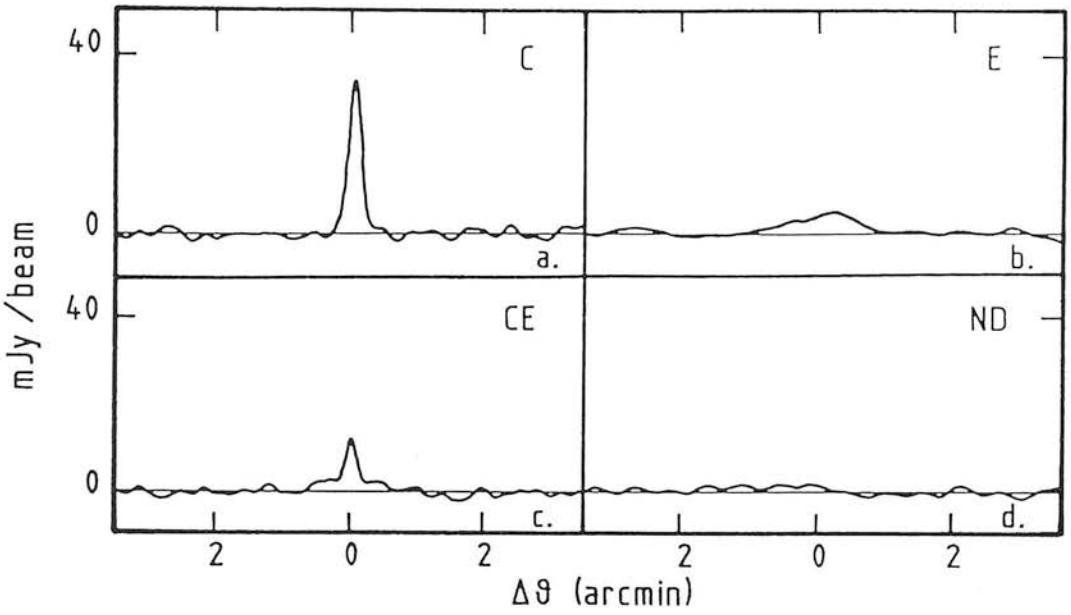

Figure 3.1: Examples of one–dimensional slices through galaxies illustrating the radio morphology classification scheme : (a) C: NGC 4419, (b) E: NGC 1832, (c) CE: NGC 3147 and (d) ND: NGC 1241.

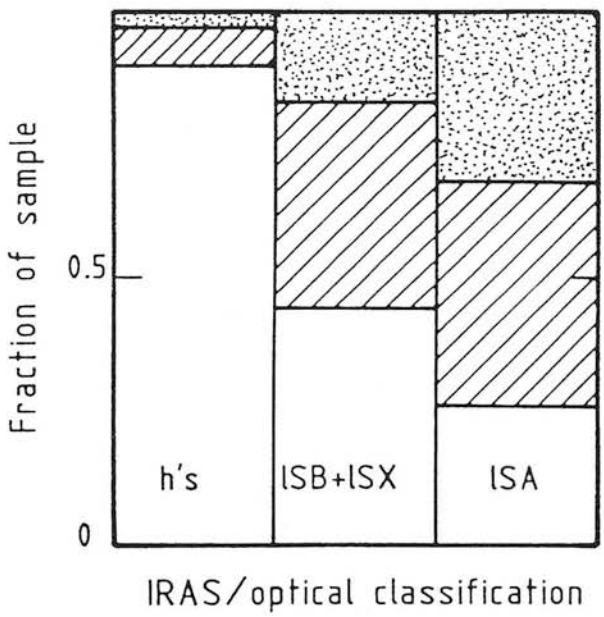

Figure 3.2: The relative fractions of central radio sources (blank), extended source (hatched), and non–detections (stippled) for three sub–samples of spirals: all h galaxies (h's), l barred and mixed–type galaxies (lSB+lSX), and unbarred l galaxies (lSA).

Table 3.2: Incidence of central and extended radio sources and non–detections as a function of *IRAS*/RC2 galaxy type. Percentages of observed number of galaxies are given in parentheses.

IRAS/RC2 type	Number observed	Radio Morphological Classification		
		C or CE	E	ND
h	30	27 (90%)	2 (7%)	1 (3%)
lSB+lSX	41	18 (44%)	16 (39%)	7 (17%)
lSA	53	14 (26%)	22 (42%)	17 (32%)

as an h system.

3.3.1 The 'l' Galaxies

In view of the excellent agreement between the *IRAS* h classification and the presence of a central radio source, there appears to be a surprisingly large number of spirals which possess central radio components but which are of *IRAS* type l. These sources are puzzling since all known Seyferts were excluded from the sample and because the l galaxies are not believed currently to have a high star formation rate.

A number of scenarios may explain the presence of these central sources:

(i) A density–wave driven inflow of material may generate a density enhancement of the interstellar medium in the central region accompanied by compression of the frozen–in magnetic field. This may suffice to produce a detectable radio source even if the density enhancement is too low to initiate vigorous star formation. Similar suggestions have been made by H81 to explain the strong central sources in early type and barred galaxies, and by van der Kruit & Allen (1976) to explain the spiral arms of M51. To investigate the feasibility of this model, the flux densities of the central sources and the extent of the disk emission given by H80 were used to calculate the ratio of central–to–disk flux density per beam, and thereby estimate the relative enhancement of the radio emission in the central regions. There exists a range of values for this ratio of between 4 and 200 for l galaxies possessing extended sources and lower limits of between 100 and 200 for those systems without detectable disk emission. Since the synchrotron radio emissivity is proportional to $nB^{1-\alpha}$, where n is the relativistic electron number density and B is the magnetic field strength, then, for a gas density enhancement factor η and assuming that the magnetic field scales as the square root of the gas density (Mouschovias, Shu & Woodward 1974), the emissivity of the compressed region will be $\eta^{(3-\alpha)/2}\, nB^{1-\alpha}$. The further assumptions of a typical synchrotron spectral index of α=–0.75 and that similar volumes of material are observed, gives the expected enhancement of the radio emission, which varies as $\eta^{1.88}$. Using the observed ratios of central–to–disk radio emission given above, this implies values for the density enhancement factor of $\eta \simeq 2 - 20$. These are consistent with empirical estimates made by Struck-Marcell &

Scalo (1987) for the critical value of the density enhancement factor ($\eta_{cr} \sim 3 - 100$) below which, they suggest, vigorous star formation does not occur. Compression, alone, cannot account for the enhanced emission in the h systems since this mechanism is unlikely to heat the dust and thereby create the steep 12–25 micron spectra exhibited by these galaxies.

There is no detectable systematic deviation in the 20 cm – far-infrared relation for l galaxies containing central radio sources. The contribution of the central source to the total radio emission in these systems, typically 10–30% (see Fig. 3.4), corresponds to an increase in the total radio power, relative to the galaxy before compression, of only about 25%. This is much smaller than the scatter in the radio – far-infrared relationship (see Fig. 3.7c).

(ii) The galaxies represent the very end of a burst of vigorous star formation. The virtual absence of stars more massive than about 5 $M_{\odot}$, which would otherwise heat the dust, is necessary to explain the low values of the 25-μm/12-μm flux density ratio in these galaxies. Synchrotron emission from relativistic electrons produced by the death of the last high mass stars could produce a detectable radio source.

In more detail: consider a subset of the *IRAS* selected sample of Shapley–Ames galaxies, described in Section 3.2, which have all been observed at 1400 MHz. A suitable example is the SB and SAB systems having $\delta > +30°$ and $B_0 < 13.0$ mag. In this essentially complete sub–sample (only one galaxy has not been observed at 20 cm), there are similar numbers of l galaxies with central radio sources and h galaxies exhibiting active star formation; being 20 and 35% respectively of the total number of spirals in the sub–sample. This suggests that the duration of these two phases must be approximately the same. The absence of stars with mass greater than 5 $M_{\odot}$ (lifetime $\sim 10^8$ yr) and other estimates for the lifetime of bursts of star formation ($\sim 10^7 - 10^8$ yr; *e.g.* Rieke *et al.* 1980; Telesco 1985) imply electron lifetimes against synchrotron losses also of about 10^8 yr. For GeV electrons this yields a reasonable upper limit on the magnetic field strength in the central regions of $\sim 10^{-9}$ T. Only a small fraction of the total energy available from supernovae is required to produce the observed mean 1.4 GHz radio power in these systems of about 2×10^{21} W Hz^{-1} (Helou, Soifer & Rowan–Robinson 1985). Nevertheless, this model has difficulty in accounting for the central

radio sources in unbarred spirals since few, if any, exhibit vigorous star formation.

(iii) The central source l galaxies contain active nuclei, possibly obscured by a thick dust shroud. It is noted that the typical 20 cm radio power of the central sources in the l galaxies ($\sim 2 \times 10^{21}$ W Hz^{-1}) is not greatly different from that seen in the very compact sources ($>$ few $\times 10^{21}$ W Hz^{-1}; van der Hulst, Crane & Keel 1981) which are thought to be powered by accretion onto massive objects. One possible candidate for an active nucleus amongst the l galaxies is NGC 3079 which shows lobes and bridges of radio emission in the VLA maps by Duric *et al.* (1983). However, note that all of the strongly barred Seyfert galaxies (de Vaucouleurs type SB) excluded from the *IRAS* sample in Chapter 2 would have been given an h classification; that is, they display a high 25-μm/12-μm ratio.

Since the strongly barred (SB) Seyfert galaxies are all classified as h, it is proposed that the central radio sources in the lSB spirals are produced by either a simple density enhancement or during the last phases of a burst of star formation. The apparent absence of vigorous star formation amongst the unbarred (SA) galaxies suggests that the latter model is inapplicable in this case and that the central sources are powered by either a density enhancement or an obscured active nucleus. The radio sources in l mixed–type (SX) galaxies may be explained by any of the three suggested models. High resolution (1 arcsec) radio continuum observations, which probe the nuclear radio morphology, may be able to distinguish between these various possibilities.

3.3.2 The 'h' Galaxies

It has been suggested (Devereux 1987) that the h barred galaxies are morphologically of earlier type than the l spirals. This would be consistent with the observed high incidence of central radio components in the h systems since it is known that early–type galaxies have stronger central radio emission than later types (Condon & Dressel 1978; H81). To investigate this suggestion, the distribution of optical morphological type (RC2 classification) for the three subclasses (all h systems, lSB + lSX galaxies, and lSA spirals) were examined. These distributions are shown in Fig. 3.3. Note that although the h galaxy sample contains a significantly higher proportion of early type

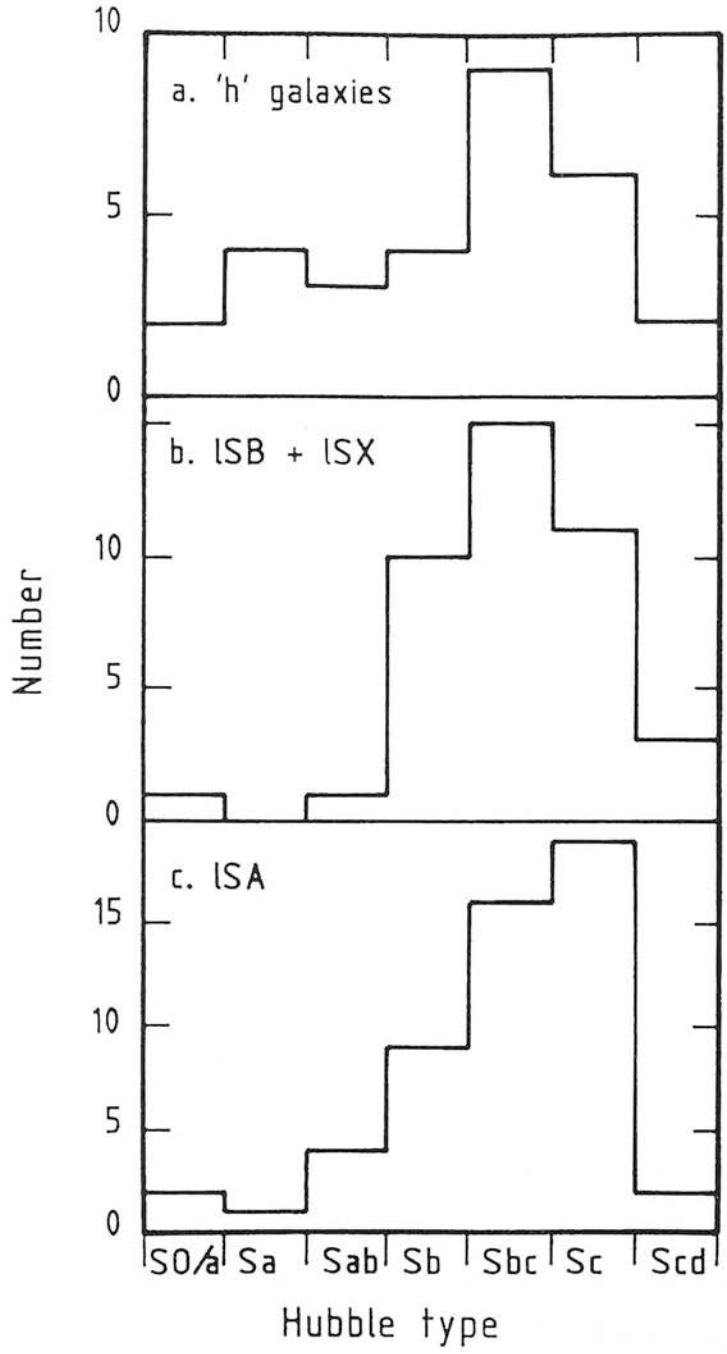

Figure 3.3: The distributions of Hubble types amongst (a) h galaxies, (b) lSB and lSX galaxies, and (c) lSA galaxies.

spirals (Sb and earlier), it is *not* dominated by them; they comprise only 13 out of 30 h systems. Therefore this suggestion cannot fully account for the higher occurrence of central radio sources in the h spirals.

The relative contribution of the central component to the total emission for the 99 detected galaxies has also been examined. In Fig. 3.4 the ratio of central–to–total 20 cm continuum flux densities for the same three subclasses is shown. Of course, since the data set is based on that of H80, the distributions for both lSA and lSB + lSX systems reproduce his result that only about one tenth of the total emission arises from the central component. However in the h galaxies, the central component supplies a much larger fraction of the total emission – typically 30–40%. As a consequence, there is a marked tendency for the total radio emission to increase with increasing central flux, as illustrated in Fig. 3.5.

One possibility not yet fully discussed is that both the radio continuum and *IRAS* emission are the result of a non–thermal active nucleus. Even though known Seyfert galaxies were excluded from the sample, an active nucleus which is deeply embedded in a dust cocoon could conceivably account for the observations thus far described since neither the data presented here, nor the *IRAS* observations, are useful for distinguishing between 'starburst' and Seyfert galaxies. High resolution ($\sim$ 1 arcsec) observations are more useful, since they can probe the central regions of these systems and investigate the near–nuclear radio morphology. Galaxies containing active nuclei are expected to have strong compact components, whilst spirals possessing regions of vigorous star formation are expected to contain extended complex components. About one half of the h systems have been observed at high resolution and frequently ($\sim$80%) show complex and/or extended central sources; for example NGC 2633 (Hummel, van der Hulst & Dicke 1984), NGC 3556 and NGC 4536 (van der Hulst, Crane & Keel 1981). A few ($\sim$20%) possess compact central components in addition to extended emission (*e.g.* NGC 2782 – van der Hulst, Crane & Keel 1981). Nevertheless, in general, the high resolution published continuum radio maps of the central components show structure consistent with, and indicative of , enhanced star formation.

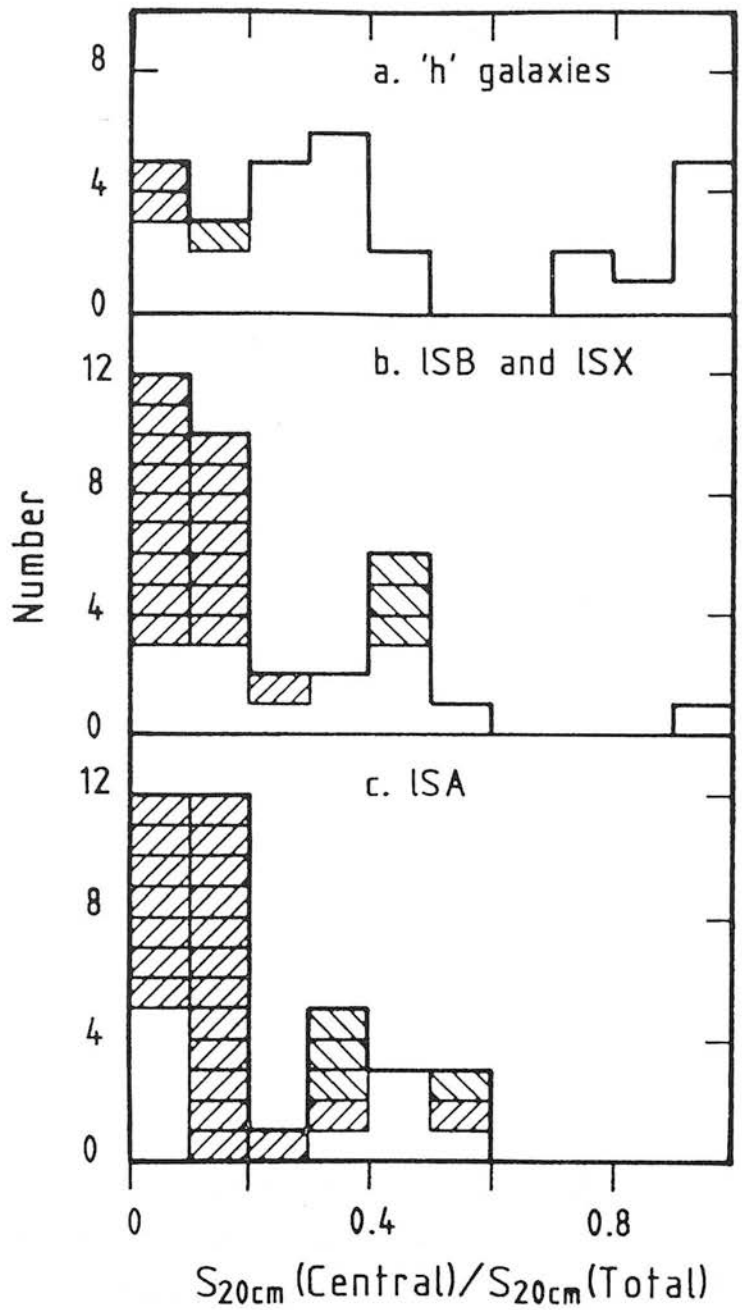

Figure 3.4: The ratio of central to total 20-cm continuum flux densities for (a) h galaxies, (b) lSB and lSX galaxies, and (c) lSA galaxies. Upper and lower limits are indicated by positively and negatively sloped hatching respectively.

3.4 Analysis of Sample — Correlations of Radio Emission with Mid- and Far-Infrared Fluxes

In this section, the ability of the radio observations to distinguish between compact 'nuclear' and extended 'disk' sources is employed to investigate the spatial origin of the mid- and far-infrared emission. This is one of the main objectives of this work, since the coarse resolution *IRAS* data generally contain little spatial information on any but the nearest galaxies.

In Fig. 3.6 a comparison between the *IRAS* point source 25-μm monochromatic power (defined as $4\pi(dist)^2\times$ *IRAS* point source flux density) and the central and total 20 cm radio powers for the h galaxies is presented. To maintain clarity, upper limits have not been included but they are consistent with the data shown. Best estimates of the typical 1σ errors are also illustrated. It is apparent that the point source 25-μm power (and to a lesser extent the 12- and 60-μm powers, not shown here) correlates better with the central radio power (Spearman rank correlation coefficient, $\rho = 0.894$) than with the total emission ($\rho = 0.779$). This result is consistent with the enhanced star formation (which dominates the 25-μm emission — see Chapter 2) being located within the central 15–20 arcsec.

The dependence of the *IRAS* point source 100-μm power on (a) central and (b) total radio power, again for the h galaxies, is illustrated in Fig. 3.7 and best estimates of the typical 1σ error bars are shown. The correlation coefficients are 0.839 and 0.838 respectively. The relationship between point source 100-μm power and total radio emission is also shown for the l galaxies and will be discussed later. Although a correlation between central and total radio emission for the h galaxies has been previously identified (Fig. 3.5), the comparable tightness of the 100-μm – radio relationships suggests that a significant fraction of the far-infrared flux must arise in the central active star formation region. The variable contribution of the central source to the total radio emission and the tightness of the 100 μm – total radio correlation (Fig. 3.7b) argue that the ratio of the far-infrared to radio flux is approximately constant over scales as small as 1 kpc. If, on average, the central source contributes about 35% to the total radio emission, then it must also contribute a similar fraction to the total far-

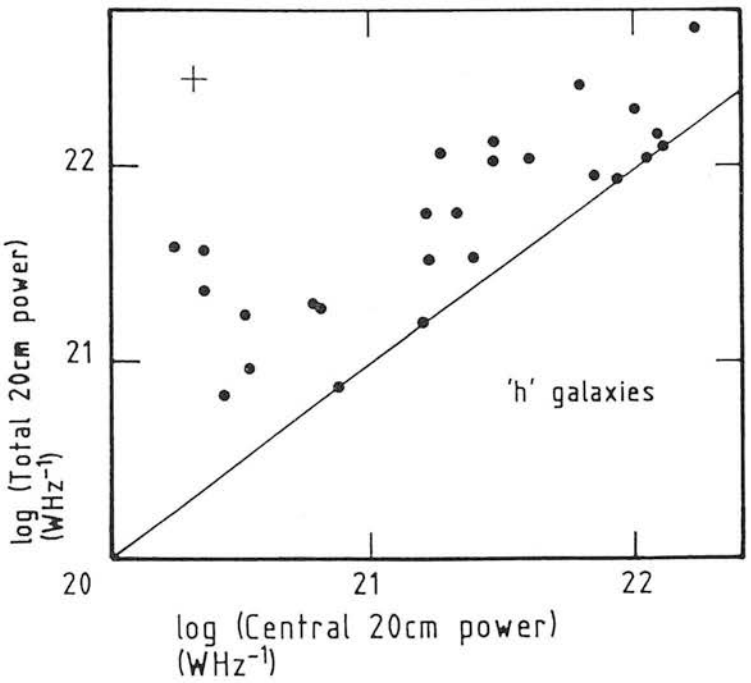

Figure 3.5: The total 20-cm radio power as a function of the power from the central source in h galaxies. The equality central=total power is indicated. Best estimates of the typical 1σ error are shown.

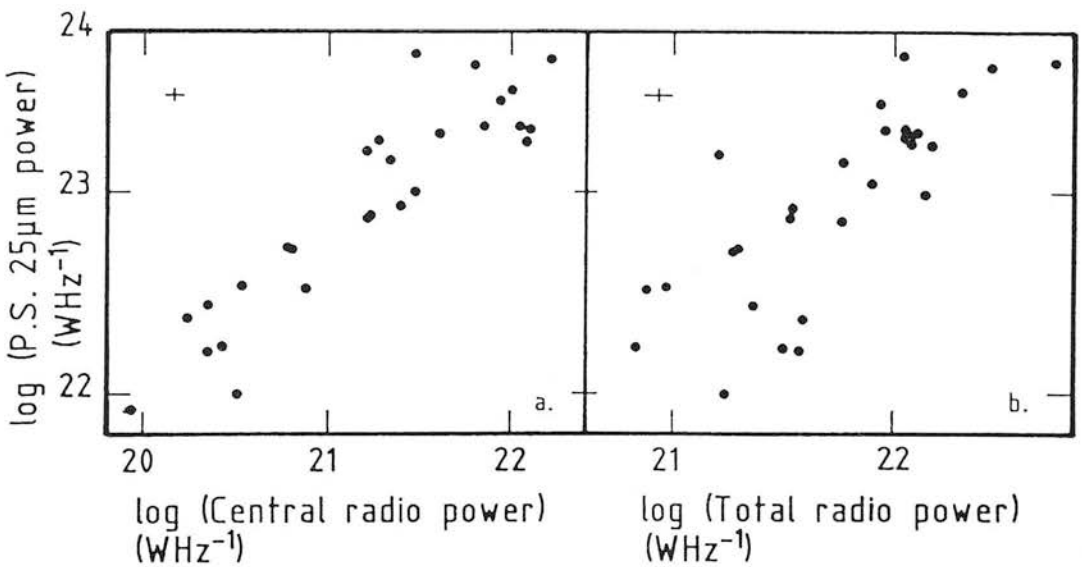

Figure 3.6: The dependences of (a) central and (b) total 20-cm continuum power on the *IRAS* point–source 25-μm monochromatic power for h galaxies. Best estimates of the typical 1σ error bars are shown.

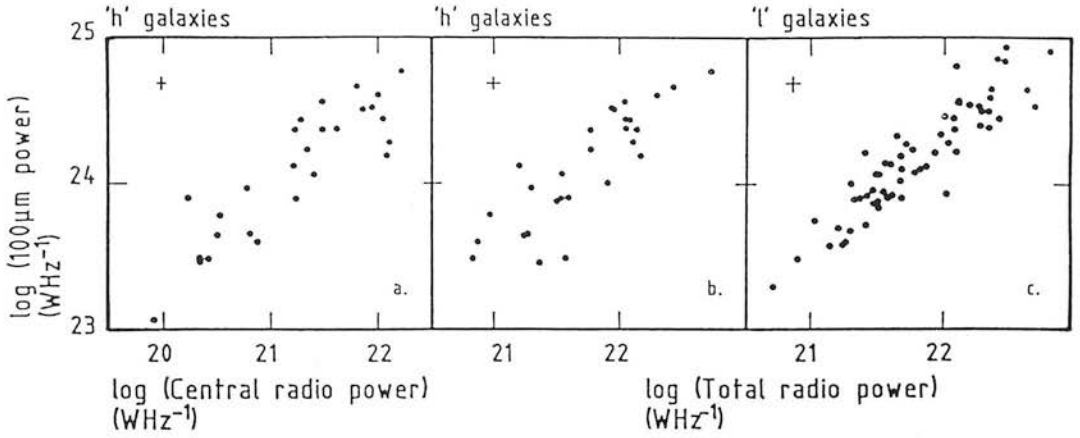

Figure 3.7: The variation of *IRAS* point–source 100-μm power with (a) central and (b) total radio power for the h galaxies, and (c) with total radio power for both barred and unbarred l galaxies. Best estimates of the typical 1σ error bars are shown.

infrared flux of the galaxy. The mean total luminosity of the h galaxies in this sample is $L_{FIR} \simeq 10^{10}$ $L_{\odot}$ (see Chapter 2 for the definition of FIR) implying that the luminosity of the central star formation complex is a few $\times 10^9$ $L_{\odot}$. Approximately 10^5 bright HII regions (mean luminosity $\sim$ few $\times 10^4$ $L_{\odot}$) are required to match this output. This is the same number of HII regions as determined in Chapter 2 from consideration of the different luminosities and spectral shapes of the h and l galaxies.

There must, however, also be a major contribution (typically 65%) to the total far-infrared flux from extended emission in the h galaxies. It is suggested that this predominantly arises in disk star formation regions (see also Haslam & Osborne 1987; Leggett, Brand & Mountain 1987). This hypothesis can be investigated a little further by examining the *IRAS Small Scale Structures Catalogue* (Helou & Walker 1986) for galaxies in the sample which possess extended ($\geq$ 1 arcmin) source associations of good or moderate flux quality. Nearly one half (43%) of the galaxies exhibit extended 25-μm emission which may originate from warm dust in the galactic disks heated by young star formation regions.

In Fig. 3.8 correlations between the extended 25-μm power (or the point source 25-μm power if no extended emission was detected) and the total 20-cm radio power for both the h and l systems are shown. The l galaxies which possess central radio sources are indicated, and the line $\log(total\,25\text{-}\mu\mathrm{m}\ power) = 4.88 + 0.84 \log(total\ radio\ power)$ is drawn in both plots as a guide for the eye. Note that there is a significant difference between the two relationships. For a given total 20-cm radio power, the total 25-μm power is about a factor of two greater in the actively star–forming h galaxies than in the l spirals. This dichotomy is also apparent when the point–source 25 μm – central radio powers are compared. Re–examination of Fig. 3.7, however, shows no difference in the correlation between point source 100-μm and radio powers for h and l galaxies. The point source 100-μm flux is sufficient for investigating this property, since the large beam size (3 x 5 arcmin) takes in virtually all of the emission from these galaxies; only one exhibits extended emission of good or moderate flux quality at 100 μm. The results in Fig. 3.7 are in concordance with the major fraction of the 100 μm emission arising in the disk and with the single tight correlation between far-infrared and radio luminosity found by Helou, Soifer & Rowan–Robinson (1985) which is independent of the level of galactic activity or Hubble type (Gavazzi, Cocito & Vettolani 1986).

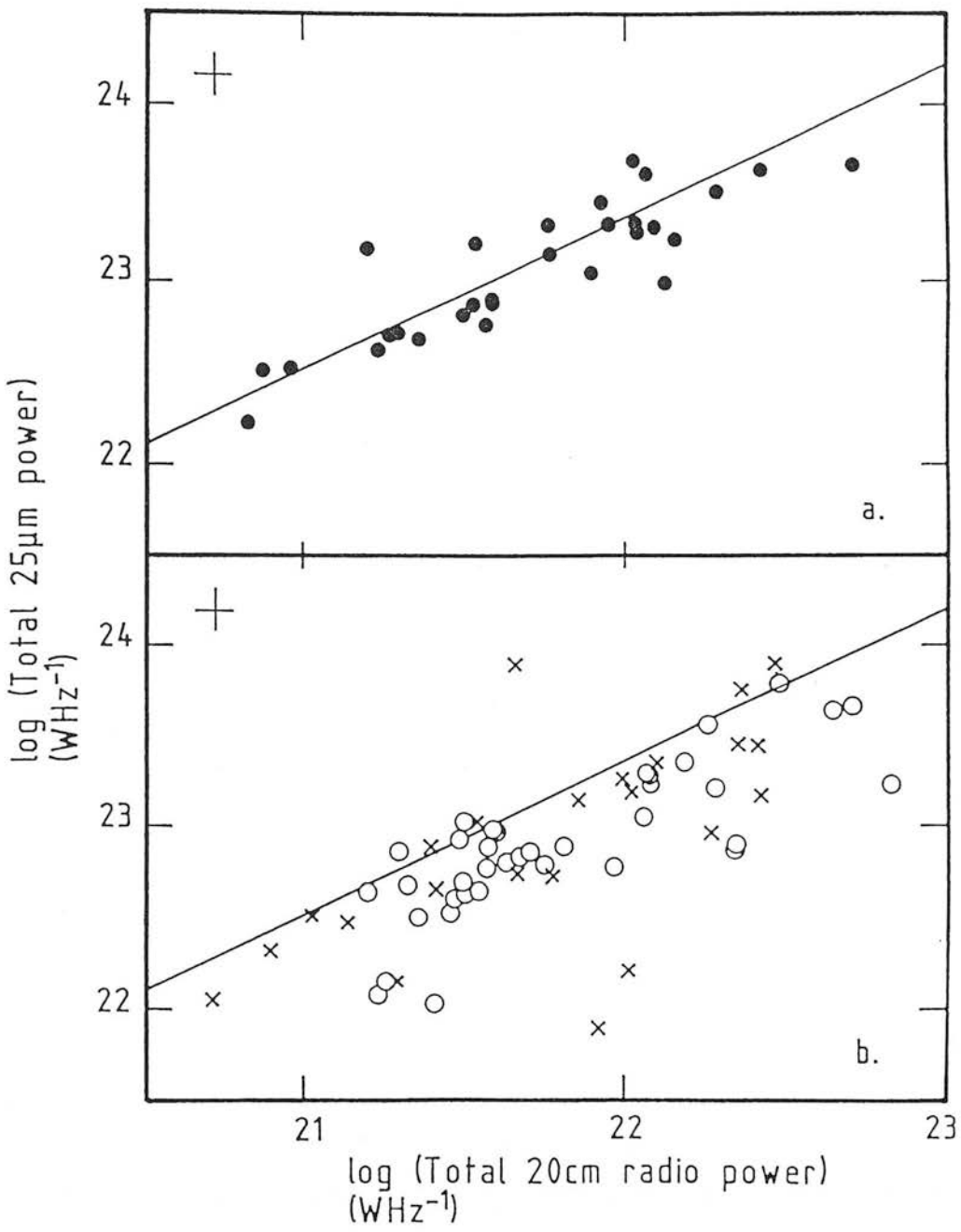

Figure 3.8: The correlations between total (point source or extended source, see text) *IRAS* 25-μm power and total 20-cm radio power for (a) h galaxies (filled circles) and (b) l galaxies (open circles and crosses). The crosses indicate l galaxies which possess central radio sources. The line log (*total* 25-μm *power*) = 4.88 + 0.84 log (*total radio power*) is shown in both plots as a guide for the eye. Best estimates of the typical 1σ error bars are shown.

Two possible explanations for the apparent dependence of the (mid-) infrared–radio correlation on the level of star formation activity are now considered.

(i) It may simply be another manifestation of the phenomenon noted in Section 3.3; namely that a surprisingly high fraction of the l galaxies possess significant radio emission but low 25-μm flux. Whilst it is true that the central source l galaxies tend to exhibit the greatest scatter about the average 25-μm/total power ratio (see Fig. 3.8b), this cannot be the complete answer since the majority of the l systems are without central radio components but still exhibit a different 25 μm–radio relationship to that seen in the h galaxies.

(ii) If the radio emission is a direct measure of the level of star formation activity (that is, the radio flux scales linearly with the supernova, and hence star formation, rate), then it is apparent that the dependence of the (mid-) infrared–radio correlation on star formation activity is most likely due to a variation in the amount of emission from warm dust per unit quantity of star formation. It is proposed that the dust heated by massive young stars is warmer in the centrally located, very active star formation regions found in the h galaxies than in the much less vigorous l spirals. A similar suggestion has been made by Helou (1986) who models the *IRAS* colour of normal galaxies by "cirrus" and variable temperature "active" components. Note that although the *IRAS* flux densities used in this paper have not been colour–corrected (Lonsdale *et al.* 1985), the correction factor at 25μm varies by less than about 7% assuming dust temperatures of between 50 and 100 K and does not significantly affect this result. Since the *IRAS* 25-μm band is close to the expected peak of the Planck function for warm dust heated by massive young stars (having a characteristic temperature of about 75K), only a small variation in the dust temperature is necessary to increase the detected flux in this band by the required factor of two.

3.5 Conclusions

The 1.4 GHz radio continuum properties of an *IRAS* selected sample of nearby spiral galaxies have been examined. This analysis shows that virtually all of the systems with *IRAS* 25-μm/12-μm flux density ratios $S_{25}/S_{12} \geq 2.22$ (the h galaxies) have central

radio sources of angular size less than about 15 arcsec. This strongly suggests that the enhanced star formation activity believed to be occurring in these galaxies is contained within regions of linear extent less than 1–3 kpc and located near or at the galactic nuclei.

The ratio of the far-infrared to radio emission is found to be approximately constant over scales as small as 1 kpc. Given this tight correlation, which is independent of the level of contribution from the central source, the typical far–infrared luminosity of the central star forming complex is estimated to be a few $\times 10^9$ $L_\odot$. This is consistent with other estimates of this parameter.

A significant fraction of galaxies believed not currently to have a high star formation rate (l systems) also possess central radio sources. Having examined three plausible models it is suggested that, amongst the strongly barred (SB) galaxies, the radio emission arises from either a simple density enhancement or from the embers of a burst of star formation. The central radio emission in the unbarred (SA) galaxies may be powered by a density enhancement or an obscured active nucleus, whilst that from the mixed–type (SX) galaxies may be due to any of the three suggested models.

A correlation between the *IRAS* 25-μm and 20 cm radio emission is identified which, in contrast to the far-infrared results, shows a marked dependence on the level of star formation activity. It is suggested that this effect is due to the presence of a warmer dust component in the actively star forming h galaxies than in the l systems.

Acknowledgements

Thijs van der Hulst is thanked for assistance at Westerbork in the reduction of these observations, and STARLINK and IPMAF for providing the hardware and software used to compile and analyse the database. The Westerbork Synthesis Radio Telescope is operated by the Netherlands Foundation for Radio Astronomy with the financial support of the Organisation for the Advancement of Pure Research. Marjorie Fretwell is thanked for production of the diagrams, as are Peter Brand, Charlie Telesco and an anonymous referee for valuable comments on this manuscript.

References

Becklin, E.E., 1987. In *Star Formation in Galaxies*, p.753, ed. Persson, C.J., US Govt. Print. Off., Washington, DC.

Biermann, P., 1980. *Highlights Astr.*, **5**, 209.

Cameron, M.J., 1971. *Mon. Not. R. astr. Soc.*, **152**, 403.

Clark, B.G., 1980. *Astr. Astrophys.*, **89**, 377.

Combes, F. & Gerin, M., 1985. *Astr. Astrophys.*, **150**, 327.

Condon, J.J. & Dressel, L.L., 1978. *Ap. J.*, **221**, 456.

Condon, J.J., 1980. *Ap. J.*, **242**, 894.

Condon, J.J., Condon, M.A., Gisler, G. & Puschell, J.J., 1982. *Ap. J.*, **252**, 102.

Cutri, R.M. & McAlary, C.W., 1985. *Ap. J.*, **296**, 90.

de Jong, T., Clegg, P.E., Soifer, B.T., Rowan-Robinson, M., Habing, H.J., Houck, J.R., Aumann, H.H. & Raimond, E., 1984. *Ap. J.*, **278**, L67.

de Vaucouleurs, G., 1959. *Handbuch der Physik*, **53**, 275.

de Vaucouleurs, G., de Vaucouleurs, A. & Corwin, H.C., 1976. *Second Reference Catalogue of Bright Galaxies*, University of Texas Press, Austin. 'RC2'.

Devereux, N., 1987. In *Star Formation in Galaxies*, p.219, ed. Persson, C.J., US Govt. Print. Off., Washington, DC.

Dressel, L.L. & Condon, J.J., 1978. *Astrophys. J. Suppl.*, **36**, 53.

Dressel, L.L., 1979. *Ph.D. Thesis.*, University of Virginia.

Duric, N., Seaquist, E.R., Crane, P.C., Bignell, R.C. & Davis, L.E., 1983. *Ap. J.*, **273**, L11.

Fairclough, J.M., 1985. In: *RAL Workshop on Extragalactic Infrared Astronomy*, p.32, ed. Gondhalekar, P.M.

Gavozzi, G., Cocito, A. & Vettolani, G., 1986. *Ap. J.*, **305**, L15.

Haslam, C.G.T. & Osborne, J.L., 1987. *Nature*, **327**, 211.

Helou, G., Soifer, B.T. & Rowan-Robinson, M., 1985. *Ap. J.*, **298**, L7.

Helou, G. & Walker, D.W., 1986. *IRAS Small Scale Structures Catalogue.* US Government Printing Office, Washington D.C.

Helou, G., 1986. *Ap. J.*, **311**, L33.

Högbom, J.A., 1974. *Astr. Astrophys. Suppl.*, **15**, 417.

Hummel, E., 1980. *Astr. Astrophys. Suppl.*,**41**, 151. 'H80'.

Hummel, E., 1981. *Astr. Astrophys.*, **93**, 93. 'H81'.

Hummel, E., van der Hulst, J.M. & Dickey, J.M., 1984. *Astr. Astrophys.*, **134**, 207.

Hummel, E., Pedlar, A., van der Hulst, J.M. & Davies, R.D., 1985. *Astr. Astrophys. Suppl.*, **60**, 293.

IRAS Explanatory Supplement, 1985. Eds. Beichman, C.A., Neugebauer, G., Habing, H.J., Clegg, P.E. & Chester, T.J. US Government Printing Office, Washington D.C.

IRAS Point Source Catalog, 1985. Joint IRAS Science Working Group, US Government Printing Office, Washington D.C.

Joseph, R.D., Meikle, W.P.S., Robertson, N.A. & Wright, G.S., 1984. *Mon. Not. R. astr. Soc.*, **209**, 111.

Joseph, R.D & Wright, G.S., 1985. *Mon. Not. R. astr. Soc.*, **214**, 87.

Kalloglyan, A.T. & Kandalyan, R.A., 1986. *Astrofizika*, **24**, 47.

Leggett, S.K., Brand, P.W.J.L. & Mountain, C.M., 1987. *Mon. Not. R. astr. Soc.*, **228**, 11p.

Lonsdale, C.J., Persson, S.E. & Matthews, K., 1984. *Ap. J.*, **287**, 95.

Lonsdale, C.J., Helou, G., Good, J.C. & Rice, W., 1985. *Cataloged Galaxies and Quasars Observed in the IRAS Survey*, Jet Propulsion Laboratory.

Mouschovias, T.C., Shu, F.H. & Woodward, P.R., 1974. *Astr. Astrophys.*, **33**, 73.

Rieke, G.H., Lebofsky, M.J., Thompson, R.I., Low, F.J. & Tokunaga, A.T., 1980. *Ap. J.*, **238**, 24.

Sandage, A. & Tammann, G.A., 1981. *A Revised Shapley Ames Catalog of Bright Galaxies*, Carnegie Institution of Washington Publication No. 635. 'RSA'.

Strom, R.G., van Someren Greve, H.W. & Miley, G.K., 1980. *Westerbork Synthesis Radio Telescope Users Manual.*

Struck-Marcell, C. & Scalo, J.M., 1987. *Astrophys. J. Suppl.*, **64**, 39.

Telesco, C.M. & Gatley, I., 1984. *Ap. J.*, **284**, 557.

Telesco, C.M., 1985. In: *Rutherford Appleton Laboratory Conference on Extragalactic Infrared Astronomy*, p.87, ed. Gondhalekar, P.M.

Ulvestad, J.S., 1982. *Ap. J.*, **259**, 96.

van der Hulst, J.M., Crane, P.C. & Keel, W.C., 1981. *Astr. J.*, **86**, 1175.

van der Kruit, P.C. & Allen, R.J., 1976. *Ann. Rev. Astr. Astrophys.*, **14**, 417.

Véron-Cetty, M.-P. & Véron,P., 1985. *ESO Scientific Report No.4.*

Wynn-Williams, C.G., 1987. *IAU Symposium No. 115, Star Forming Regions*, p125, eds. Peimbert, M. & Jugaku, J., Reidel, Dordrecht, Holland.

Chapter 4

Fluorescent Molecular Hydrogen In Galaxies

Preface : This chapter presents the first results from a near–infrared spectrophotometric survey of spiral galaxy nuclei. All seven of the galaxies discussed here are barred and display evidence of near–nuclear star–formation. The near–IR atmospheric windows, being rich in lines of atomic and molecular hydrogen which suffer less extinction than any optical counterparts, allow the dust–obscured nuclear star–forming complexes to be studied. This work has been published : Puxley, Hawarden & Mountain, 1988. *Mon. Not. R. astr. Soc.*, **234**, 29P.

Summary

New near–infrared spectrophotometric observations of seven nearby spiral galaxies with vigorous central star–forming complexes are presented. Emission from molecular hydrogen has been detected from near the nucleus of each of these galaxies and in every case it proves to be fluorescent, not shock excited. Comparison with the Brγ emission shows that excitation and ionization by ultraviolet radiation of power–law slope, as expected from an active nucleus, may not be a viable mechanism. Instead, the observed molecular and atomic hydrogen line fluxes can be understood if the source of UV is an ensemble of stars having an initial mass function consistent with that of the solar neighbourhood. These results contrast sharply with those so far available, for interacting, merging and some Seyfert galaxies, in which the excitation mechanism appears to be shocks. This difference may perhaps be due to beam size effects; if not, there appears to be a qualitative difference between the star–forming complexes in merging and interacting galaxies, on the one hand, and in barred spiral galaxies, on the other.

4.1 Introduction

Emission from molecular hydrogen in astronomical sources can be excited in two ways: by absorption of soft UV radiation in the Lyman and Werner bands (91.2–110.8 nm) followed by fluorescence down to the excited vibrational/rotational levels of the ground electronic state and subsequent radiative decay, or by collisional excitation with X–ray or shock–heated gas (Shull & Hollenbach 1978; Lepp & McCray 1983; Black & van Dishoeck 1987,'BVD'). In both cases, the v=1–0 S(1) line at 2.122 μm is generally the most easily detected transition. Discrimination between the two mechanisms is possible on the basis of the strength, relative to this line, of the v=1–0 S(0) and v=2–1 S(1) lines at 2.223 and 2.248 μm. These approach 50% of the strength of v=1–0 S(1) only in the case of fluorescence and are expected to be much weaker from shocked sources. Note, however, that it is in principle possible for shock–like line ratios to arise from dense gas which is *radiatively* excited by an intense UV field; see Sternberg (1986).

The measured line ratios in most Galactic sources (which include bipolar flows, planetary nebulae and supernova remnants) are consistent with the theoretical values for shock excitation (Shull & Beckwith 1982). It is therefore natural to associate the molecular hydrogen emission from other galaxies with shock heated gas; indeed, almost all systems observed thus far with sufficient spectral coverage and signal to noise to permit measurement of the strengths of the discriminant lines exhibit ratios appropriate to shock excitation *e.g.* NGC 1068 (Thompson *et al.* 1978; Hall *et al.* 1981); NGC 6240 and Arp 220 (Joseph, Wright & Wade 1984; DePoy, Becklin & Wynn–Williams 1986). Although models of outflow sources in star–forming regions are only able to account for about 1% of the observed H_2 emission (*e.g.* Kawara, Nishida & Gregory 1987, hereinafter KNG; see also Oliva & Moorwood 1986) supernovae, cloud–cloud collisions (*c.f.* NGC 6240 and Arp 220), or the wind from an active nucleus (*c.f.* NGC 1068) have been suggested, quite credibly, to make up the deficit.

In this chapter observations of the v=1–0 S(1), v=2–1 S(1), v=1–0 S(0) and v=1–0 Q–branch lines of molecular hydrogen, and the Brγ (7–4) line of atomic hydrogen are presented for a number of galaxies. In all but one of these systems, the line ratios do *not* indicate collisional excitation, but are, instead, very suggestive of radiative pumping by

the UV field from an ensemble of stars. Fischer *et al.* (1987) have recently argued that molecular hydrogen emission from the Seyfert 1 galaxies NGC 3227 and NGC 4151 is fluorescent, albeit with the excitation produced by the power–law UV continua of the Seyfert nuclei. Observations of fluorescent emission in a few other sources have also been made recently: in Orion's Bar (Hayashi *et al.* 1985), in the reflection nebulae NGC2023 (Gatley *et al.* 1987) and Parasamyan 16 (Sellgren 1986), in the planetary nebula Hubble 12 (Dinerstein *et al.* 1988), in the extra–nuclear HII region NGC 604 in M33 (Israel *et al.* 1988), and possibly in the SMC HII region N88 (Israel & Koornneef 1988).

4.2 Observations of H_2 Emission in Nearby Bright Galaxies

The observations were obtained on the 3.8m UK Infrared Telescope (UKIRT) with the facility single–channel photometer–spectrometer UKT9, using a Circularly Variable Filter (CVF) operated at a spectral resolution ($\lambda/\delta\lambda$) of 120 (see Appendix A for details of the data reduction). This cryostat is equipped with Fabry optics which make the spectral resolution of the system effectively independent of the size of the acceptance solid angle on the sky. All of these observations were carried out using a beam FWHM of 19.6 arcsec; the sensitivity variations within most of this beam are only a few percent and there are no spectral variations across it. This permits photometry to be performed at consecutive CVF settings with very great internal precision and thus measurements can be made of lines which are a small fraction of the strong continuum against which they are observed: the practical limit is probably about 1%.

Fig. 4.1 (a) to (g) shows the K–window spectra of the nearby spiral galaxies NGC 1365, 1808, 3504, 4102, 4536, 5236 and 6946. Identifications for the emission features and their redshifted central wavelengths are shown. The spectra were divided by photometric standard stars observed at a similar airmass and fitted continua have been subtracted (see Appendix A for further details). Late–type giant stars were used for the range 2.08–2.20 μm and earlier types, without stellar CO absorption features, for 2.20–2.50 μm. Emission line strengths were determined by fitting Gaussian functions to the lines, all of which were found to be unresolved at the resolution of the CVF. Table 4.1 lists the observed integrated line fluxes. The indicated errors include a contribution

Figure 4.1: New 2-μm continuum–subtracted large–aperture spectra of (a) NGC 1365, (b) NGC 1808, (c) NGC 3504, (d) NGC 4102, (e) NGC 4536, (f) NGC 5236, and (g) NGC 6946.

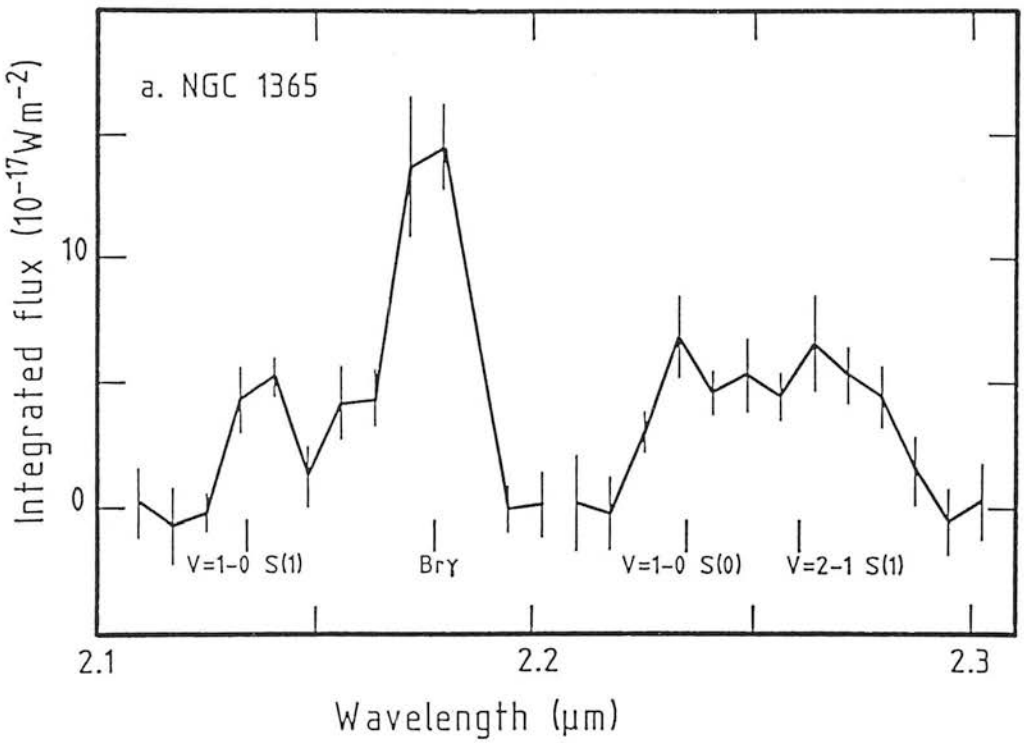

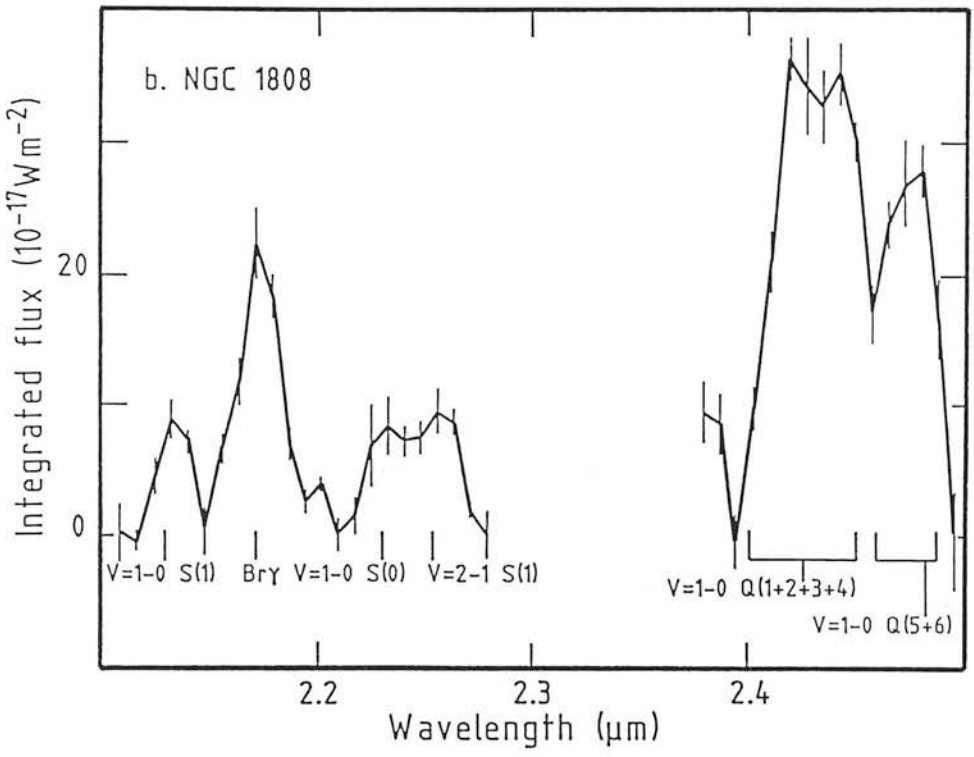
b. NGC 1808
Integrated flux (10^{-17}Wm^{-2})
20
0
V=1-0 S(1)
Brγ
V=1-0 S(0)
V=2-1 S(1)
V=1-0 Q(1+2+3+4)
V=1-0 Q(5+6)
2.2
2.3
2.4
Wavelength (μm)

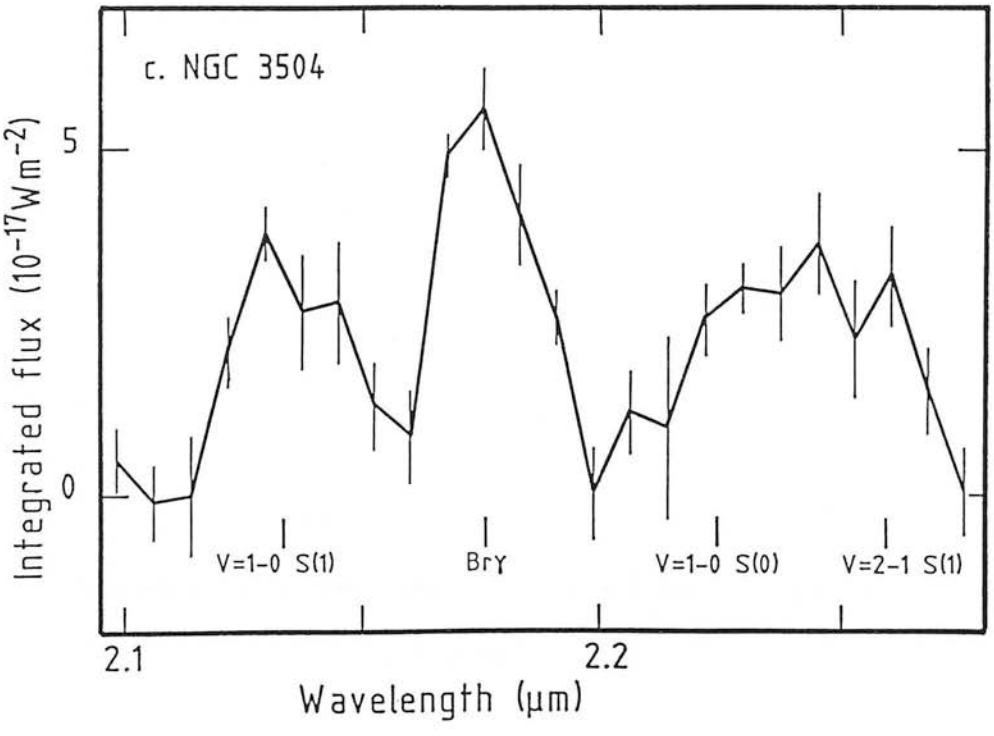
c. NGC 3504
Integrated flux (10^{-17}Wm^{-2})
5
0
V=1-0 S(1)
Brγ
V=1-0 S(0)
V=2-1 S(1)
2.1
2.2
Wavelength (μm)

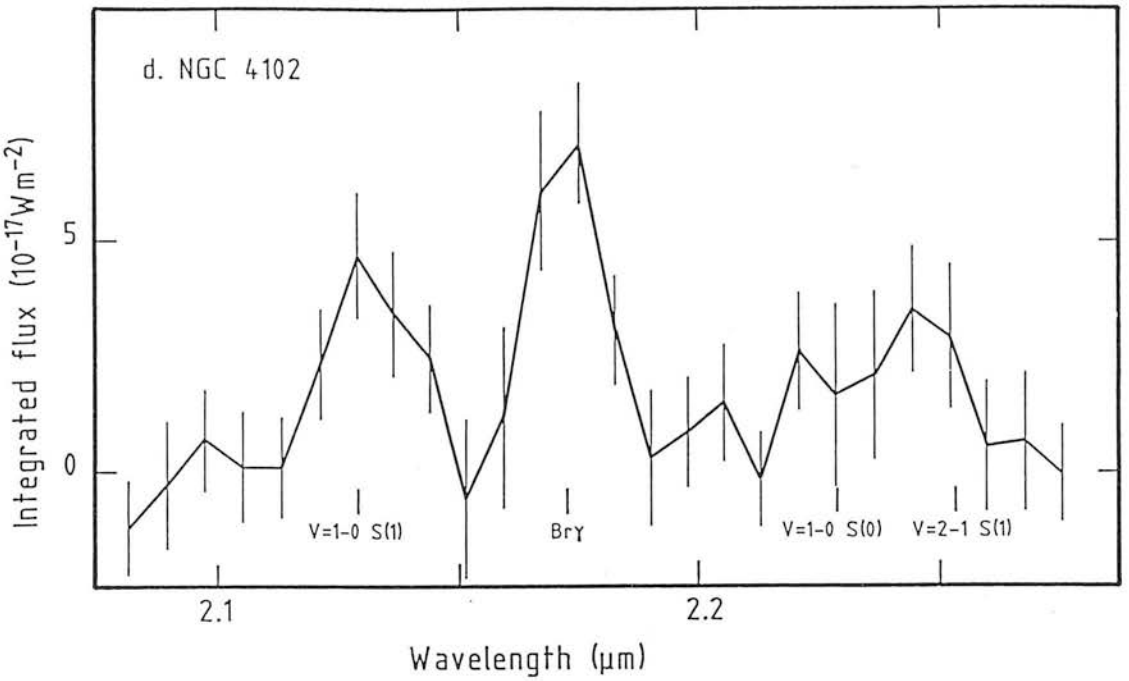
d. NGC 4102
Integrated flux (10^{-17}Wm^{-2})
5
0
V=1-0 S(1)
Brγ
V=1-0 S(0)
V=2-1 S(1)
2.1
2.2
Wavelength (μm)

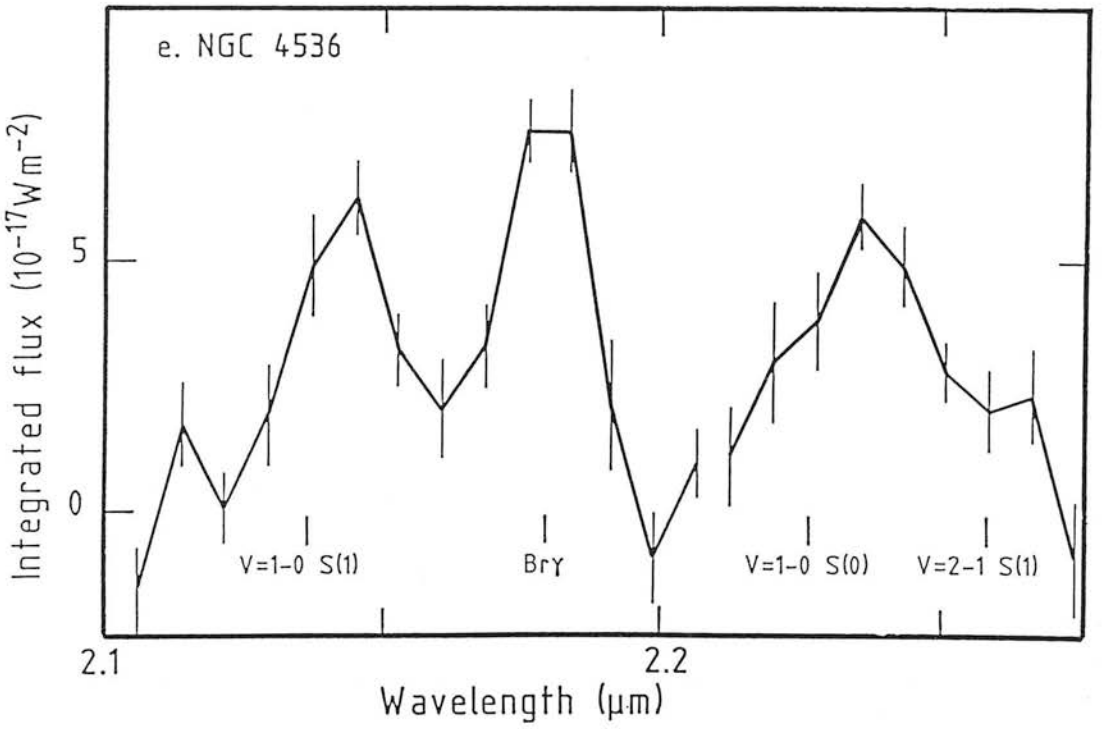
e. NGC 4536
Integrated flux (10^{-17}Wm^{-2})
5
0
V=1-0 S(1)
Brγ
V=1-0 S(0)
V=2-1 S(1)
2.1
2.2
Wavelength (μm)

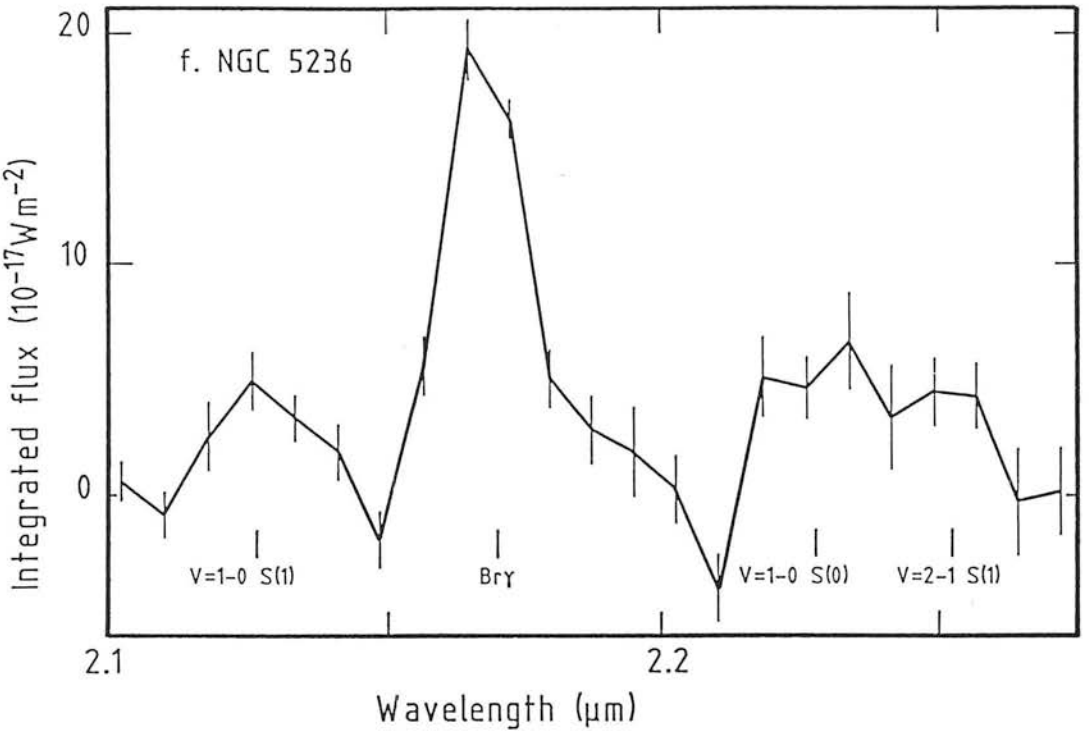
f. NGC 5236
20
10
0
Integrated flux (10^{-17}Wm^{-2})
V=1-0 S(1)
Brγ
V=1-0 S(0)
V=2-1 S(1)
2.1
2.2
Wavelength (μm)

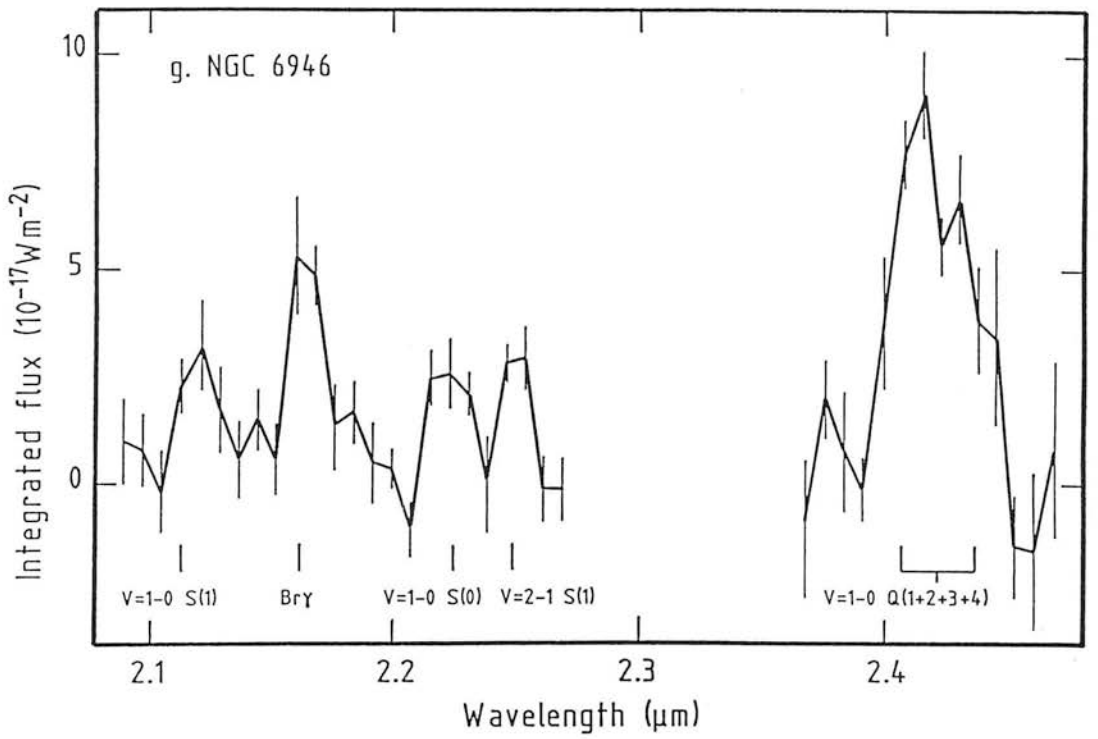
g. NGC 6946
10
5
0
Integrated flux (10^{-17}Wm^{-2})
V=1-0 S(1)
Brγ
V=1-0 S(0)
V=2-1 S(1)
V=1-0 Q(1+2+3+4)
2.1
2.2
2.3
2.4
Wavelength (μm)

Table 4.1: Two micron spectrophotometric data for nearby spiral galaxies and theoretical line flux ratios. The column headed 1–0 Q(1,2,3,4) represents the sum of the emission in the v=1–0 Q-branch lines, Q(1) through Q(4).

Galaxy	Integrated Line Fluxes in 10^{-17} Wm^{-2}					
name	1–0 S(1)	Brγ	1–0 S(0)	2–1 S(1)	1–0 Q(1,2,3,4)	1–0 Q(5,6)
NGC 1365	7.5 ± 0.8	19.6 ± 1.1	5.7 ± 1.3	6.1 ± 1.3	–	–
NGC 1808	9.8 ± 0.8	22.3 ± 0.7	6.5 ± 1.2	8.9 ± 0.9	52 ± 7	28 ± 4
NGC 3504	4.8 ± 1.2	6.8 ± 1.2	3.9 ± 0.7	3.1 ± 0.7	–	–
NGC 4102	4.1 ± 0.6	5.9 ± 0.4	2.1 ± 0.7	2.1 ± 0.7	–	–
NGC 4536	6.4 ± 0.4	8.4 ± 0.5	5.4 ± 0.9	3.0 ± 0.8	–	–
NGC 5236	5.1 ± 0.7	19.6 ± 1.3	6.4 ± 1.4	4.6 ± 1.2	–	–
NGC 6946	3.2 ± 0.5	6.1 ± 1.2	2.6 ± 0.7	2.5 ± 0.7	16 ± 3	–
Fluorescent H_2 model	1.00	–	0.52 ± 0.06	0.54 ± 0.02	2.63 ± 0.14	0.43
Shocked H_2 model	1.00	–	0.23	0.08	1.97	0.53

from uncertainties in the level of the continuum fit. The final two rows of this Table give the expected theoretical values for the fluorescent and shock excited molecular hydrogen line ratios, relative to the v=1–0 S(1) line (BVD; P.W.J.L. Brand, personal communication). In the former case, the errors reflect the ranges assumed for the model parameters, whilst the latter ratios are essentially constant (Brand *et al.* 1988).

There are no published measures of the fluxes of these lines in the galaxies with which to make direct comparisons, because of the large beam size. However, it is noted that the Brγ and v=1–0 S(1) fluxes listed here for NGC 1365 and 1808 are 4-5 times larger than those measured by KNG through a $7\widehat{''} \times 4.5\widehat{''}$ aperture (*c.f.* Kawara, Nishida & Taniguchi 1988). This is consistent with their inference from line observations that star formation extends over at least the central 1 kpc (see also Chapter 3).

4.3 Discussion

It is apparent, from Table 4.1, that the H_2 S–branch line ratios observed in all of these galaxies are not consistent with shock heating but are approximately those predicted by the UV pumping model. These ratios cannot be simulated by any reasonable amount of extinction applied to a shock excited source because of the small wavelength differences of the lines. The effect of reddening on the ratios is discussed in detail in Section 4.3.1, below. In Section 4.3.2, it is argued that an ensemble of stars can produce sufficient ionizing and non–ionizing ultraviolet flux to excite both the atomic and molecular hydrogen line emission which have been observed. In Section 4.3.3, the implications of these results for models of central starbursts in galaxies are briefly addressed.

4.3.1 Molecular Line Emission and Reddening

Although the extinction in the near–infrared is much less than in the visible, the large amounts of dust observed towards the nuclei of IR–bright galaxies (*e.g.* DePoy 1987) implies that there can be significant differential absorption even between the 2-μm lines of molecular hydrogen; thus, for example, between v=1–0 S(1) and Q–branch $A_{1-0S(1)} - A_Q \simeq 0.02\ A_V$.

To make some correction for this, the visual extinction (A_V) for each galaxy was estimated using the observed Brγ line strength (Table 4.1) together with values for the Hα or Hβ flux – taken from the literature – by assuming case B recombination theory (Baker & Menzel 1938) and simple foreground reddening. The extinction derived in this way is only a *lower* limit since the sources are probably spatially distributed amongst intervening dust. If so, and if there exists a significant amount of dust *between* the HII regions producing the recombination lines, then the reddening within these galaxies may have been severely underestimated (see Appendix B, and also Mathis 1970). This is because the optical lines, which are the most affected, will tend to arise near the front surface of any such distributed region, whereas the longer–wavelength Brγ line will come from all sources to a greater physical, and far greater optical, depth. For example, if the observed ratio of the Hβ/Brγ emission is 4 then an apparently low extinction $A_V \sim 2.2$ would be inferred from the conventional model of a point source and dust blanket, but a much higher value $A_V \sim 20$ is implied if the sources and dust are homogeneously mixed. Recognizing this, the following section proceeds using the conventional technique and, later, its viability is investigated.

The optical line fluxes were corrected to the 20 arcsec aperture of the CVF by assuming that the recombination line emission is co-extensive with the 10 μm or radio continuum emission. References to the line strengths and source extents are given beneath Table 4.2. No correction has been made in the case of NGC 1365 due to uncertainty regarding the relative contributions of the active nucleus, for which case B is probably not applicable, and the inner star–forming region. For NGC 5236 (M83), $A_V = 20$ is adopted (Turner, Ho & Beck 1987). Table 4.2 shows the derived values for the visual extinction (column 2) together with the corrected line fluxes and ratios – using the reddening law of Rieke & Lebofsky (1985) – in columns 3–7. It is noted that Phillips, Aitken & Roche (1984) find that the reddening inferred from optical and infrared recombination lines in NGC 1808 and NGC 6946 is considerably less than that implied by the depths of their 10 μm silicate features.

Although the observed H_2 S–branch line ratios are roughly those predicted by the UV pumping model, relative to the v=1–0 S(1) line, the blended Q–branch lines are stronger than expected in both NGC 1808 and NGC 6946 – the only two objects observed at 2.3–2.5 μm. This is probably due to the sources being spatially distributed

Table 4.2: Extinction corrected line fluxes and ratios for nearby galaxies.

Galaxy name	A_V [1]	Corrected Line Fluxes (in 10^{-17} Wm^{-2}) and Ratios				
		$1-0\,S(1)$	$Br\gamma$	$\frac{1-0\,S(0)}{1-0\,S(1)}$	$\frac{2-1\,S(1)}{1-0\,S(1)}$	$\frac{1-0\,Q(1,2,3,4)}{1-0\,S(1)}$
NGC 1365	–	7.5 ± 0.8	19.6 ± 1.1	0.76 ± 0.19	0.81 ± 0.19	–
NGC 1808	5	17.1 ± 1.4	37.9 ± 1.2	0.64 ± 0.13	0.86 ± 0.11	4.8 ± 0.8
NGC 3504	4	7.5 ± 1.9	10.4 ± 1.8	0.78 ± 0.24	0.62 ± 0.21	–
NGC 4102	4	6.4 ± 0.9	9.0 ± 0.6	0.49 ± 0.20	0.49 ± 0.20	–
NGC 4536	6	12.5 ± 0.8	15.9 ± 0.9	0.80 ± 0.14	0.44 ± 0.12	–
NGC 5236	20	46.9 ± 6.4	164 ± 11	1.06 ± 0.27	0.74 ± 0.22	–
NGC 6946	6	6.2 ± 1.0	11.5 ± 2.3	0.78 ± 0.24	0.74 ± 0.24	4.4 ± 1.1

[1] References used for calculation of visual extinction (see text): NGC 1808 – Véron–Cetty & Véron (1986); Telesco *et al.* (1987); NGC 3504 – Stauffer 1982; Hummel, van der Hulst & Dickey (1984); NGC 4102 – Keel 1983a; Condon *et al.* (1982); NGC4536 – Keel (1983b); Telesco *et al.* (1987); NGC 5236 – Turner, Ho & Beck (1987); NGC 6946 – Heckman, Balick & Crane 1980; Condon *et al.* (1982).

through the dust, and the reddening consequently underestimated, as outlined above. Making the assumption that all of the molecular hydrogen emission in these galaxies is fluorescent, allows a more realistic value of the reddening to be derived since the S– and Q–branch lines are relatively close to one another in wavelength and thus probe approximately the same depth of material. Using an intrinsic value for the ratio v=1–0 Q(1+2+3+4) / v=1–0 S(1) of 2.63±0.14 (Black & van Dishoeck 1987), the visual extinction in NGC 1808 and NGC 6946 is estimated to be A_V=33±11 and A_V=30±15 respectively. These values are consistent with those inferred by Phillips, Aitken & Roche (1984) from the 10-μm optical depth *i.e.* A_V=16±9 and 31±8 respectively. Adopting the values for A_V derived from the Q–branch and 1–0 S(1) lines also brings the other ratios into closer agreement with the theoretical fluorescent model.

4.3.2 The Source of the UV

Recently, Fischer *et al.* (1987) have detected molecular and atomic hydrogen emission from the Seyfert galaxies NGC 1275, NGC 4151 and NGC3227. In the latter they interpret the H_2 line ratios as indicating fluorescence. By assuming a power-law spectrum for the ultraviolet to X–ray continua of the Seyfert nuclei, they use the Brγ flux to calculate the number of UV photons in the range 91.2–110.8 nm that are available to excite the molecular hydrogen. This is then compared with the observed v=1–0 S(1) flux by assuming that one S(1) photon is emitted for every 50 UV photons absorbed, as predicted by the UV pumping model of BVD. Hence they derive a relationship :

$$R_{UV,\beta=1.6} = 0.64 f \frac{F(Br\gamma)}{F(1-0\,S(1))} \tag{4.1}$$

where $(1-f)$ is the fraction of non–ionizing UV photons absorbed by dust before being able to excite the molecular gas, β=1.6 is the power–law slope ($f_\nu \propto \nu^{-\beta}$), and $F(Br\gamma)$ and $F(1-0\,S(1))$ are the measured fluxes. Essentially, R_{UV} is the number of ultraviolet photons available in the Lyman and Werner bands relative to the number required to produce the observed S(1) emission. A value of $R_{UV} \geq 1$ means that there are sufficient photons available to excite the gas. Adopting f$\sim$0.3 (Sternberg 1986), Fischer *et al.* conclude that UV fluorescence is a viable mechanism in NGC 4151 (with R_{UV}=1.21) and, possibly, in NGC 3227 (R_{UV}=0.4), in which the diagnostic lines were actually

detected. In Table 4.3 (column 2), the values of $R_{UV,\beta=1.6}$ calculated for the galaxies presented in this chapter are given. No correction has been made for reddening since the differential extinction between 2.122 and 2.166 μm is negligible even for $A_V \sim 30$. In each case the value of R_{UV} is much less than unity implying that excitation by a power–law UV field can probably be ruled out. Thus, other sources of UV must be considered – the most obvious being stars. (Note in passing, however, that of the galaxies with the largest values of R_{UV}, NGC 1365 and NGC 1808 are known to possess active nuclei (Edmunds & Pagel 1982; Véron–Cetty & Véron 1985). It is possible that in these two cases there is a contribution to the fluorescent excitation by the nucleus itself, though given the small Brγ and 1–0 S(1) fluxes measured by KNG it by no means dominates this process.)

The UV excitation of H_2 by an ensemble of stars is now briefly considered. For the purposes of the simple description intended, it is sufficient to assume f$\sim$0.3, although this may be of only limited applicability (see Chapter 5 for a detailed discussion). In general, the value of some observable property in a 'starburst' can be written (*e.g.* Gehrz, Sramek & Weedman 1983; see also Appendix C):

$$S_{obs} = N_0 \left[t \int_{m_l}^{m_0} S(m)\psi(m)dm + \int_{m_0}^{m_u} S(m)\psi(m)\tau(m)dm \right] \qquad (4.2)$$

where $S(m)$ is the emission from a star of mass m, $\tau(m)$ is the main sequence lifetime of this star, $\psi(m)$ is the initial mass function (IMF) with upper and lower limits of m_u and m_l respectively, t is the time since star formation began and N_0 is a scaling factor. This equation is simply the sum of the emissions from stars whose main sequence lifetimes are larger than t (so that m_0 is the mass of a star having $\tau(m_0) = t$), and from those which have been dying. A constant star formation rate was assumed. Using the integrated model stellar atmospheres of Kurucz (1979), described in Appendix C, the ionizing ($\lambda \leq 91.2$ nm) and non–ionizing ($91.2 < \lambda < 110.8$ nm) photon production rates were calculated as a function of stellar mass. The IMF given by Scalo (1986) and the lifetime–mass relation from Bahcall & Piran (1983), were also adopted. Assuming that 70 ionizing photons are required to produce each Brγ photon, as for Case B with $T=10^4$ K and $n_e=10^4$ cm^{-3} (Hummer & Storey 1987), and that 50 non–ionizing photons produce one 1–0 S(1) photon (BVD), a relationship analogous to that in Eqn. (4.1) can be constructed. For a "zero–age" starburst (*i.e.* dropping the second term in Eqn.

Table 4.3: Results from the power–law and 'starburst' ionization/excitation modelling described in the text.

Galaxy	Power–law	'Starburst' Model		
name	$R_{UV,\beta=1.6}$	$R_{UV}(100\,M_\odot)$	$R_{UV}(30\,M_\odot)$	$R_{UV}(3.5\times10^7 yr, 100\,M_\odot)$
NGC 1365	0.50	1.06	2.34	1.54
NGC 1808	0.43	0.90	1.99	1.31
NGC 3504	0.27	0.56	1.24	0.82
NGC 4102	0.27	0.57	1.26	0.83
NGC 4536	0.24	0.52	1.18	0.75
NGC 5236	0.67	1.42	3.14	2.07
NGC 6946	0.36	0.75	1.66	1.10

(4.2) and setting m_0=m_u=100 $M_\odot$, m_l=0.8 $M_\odot$ and t=1) :

$$R_{UV,s/burst} = 1.35 f \frac{F(Br\gamma)}{F(1-0\,S(1))} \tag{4.3}$$

Values for this parameter were also calculated assuming m_u=30 $M_\odot$ and for an episode of star formation with age t=3.7x10^7 yr (and having m_u=100 $M_\odot$). In these cases, the numerical factor in Eqn. (4.3) becomes 2.99 or 1.97 respectively. The effect of decreasing the upper mass limit or increasing the age of the starburst (keeping a constant star formation rate) is just to increase the relative number of low–mass stars present, which in turn increases the relative fraction of non–ionizing UV photons. The effect on $R_{UV,s/burst}$ of increasing the lower mass limit up to about 5 $M_\odot$ is negligible for a starburst of age 3.7x10^7 yr. In columns 3–5 of Table 4.3, the values of $R_{UV,s/burst}$ are given for the galaxies taking f$\sim$0.3. It can be seen that, though dependent on the upper mass cut–off and the age of the starburst, the proposed mechanism of UV pumping by an ensemble of stars is viable. This mechanism is examined further in Chapter 5.

4.3.3 H_2 Excitation and the Properties of Starbursts

The galaxies in which the lines diagnostic of the H_2 excitation mechanism have previously been observed comprise the ultraluminous objects NGC 6240 and Arp 220, several Seyferts, including NGC 3227, hitherto the lone confirmed example of fluorescent molecular hydrogen emission, and about 10 galaxies selected as being IR–luminous interacting or post–merging systems, which are being studied by R.D. Joseph, G.S. Wright and collaborators (G.S. Wright, personal communication; see also Joseph *et al.* 1987). All except one, NGC 1068, are highly disturbed, with every indication that their gaseous components contain an abundance of kinetic energy. In contrast, the galaxies in the present study are morphologically quite normal spirals. Intuitively, therefore, it is perhaps not surprising that the H_2 emission from most of the former is shock excited, but from most of the latter it is not.

Unfortunately, except in that minority of interactors in which actual collisions of large masses of ISM are taking place (*c.f.* NGC 6240), this comfortable intuition does not agree particularly well with the limited knowledge concerning the physical causes

of vigorous star formation, or the properties of star–forming complexes. In "normal" galaxies, such star formation is most frequent in barred systems (Chapter 2) which strongly suggests that it owes its existence to the presence of the bar. In so far as it can be claimed that the causes of the more luminous starbursts in the interacting and merging galaxies are understood, it would appear that the underlying mechanism is the same — the rotating non–axisymmetric potential produced by the bar or the companion galaxy drives an inflow of interstellar material which fuels, and perhaps even initiates, the star formation (Combes & Gerin 1985; Combes 1988). Thus there is no good reason to expect that the kinetic energy per unit mass of ISM in the starbursts in the two groups of galaxies is radically different, as the observational results appear to imply.

Perhaps more likely is that the difference between the spectroscopic properties of the two groups is the result of a selection effect. The disturbed systems are on average at a markedly larger distance than the normal galaxies, so that the spectrophotometry samples a larger spatial region around the nucleus. Observations of the former systems (covering 5 kpc, or more, in extent) may therefore be dominated by emission from shocked material being moved inwards, outside the central starburst, whilst the measurements presented in this chapter (over $\sim$1 kpc) may be dominated by the UV–rich central regions. Unpublished observations of the nearby system NGC 253 by G.S. Wright and collaborators (private communication) show a substantial increase in the strength of v=1–0 S(1) relative to Brγ at increasing radial distances from the nucleus. The situation is not simple, however, as these workers also find that their spectrum taken through a 20 arcsec aperture, in common with those of Rieke *et al.* (1988) using an 7.8 arcsec beam, and F.P. Israel (personal communication) in a 6 arcsec aperture, shows that the H_2 emission from the 'nuclear' regions of this galaxy is shock excited, not fluorescent.

The luminosities in the v=1–0 S(1) line of the galaxies studied here are between 1×10^{31} and 4×10^{32} W (for H_0=75 km s^{-1} Mpc^{-1}), very much less than the $\sim 10^{34}$ W emitted in this line by shocked H_2 in the ultraluminous *IRAS* galaxies such as Arp 220, NGC 6240 and IRAS 14348-1447 (Geballe 1988), but comparable to the 4×10^{32} W from shocked gas in NGC 1068. Sanders *et al.* (1988) have suggested that the ultraluminous *IRAS* galaxies are generically related to the most luminous AGNs and, perhaps, draw their power from a buried central quasar. It might therefore be speculated that in these

and the other luminous (disturbed) systems the shocked H_2 emission is caused by a wind from an active nucleus, rather than by mass motions of the molecular material itself. This is certainly true of the nearby low–luminosity active spiral NGC 3079 (Hawarden *et al.* 1988) and is consistent with the observation by KNG that the AGNs in their sample have markedly higher luminosity in 1–0 S(1) than do the starburst systems. However it should be noted that on their figure Arp 220, an excellent candidate for an ultraluminous galaxy containing a buried quasar, lies amongst the starburst systems, while NGC 6240, which may only contain a mere LINER nucleus, has an order of magnitude more luminosity in S(1), for its total luminosity, than do the rest of the AGNs.

These results clearly demonstrate the need for caution in using spectrophotometry of H_2 emission in one or a few galaxies to infer an evolutionary sequence for starbursts such as that by Rieke *et al.* (1988). While the general picture proposed by these workers may be correct, it now appears that the H_2 emission from NGC 253 which inspired it may be quite atypical in its excitation mechanism. Similar reservations apply to the use of the v=1–0 S(1) line strengths, alone, to examine the physics of galactic nuclei. At present it seems clear only that if meaningful progress is to be made in understanding these problems, an increase in the sample of *adequately* studied galaxies, and much more information on radial variations of the excitation mechanism, are essential.

Acknowledgements

Most of the data upon which this paper is based were obtained in observing time awarded by the UK Panel for the Allocation of Telescope Time (PATT). The successful employment of this time is a tribute to the skill and efficiency of telescope operators Joel Aycock, Dolores Walther and Thor Wold. Certain important supplementary and confirming observations were obtained as part of the UKIRT Service Observing programme. Special thanks are due to Gillian Wright and Bob Joseph for showing, discussing and allowing reference to their unpublished spectroscopy of interacting and merging starburst galaxies. Toby Moore, Peter Brand, Frank Israel and Tom Geballe all

contributed help, advice and stimulus to this work, and its presentation was improved by the helpful comments of the referee. Marjorie Fretwell is thanked for drawing the diagrams.

References

Bahcall, J.N. & Piran, T., 1983. *Ap. J.*, **267**, L77.

Baker, J.G. & Menzel, D.H., 1938. *Ap. J.*, **88**, 52.

Black, J.H. & van Dishoeck, E.F., 1987. *Ap. J.*, **322**, 412. 'BVD'.

Brand, P.W.J.L., Moorhouse, A., Burton, M.G., Geballe, T.R., Bird, M. & Wade, R., 1988. Submitted to *Astrophys. J.*

Combes, F., 1988. In *Galactic and Extragalactic Star Formation*, p.475, eds. Pudritz, R.E. & Fich, M., Kluwer Acad. Publ., Dordrecht.

Combes, F. & Gerin, M., 1985. *Astr. Astrophys.*, **150**, 327.

Condon, J.J., Condon, M.A., Gisler, G. & Puschel, J.J., 1982. *Ap. J.*, **252**, 102.

DePoy, D.L., 1987. *Ph.D. Thesis*, University of Hawaii.

DePoy, D.L., Becklin, E.E. & Wynn–Williams, C.G., 1986. *Ap. J.*, **307**, 116.

Dinerstein, H.L., Lester, D.F., Carr, J.S. & Harvey, P.M., 1988. *Ap. J.*, **327**, L27.

Edmunds, M.G. & Pagel, B.E.J., 1982. *Mon. Not. R. astr. Soc.*, **198**, 1089.

Ferland, G.J. & Osterbrock, D.E., 1986. *Ap. J.*, **300**, 658.

Fischer, J., Geballe, T.R., Smith, H.A., Simon, M. & Storey, J.W.V., 1987. *Ap. J.*, **320**, 667.

Gatley, I., Hasegawa, T., Suzuki, H., Garden, R., Brand, P., Lightfoot, J., Glencross, W., Okuda, H. & Nagata, T., 1987. *Ap. J.*, **318**, L73.

Geballe, T.R., 1988. *Mon. Not. R. astr. Soc.*, in press.

Gehrz, R.D., Sramek, R.A. & Weedman, D.W., 1983. *Ap. J.*, **267**, 551.

Hall, D.N.B., Kleinmann, S.G., Scoville, N.Z. & Ridgway, S.T., 1981. *Ap. J.*, **248**, 898.

Hawarden, T.G., Wade, R., Israel, F.P. & Geballe, T.R., 1988. Submitted to *Mon. Not. R. astr. Soc.*

Hayashi, M., Hasegawa, T., Gatley, I., Garden, R. & Kaifu, N., 1985. *Mon. Not. R. astr. Soc.*, **215**, 31P.

Heckman, T.M., Balick, B. & Crane, P.C., 1980. *Astr. Astrophys. Suppl.*,**40**, 295.

Hummel, E., van der Hulst, J.M. & Dickey, J.M., 1984. *Astr. Astrophys.*, **134**, 207.

Hummer, D.G. & Storey, P.J., 1987. *Mon. Not. R. astr. Soc.*, **224**, 801.

Israel, F.P., Hawarden, T.G., Wade, R., Geballe, T.R. & van Dishoeck, E.F., 1988. Submitted to *Mon. Not. R. astr. Soc.*

Israel, F.P. & Koornneef, J., 1988. *Astr. Astrophys.*, **190**, 21.

Joseph, R.D., Wright, G.S. & Wade, R., 1984. *Nature*, **311**, 132.

Joseph, R.D., Wright, G.S., Wade, R., Graham, J.R., Gatley, I. & Prestwich, A.H., 1987. In *Star Formation in Galaxies*, p.421, ed. Persson, C.J., US Govt. Print. Off., Washington, DC.

Kawara, K., Nishida, M. & Gregory, B., 1987. *Ap. J.*, **321**, L35.

Kawara, K., Nishida, M. & Taniguchi, Y., 1988. *Ap. J.*, **328**, L4.

Keel, W.C., 1983a. *Ap. J.*, **269**, 466.

Keel, W.C., 1983b. *Astrophys. J. Suppl.*,**52**, 229.

Kurucz, R.L., 1979. *Astrophys. J. Suppl.*, **40**, 1.

Lepp, S. & McCray, R., 1983. *Ap. J.*, **269**, 560.

Mathis, J.S., 1970. *Ap. J.*, **159**, 263.

Oliva, X. & Moorwood, A.F.M., 1986. *Astr. Astrophys.*, **164**, 104.

Phillips, M.M., Aitken, D.K. & Roche, P.F., 1984. *Mon. Not. R. astr. Soc.*, **207**, 25.

Rieke, G.H. & Lebofsky, M.J., 1985. *Ap. J.*, **288**, 618.

Rieke, G.H., Lebofsky, M.J. & Walker, C.E., 1988. *Ap. J.*, **325**, 679.

Sanders, D.B., Soifer, B.T., Elias, J.M., Madore, B.F., Matthews, K., Neugebauer, G., & Scoville, N.Z., 1988. *Ap. J.*, **325**, 74.

Scalo, J.M., 1986. *Fund. Cosm. Phys.*,**11**, 1.

Sellgren, K., 1986. *Ap. J.*, **305**, 399.

Shull, J.M. & Beckwith, S., 1982. *Ann. Rev. Astr. Astrophys.*, **20**, 163.

Shull, J.M. & Hollenbach, D.J., 1978. *Ap. J.*, **220**, 525.

Stauffer, J.R., 1982. *Astrophys. J. Suppl.*,**50**, 517.

Sternberg, A., 1986. *Ph.D. Thesis*, Columbia University.

Telesco, C.M., Decher, R., Ramsey, B.D., Wolstencroft, R.D. & Leggett, S.K., 1987. In *Star Formation in Galaxies*, p.497, ed. Persson, C.J., US Govt. Print. Off., Washington, DC.

Thompson, R.I., Lebofsky, M.J. & Rieke, G.H., 1978. *Ap. J.*, **222**, L49.

Turner, J.L., Ho, P.T.P. & Beck, S.C., 1987. *Ap. J.*, **313**, 644.

Véron–Cetty, M.–P. & Véron, P., 1985. *Astr. Astrophys.*, **145**, 425.

Véron–Cetty, M.–P. & Véron, P., 1986.*Astr. Astrophys. Suppl.*, **66**, 335.

Chapter 5

Molecular and Atomic Hydrogen Line Emission from Star–Forming Galaxies

Preface : This chapter expands on the discovery in the last section of widespread fluorescent molecular hydrogen in star–forming galaxies. The excitation of H_2 in these regions is given a firmer basis and the potential of such measurements, in conjunction with those of hydrogen recombination lines, for probing the physical conditions is explored. This work has been prepared for publication : Puxley, Hawarden & Mountain, 1988. *Mon. Not. R. astr. Soc.*, to be submitted.

Summary

Models of the generation of molecular and atomic hydrogen line emission from star–forming regions are discussed. These take into account the variations in the efficiency with which fluorescent H_2 emission is produced as the ratio of the incident soft UV to the gas density changes (the lower this ratio, the higher the efficiency). The models deal with hot stars embedded within molecular clouds, large compact clusters of young stars generating intense UV fields, and emission from clouds bathed in a relatively diffuse UV field. The results are compared with the ratio of the observed intensities of the H_2 v=1–0 S(1) and Brγ lines from the nuclear regions for a sample of 28 star–forming galaxies. The results for 14 of these are derived from new measures of the total nuclear line fluxes from spirals, and another 14 are taken from the literature. Unlike the results of previous investigations, the scatter in the ratio of the S(1) line to Brγ is found to be quite small. This, together with the observed dominance of radiative excitation in at least eight galaxies from the sample, suggests a common mechanism for the H_2 excitation, that is, ultraviolet pumping. Most galaxies can be understood in terms of ensembles of hot stars intimately mixed with molecular clouds, but a few require

much higher ratios of the UV intensity to the gas density, conditions which suggest the presence of large numbers of massive stars in compact clusters.

5.1 Introduction

Until recently, it was believed that the molecular hydrogen emission from star–forming regions was dominated by collisional excitation in the shock fronts created by expanding HII regions and by stellar winds (see Shull & Beckwith 1982 for a review). Further, the luminous shock–excited emission from supernova remnants such as IC 443 (Burton *et al.* 1988) made it natural to attribute the H_2 emission from galaxies to the same mechanism. Early observational evidence from a few luminous systems (NGC 1068, NGC 6240 and Arp 220) suggested this was, indeed, the case (Thompson *et al.* 1978; Hall *et al.* 1981; Joseph, Wright & Wade 1984). However, the first extragalactic H_2 emission measured from an extra–nuclear HII region (NGC 604 in M33) by Israel *et al.* (1988) proved to be excited by absorption of UV photons. Recently, nuclear H_2 emission from spiral galaxies where the luminosity can be ascribed mostly to young stars has also proven to be radiatively excited (see Chapter 4). Even Orion, traditionally the abode of shock–excited H_2, exhibits widespread fluorescent emission (Hayashi *et al.* 1985) which may dominate the integrated flux (*e.g.* Israel & Koornneef 1988). Thus, apart from galaxies exhibiting peculiar morphologies or containing nuclear–driven winds (NGC 1068; NGC 3079, Hawarden *et al.* 1988), it now seems quite conservative to associate extragalactic H_2 emission with radiative excitation.

In Chapter 4 a simple model of the atomic (Brγ) and molecular (v=1–0 S(1)) hydrogen line emission from star–forming complexes, was presented. There, it was assumed that the conversion efficiency of ultraviolet (λ = 91.2 – 110.8 nm) to infrared H_2 line photons was constant (*q.v.* Fischer *et al.* 1987), and the strength of the Brγ line suggested that sufficient UV photons were available to produce the observed H_2 emission. This chapter presents a much more detailed analysis of the factors affecting the molecular and atomic hydrogen line emission (§5.2), employing recent models describing the radiative excitation of H_2 (Black & van Dishoeck 1987, hereinafter BVD;

Sternberg 1988, hereinafter S88). The implications of the assertion that the molecular hydrogen is fluorescent are examined by comparison of predicted S(1)/Brγ ratios with new and published near–IR spectra of galaxies (§5.3).

5.2 Modelling the Line Emission

The assumption in Chapter 4 that the absorption by molecular hydrogen of non–ionizing UV radiation and the subsequent re–emission of infrared line photons occurs with constant efficiency is only of limited validity. As demonstrated by BVD and S88, the H_2 excitation efficiency, that is, the ratio of output IR line to incident UV continuum flux, depends primarily on the intensity of the incident ultraviolet radiation (χ), and the gas density ($n = 2n_{H_2} + n_H$). The efficiency of H_2 excitation is maximised for small χ/n, when the attenuation of UV radiation is dominated by line absorption (see Fig. 5.1, adapted from BVD). For larger values of χ/n, the efficiency is reduced because of the removal of UV photons by dust. Thus, the extent to which the stellar radiation is diluted by geometry is pivotal in determining the molecular hydrogen luminosity. It is unfortunate, therefore, that the morphologies of star–forming complexes are not well known.

Before examining the models in detail, some of their common sources of uncertainty are described. The theoretical H_2 excitation calculations by BVD have been employed throughout to convert the incident UV radiation into v=1–0 S(1) line emission. Besides the UV photon flux and gas density, there are several factors incorporated within these calculations which can affect the emitted S(1) intensity. An enhanced H_2 formation rate may increase the UV–to–IR efficiency by up to a factor of 2.5 for high UV intensities and low gas densities ($\chi/n > 0.1$ cm^{-3}, S88, where χ is the strength of the UV field relative to that in the solar neighbourhood, see §5.2.1). This rate depends in an uncertain way on grain properties such as temperature and chemical composition, and it is noted that the value adopted here (from BVD) is three times larger than that assumed by S88. Raising the gas temperature can also increase the H_2 formation rate and alters the lower level populations through collisions. BVD calculate a factor of 4 increase in the emitted line intensity over the temperature range 30 to 300 K; for convenience I follow BVD and assume 100 K throughout this work. Finally, the gas–to–dust ratio

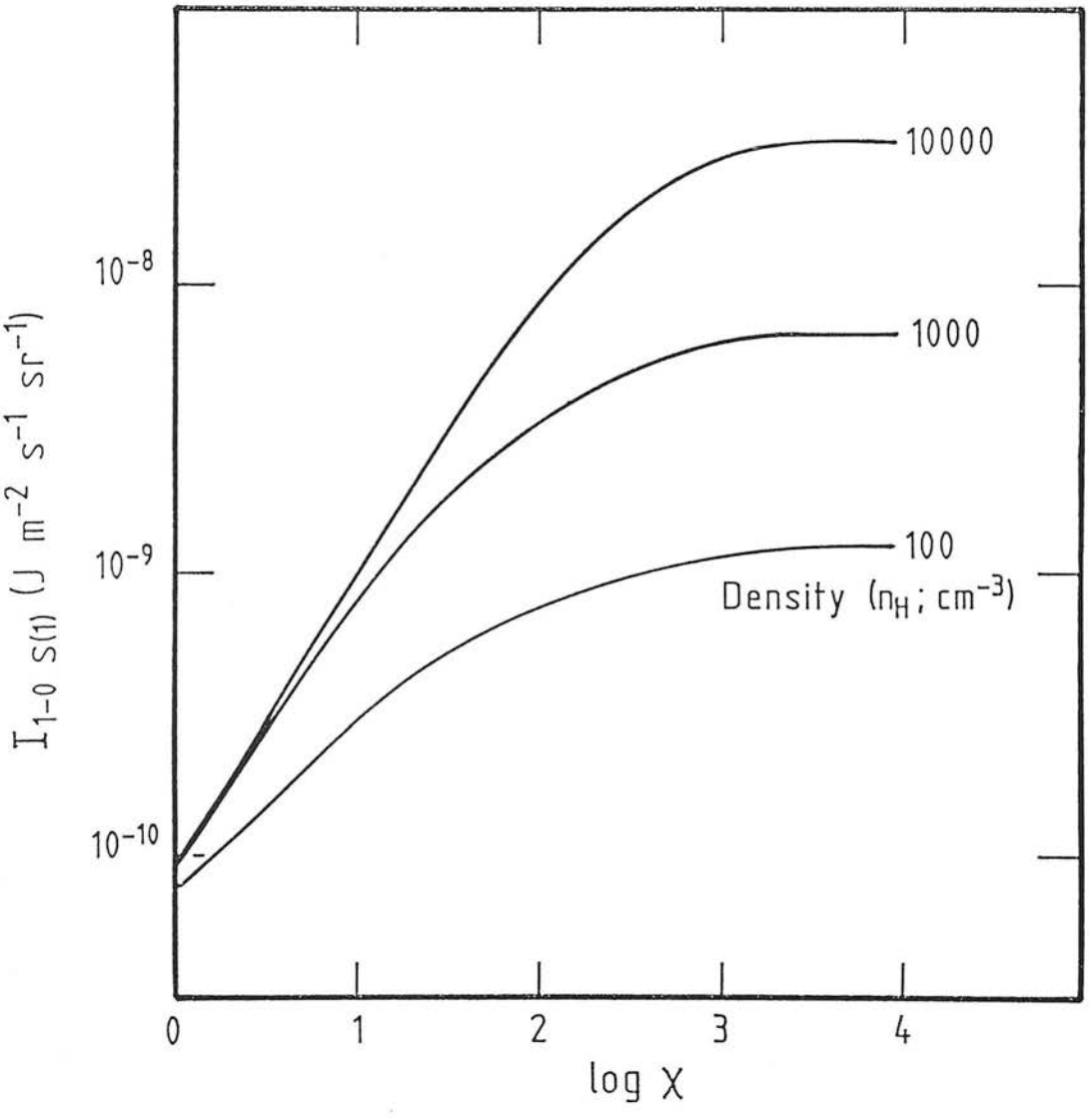

Figure 5.1: Emitted intensity in the v=1–0 S(1) line of H_2 as a function of the incident UV radiation (given relative to the background in the solar neighbourhood) for various values of the total gas density (adapted from Black & van Dishoeck 1987).

affects the excitation efficiency since dust competes with H_2 for UV photons. The models presented in this chapter all assume a 'normal' ratio ($N_H = 1.6 \times 10^{21} A_V$ cm^{-2}, equivalently, a gas–to–dust mass ratio of 100). They may be adjusted using the scaling–law of S88 who shows that the emitted intensity increases as the square root of the gas–to–dust ratio.

5.2.1 Common Properties and Parameters of the Models

The models described in Section 5.2.2 all have a common basis — namely, calculation of the relative fractions of ionizing ($\lambda < 91.2$ nm) and non–ionizing ($91.2 < \lambda < 110.8$ nm) ultraviolet photons emitted by hot stars and their conversion into atomic (Brγ) and molecular (v=1–0 S(1)) hydrogen line luminosities, respectively. Some of the more general aspects of these procedures are given below, the model–specific details, and results, being described in Section 5.2.2.

In order to determine the UV emission from the stars comprising the complex, ionizing and non–ionizing ultraviolet photon fluxes were evaluated as a function of stellar mass by integrating under Kurucz (1979) model atmospheres. Other stellar properties, such as the conversion from effective temperature (T_{eff}) to mass, and stellar radii, were taken from the compilation by Landolt–Börnstein (1982). The resultant fluxes are given in Table C.1 of Appendix C where further details may be found. Using these data, Brγ hydrogen recombination line luminosities were derived from the ionization rate assuming Case B recombination theory for an electron temperature and density of 10^4 K and 10^4 cm^{-3}, respectively. Under these conditions, in dust–free nebulae, 70 Lyman continuum photons are required to produce one Brγ photon (Hummer & Storey 1987).

As the first stage in calculating the luminosity in the v=1–0 S(1) transition of H_2, the intensity of the ultraviolet radiation incident on the molecular clouds was computed. For two of the models (A and B, see §5.2.2), the molecular gas was assumed to envelop the Strömgren spheres of ionized gas surrounding hot stars. The incident UV intensity may then be written :

$$\chi = 1.24 \times 10^{-14} \left(\frac{N_{NUV}}{s^{-1}}\right) \left(\frac{N_{LyC}}{s^{-1}}\right)^{-2/3} R^{-2} \qquad (5.1)$$

where χ is the 91.2 – 110.8 nm photon flux per unit surface area relative to the mean starlight background in the solar neighbourhood : 2.7×10^{11} photon s^{-1} m^{-2}, from Draine (1978) as quoted by Roberge, Dalgarno & Flannery (1981) – see BVD for details. N_{LyC} and N_{NUV} are the ionizing and non–ionizing photon fluxes, either from individual stars (model A, taken from Table C.1) or from a cluster of sources (model B), and R is a dimensionless cloud–radiation source separation in units of the Strömgren radius. (The latter is left as a free parameter since evolution may result in HII regions much larger than their Strömgren radii). For a given gas density, the incident UV flux was converted into an emitted 1–0 S(1) intensity using results from the detailed models of H_2 excitation by BVD (*i.e.* Fig. 5.1). Gas densities larger than 10^4 cm^{-3} were not considered since the observed H_2 line ratios (Chapter 4) argue against such values because of the consequent distortion of the level populations due to multiple pumping (Sternberg 1986; S88). In the third model, the conversion of ultraviolet continuum into H_2 line photons was assumed to operate at maximum efficiency, *i.e.* the linear regime in Fig. 5.1, and therefore the S(1) luminosity was derived directly from the non–ionizing photon flux, by–passing calculation of the incident UV intensity.

5.2.2 The Three Models

The geometry of the star–forming complex governs the dilution of the UV radiation and, hence, the H_2 excitation efficiency for a given gas density. Since the morphologies of these regions are poorly known, for modelling purposes three configurations of young stars and molecular clouds were selected which aim to encompass the range of plausible distributions. These are shown schematically in Fig. 5.2, and consist of : (A) concentric photodissociation zones and HII regions surrounding individual stars, (B) a single vast ionized region, surrounded by H_2 line–emitting clouds, and enclosing the clustered young stellar population, and (C) H_2 emission from clouds bathed in a relatively diffuse UV field. These models may also be viewed as snapshots taken at various stages in the evolution of a star–forming complex : from formation of embedded massive stars (model A), to disruption and dispersion of the parent molecular clouds (model C).

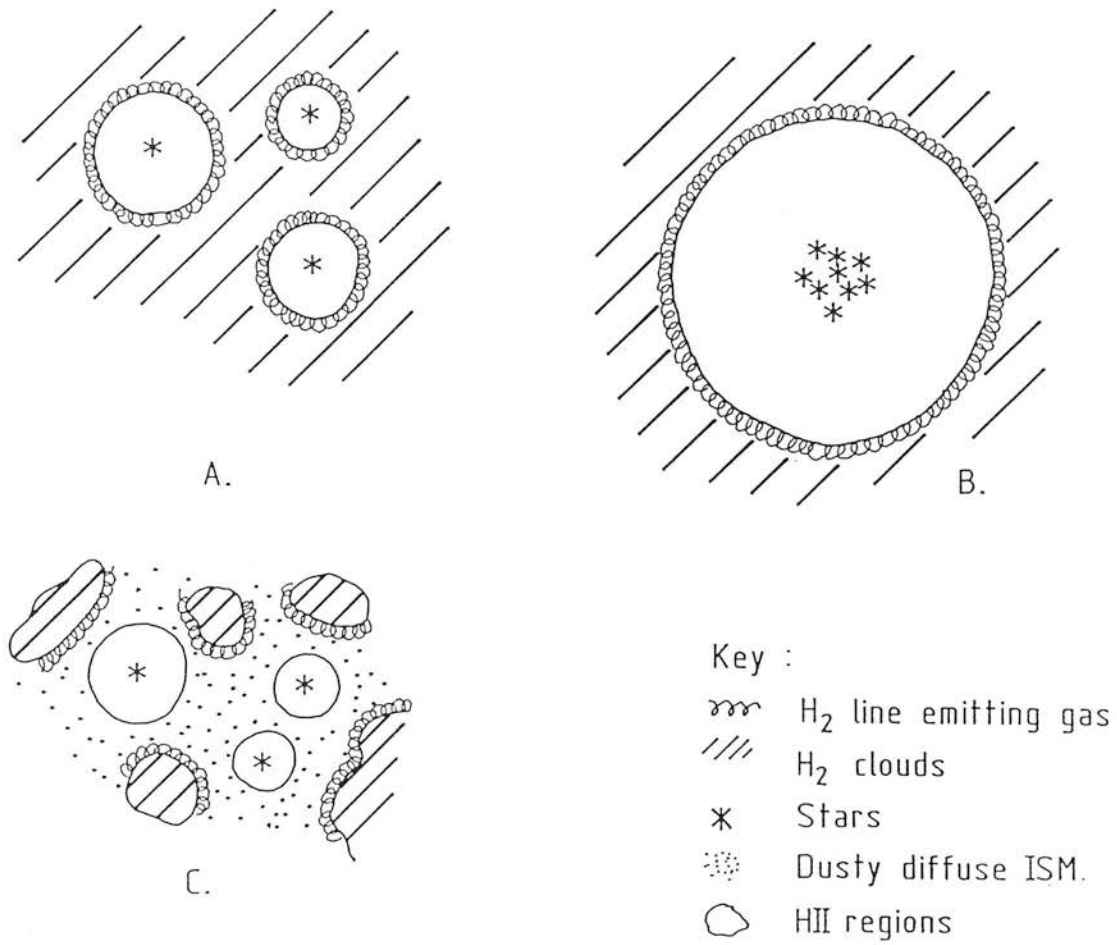

Figure 5.2: Schematic representation of the distribution of stars, HII regions, and molecular gas for the three models discussed in the text.

These three models are now examined in detail.

5.2.2.1 *Model A : Embedded Stars*

For stars of mass 2–100 $M_\odot$ (*i.e.* effective stellar temperatures in the range $(8-50)\times10^3$ K), the luminosity in the Brγ line was calculated using the ionizing fluxes given in Table C.1. The non–ionizing UV flux incident on the molecular clouds, assumed to be located at the edge of the Strömgren sphere with $R = 1$, was evaluated using Eqn. 5.1 and the S(1) emission determined from Fig. 5.1 and integrated over the surface of the sphere to yield the luminosity in the line. The results of these calculations for individual embedded stars are given in Table 5.1 as a function of their effective stellar temperature for total hydrogen densities of 10^2, 10^3, and 10^4 cm^{-3}.

The total line emission from the star–forming complex was calculated by integrating over an ensemble of stars distributed according to the Scalo (1986) initial mass function (IMF) and which are assumed to have formed simultaneously, see Chapter 4 and Appendix C for details. The resultant ratio of S(1)/Brγ luminosities is dominated by the relatively short–lived massive stars (see Table 5.1). Consequently, its value is insensitive to the lower mass limit (m_l) of the IMF (decreasing by less than 20% as m_l is increased from 5 to 25 $M_\odot$), and to the evolutionary state of the region (assuming a constant rate of star formation). The S(1)/Brγ ratio is more responsive to alterations of the IMF upper mass limit (m_u), though even in these circumstances the variations are minor compared to those produced by adjustment of the gas density. The predicted S(1)/Brγ ratios for an unevolved burst and for several values of m_u and the gas density are given in Table 5.2.

5.2.2.2 *Model B : Clustered Stars*

In this model, the entire young stellar population is imagined to reside within a communal HII region. The covering factor of this region by molecular clouds is again assumed to be unity and the intensity of UV radiation incident upon them is governed by Eqn. 5.1. If the stars are tightly grouped near the centre of this region, then, for computa-

Table 5.1: Atomic (Brγ) and molecular (v=1–0 S(1)) line luminosities from embedded stars of effective temperature, T_{eff}, for photodissociation–zone gas densities of 10^2 – 10^4 cm^{-3}. (1.5(–2) means 1.5×10^{-2}.)

T_{eff} (10^3 K)	Line Luminosity (10^{20} W)			
	Brγ	v=1–0 S(1)		
		$n = 10^2$ cm^{-3}	$n = 10^3$ cm^{-3}	$n = 10^4$ cm^{-3}
8	1.34(–7)	5.49(–4)	1.37(–3)	1.67(–3)
8.5	1.57(–6)	3.47(–3)	1.00(–2)	1.37(–2)
9	3.53(–5)	3.22(–2)	1.07(–1)	1.59(–1)
9.4	2.67(–4)	1.44(–1)	5.35(–1)	9.20(–1)
9.5	3.78(–4)	2.21(–1)	9.20(–1)	1.83(0)
10	2.17(–3)	1.13(0)	6.27(0)	2.47(1)
11	2.28(–2)	6.40(0)	3.55(1)	1.66(2)
12	1.47(–1)	2.22(1)	1.23(2)	5.77(2)
13	8.08(–1)	6.64(1)	3.69(2)	1.72(3)
14	3.53(0)	1.88(2)	1.05(3)	4.88(3)
15	1.37(1)	4.60(2)	2.55(3)	1.19(4)
16	4.87(1)	1.06(3)	5.90(3)	2.76(4)
17	1.69(2)	2.65(3)	1.47(4)	6.87(4)
18	4.98(2)	5.31(3)	2.95(4)	1.38(5)
20	2.93(3)	1.65(4)	9.45(4)	4.29(5)
22.5	1.94(4)	5.77(4)	3.20(5)	1.50(6)
25	1.09(5)	1.79(5)	1.02(6)	4.77(6)
30	2.38(6)	1.29(6)	7.34(6)	2.98(7)
35	2.87(7)	5.82(6)	2.97(7)	1.04(8)
40	1.40(8)	1.59(7)	7.96(7)	2.58(8)
45	3.78(8)	3.11(7)	1.54(8)	5.11(8)
50	9.06(8)	5.25(7)	2.63(8)	8.52(8)

tional convenience, the relative total ionizing and non–ionizing UV photon fluxes can be characterised by an effective temperature (T_{eff}) set by the stellar mass function. Thus the intensity of incident UV radiation becomes :

$$\chi = 1.24 \times 10^{-14}\, \Theta(T_{eff}) \left(\frac{N_{LyC}}{s^{-1}}\right)^{1/3} R^{-2} \tag{5.2}$$

Values of the factor $\Theta(T_{eff})$ were derived by integrating the ionizing and non–ionizing UV photon fluxes over the mass–weighted ensemble of stars described in Section 5.2.2.1. These values are given in Table 5.3 along with the effective temperature of the radiation field (interpolated from Table C.1) for mass functions extending between $m_l = 4 - 13$ and $m_u = 30 - 100$ $M_\odot$. It is apparent from Eqn. 5.2 and Table 5.3 that, for this geometry, the UV intensity is fairly insensitive to both the total ionization rate and initial mass function. Total S(1) and Brγ luminosities for the cluster were derived in similar fashion to those for an individual star in model A. Their ratio is displayed in Table 5.4 assuming an effective UV temperature of 35,000 K and various values of the gas density, source–cloud separation, and integrated ionization rate. It is noted that the S(1)/Brγ ratios for these models are generally much smaller than those found using model A, unless the line–emitting clouds are dense and separated from the sources of UV radiation by more than one Strömgren radius. Their low value arises partly because the surface area to volume ratio (very roughly, the S(1) to Brγ ratio) of the communal HII region is considerably smaller than for the individual stars in Model A. Furthermore, and as a consequence, the non–ionizing UV field incident on the molecular clouds in Model B is much more intense and therefore the H_2 excitation efficiency is lower (see Fig. 5.1). The predicted line ratios increase dramatically if the UV radiation is diluted by increasing the size of the ionized region, and thus reproduction of a given ratio is very sensitive to the choice of cloud–source separation and gas density.

5.2.2.3 *Model C : H_2 Excitation in a Diffuse UV Field*

In the case of diffuse ultraviolet radiation, the UV–to–IR conversion efficiency tends to a maximum value. For the parameters adopted by BVD, one v=1–0 S(1) photon is produced for every 21 soft UV photons falling on the cloud. This figure is independent of the gas density provided that $\chi/n \lesssim 0.01$ cm^{-3}. The creation of a diffuse UV

Table 5.2: Predicted v=1–0 S(1)/Brγ ratios from model A, for several values of the IMF upper mass limit and total gas density in the photodissociation zone. A lower mass limit of 5 $M_\odot$ and source–cloud separation of $R = 1$ were assumed.

Density	Upper Mass Limit ($M_\odot$)		
(cm^{-3})	30	60	100
10^2	0.19	0.13	0.11
10^3	0.97	0.65	0.56
10^4	3.50	2.23	1.89

Table 5.3: Dependence of the relative non–ionizing and ionizing photon fluxes (Θ), and equivalent effective temperature of the radiation field (T_{eff}), for a mass–weighted ensemble of stars on the lower and upper limits of the initial mass function.

IMF Limits		Θ	T_{eff}
lower (m_l)	upper (m_u)		(10^3 K)
4	30	2.08	34
4	60	1.16	37
4	100	0.94	38
13	30	1.72	35
13	100	0.86	39

Table 5.4: Predicted S(1)/Brγ ratios from model B, showing the dependence on ionization rate (N_{LyC}), dimensionless source–cloud separation (R) and gas density, assuming an effective temperature for the radiation field of 35,000 K.

N_{LyC}	R	S(1)/Brγ		
		$n = 10^2$ cm^{-3}	$n = 10^3$ cm^{-3}	$n = 10^4$ cm^{-3}
10^{52}	1	0.02	0.09	0.41
10^{53}	1	0.01	0.04	0.19
10^{54}	1	<0.01	0.02	0.09
10^{53}	2	0.03	0.16	0.76
10^{53}	3	0.06	0.37	1.60

field is the natural result of increasing the cloud–source separation (R) in models A and B, for example by dispersion of the molecular material as the star–forming region evolves. For maximum excitation efficiency, the clouds need only be 3–10 pc from the stars dominating the emission (depending on stellar temperature) for a gas density of 10^4 cm^{-3}. This corresponds to $R > 1.5$ for 100 $M_\odot$ and $R > 3$ for 18 $M_\odot$ stars; the separation required being progressively larger for lower gas densities (factors of approximately 3 and 9 for n=10^3 and 10^2 cm^{-3}, respectively).

At peak efficiency, the S(1) emission is directly proportional to the incident ultraviolet flux (Fig. 5.1). Thus the S(1)/Brγ ratio, integrated over the star–forming region, is only dependent upon the effective temperature of the radiation field for this geometry :

$$\frac{S(1)}{Br\gamma} = 3.43\,\Theta(T_{eff}) \tag{5.3}$$

For stellar mass functions extending up to 30 or 100 $M_\odot$ (*i.e.* T_{eff} = 35,000 or 40,000 K), the values of $\Theta(T_{eff})$ in Table 5.3 give predicted line ratios of 6.2 and 2.7, respectively, assuming that all of the UV radiation impinges on molecular clouds. These ratios are markedly higher than those produced in other geometries, except for the high density case of model A which also verges on maximum UV–to–IR efficiency.

5.3 Comparison with Observations

5.3.1 New Near–Infrared Spectrophotometry

5.3.1.1 *Observational Techniques*

The 2-μm measurements were made with the 3.8m United Kingdom Infrared Telescope (UKIRT) on Mauna Kea, Hawaii, during 1986 March, October and December, and 1987 June, using the facility photometer/spectrometer UKT9 employing a circular variable filter (CVF). The spectral resolution at 2.17 μm was determined from observations of the Brγ line in the planetary nebulae NGC 6210 and NGC 3242 to be $\sim$2650 km s^{-1}. These observations also provided the wavelength calibration. All of the galaxies were

observed through a 19.6 arcsec aperture, with the exception of NGC 7714 for which a 12.4 arcsec aperture was used. The data were taken at wavelength steps corresponding to about 0.4 times the instrumental resolution. Typically, each scan consisted of 10s integrations at successive spectral points. Usually, eight such scans were coadded to produce the final spectrum, and resulting in a total integration time of 80s per spectral point.

To correct for the wavelength–dependent responses of the instrument and of the atmospheric transmission, the galaxy measurements were divided by the spectra of nearby stars with spectral types between about G8III and K4III, which exhibited no spectral features in the wavelength ranges observed. Flux calibration was performed by observations of nearby photometric standard stars, which were frequently spectral standards also. The absolute flux density of Vega was assumed to be 4.13×10^{-10} W m^{-2} μm^{-1} at 2.20 μm (Mountain *et al.* 1985). Comparison of the photometric standard stars used indicates the flux calibration to be accurate to within 10%. Further details concerning data reduction are given in Appendix A.

The observations were most commonly centred on the peak of the galaxian 2.2 μm emission, which permitted accurate photometry to be performed at consecutive CVF settings. The effects of seeing on an eccentric 2-μm peak would result in a dramatic increase in the uncertainty on the level of the strong continuum, thus making measurement of the weak lines impossible. The pointing was checked using 2 or 3 nearby SAO stars and the quoted positions are therefore accurate to within $\sim$1–2 arcsec. Occasionally, the aperture was positioned on the high–resolution radio–continuum peak or on the optical peak; the latter being estimated from the television guider screen.

5.3.1.2 *Observational Results*

In Table 5.5 results of the observations of nearby IR–bright spiral galaxies are presented. All of the spirals have *IRAS* 25-μm flux densities $S_{25} \gtrsim 1.5$ Jy, and represent a subset of the complete sample of such systems being observed as part of a long–term programme at UKIRT. In addition, except for NGC 613, all of the galaxies in this Table have optical spectra which are indicative of a dominant population of young stars. In the

Table 5.5: Results of new large–aperture 2-μm spectrophotometric observations of star–forming galaxies.

Name	Aperture Position		Aper.	Line Flux (10^{-17} W m^{-2})	
	RA (h,m,s)	DEC (°,′,″)	ID	Brγ	1–0 S(1)
NGC 278	00 49 14.8	+47 16 44.8	O	1.8 ± 0.4	1.0 ± 0.3
NGC 613	01 31 59.7	−29 40 28.5	O	5.4 ± 0.8	4.7 ± 1.5
NGC 2782	09 10 53.6	+40 19 15.0	R	4.7 ± 0.7	2.8 ± 0.7
NGC 2964	09 39 56.7	+32 04 34.4	R	1.2 ± 0.3	< 1.2
NGC 3310	10 35 40.0	+53 45 48.8	K	8.5 ± 0.6	< 2.1
NGC 3351	10 41 23.0	+11 58 15.3	O	8.1 ± 1.2	3.8 ± 0.7
NGC 3690	11 25 40.6	+58 50 13.1	K	13.6 ± 0.5	6.3 ± 1.1
IC 694	11 25 43.6	+58 50 14.7	K	9.5 ± 1.0	8.7 ± 0.6
NGC 4527	12 31 35.4	+02 55 46.4	K	6.2 ± 1.2	5.9 ± 1.0
NGC 4536	12 31 53.4	+02 27 48.0	K	8.0 ± 0.6	4.6 ± 0.5
NGC 4691	12 45 39.4	−03 03 37.2	K	3.7 ± 0.5	3.2 ± 1.0
NGC 5236	13 34 11.1	−29 36 41.3	K	20.8 ± 1.6	8.1 ± 1.7
NGC 5713	14 37 37.6	−00 04 31.9	K	3.5 ± 0.2	1.8 ± 0.2
NGC 7714	23 33 40.3	+01 52 35.7	K	5.0 ± 0.7	< 1.8

References to optical spectra : NGC 278 — Heckman, Balick & Crane 1980; NGC 613 — Véron–Cetty & Véron 1986; NGC 2782 — Heckman *et al.* 1983; NGC 2964 — Keel *et al.* 1985; NGC 3310 — Heckman, Balick & Crane 1980; NGC 3351 — Keel 1983; NGC 3690 and IC 694 — Augarde & Lequeux 1985; NGC 4527 — Véron–Cetty & Véron 1986; NGC 4536 — Keel 1983; NGC 4691 — Keel 1983; NGC 5236 — Véron–Cetty & Véron 1986; NGC 5713 — Véron–Cetty & Véron 1986; NGC 7714 — Keel *et al.* 1985.

case of NGC 613, the optical spectrum is "composite", *i.e.* the emission lines indicate excitation conditions in the central region which are intermediate between those found in Seyfert nuclei and those in HII regions. However, the infrared line fluxes measured through the large ($20\widehat{''}$) aperture are considerably greater than those found by Moorwood & Oliva (1988; hereinafter MO88) in a $6\widehat{''} \times 6\widehat{''}$ beam, which can be interpreted as evidence for extended star formation around an active nucleus. Therefore, this galaxy has been included in the sample of star–forming systems. The columns in Table 5.5 are :

1. Galaxy name.
2. & 3. Position of the aperture (1950 co–ordinates).
4. Aperture identification, *i.e.* 2-μm peak (K), radio (R) or optical (O) nucleus.
5. & 6. Integrated fluxes (and 1σ uncertainties) in the v=1–0 S(1) transition of H_2 (λ=2.122μm) and Brγ hydrogen recombination line (λ=2.167μm).

References to the optical spectra used to identify the galaxies as predominantly star–forming are given beneath Table 5.5.

5.3.2 Description of the Sample

In Table 5.6 the results of the new observations are listed, together with data taken from the literature for galaxies whose optical spectra are dominated by HII regions and which have measured v=1–0 S(1) and Brγ fluxes. The galaxies NGC 1365 and 1808 have composite optical spectra and have been treated similarly to NGC 613, above, since the measured fluxes from Chapter 4 are much greater than those obtained by Kawara, Nishida & Gregory (1987; hereinafter KNG87) and MO88 through a small aperture. The columns in Table 5.6 are :

1. Galaxy name.
2. Distance in Mpc (H_0 = 75 km s^{-1} Mpc^{-1} is adopted throughout).
3. Ratio of v=1–0 S(1)/Brγ, and 1σ uncertainty. For non–detections, the 3σ upper limit is assumed.

Table 5.6: Observed properties for the sample of 28, predominantly star–forming, galaxies.

Name	Distance (Mpc)	$S(1)/Br\gamma$	Beam Area $(\text{kpc})^2$	N_{LyC} (s^{-1})	Ref.
NGC 253	3.4	< 0.34	0.01	3.1×10^{52}	a^*
		0.62 ± 0.04	0.01	1.9×10^{52}	b
NGC 278	12	0.56 ± 0.21	1.1	2.4×10^{52}	c^*
NGC 613	20	0.87 ± 0.31	2.8	1.7×10^{53}	c^*
		1.29 ± 0.48	0.3	5.2×10^{52}	b
NGC 986	26	0.43 ± 0.13	0.4	1.3×10^{53}	d
NGC 1365	20	0.38 ± 0.05	2.8	7.2×10^{53}	e^*
		0.40 ± 0.09	0.3	1.5×10^{53}	d
		0.67 ± 0.21	0.3	1.1×10^{53}	b
NGC 1614	60	0.20 ± 0.04	2.0	2.0×10^{54}	b
		0.55 ± 0.10	26.6	—	f^*
NGC 1808	10	0.44 ± 0.04	0.8	2.1×10^{53}	e^*
		0.34 ± 0.07	0.07	5.6×10^{52}	d
		0.82 ± 0.25	0.08	4.6×10^{52}	b
NGC 2782	34	0.60 ± 0.17	8.6	5.0×10^{53}	c^*
NGC 2964	17	< 1.0	2.0	3.2×10^{52}	c
NGC 3034	3.3	< 0.18	0.01	2.2×10^{52}	a
		$0.1 - 0.8$	0.01	—	g^*
NGC 3310	14	< 0.25	1.5	1.5×10^{53}	c
NGC 3351	9	0.47 ± 0.11	0.6	6.0×10^{52}	c
NGC 3504	20	0.71 ± 0.05	2.8	2.5×10^{53}	e^*
NGC 3690	43	0.46 ± 0.14	13.9	2.3×10^{54}	c
		0.64 ± 0.15	15.6	1.7×10^{54}	h
		1.12 ± 0.27	39.5	4.4×10^{54}	h^*
IC 694	43	0.92 ± 0.12	13.9	1.6×10^{54}	c

Table 5.6: (cont.)

Name	Distance (Mpc)	$S(1)/Br\gamma$	Beam Area $(\mathrm{kpc})^2$	N_{LyC} (s^{-1})	Ref.
NGC 4102	13	0.69 ± 0.11	1.3	9.2×10^{52}	e
NGC 4527	22	0.95 ± 0.24	3.5	2.8×10^{53}	c
NGC 4536	23	0.67 ± 0.12	3.8	4.0×10^{53}	c, e^*
NGC 4691	13	0.86 ± 0.29	1.3	5.8×10^{52}	c
NGC 5236	3.7	0.33 ± 0.08	0.1	2.5×10^{52}	c, e^*
		< 0.34	0.01	3.7×10^{51}	b
NGC 5253	4	< 0.16	0.08	2.2×10^{52}	d
		< 0.11	0.01	1.3×10^{52}	b
NGC 5713	25	0.51 ± 0.07	4.5	2.0×10^{53}	c
NGC 6810	24	1.5 ± 0.6	0.5	6.4×10^{52}	b
NGC 6946	10	0.52 ± 0.13	0.8	5.6×10^{52}	e
NGC 7552	20	0.48 ± 0.06	0.3	2.4×10^{53}	d
		0.35 ± 0.08	0.3	3.1×10^{53}	b
NGC 7714	40	< 0.36	4.6	7.4×10^{53}	c
		< 0.33	1.4	4.4×10^{53}	b
He 2–10	6	0.20 ± 0.05	0.02	1.5×10^{52}	d
		0.15 ± 0.03	0.03	3.1×10^{52}	b
IIZw40	10	0.30 ± 0.11	0.08	6.2×10^{52}	b

(a) Rieke *et al.* 1980; (b) Moorwood & Oliva 1988; (c) This work; (d) Kawara, Nishida & Gregory 1987; (e) Chapter 4; (f) Joseph *et al.* 1987; (g) Lester *et al.*, cited by Telesco 1988; (h) Fischer *et al.* 1983.

4. Projected beam area on galaxy in $(\mathrm{kpc})^2$.

5. Ionization rate, calculated assuming a photon ratio of $N_{LyC}/N_{Br\gamma} = 70$. No corrections for extinction at $2.2\,\mu$m were applied, and thus the ionization rate is a lower limit.

6. References to the sources of data.

The references to data taken from the literature are given beneath Table 5.6. Notes concerning individual galaxies are indicated by an asterisk in column 6 and detailed below :

NGC 253 : The H_2 emission appears to be shock excited (G.S. Wright, personal communication), but the ratio $S(1)/Br\gamma$ increases with radial distance from the nucleus. There is a discrepancy between the Brγ observation by Rieke *et al.* (1980), taken using a Fourier transform spectrometer, and that of MO88 using a grating spectrometer. The latter measurement is adopted due to its higher precision.

NGC 278 : The detection of molecular hydrogen emission is marginal, but observations at the wavelengths of the discriminant lines v=1–0 S(0) and 2–1 S(1) suggests it may be fluorescent.

NGC 613 : Measurements of the discriminant H_2 lines made at the same time as v=1–0 S(0) and Brγ, show that the gas is radiatively excited.

NGC 1365 : The H_2 emission sampled through the large aperture is fluorescent (Chapter 4). This galaxy contains an active nucleus (*e.g.* Edmunds & Pagel 1982) which may affect the measurements made with smaller beams, although there is no evidence for any variation in the $S(1)/Br\gamma$ ratio. The Brγ line measured in a small beam by KNG87 was velocity resolved ($\Delta V = 1500 \pm 380$ km s^{-1}).

NGC 1614 : The large aperture line flux ratio was measured from the spectrum by Joseph *et al.* (1987). A conservative error, reflecting uncertainty in the level of the continuum, was assigned. In this spectrum, the brighter

feature seen in the wavelength range 2.25 – 2.3 μm may be the blended lines v=1–0 S(0) and v=2–1 S(1) of H_2, and are at a level indicative of fluorescent excitation. There is a significant (3σ) increase in the $S(1)/Br\gamma$ ratio with aperture.

NGC 1808 : The H_2 emission sampled through the $20\widehat{''}$ aperture is fluorescent. This galaxy contains an active nucleus (*e.g.* Véron–Cetty & Véron 1985) and the Brγ line measured by KNG87 was velocity resolved ($\Delta V = 1100 \pm 190$ km s^{-1}). The small aperture measurements may therefore be affected by the central source. There is marginal evidence for variation in the $S(1)/Br\gamma$ ratio with aperture.

NGC 2782 : Observation of the discriminant H_2 lines are suggestive of radiative excitation, but this result is tentative since insufficient continuum measurements were made.

NGC 3034 : (M82) Observations taken along the major axis indicate a low ratio $S(1)/Br\gamma \simeq 0.1$ within the central $20\widehat{''}$, but much larger values exterior to this (0.5 – 0.8). The relatively strong S(1) emission appears shock–excited and is coincident with the peaks of the ^{12}CO J=1–0 emission (Nakai *et al.* 1987; Lester *et al.* quoted in Telesco 1988).

NGC 3504 : The H_2 emission is fluorescent. The galaxy contains a compact radio continuum source (Condon *et al.* 1982). Its optical spectrum resembles that of an HII region although there is some suggestion of contribution from a LINER component (Heckman *et al* 1983, and references therein).

NGC 3690 : Observations made through the largest aperture ($34\widehat{''}$) sample the emission from both NGC 3690 and its companion, IC694.

NGC 4536 : The adopted line fluxes are the average of the two independent measurements. The H_2 emission is fluorescent (Chapter 4).

NGC 5236 : The adopted line fluxes, for the $20\widehat{''}$ beam, are the average of the two independent measurements. The H_2 emission is fluorescent (Chapter 4).

5.3.3.1 *The H_2 Excitation Mechanism*

Prior to comparing the models of fluorescent H_2 emission with observations, it is necessary to investigate whether this is in fact the dominant excitation mechanism. In Figure 5.3 the Brγ and v=1–0 S(1) fluxes for the galaxies listed in Table 5.6 are plotted, together with similar data for several systems in which the H_2 appears to be shock–excited. A typical error bar representing 20% uncertainty in the line flux is shown, as is a vector illustrating the effect on the S(1)/Brγ ratio (*not* the individual line strengths) of 10 magnitudes of visual extinction. Since the lines are close in wavelength, the effects of dust are negligible : $A_V = 10$ amounts to a differential extinction between Brγ and S(1) of only 0.05 mag, using the reddening law by Rieke & Lebofsky (1985).

In Fig. 5.3 the star–forming galaxies display a tendency for the S(1) emission to increase with the Brγ line strength (*c.f.* the shock–excited systems). This is contrary to the conclusions by Fischer *et al.* (1987) and DePoy (1987). This contradiction is probably due to their inhomogeneous, and smaller, samples. Fig. 5.3 indicates a close association between extragalactic molecular hydrogen line emission and star formation.

Aside from NGC 613, the seven galaxies identified in Chapter 4 as possessing radiatively excited molecular hydrogen, and NGC 253 which probably contains shock–excited gas, the discriminant H_2 lines have not been measured in the "normal" spirals and consequently no definitive statement concerning the excitation mechanism in the rest of the sample can be made. However, galaxies in which the molecular hydrogen has been found to be shock–excited, generally exhibit large ratios of $S(1)/Br\gamma$: NGC 1275, 3079, 6240 and Arp 220 have ratios of >2.7, $\sim$ 4, >5.6–21, and 2.4 respectively (Fischer *et al.* 1987; Hawarden *et al.* 1988, in preparation; Joseph, Wright & Wade 1984; DePoy, Becklin & Wynn–Williams 1986; Lester, Harvey & Carr 1988), although the ratio in NGC 1068 is $\sim$1 (Thompson *et al.* 1978; Hall *et al.* 1981). In addition, the ratio of $S(1)/Br\gamma$ in shock–excited galactic sources is generally much greater than unity : for example, at OMC1 peak 1, Burton *et al.* (1988) measure a ratio of $\sim$10,

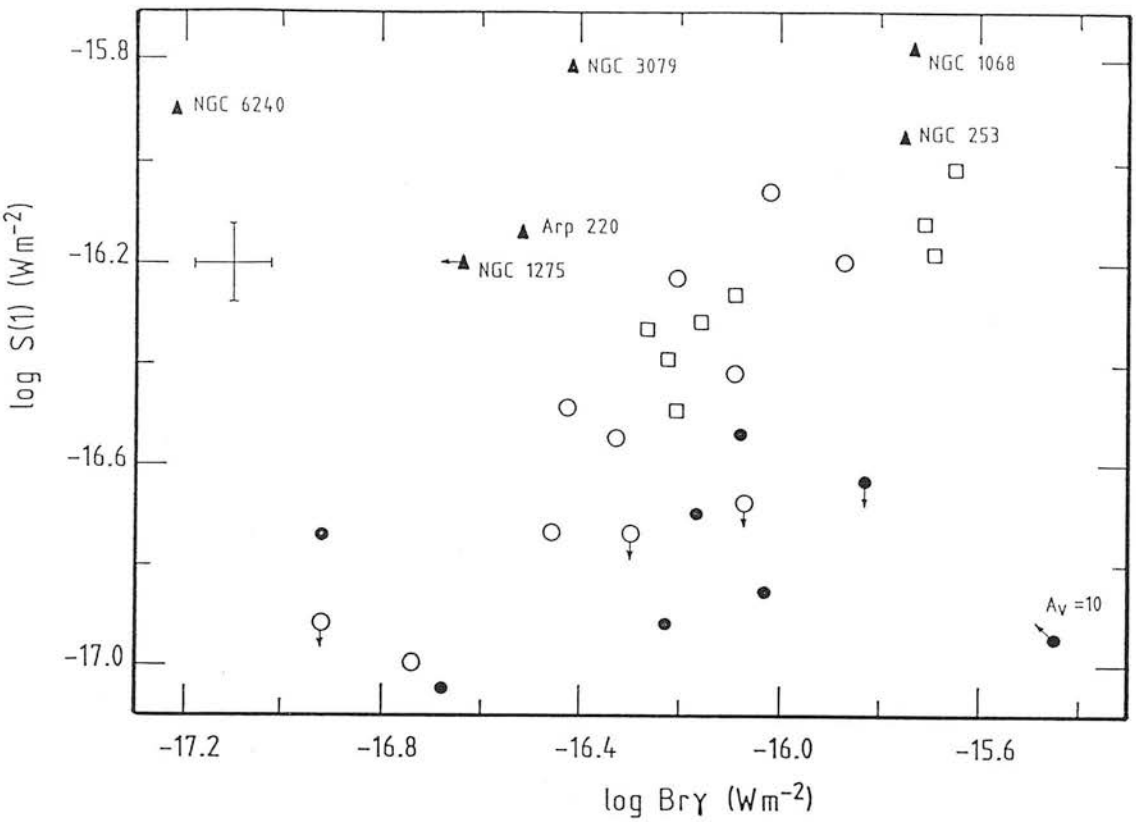

Figure 5.3: Observed Brγ and v=1–0 S(1) fluxes for the sample of star–forming galaxies : open circles — new results from Chapters 4 and 5; open squares — new results for which measurements of several H_2 lines suggest radiative excitation; filled circles — data taken from the literature. Several galaxies thought to contain shock–excited H_2 are represented by filled triangles. The error bar corresponds to 20% uncertainty in the line fluxes and the vector shows the effect of 10 magnitudes of visual extinction on their ratio.

whilst in the supernova remnant IC443 they find $S(1)/Br\gamma > 30$.

The sample galaxies generally possess low values of the S(1)/Brγ ratio and display a relatively small scatter suggestive of a common excitation mechanism. Given the inferred dominance of radiative excitation in eight out of nine nearby spirals in which the mechanism has been identified, it is therefore proposed that the integrated S(1) emission from star–forming galaxies be attributed to pumping by UV radiation. Hence comparison of the observational data with the fluorescent models will test if this assertion is a self–consistent physical description of the H_2 excitation.

To illustrate better the S(1)/Brγ ratio and the variation therein, Fig. 5.4 presents the observed line ratio as a function of the projected beam area on the galaxy. In this diagram, the horizontal lines indicate 1σ uncertainties, and multi–aperture measurements are connected via dashed lines. The galaxies exhibiting S(1)/Brγ ratios in the range 0.4–0.9, which comprise the majority of the sample, are considered first and their values compared with those predicted by the three models.

5.3.3.2 *Galaxies With Ratios S(1)/Br$\gamma \simeq$ 0.4–0.9*

Ratios in the range 0.4–0.9 are easily reproduced by model A (embedded stars) if the galaxies possess stellar mass functions extending above 30 $M_\odot$ and gas densities within the photodissociation zones of approximately 10^3 cm^{-3} (see Table 5.2). Lower density regions cannot contribute significantly to the total emission since their UV–to–IR efficiencies, and thus S(1)/Brγ ratios, are too low. This conclusion is consistent with that by Crawford *et al.* (1985) who argue for $n > 10^3$ cm^{-3} in photodissociation zones, from comparison of the [CII]λ158 μm emission and infrared energy density. The enhanced H_2 excitation efficiency in gas much denser than 10^3 cm^{-3} (see Fig. 5.1) precludes the dominance of such regions, provided that the stars remain embedded within the molecular clouds. Gas densities up to about 10^4 cm^{-3} are permitted if the evolution of the stars causes cloud disruption, or, equivalently, if the stars are born close to the edge such that their HII regions constitute "blisters" on the surface. In such a case, large fractions of the non–ionizing UV emission may escape into the surrounding interstellar medium. The morphology then resembles that of model C. At

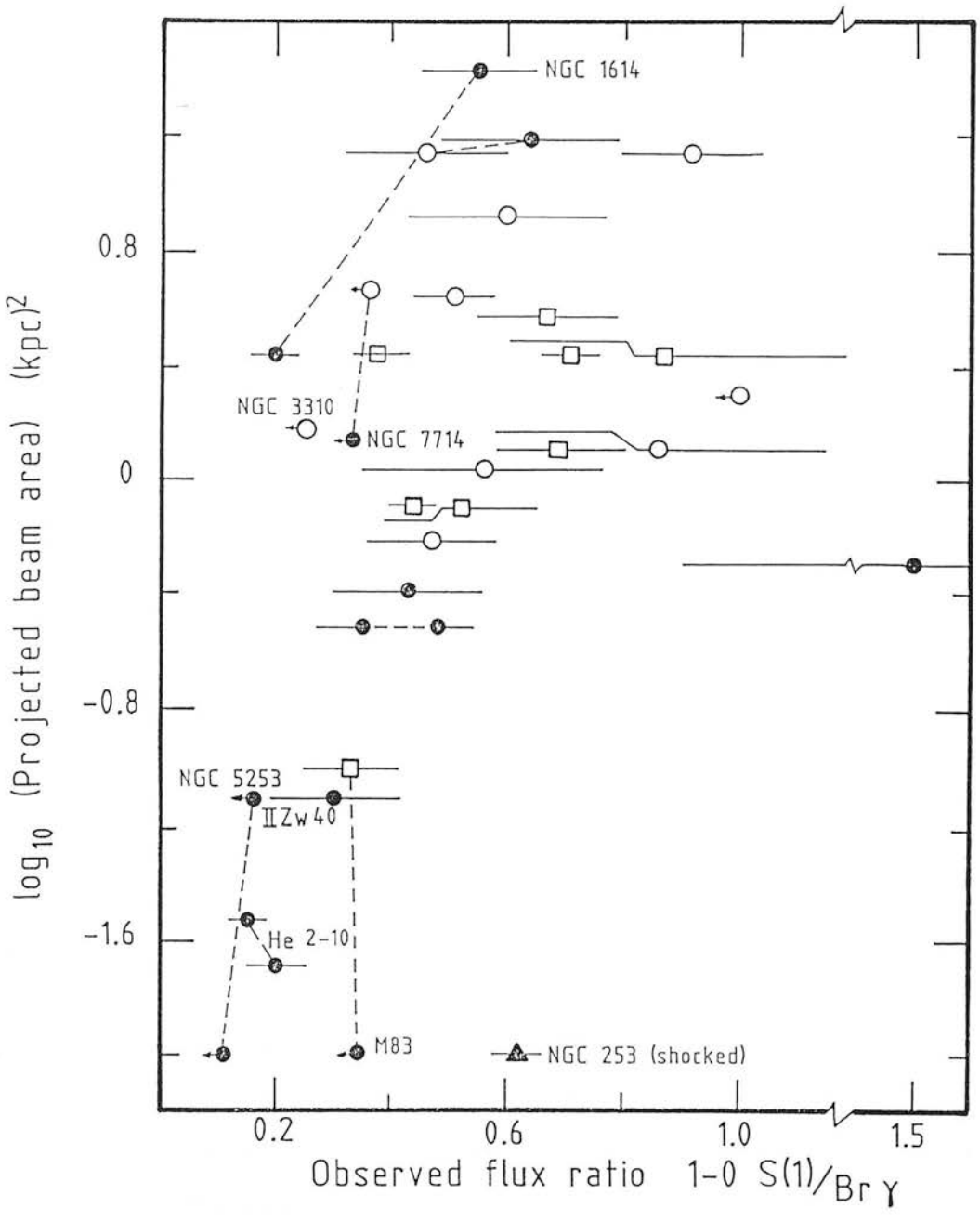

Figure 5.4: Ratio of observed S(1)/Brγ fluxes plotted as a function of the projected beam area on the target. The symbols are as in Figure 5.3.

first sight it might seem that this diffuse UV radiation creates an even larger S(1)/Brγ ratio (*c.f.* §5.2.2.3). However, the presence of dust in the intercloud medium may absorb the 'excess' UV photons. If one takes the extreme case and assumes that all HII regions exist as blisters on cloud surfaces, then for a photodissociation–zone gas density of 10^4 cm^{-3} and an upper mass limit of 60 $M_\odot$, more than half of the soft UV radiation must be absorbed by dust to produce the typical observed S(1)/Brγ ratio. This fraction obviously decreases as the morphology tends to that of model A. In the case of complete disruption of the parent molecular clouds, a high effective temperature of the radiation field (*i.e.* relatively high lower and upper IMF limits) is favoured since it creates a relatively low line ratio, unless the dust content of the intercloud medium is considerable.

Examination of Table 5.4 suggests that a large, central, cluster of stars cannot readily reproduce the typical S(1)/Brγ ratio. Displacement of the molecular clouds to further distances from the sources of UV radiation would increase the excitation efficiency and H_2 luminosity, but, as noted above, the resultant line ratio is very sensitive to the separation and gas density. To construct a line ratio in the range 0.4–0.9 employing model C requires cloud–source separations of 0.1–0.15 kpc ($n = 10^4$ cm^{-3}) or 0.2–0.4 kpc ($n = 10^3$ cm^{-3}). It seems unreasonable to assume that all of the galaxies with S(1)/Brγ ratios in this range and which are, presumably, at various stages in their evolution, should possess such restricted combinations of density–distance parameters. This result has important implications, for it is precisely this cloud–source configuration that is implicitly assumed when the galaxian extinction due to dust is inferred from measurements of two hydrogen recombination lines. As emphasized in Appendix B, if the dust is not entirely foreground (*i.e.* model C) but, instead, is distributed amongst the ionizing sources then the total extinction, and consequently the inferred total ionization rate, may be severly underestimated.

5.3.3.3 *Galaxies With Ratios S(1)/Brγ<0.4*

Now consider the galaxies which exhibit unusually small values of the S(1)/Brγ ratio. The fluorescent models discussed above predict relatively low line ratios when $\chi/n > 1$, that is, when the UV field is intense or the gas density low ($n \lesssim 100$ cm^{-3}, in the case of

model A). The latter suggestion is inconsistent with the density estimates by Crawford *et al.* (1985). Their measurement of collisionally–excited C^+ emission from M83, which displays $S(1)/Br\gamma \simeq 0.3$, indicates the density of gas in the photodissociation zones is likely to be greater than 10^3 cm^{-3}. However, M83 presents rather a special case since analysis of the infrared recombination line and thermal radio continuum emission from the central star–forming region suggests that the hydrogen line strengths are enhanced due to Balmer, in addition to the usual Lyman, continuum ionization in young HII regions (Turner, Ho & Beck 1983). Consequently, the observed $S(1)/Br\gamma$ ratio of this galaxy may be artificially depressed.

In regions of recent star formation, the S(1) emission might be expected to be relatively low because of the intensity of UV radiation incident on molecular clouds. However, the rapidity with which the radius of an ionized region tends to the Strömgren radius makes this argument unconvincing for individual stars or small clusters. For example, assuming a gas density of 10^3 cm^{-3} and a target line ratio of $S(1)/Br\gamma = 0.2$, model A requires geometrical dilution of the UV radiation characterised by $R \simeq 0.5$. Simple consideration of the expansion of an ionization front in a medium of this density (*e.g.* Dyson & Williams 1980), would imply an age less than 100 yr.

A large cluster of stars, such as that represented by model B, can more readily produce low $S(1)/Br\gamma$ ratios, as shown in Table 5.4. A similar configuration has been suggested for NGC 5253 by Aitken *et al.* (1982) from analysis of its high–excitation [SIV] emission. The absence in this galaxy of the narrow 8.7 and 11.3 μm emission features is unusual for systems experiencing episodes of active star formation (*e.g.* Roche & Aitken 1985). This may indicate exceptionally intense UV radiation, which can destroy the small particles responsible for these emission features, and the resulting low H_2 excitation efficiency would be consistent with the low upper limits to the S(1) flux. A similar situation may pertain to IIZw40 in which the narrow emission features are also absent (P. Roche, personal communication). The explanation may not be this straightforward, however, since mid–IR spectra of several other galaxies having weak H_2 lines show emission at 11.3 μm and the lower–excitation [NeII] line.

One further factor to be considered is metallicity, since this affects the dust content. For galaxies with low $S(1)/Br\gamma$ ratios, the oxygen abundance varies from

about one–tenth (NGC 5253 and IIZw40; Gonzáles–Riestra, Rego & Zamorano 1987; Arnault *et al.* 1988) through approximately one half (NGC 3310, 7714 and He 2–10; Hunter, Gallagher & Rautenkratz 1982; French 1980; Johansson 1987) to slightly more than the solar value (M83; Dufour *et al.* 1980). However, the influence of this diversity is unclear. BVD demonstrate that decreasing the dust content enhances the H_2 line intensity, since fewer UV photons are absorbed by grains, but the extent to which this is offset by a lowering of the H_2 formation efficiency is uncertain (see also S88). Indeed, it is possible that, in some instances, the relatively weak S(1) emission from vigorous nuclear star–forming complexes results from a reduced H_2 formation rate on warm dust grains. This picture may account for the low S(1)/Brγ ratios in the compact regions in NGC 7714 and He 2–10.

The discussion above illustrates the dependence of the molecular and atomic hydrogen emission on geometry and the H_2 excitation conditions. Further progress in understanding the emission from these regions requires mapping in several lines to be performed, to determine the H_2 excitation mechanism and the spatial distribution of molecular clouds and stars.

5.4 Conclusions

Models of vigorous star–forming regions have been constructed. These allow investigation of the factors affecting the observed ratio of molecular (v=1–0 S(1)) to atomic (Brγ) hydrogen line emission. Of dominant importance is the morphology of the region which determines the dilution of the ultraviolet radiation, and, together with the gas density, controls the efficiency with which H_2 is radiatively excited.

The measured S(1)/Brγ ratios in a sample of star–forming galaxies show relatively little scatter, compared with systems in which the molecular hydrogen appears to be shock–excited. Since the S(1) emission from several of the former has been shown to be fluorescent, it is asserted that this mechanism is common to galaxies undergoing vigorous star formation.

Most systems have S(1)/Brγ ratios in the range 0.4–0.9. These ratios are readily reproduced by a model comprising molecular clouds of density 10^3–10^4 cm^{-3} surrounding Strömgren spheres of ionized hydrogen and illuminated by individual hot stars at their centres. For gas at the upper end of the density range, the dominant emitting regions are likely to constitute blisters on the cloud surfaces and significant fractions of the non–ionizing UV radiation must be absorbed by dust in the intercloud medium. Compact clusters comprising many massive stars have difficulty in reproducing these line ratios.

A number of galaxies exhibit very small S(1)/Brγ line ratios. For several of these, at least, the ratios appear to be caused by unusually intense UV radiation, probably generated by a large compact cluster of hot stars.

Acknowledgements

Peter Brand, Pat Roche and Toby Moore are acknowledged for invigorating discussions on the excitation of molecular hydrogen in the interstellar medium. As usual, all of the staff, and particularly the telescope operators (Joel Aycock, Dolores Walther, and Thor Wold), of UKIRT are thanked for making these observations possible. Marjorie Fretwell is also thanked for the diagrams.

References

Aitken, D.K., Roche, P.F., Allen, M.C. & Phillips, M.M., 1982. *Mon. Not. R. astr. Soc.*, **199**, 31P.

Arnault, P., Casoli, F., Combes, F. & Kunth, D., 1988. *Astr. Astrophys.*, in press.

Augarde, R. & Lequeux, J., 1985. *Astr. Astrophys.*, **147**, 273.

Black, J.H. & van Dishoeck, E.F., 1987. *Ap. J.*, **322**, 412. 'BVD'.

Burton, M.G., Geballe, T.R., Brand, P.W.J.L. & Webster, A.S., 1988. *Mon. Not. R. astr. Soc.*, **231**, 617.

Condon, J.J., Condon, M.A., Gisler, G. & Puschel, J.J., 1982. *Ap. J.*, **252**, 102.

Crawford, M.K., Genzel, R., Townes, C.H. & Watson, D.M., 1985. *Ap. J.*, **291**, 755.

DePoy, D.L., Becklin, E.E. & Wynn–Williams, C.G., 1986. *Ap. J.*, **307**, 116.

DePoy, D.L., 1987. *Ph.D. Thesis*, University of Hawaii.

Draine, B.T., 1978. *Ap. J. Suppl.*, **36**, 595.

Dufour *et al.*, 1980. *Ap. J.*, **236**, 119.

Dyson, J.E. & Williams, D.A., 1980. *Physics of the Interstellar Medium*, Manchester University Press, Manchester.

Edmunds, M.G. & Pagel, B.E.J., 1982. *Mon. Not. R. astr. Soc.*, **198**, 1089.

Fischer, J., Geballe, T.R., Smith, H.A., Simon, M. & Storey, J.W.V., 1987. *Ap. J.*, **320**, 667.

French, 1980. *Ap. J.*, **240**, 41.

González–Riestra, R., Rego, M. & Zamorano, J., 1987. *Astr. Astrophys.*, **186**, 64.

Hall, D.N.B., Kleinmann, S.G., Scoville, N.Z. & Ridgway, S.T., 1981. *Ap. J.*, **248**, 898.

Hawarden, T.G., Wade, R., Israel, F.P. & Geballe, T.R., 1988. In preparation.

Hayashi, M., Hasegawa, T., Gatley, I., Garden, R. & Kaifu, N., 1985. *Mon. Not. R. astr. Soc.*, **215**, 31P.

Heckman, T.M., Balick, B. & Crane, P.C., 1980. *Astr. Astrophys. Suppl.*, **40**, 295.

Heckman, T.M., van Breugel, W., Miley, G.K. & Butcher, H.R., 1983. *Astron. J.*, **88**, 8.

Hummer, D.G. & Storey, P.J., 1987. *Mon. Not. R. astr. Soc.*, **224**, 801.

Hunter, D.A., Gallagher, J.S. & Rautenkratz, R., 1982. *Astrophys. J. Suppl.*, **49**, 53.

Israel, F.P., Hawarden, T.G., Wade, R., Geballe, T.R. & van Dishoeck, E.F., 1988. *Mon. Not. R. astr. Soc.*, in press.

Israel, F.P. & Koornneef, J., 1988. *Astr. Astrophys.*, **190**, 21.

Johansson, L., 1987. *Astr. Astrophys.*, **182**, 179.

Joseph, R.D., Wright, G.S. & Wade, R., 1984. *Nature*, **311**,132.

Joseph, R.D., Wright, G.S., Wade, R., Graham, J.R., Gatley, I. & Prestwich, A.H., 1987. In *Star Formation in Galaxies*, p.421, ed. Persson, C.J., US Govt. Print. Off., Washington, DC.

Kawara, K., Nishida, M. & Gregory, B., 1987. *Ap. J.*, **321**, L35. 'KNG87'

Keel, W.C., 1983. *Astrophys. J. Suppl.*, **52**, 229.

Keel, W.C., Kennicutt, R.C., Hummel, E. & van der Hulst, J.M., 1985. *Astron. J.*, **90**, 708.

Kurucz, R.L., 1979. *Astrophys. J. Suppl.*, **40**, 1.

Landolt–Börnstein 1982. *Astronomy & Astrophysics*, **2b**, Stars & Star Clusters. Eds. Schiaffers, K. & Voigt, H.H.

Lester, D.F., Harvey, P.M. & Carr, J., 1988. *Ap. J.*, **329**, 641.

Moorwood, A.F.M. & Oliva, E., 1988. *Astr. Astrophys.*, **203**, 278. 'MO88'

Mountain, C.M., Leggett, S.K., Selby, M.J., Blackwell, D.E. & Petford, A.D., 1985. *Astr. Astrophys.*, **151**, 399.

Nakai, N., Hayashi, M., Handa, T., Sofue, Y. & Hasegawa, T., 1987. *Pub. A.S.J.*, **39**, 685.

Rieke, G.H. & Lebofsky, M.J., 1985. *Ap. J.*, **288**, 618.

Rieke, G.H., Lebofsky, M.J., Thompson, R.I., Low, F.J. & Tokunaga, A.T., 1980. *Ap. J.*, **238**, 24.

Roberge, W.G., & Dalgarno, A. & Flannery, B.P., 1981. *Ap. J.*, **243**, 817.

Roche, P.F. & Aitken, D.K., 1985. *Mon. Not. R. astr. Soc.*, **213**, 789.

Scalo, J.M., 1986. *Fund. Cosm. Phys.*,**11**, 1.

Shull, J.M. & Beckwith, S., 1982. *Ann. Rev. Astr. Astrophys.*, **20**, 163.

Sternberg, A., 1986. *Ph.D. Thesis*, Columbia University.

Sternberg, A., 1988. *Ap. J.*, **332**, 400. 'S88'

Telesco, C.M., 1988. *Ann. Rev. Astr. Astrophys.*, **26**, 343.

Thompson, R.I., Lebofsky, M.J. & Rieke, G.H., 1978. *Ap. J.*, **222**, L49.

Turner, J.L., Ho, P.T.P. & Beck, S.C., 1987. *Ap. J.*, **313**, 644.

Véron–Cetty, M.–P. & Véron, P., 1985. *Astr. Astrophys.*, **145**, 425.

Véron–Cetty, M.–P. & Véron, P., 1986. *Astr. Astrophys. Suppl.*, **66**, 335.

Chapter 6

Detection of H53α Emission from M82 : A Reliable Measure of the Ionization Rate and its Implications

Preface : One of the recurring themes in this thesis has been the importance of the geometry of the star–forming region, not just in its control of the molecular gas excitation, described in the preceeding chapter, but also the way in which it may modify the observed emission via distribution of the extinction. To circumvent the problems posed by the latter when determining the intrinsic ionization rate from optical or near–IR recombination lines, a long (mm-) wavelength hydrogen line from the archetypal starburst galaxy M82 was measured. The results demonstrate the strong constraints that may be placed on the properties of extragalactic star–forming regions once reliable measurements become available. This work was performed in collaboration with colleagues both in Edinburgh and in Japan, and has been submitted for publication : Puxley, Brand, Moore, Mountain, Nakai & Yamashita, 1988. Submitted to *Ap. J.*

Summary

Emission in the hydrogen recombination line H53α has been detected, for the first time, in another galaxy : the nearby 'starburst' system M82. This line is produced primarily by spontaneous emission and provides the most direct, extinction independent, estimate of the ionization rate in the star–forming complex. The line strength implies an ionization rate of 1.1×10^{54} s^{-1}, approximately 5 times larger than that inferred from Brα observations, and indicates a dust extinction at 4 μm of more than 1 mag ($A_V \simeq 27$ mag). Comparison of the 3.3-mm free–free continuum and H53α fluxes implies an average electron temperature of $T_e \sim 5 \times 10^3$ K. Analysis of the line excitation conditions,

using the H53α emission in conjunction with that in the far–IR O^{2+} and N^{2+} forbidden lines, together with the IR luminosity, suggests that only a very restricted range of stellar masses are formed. Less plausible explanations are that (i) approximately two thirds of the direct stellar emission escapes from the central $40''$ without encountering dust, or (ii) much of the line emission and IR luminosity arises via fast ($\sim$100 km s^{-1}) shocks.

6.1 Introduction

The galaxy M82 has been well–studied throughout the observable electromagnetic spectrum due to its propinquity. Infra–red observations, which are less affected by the heavy extinction within this edge–on system, have been instrumental in revealing that the IR luminosity of the galaxy is dominated by a population of young stars in the central regions; see Telesco (1988) for a review. However, even in the near–IR, attenuation by dust cannot be ignored. In this chapter, the first detection of another galaxy in the n=54$\rightarrow$53 transition of atomic hydrogen (H53α), which occurs at a rest frequency of 42.952 GHz, is presented. At this frequency the line emission is dominated by spontaneous emission and thus provides a reddening–independent estimate of the photo–ionization rate and physical conditions within the ionized regions (§6.3). In Section 6.4, a simple model for the far–IR and mm–wavelength line emission and IR luminosity is constructed in terms of an ensemble of dust–enshrouded photo–ionized regions, and the implications of this model for the stellar initial mass function, elemental abundances and source geometry are investigated.

6.2 Observations

Observations of M82 were made during 1988 April using the 45m telescope of the Nobeyama Radio Observatory, simultaneously in the 53α and 40α transitions of hydrogen at frequencies of 43 and 99 GHz respectively. The instrumentation comprised SIS (H53α) and cooled Schottky diode (H40α) frontends together with 2048–channel wide–band acousto–optical spectrometer backends, which gave a frequency resolution of 250

kHz and an instantaneous band–width of 256 MHz. The system noise temperatures (T_{SSB}) during the observations were ~300 and ~670 K at 43 and 99 GHz respectively, and the aperture efficiencies were η_A=0.60 and 0.34. The half–power beam widths were $41\widehat{''}$ and $19\widehat{''}$.

The telescope was pointed at $\alpha(1950) = 9^h\,51^m\,42.5^s$, $\delta(1950) = +69°\,55\widehat{'}\,00\widehat{''}$, *i.e.* $5\widehat{''}$ W of the 2-μm peak and HI dynamical centre (Joy, Lester & Harvey 1987; Weliachew, Fomalont & Greisen 1984) and coincident with the 10-μm centroid (Rieke *et al.* 1980). The extent of the central star–forming complex is about $25\widehat{''}$ as determined from Brγ recombination line observations by Lester *et al.* (quoted in Telesco 1988), and thus the H53α beam is expected to encompass all of the detectable emission. The pointing was checked regularly using a nearby SiO maser source, and the overall accuracy is estimated to be $\pm 3\widehat{''}$. Calibration was performed using a warm chopper in front of the receiver, and converted to flux density using the efficiencies quoted above. Linear baselines were removed and the data re–binned into channels of width 8 MHz. The resulting spectra are shown in Figure 6.1, together with the [OIII]λ88 μm profile from Duffy *et al.* (1987).

The line fluxes integrated between –100 and +500 km s^{-1} are $F(H53\alpha) = (1.87 \pm 0.28) \times 10^{-20}$ W m^{-2} and $F(H40\alpha) = (9.22^{+1.38}_{-1.84}) \times 10^{-20}$ W m^{-2}. The error in the former value is primarily the result of uncertainty in the exact aperture efficiency, whilst the larger asymmetric error of the latter reflects uncertainty in the baseline, which may not be linear. Detection of H53α emission from M82 was confirmed the following night, although the weather conditions were poor and therefore these data are not included in the following analysis. Comparison with measurements of the radio hydrogen recombination lines (*e.g.* Bell & Seaquist 1978; Shaver, Churchwell & Walmsley 1978), which are due to stimulated emission and whose strength decreases with increasing frequency (primarily due to the slope of the non–thermal stimulating continuum radiation), indicates that less than 3% of the H53α flux is produced in this way : the line is generated primarily by spontaneous emission. Negligible contributions to the integrated line fluxes from the equivalent helium transitions He40α and He53α ($\lesssim$5%, Peimbert & Spinrad 1970; velocity shift –122 km s^{-1}), and from other high n–level hydrogen lines are expected.

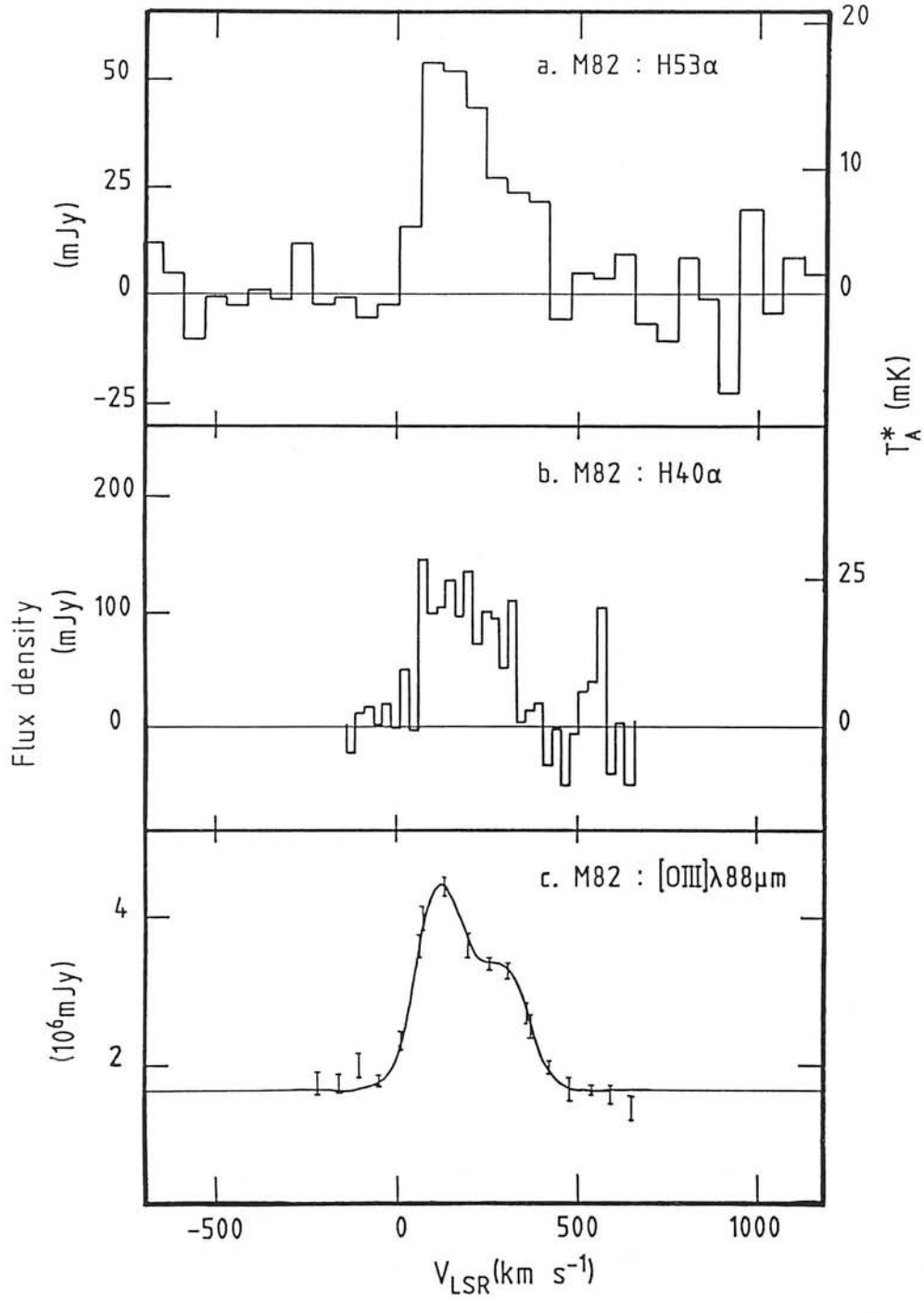

Figure 6.1: (a) H53α and (b) H40α recombination–line spectra of the central star–forming complex in M82, together with (c) the [OIII]λ88 μm profile from Duffy *et al.* (1987) for comparison.

6.3 Hydrogen Recombination Line Emission

Examination of Figure 6.1 shows that the H53α profile, in particular, bears a strong resemblance to the far–IR line [OIII]λ88 μm (and also [OIII]λ52 and [NIII]λ57 μm; Lugten *et al.* 1986; Duffy *et al.* 1987), as expected due to their common origin in regions of ionized gas. The shapes of the H40α and H53α lines appear somewhat different, but are probably consistent within the errors. In Table 6.1, rows 1 & 2, theoretical intensities in the H40α and H53α transitions relative to Hβ are presented for a range of electron temperatures and densities, and are accurate to about 1% (P.J. Storey – personal communication; see Hummer & Storey (1987) for details of the methods used). Case B recombination was assumed (Baker & Menzel 1938). The observed line ratio $H40\alpha/H53\alpha = (4.9^{+1.0}_{-1.2})$ is consistent with the theoretical values for the range of electron densities and temperatures considered here. However, the measured H40α flux is likely to be an underestimate since the telescope beam at 99 GHz ($19\widehat{''}$) is somewhat smaller than the extent of the recombination line emission ($\sim 25\widehat{''}$). This suggests that the electron density may lie towards the lower end of the range, although it is not possible to provide much constraint on its value. Given the lower signal–to–noise ratio of the H40α detection, and its less certain baseline, only the H53α measurement is considered in the rest of this chapter.

The electron density in M82 has been determined using a variety of techniques, but those involving far–IR forbidden or radio recombination lines are much preferred since they are less affected by extinction. Observations of the density–sensitive ratios [OIII]λ88/λ52 and [SIII]λ33/λ18 imply an electron density of $n_e \simeq 200$ cm^{-3} (Duffy *et al.* 1987; Houck *et al.* 1984), which is consistent with *some* analyses of the radio hydrogen recombination lines (*e.g.* Bell & Seaquist 1978; Rodriguez & Chaisson 1980). However, Lugten *et al.* (1986) have also measured the ratio [OIII]λ88/λ52 and, whilst agreeing with Duffy *et al.*'s value of n_e for a single–density model, they find that the data can also be decomposed into two components. One component, having $V_{LSR} \sim 150$ km s^{-1} and contributing $\sim$2/3 of the integrated line flux (see also Fig. 6.1), implies $n_e \sim 600$ cm^{-3}, whereas the other gives $n_e \sim 60$ cm^{-3}. This two–component density model is supported by the radio hydrogen recombination line results of Seaquist, Bell & Bignell (1985). This disagreement probably arises in part from the different flux calibrations and beam

Table 6.1: Theoretical recombination line ratios for a range of electron temperatures and densities assuming case B.

Ratio	$T_e = 5 \times 10^3$ K		$T_e = 10^4$ K	
	$n_e = 100cm^{-3}$	$n_e = 10^4cm^{-3}$	$n_e = 100cm^{-3}$	$n_e = 10^4cm^{-3}$
$I_{H53\alpha}/I_{H\beta}$	4.54×10^{-8}	5.16×10^{-8}	3.16×10^{-8}	3.38×10^{-8}
$I_{H40\alpha}/I_{H\beta}$	2.58×10^{-7}	2.28×10^{-7}	1.76×10^{-7}	1.59×10^{-7}
$N_{H53\alpha}/N_{LyC}$	7.76×10^{-5}	8.82×10^{-5}	5.31×10^{-5}	5.68×10^{-5}
$I_{Br\alpha}/I_{H53\alpha}$	2.29×10^{6}	1.92×10^{6}	2.53×10^{6}	2.30×10^{6}
$I_{Br\gamma}/I_{H53\alpha}$	7.72×10^{5}	6.28×10^{5}	8.80×10^{5}	8.14×10^{5}

sizes used for the [OIII] measurements, and also from low signal–to–noise ratios in the higher frequency radio recombination line data. In this chapter, a single–component electron density model with n_e=100 cm^{-3} has been adopted for simplicity, but, where appropriate, the effects of employing a two–component model with n_e=100 and 1000 cm^{-3} (comprising 1/3 and 2/3 of the total line fluxes, respectively) are investigated.

Together with observations of the 3.3-mm continuum emission, the measurement of the H53α flux allows calculation of the average electron temperature in the ionized gas. Following Rubin (1968), one may write :

$$\left(\frac{F(H53\alpha)}{Wm^{-2}}\right) = 1.78 \times 10^{-16}\left(\frac{N_{H53\alpha}}{N_{LyC}}\right)_{CaseB}\left(\frac{S_\nu^{th}}{Jy}\right)\left(\frac{\nu}{GHz}\right)^{0.1}\left(\frac{T_e}{10^4K}\right)^{-0.45} \quad (6.1)$$

where $N_{H53\alpha}/N_{LyC}$ is the predicted number of H53α photons produced per recombination (see Table 6.1, row 3) and S_ν^{th} is the free–free flux density at a frequency ν. This relation is insensitive to the electron density. Integration over the aperture–synthesis map by Carlstrom (1988) gives $S(91GHz) = 0.55$ Jy, which is consistent with the large beam ($\sim 75''$) measurement by Jura, Hobbs & Maran (1978) of $S(87GHz) = (0.54 \pm 0.08)$ Jy. Assuming that this emission is entirely due to bremsstrahlung, Eqn. 6.1 yields an electron temperature of $T_e \sim 5 \times 10^3 K$. Thence, contributions to the 90 GHz flux due to thermal emission from cold dust and from synchrotron emission must be negligible (*c.f.* Klein, Wielebinski & Morsi 1988), otherwise the inferred electron temperature would be unfeasibly low. For example, if 10% of the observed 90 GHz continuum radiation was non–thermal (*c.f.* the predicted contribution from known supernova remnants of about 3%, assuming a spectral index for the discrete sources studied by Kronberg, Biermann & Schwab (1985) of -0.9), then the electron temperature implied by Eqn. (6.1) would be less than 2900 K.

The ionization rate implied by the H53α flux is also insensitive to the electron density. Using the recombination coefficients given by Hummer & Storey (1987) and a distance to M82 of 3.25 Mpc (Tammann & Sandage 1968), gives $N_{LyC} = (1.08 \pm 0.16) \times 10^{54}$ s^{-1} for n_e=100 cm^{-3} and $T_e = 5 \times 10^3$ K. For the two–component density model this becomes $N_{LyC} = 1.03 \times 10^{54}$ s^{-1}. These values are more than 5 times larger than the ionization rate derived from the large–aperture Brα measurement by Willner *et al.* (1977), and imply significant extinction by dust even at 4 μm. Assuming an

intrinsic Case B line ratio of $I(Br\alpha)/I(H53\alpha) = 2.29 \times 10^6$ (see Table 6.1) and that the attenuation at $4\,\mu$m is given by $A_{4-\mu m} = 0.04 A_V$ (Rieke & Lebofsky 1985), the measured Brα flux of 1.6×10^{-14} W m^{-2} implies $A_V = 27 \pm 4$ mag. This is consistent within errors with estimates of the visual extinction deduced from the depth of the 10-μm silicate feature after correction for the narrow dust emission features ($A_V = 20 \pm 4$ mag; Aitken & Roche 1984).

The visual extinction derived from the H53α and Brα lines is considerably greater than that inferred from the optical Hβ and Hα lines, *e.g.* $A_V \sim 4$ mag (Peimbert & Spinrad 1970). Furthermore, the Hα flux of 1.2×10^{-12} W m^{-2} measured through a $35''$ aperture centred on the nucleus of M82 (J. Bland, personal communication, from data in Bland & Tully 1988), implies an ionization rate of 1.4×10^{54} s^{-1} *without reddening corrections* and using the same assumptions as those adopted above. This is clearly inconsistent with the H53α and Brα results, and the problem is exacerbated when one includes the effects of dust extinction. This disagreement cannot be caused patchy extinction. To explain this discrepancy it is suggested that much of the observed hydrogen line emission from the low n–levels arises in front of the star formation region and is generated by collisional excitation via shocks (see also McCarthy, Heckman & van Breugel 1987).

6.4 Modelling the Emission from M82

6.4.1 The Far–IR Forbidden and mm–Wavelength Lines

The recent availability of high quality long–wavelength spectral line measurements of M82, made through similar large apertures, allows quantitative investigation of the global properties of the central star formation complex without the usual problems associated with dust obscuration and beam–size effects. Therefore, given the spectral similarity of the [OIII], [NIII] and H53α lines, and the expectation that the dominant sources of emission are the same (namely, ionized regions around hot stars), a simple model of the far–IR and mm line emission from M82 in terms of an ensemble of such regions was constructed using the numerical calculations of Rubin (1985, henceforth R85). Below, the values adopted for the model parameters are described (see Appendix

C for further details).

Using the compilation of stellar properties in Landolt–Börnstein (1982), ionization rates (N_{LyC}) were calculated by integrating under the Kurucz (1979) model atmospheres of stars with effective temperatures in the range $31,000 \leq T_{eff} \leq 45,000$ K. The [OIII]λ88 μm and [NIII]λ57 μm line intensities were scaled from R85 (where fixed values of N_{LyC} were adopted) to be consistent with the derived ionization rates (see Appendix C for the values of $N_{LyC}(mass)$ employed). The H53α fluxes were calculated from the adjusted tabulated Brγ strengths using the predicted Case B ratio given in Table 6.1 for n_e=100 cm^{-3} and T_e=5 $\times 10^3$ K. Stars with temperatures outside the range considered here do not affect the results; the UV fluxes from those with lower T_{eff} are insufficient to provide significant H^+, O^{2+} or N^{2+} abundances, whilst there are no stars with higher T_{eff} (see below).

Analysis of the argon and neon mid–IR line emission (Willner *et al.* 1977) suggests that Ar^+ and Ne^+ are the dominant ionization states. Following Willner *et al.*, and setting A_V=27 mag and $T_e = 5 \times 10^3$ K, the inferred abundances of these two elements are within $\pm$50% of their solar values. This result is insensitive to the range of electron densities considered here, and a similar value is obtained using $T_e = 10^4$ K. Initially, therefore, solar abundances of oxygen and nitrogen were adopted. Note that if the elemental abundances were significantly less than their solar values (*e.g.* $Z = Z_\odot/10$), then the electron temperature within the nebulae would be more than 10^4 K due to the decreased abundance of the coolant species (R85). This would be inconsistent with the value of $T_e \sim 5 \times 10^3$ K found in Section 6.3, though one must be slightly cautious since the free–free emission coefficient decreases with increasing T_e and thus the observed emission is weighted to lower temperature regions. McCarthy, Heckman & van Breugel (1987) have analysed the optical line emission towards the nucleus of M82 and also concluded that the elemental abundances have roughly their solar values.

The values for the line emission arising in photo–ionized regions around individual stars together with the compilation of stellar main–sequence lifetimes and the initial mass function (IMF) given by Scalo (1986) were used to calculate the total [OIII]λ88, [NIII]λ57 and H53α fluxes from an ensemble of stars having masses distributed according to various present day mass functions; see Gehrz, Sramek & Weedman (1983),

Telesco (1985), and Appendix C for further details of the methods used. The results of this modelling are shown in Figure 6.2.

The cross in the lower left corner of Figure 6.2 shows the observed line ratios, and 1σ uncertainties, calculated using the forbidden line fluxes in Duffy *et al.* (1987): $F([OIII]) = (9.2 \pm 0.3) \times 10^{-14}$ W m^{-2} and $F([NIII]) = (4.3 \pm 0.3) \times 10^{-14}$ W m^{-2}, both measured through a $48''$ aperture. Representing the star formation complex as a single object yields an effective temperature for the ionizing source of T$\simeq$35,500 K, equivalent to an O8 star (Landolt–Börnstein 1982). This is in agreement with the upper limit of T<37,000 K implied by the non–detection of [ArIII]λ9 μm (Gillett *et al.* 1975; Willner *et al.* 1977; R85), and the value T$\sim$30,000 K from analysis of the ionization state of helium (Peimbert & Spinrad 1970).

In Figure 6.2 the point marked O represents the predicted [OIII]λ88/H53α and [NIII]λ57/H53α flux ratios for an unevolved ("zero–age") starburst with stellar masses distributed according to the initial mass function (IMF) of Scalo (1986) (effectively $\alpha = -2.85$, $\psi(m) \propto m^{\alpha}$), and an upper mass limit of m$_u$=64 M$_\odot$ corresponding to T$_{eff}$=45,000 K. Point S shows the effect of using a flatter IMF ($\alpha = -2.35$, Salpeter 1955), and keeping the other model parameters constant. The line connecting O–E represents evolution with a constant rate of star formation. After 10^7 yr the stellar birth and death rates become equal and the line fluxes do not change (point E). It is immediately apparent that neither the original model, nor evolution, nor reasonable values for the IMF slope can reproduce the observed line ratios. Even employing a model in which the star formation rate varies as e^{-t/τ_0} (with $\tau_0 \sim 10^7 - 10^8$ yr; Rieke *et al.* 1980) can not reproduce the observed values – in fact this model is very similar to that with constant evolution. The reason for this, and for why evolution and IMF variations have only a small effect, is that the predicted line fluxes, and thus the line ratios, are dominated by the most massive stars. For example, the predicted [OIII] and [NIII] fluxes vary by roughly a factor of 10^5 over the range 18–64 M$_\odot$. Thus an exponential decrease in the rate of star formation having a time constant one order of magnitude larger than the lifetime of the most massive stars simply does not occur quickly enough to dramatically affect the line ratios. The presence of dust within the ionized regions can also be rejected as an explanation for the low excitation conditions, since this would require an unfeasible increase in the dust photo–absorption cross–

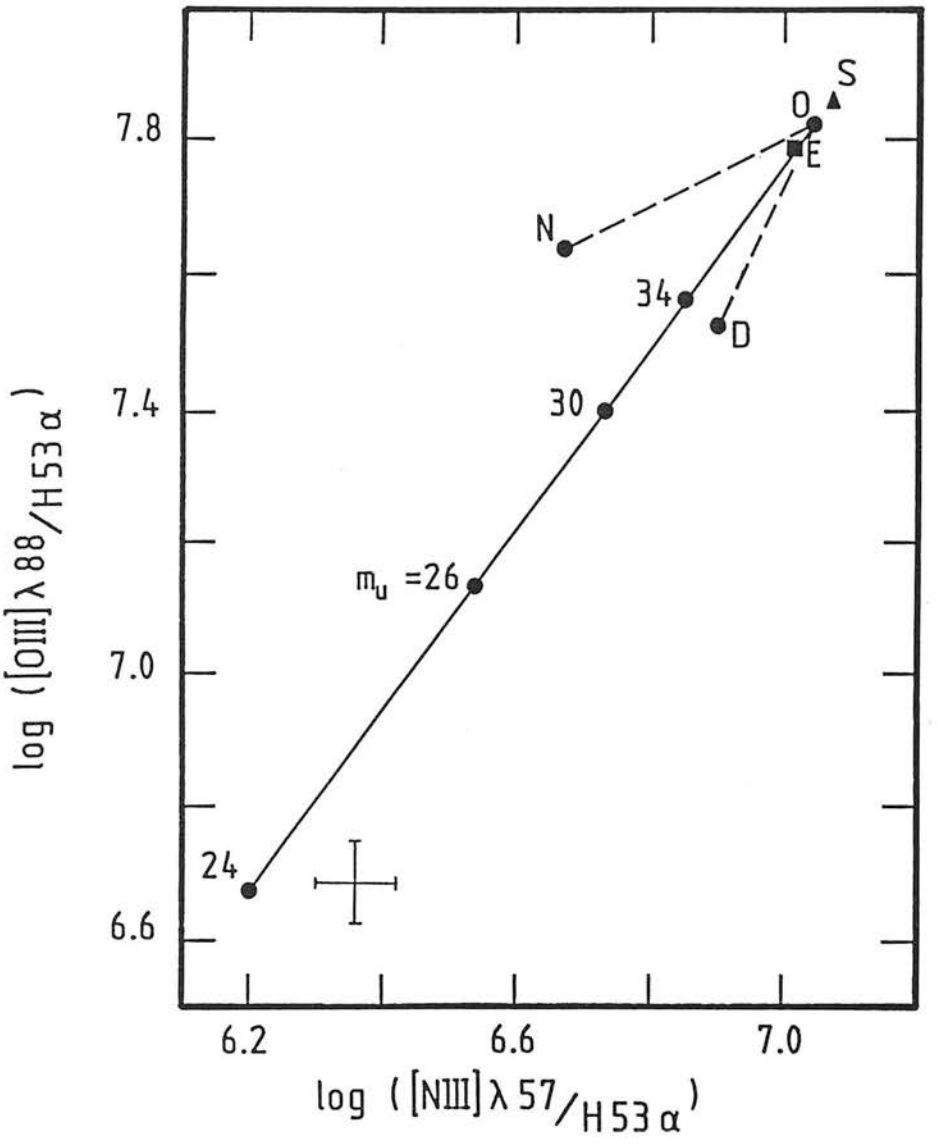

Figure 6.2: Theoretical and observed [OIII]λ88/H53α and [NIII]λ57/H53α line ratios for M82. The cross in the lower–left corner indicates the observed values and 1σ uncertainties. The points labelled O (unevolved starburst model with upper mass limit m_u=64 $M_\odot$, electron density n_e=100 cm^{-3} and solar abundances), N (as O but with lower elemental abundances), S (filled triangle; as O but with a flatter stellar mass function), D (as O but assuming a two–component density model), and E (filled square; as O but assuming constant evolution for $\sim 10^7$ yr) are described in detail in the text. The solid line represents the basic model (O) but adopting various values for the upper mass limit, which are marked along it.

section from the ionization potential of hydrogen to that of O^+ and N^+ ($\sim$35 eV); see Mathis (1986).

Two other vectors of note in Figure 6.2 are those ending in the points labelled D and N. The former illustrates the predicted line ratios for the unevolved model with m_u=64 $M_\odot$ but adopting the two–component density model described in Section 6.3. The line ratios decrease by about 0.2 dex due to collisional de–excitation of the excited states of [OIII] and [NIII] in the n_e=1000 cm^{-3} component. Point N shows the effect on the single–component (n_e=100 cm^{-3}) model of reducing the oxygen and nitrogen abundances to 0.6$\times$ and 0.4$\times$ their solar values, respectively (*i.e.* model series N from R85). This decrease in the abundances dominates over the slight increase in the fractional abundances of O^{2+} and N^{2+}, which is due to a hardening of the stellar UV spectra with lower metallicity. The net result is a decrease in the line ratios in proportion to the change in the elemental abundances.

Figure 6.2 shows that the most dramatic variations in the predicted line ratios are due to changes in the upper mass limit (m_u) of the IMF. The solid line represents an unevolved starburst having $\alpha = -2.85$, and has various values of m_u marked along it. This line essentially also illustrates the evolution of the line ratios after a rapid switch–off of star formation (*i.e.* small τ_0 in Rieke *et al.'s* model), so that stars of progressively lower mass dominate the observed line emission. This locus clearly demonstrates that there cannot currently be any stars in the central star–formation complex of M82 which are more massive than about 24 $M_\odot$ (n_e=100 cm^{-3}, Z= $Z_\odot$) or 30 $M_\odot$ if Z$\sim$ $Z_\odot/2$ and the two–component density model are assumed. The absence of stars with masses greater than 24–30 $M_\odot$ implies that, unless there has been a dramatic decrease in the star–formation rate during the last $\sim 10^7$ yr [$\tau(25\,M_\odot) \sim 8 \times 10^6$ yr], the stellar *initial* mass function in M82 must also terminate at about this mass. In the following section the constraints on the lower IMF bound (m_l) implied by this value of m_u are investigated.

Stellar luminosities and ionization rates were calculated for stars in the mass range 0.8 – 100 $M_\odot$ by integrating under the same Kurucz (1979) model atmospheres, for consistency. The total IR luminosity from the ensemble of stars was derived following the method of Section 6.4.1 and assuming that the entire stellar output is thermalised by dust within the effective IR beam used for the observations ($\sim 40''$). For any star formation model, the maximum value of the ratio of the ionization rate to IR luminosity occurs before any stars have started dying (provided, of course, that the IMF is constant in time), and is thus independent of the star formation rate. Since the ionization rate inferred from the H53α measurement is considerably larger than previously believed, this maximum value of N_{LyC}/L_{IR} was used to characterise a particular lower—upper mass limit (m_l,m_u) model. The observed ratio for the central $40''$ of M82 is $\log(N_{LyC}/L_{IR}) = (43.56 \pm 0.11)$ assuming an IR luminosity of 3×10^{10} $L_\odot$ (Telesco & Harper 1980). The dependence of the predicted ratio on the value of the IMF slope is small: $\Delta\log(N_{LyC}/L_{IR}) \sim 0.05$ for α=–2.85 and α=–2.35. For a given value of the upper mass limit there is a minimum value of m_l which can reproduce the observed ratio; a smaller m_l produces too much relative luminosity since the lower mass stars make no contribution to the integrated ionization rate. The permitted ranges of m_l and m_u are explored in Figure 6.3, where constraints on m_u imposed by the line excitation conditions are also illustrated.

If the assumptions outlined above for this model hold, then it is apparent that star formation in the centre of M82 is restricted to only a narrow range of stellar masses. For n_e=100 cm^{-3} and Z= $Z_\odot$ it can be seen that only stars having $m_* = 20 - 24$ $M_\odot$ are allowed (for 2σ uncertainty in the ratio N_{LyC}/L_{IR}). Taking values of the metallicity ($Z \simeq Z_\odot/2$) and electron density (two–component model; §6.3) which permit the widest range of stellar masses, the extent becomes $m_* = 17 - 30$ $M_\odot(2\sigma)$. Even if the ratio was $N_{LyC}/L_{IR} = 10^{43.23}$ (reflecting 3σ uncertainty), the allowed range would still be only 17 – 24 or 12 – 30 $M_\odot$, depending on Z and n_e. Further relaxation of these stringent constraints on the mass function would require greater uncertainty in the infrared luminosity (since this dominates the error quoted for N_{LyC}/L_{IR}), a metallicity of one half the solar value, adoption of the two–component density model,

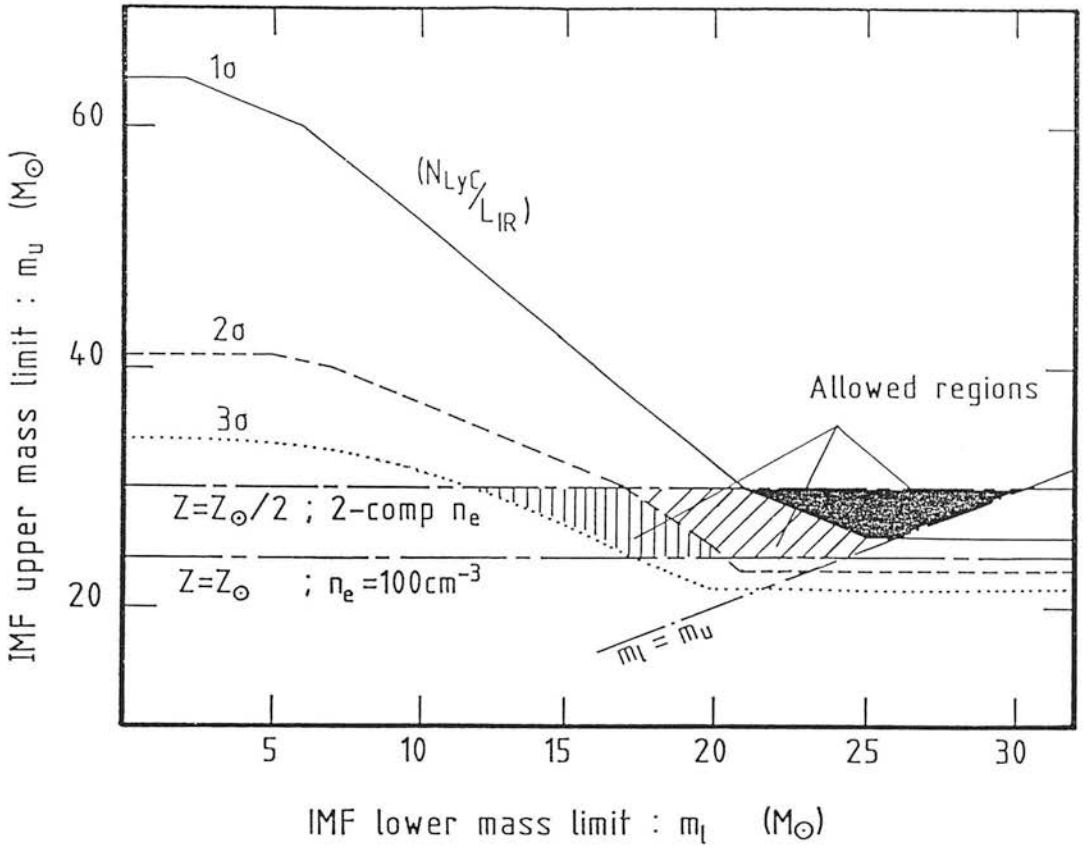

Figure 6.3: Constraints on the lower (m_l) and upper (m_u) mass limits of the initial mass function in M82 identified using the models described in the text. The allowed ranges of m_l and m_u are indicated by the solid (1σ uncertainty), diagonally hatched (2σ), and vertically ruled (3σ) regions. Areas of the (m_l,m_u) parameter space above the dash-dot line labelled $Z = Z_\odot/2$ and below that labelled $Z = Z_\odot$ are forbidden by the line-excitation conditions. The region below the solid line (1σ uncertainty, short dashed line for 2σ, or dotted line representing 3σ) is forbidden by the observed ratio of the ionization rate to IR luminosity. A line indicating equivalence of m_l and m_u is also shown.

and that the starburst be unevolved. The evolutionary phase of the starburst affects the inferred lower mass limit because, as time progresses, the longer–lived lower mass stars, which exhibit relatively small values of the ratio N_{LyC}/L_{IR}, accumulate on the main sequence and thereby lower the integrated ratio. The high value of N_{LyC}/L_{IR} observed at the present epoch would therefore imply an even larger ratio, and thus greater predominance of massive stars, in the past.

The permitted range of stellar masses is uncomfortably small, particularly since the 2-μm spectrophotometry by Rieke *et al.* (1980) of the stellar CO absorption feature produced in the atmospheres of red giant and supergiant stars may require a mass function extending to considerably lower mass than identified above, though the exact value is not specified by the simple model presented here. Assuming that the stellar–atmosphere and ionized–region models are correct, two other possible explanations for this discrepancy are suggested.

(i) The assumption of complete thermalisation of the stellar radiation by dust within the central $40''$ may be incorrect. If sufficient stellar luminosity ($L_{ESC} \gtrsim 5 \times 10^{10}$ $L_\odot$) can escape from the star–forming complex without encountering dust, then the ratio $N_{LyC}/(L_{IR}+L_{ESC})$ provides no constraint on the lower mass limit of the IMF. In other words, increasing the total luminosity ($L_{IR} + L_{ESC}$) allows the permitted range of stellar masses to extend to lower values.

Rieke *et al.* (1980) speculated that a luminosity of 10^{10} $L_\odot$, emanating directly from the photospheres of red giants, escapes perpendicular to the plane. Assuming their value for the total intrinsic luminosity ($L_{IR} = 4 \times 10^{10}$ $L_\odot$) broadens the allowed range of stellar masses to 17 – 24 $M_\odot$ (2σ) for n_e=100 cm^{-3} and Z= $Z_\odot$. This range is still very narrow, despite having allowed one quarter of the stellar radiation to escape. At least 60% of the total luminosity must escape for complete relaxation of the constraints on m_l (*i.e.* $L_{TOT} \gtrsim 8 \times 10^{10}$ $L_\odot$, which implies $L_{ESC} \gtrsim 5 \times 10^{10}$ $L_\odot$).

The central hollow cylinder geometry proposed by Nakai *et al.* (1987) may provide a dust–free escape route, although this would further require that the stars responsible for L_{ESC} are situated away from the dusty molecular clouds in which they were born, or have since dispersed.

(ii) The dominant excitation mechanism of the far–IR and mm–wavelength line emission is not photo–excitation by stars but by the UV–precursors of fast shocks. The theoretical calculations by Shull & McKee (1979) are able approximately to reproduce the observed [OIII]λ52 and 88 μm and H53α relative strengths for shock velocities of $\sim$100 km s^{-1}. Exploring this model further, the Hβ line intensity from Shull & McKee ($\sim 3 \times 10^{-9}$ W m^{-2} sr^{-1}), together with Table 6.1, imply a source emitting area of $\sim$1000 kpc^2 if the entire measured H53α flux is produced by shocks of velocity 100 km s^{-1}. Further, if the shocks were due to identical supernova remnants with diameters of about 50 pc (*i.e.* $V_s \sim 100$ km s^{-1}), it would require the existence of $\sim 2 \times 10^5$ such remnants, with a mean separation of $\sim$ 5 pc (assuming that they are equally distributed within a pillbox of dimensions: 500 pc diameter and 150 pc thickness). This calculation assumes an ambient density for the ISM of 1 cm^{-3}. Moreover, if the time dependences of the star–formation and supernova rates are equal then the predicted SN rate is $\sim 0.1 - 1$ yr^{-1} (see Gehrz, Sramek & Weedman 1983), depending on the stellar mass range and assuming that each star with mass $m_* > 8$ M$_\odot$ produces a SN remnant. Thus the lifetime of a remnant in the far–IR line–emitting phase would have to be $2 \times 10^5 - 2 \times 10^6$ yr to match the required number of remnants. This seems implausibly long, particularly when one considers that only a relatively narrow range of remnant velocities ($\sim$ 80–120 km s^{-1}, depending on ambient density) can reproduce the observed low–excitation conditions. Furthermore, the required number of line–emitting supernova remnants is many orders of magnitude larger than that actually observed using VLBI techniques ($\sim$40; Unger *et al.* 1984; Kronberg, Biermann & Schwab 1985). The supernova rate inferred from observations of the radio–emitting remnants ($\sim$0.2 yr^{-1}) is in agreement with that deduced above, using the ionization rate, only if the line emission arises primarily from ionized regions around stars.

A more detailed study of the line excitation in M82 is required to help examine the two possibilities described above; however both explanations are regarded as unlikely due to the extreme conditions they imply.

6.5 Conclusions

The first detection of H53α emission from another galaxy has been made. At the frequency of this transition (43 GHz), spontaneous emission dominates and extinction by dust can be totally ignored. Thus, this detection provides a reliable measure of the photo–ionization rate ($N_{LyC} = 1.1 \times 10^{54}$ s^{-1}) and electron temperature ($T_e \sim 5 \times 10^3$ K). Comparison of the H53α line strength with large aperture Brα observations shows there to be significant attenuation by dust, even in the near–infrared ($A_{4\mu m} \sim 1$ mag).

In combination with the observed IR luminosity and far–IR forbidden line measurements of O^{2+} and N^{2+}, the H53α emission has been used to constrain the allowed mass–range of stars present. This is found to be very narrow : approximately 20 – 30 $M_\odot$ depending on the electron density and elemental abundances. This restriction is lifted if a large fraction (~60%) of the stellar light escapes from the central regions without being absorbed by dust, or if significant amounts of the line radiation and luminosity are produced in fast shocks. Neither of these two situations is regarded as likely.

Acknowledgements

Thanks are due to Tetsuo Hasegawa for assistance with tuning of the receivers and to the staff of NRO for their support and hospitality. Peter Storey is thanked for calculating the H40α and H53α recombination line strengths, as are Joss Bland for providing the Hα data, Pat Roche for stimulating discussions and Marjorie Fretwell for drawing the diagrams. James Houck provided several helpful comments which improved the presentation of this material.

References

Aitken, D.K. & Roche, P.F., 1984. *Mon. Not. R. astr. Soc.*, **208**, 751.

Baker, J.G. & Menzel, D.H., 1938. *Ap. J.*, **88**, 52.

Bell, M.B. & Seaquist, E.R., 1978. *Ap. J.*, **223**, 378.

Bland, J. & Tully, R.B., 1988. *Nature*, **334**, 43.

Carlstrom, J.E., 1988. In *Galactic and Extragalactic Star Formation*, p.571, eds. Pudritz, R.E. & Fich, M., Kluwer Acad. Publ., Dordrecht.

Duffy, P.B., Erickson, E.F., Haas, M.R. & Houck, J.R., 1987. *Ap. J.*, **315**, 68.

Gehrz, R.D., Sramek, R.A. & Weedman, D.W., 1983. *Ap. J.*, **267**, 551.

Gillett, F.C., Kleinmann, D.E., Wright, E.L. & Capps, R.W., 1975. *Ap. J.*, **198**, L65.

Houck, J.R., Shure, M.A., Gull, G.E. & Herter, T., 1984. *Ap. J.*, **287**, L11.

Hummer, D.G. & Storey, P.J., 1987. *Mon. Not. R. astr. Soc.*, **224**, 801.

Joy, M., Lester, D.F. & Harvey, P.M., 1987. *Ap. J.*, **319**, 314.

Jura, M., Hobbs, R.W. & Maran, S.P., 1978. *Astron. J.*, **83**, 153.

Klein, U., Wielebinski, R. & Morsi, H.W., 1988. *Astr. Astrophys.*, **190**, 41.

Kronberg, P.P., Biermann, P. & Schwab, F.R., 1985. *Ap. J.*, **291**, 693.

Kurucz, R.L., 1979. *Ap. J. Suppl.*, **40**, 1.

Landolt–Börnstein 1982. *Astronomy & Astrophysics*, **2b**, Stars & Star Clusters. Eds. Schiaffers, K. & Voigt, H.H.

Lugten, J.B., Watson, D.M., Crawford, M.K. & Genzel, R., 1986. *Ap. J.*, **311**, L51.

McCarthy, P.J., Heckman, T. & van Breugel, W., 1987. *A. J.*, **93**, 264.

Mathis, J.S., 1986. *Pub. A.S.P.*, **98**, 995.

Nakai, N., Hayashi, M., Handa, T., Sofue, Y. & Hasegawa, T., 1987. *Pub. A.S.J.*, **39**, 685.

Peimbert, M. & Spinrad, H., 1970. *Ap. J.*, **160**, 429.

Rieke, G.H. & Lebofsky, M.J., 1985. *Ap. J.*, **288**, 618.

Rieke, G.H., Lebofsky, M.J., Thompson, R.I., Low, F.J. & Tokunaga, A.T., 1980. *Ap. J.*, **238**, 24.

Rodriguez, L.F. & Chaisson, E.J., 1980. *Ap. J.*, **238**, 41.

Rubin, R.H., 1968. *Ap. J.*, **153**, 761.

Rubin, R.H., 1985. *Ap. J. Suppl.*, **57**, 349. R85.

Salpeter, E.E., 1955. *Ap. J.*, **121**, 161.

Scalo, J.M., 1986. *Fund. Cosm. Phys.*, **11**, 1.

Seaquist, E.R., Bell, M.B. & Bignell, R.C., 1985. *Ap. J.*, **294**, 546.

Shaver, P.A., Churchwell, E. & Walmsley, C.M., 1978. *Astr. Astrophys.*, **64**, 1.

Shull, J.M. & McKee, C.F., 1979. *Ap. J.*, **227**, 131.

Tammann, G.A. & Sandage, A., 1968. *Ap. J.*, **151**, 825.

Telesco, C.M., 1985. In: *Extragalactic Infrared Astronomy*, p87, Rutherford Appleton Laboratory. Ed. Gondhalekar, P.M.

Telesco, C.M., 1988. *Ann. Rev. Astr. Astrophys.*, **26**, 343.

Telesco, C.M. & Harper, D.A., 1980. *Ap. J.*, **235**, 392.

Unger, S.W., Pedlar, A., Axon, D.J., Wilkinson, P.N. & Appleton, P.N., 1984. *Mon. Not. R. astr. Soc.*, **211**, 783.

Weliachew, L., Fomalont, E.B., Greisen, E.W., 1984. *Astr. Astrophys.*, **137**, 335.

Willner, S.P., Soifer, B.T., Russell, R.W., Joyce, R.R. & Gillett, F.C., 1977. *Ap. J.*, **217**, L121.

Chapter 7

Conclusions and Suggestions for Research

7.1 Conclusions

This dissertation has presented a study of vigorous star–formation in the nuclei of nearby galaxies. The aims of this work have been to identify the causes and quantify the properties of this phenomenon. To this end, several observational programmes involving a variety of techniques have been initiated. These are described below.

The database produced by the *Infrared Astronomical Satellite (IRAS)* was used to construct a sample of infrared–bright galaxies suitable for study. These systems are an infrared–luminous subset of nearby spirals from the optical Shapley–Ames catalogue of galaxies. Examination of the *IRAS* properties of this sample led to the identification of a population which display evidence for a substantial component of warm dust. This excess emission, which is most prominent at 25 μm, is interpreted as resulting from an episode of high–mass star formation in the dusty central regions, and which contributes about one third of the galaxies luminosity ($\sim 10^{10}$ $L_{\odot}$). The galaxies containing warm dust usually have a stellar bar which prompts the hypothesis that the star–formation is fuelled, and perhaps even initiated, by a bar–driven inflow of disk material.

The results of the *IRAS* investigation are strengthened by analysis of new, and published, radio continuum observations. These measurements, having a spatial resolution of about $15\widehat{''}$, are able to separate nuclear and disk components. Virtually all of the galaxies thought to be undergoing enhanced star formation exhibit central radio sources, their detection rate being much higher than that of comparison samples not having 25-μm excesses. The radio emission is predominantly non–thermal and is believed to arise from supernova remnants, which trace regions of recent high–mass star formation, and from the energetic particles which they inject into the interstellar

medium. Supporting evidence for the presence of hot young stars intimately mixed with dust comes form the ratio of mid–infrared to radio continuum emission which is significantly larger in the galaxies displaying 25-μm excesses.

Sizeable fractions of the comparison samples also contain central radio sources. These present something of a puzzle since the host galaxies are not thought to be currently undergoing active star formation, due to the absence of warm dust, nor have compact massive nuclei, on the basis of optical spectroscopy. Their radio emission may result from compression of the gas, from the supernova embers of a previous episode of star formation, or from a highly dust–obscured active nucleus.

In order to study the properties of the actively star–forming regions, near–infrared spectrophotometric measurements were made. Detection of the Brγ hydrogen recombination line, which arises in the ionized gas surrounding hot stars, is supporting evidence for high–mass star formation in these galaxies. In many of the galaxies, line emission from molecular hydrogen was also detected, and in a number of these systems several transitions were measured.The relative line strengths unambiguously demonstrate that the H_2 is excited by the absorption of non–ionizing UV photons. This contrasts with previous studies of interacting/merging and active galaxies in which the molecular hydrogen appears to be shock excited.

To account for the observed line emission from star–forming galaxies, detailed models of the excitation of molecular and atomic hydrogen were constructed. One of the most important parameters in these models is found to be the geometry of the star–forming complex since this controls the intensity of UV photons incident on molecular clouds, and thence the efficiency with which this radiation is converted into H_2 line emission. The ratios of the observed molecular (v=1–0 S(1)) to atomic (Brγ) hydrogen emission from galaxies, using new and published data, are compared with model predictions. Most galaxies can be understood in terms of hot stars intimately mixed with molecular gas, but a few require the existence of large compact clusters of massive stars within a communal ionized region.

Another difficulty arising from the uncertain geometry of star–forming regions is that of the correction for attenuation of radiation by dust. If the sources of emission

are distributed amongst a considerable quantity of dust, then the extinction correction required will be very different from that in a geometry where all of the dust lies foreground to the sources. One way of avoiding this difficulty is to observe lines of sufficiently long wavelength that they suffer no attenuation by dust. This philosophy was applied to the archetypal starburst galaxy M82 in which the H53α and H40α lines were measured. Their observed relative intensities are consistent with the predictions of atomic physics. Comparison with the near–infrared Brα line, however, implies an extinction at 4 μm of more than 1 mag. The ionization rate inferred from the H53α measurement allows further examination of the global properties of star formation. In conjunction with far–infrared lines of doubly–ionized oxygen and nitrogen, it places strong constraints on the maximum mass of star that can be present in this galaxy, and, together with the total luminosity, it constrains the lower mass limit. Analysis of these data suggests that star formation in M82 may be restricted to only a very narrow range of masses (approximately 20–30 $M_{\odot}$, depending on various model parameters).

7.2 Suggestions for Further Research

The results outlined above go some way to attacking the goals of this study, however there are many unanswered questions. Perhaps the most fundamental is : what triggers near–nuclear star formation in barred spirals? Although the hypothesised bar–driven inflow of gas represents a self–consistent physical picture of these galaxies, only 8% of all Shapley–Ames barred spirals display such behaviour. There are several possible explanations for this. The small fraction may represent the "on" phase of a star–forming duty–cycle. Episodes of active star formation must end when the stockpile of raw material drops below some critical limit, either because of use or dispersion (*e.g.* by supernovae). Active star formation may then only begin again once sufficient material has accumulated. Observations of the molecular and atomic gas contents of barred spirals, for example via tracers such as dust or CO, may be employed to investigate this suggestion. Alternatively, the strength of the bar potential, which plays a role in governing the rate of gas inflow, may determine the level of nuclear star formation activity. One observational test of this suggestion would be to use near–infrared images of the bar as a guide to its mass via the stars it contains.

Progress in understanding the molecular hydrogen emission from galaxies will be driven by the advent of new near–infrared 2D–array spectrometers. Their capability for simultaneously measuring many transitions at various positions and with great sensitivity will revolutionize this field of research. However, much useful work can be done with present instrumentation. For example, the causes of the differing H_2 excitation mechanisms in barred and interacting/merging galaxies are not understood. The suggestion that this is a selection effect due to the projected extent of the aperture may be tested by small beam ($\sim 5''$) observations at several positions. As the unexpected discovery of widespread fluorescent H_2 emphasises, measurement of more than one transition is essential for identifying the excitation mechanism. The nearby starburst galaxy NGC 253 may hold the key to the problem since, although being an isolated barred spiral, it exhibits shock–excited H_2 emission. The proximity and brightness of this system make it an ideal candidate for mapping in several lines. Observations should also be made in higher ro–vibrational transitions since the apparently shock–excited line ratios may arise due to the impingement of intense UV radiation on dense gas.

The systems variously called extragalactic HII regions or blue compact galaxies (BCGs) have the potential for clarifying some of the processes involved in radiative excitation of H_2 in galaxies. The influence of factors such as the metallicity and dust content of the interstellar medium, which vary widely in BCGs, is currently poorly understood. Indeed, it must be remembered that detailed models of H_2 fluorescence have only recently been developed and thus *many* aspects of this mechanism require investigation. In particular, observations of nearby Galactic star–forming regions, where the structure may be expected to be more comprehensible than that of extragalactic complexes, are urgently needed. This point is highlighted by the fact that, in terms of the number of sources studied, fluorescent H_2 in extragalactic systems currently overwhelms that from Galactic objects.

The role played by geometry in governing the observed radiation from star–forming complexes has been emphasized several times in this dissertation. The relative spatial distributions of hot stars and dust are unknown at present but may be studied, in two dimensions, by mapping. The three dimensional structure is more difficult to determine but may be investigated via multi–line observations and by consideration of radiative transfer through regions of distributed emission. An observational programme

incorporating these techniques is scheduled.

The stellar content in active extragalactic star–forming regions is also a subject that warrants comprehensive investigation. Amongst the many questions requiring consideration, perhaps the most interesting is : how does the permitted range of stellar masses depend on the physical properties of the star–forming environment ? To answer this question it will first be necessary to determine what stars *are* present. This problem is not at all simple but the advent of sensitive spaced–based mid–infrared spectrometers on satellites such as *ISO* will enable investigation of the high–mass stellar content in many galaxies via the ionization state of the gas. For the low–mass end of the mass function, the near–infrared photospheric absorption features, such as CO, may be used for examining the stellar content.

The forthcoming availability of several new instruments with greatly enhanced characteristics guarantees a bright future for the study of star formation in extragalactic environments, and must surely help to unravel the complex phenomena involved.

Appendix A

Reduction of Infrared Spectroscopy Data

This section briefly describes the reduction of the infrared spectra analysed in Chapters 4 and 5. There are several steps in this process : (1) correction for wavelength–dependent atmospheric and instrumental responses, (2) flux calibration, (3) wavelength calibration, and (4) evaluation of line flux and continuum flux density. The techniques discussed are completely general, but particular details relevant to analysis of the 2-μm spectrophotometric data contained in this thesis, obtained with the UKIRT common–user instrument UKT 9, are given.

A.1 Wavelength–dependent Effects

The spectrum produced by an instrument at the surface of the Earth will, in general, be different from that incident upon the top of the atmosphere due to the wavelength–dependent attenuation by atmospheric gases (principally H_2O and CO_2) and the response of the detecting device. To correct for these effects, the radiation from the object of interest must be compared with that from an astronomical source having known spectral shape.

Let the flux density at a wavelength λ from the source be S_λ, from the "spectral standard" (also called the 'ratio–ing' source) be R_λ, the atmospheric transmission T_λ, and the instrumental response I_λ. As illustrated schematically in Figure A.1, the measured signals from the source and spectral standard are simply proportional to $S_\lambda\, T_\lambda\, I_\lambda$ and $R_\lambda\, T_\lambda\, I_\lambda$, respectively. In practice, early–type stars (*e.g.* spectral type A) are often used as spectral standards since they closely approximate black bodies (*e.g.* Mountain *et al.* 1985), deviating significantly only by the presence of atomic hydrogen absorption lines. Thus for a star of known spectral type and luminosity class (*i.e.* known effective temperature, T_{eff}), the undistorted spectrum of the source can

be reconstructed by evaluating :

$$\frac{\text{source flux density}}{\text{spectral standard flux density}} \times \text{black body flux density}$$

$$= \frac{S_\lambda\, T_\lambda\, I_\lambda}{R_\lambda\, T_\lambda\, I_\lambda}\, BB_\lambda(T_{eff})$$

$$\cong k_\lambda\, S_\lambda \qquad \text{(A.1)}$$

where k_λ is a constant introduced because of the arbitrary brightness of the spectral standard ($BB_\lambda(T_{eff}) \simeq k_\lambda\, R_\lambda$).

Often, the spectral region of interest lies close to a hydrogen absorption line in the stellar reference spectrum (*e.g.* attempted measurement of the Brγ recombination emission line). There are two solutions to this problem. A later–type star may be used as the spectral standard since it is cooler and exhibits no hydrogen lines, but the many molecular features (mostly CO and H_2O) may offset this advantage if measurement at other wavelengths is also required. Alternatively, one can extrapolate linearly across the absorption feature in the early–type stellar reference spectrum provided that the atmospheric transmission and instrumental response do not vary dramatically with wavelength. Both of these techniques were tried and found to give indistinguishable results.

One further important point to note is that the attenuation of radiation depends on the path length of atmosphere (the "airmass") through which it propagates. Thus, to obtain reliable results, the source and spectral standard should have similar airmasses (equivalently, similar sec z, where z is the zenith distance in degrees) and, preferably, be close together in projection on the sky. This avoids the problems associated with wavelength–dependent variations in the extinction—airmass relationship.

A.2 Flux Calibration

Most often, flux calibration of an infrared spectrum involves comparison with another astronomical source of known brightness. As in section A.1, stars are frequently used as

flux standards, there being several comprehensive tabulations of suitable measurements. All of these quote the stellar emission in magnitudes, that is, relative to the star Vega (αLyra, BS 7001) defined to have zero magnitude at every wavelength. Measurements of the absolute flux from Vega (Mountain *et al.* 1985) :

$$\left(\frac{F_\lambda}{\mathrm{W\ m^{-2}\ \mu m^{-1}}}\right) = \frac{1.965 \times 10^{-8}}{\lambda^5\,(\exp(1.4388/\lambda) - 1)} \tag{A.2}$$

(where λ is the wavelength in microns) thus give the flux density from a star of magnitude m :

$$F_\lambda(m) = F_\lambda(Vega)\, 10^{-0.4m} \tag{A.3}$$

For example, at $2.2\,\mu$m :

$$\left(\frac{F_{2.2}(m)}{\mathrm{W\ m^{-2}\ \mu m^{-1}}}\right) = 4.13 \times 10^{-10}\, 10^{-0.4m} \tag{A.4}$$

where m is the infrared K ($2.2\,\mu$m) magnitude of the star.

In cases where the flux standard is also the spectral standard (§A.1), the constant, k_λ, in Eqn. A.1 is known. Hence, multiplication of $(source/standard) \times BB$ by the appropriate value of $F_\lambda(m)$ from Eqn. A.3 immediately yields a flux calibrated spectrum. Generally, however, the flux and spectral standards are not the same and one must first determine the relative brightness of the two stars (*i.e.* flux calibrate the spectral standard).

The standard stars used for flux calibration of the spectrophotometry data are given in Table A.1. The two columns give (1) the name from the *Bright Star Catalogue* (Hoffleit & Jascheck 1982), and (2) the broad–band K magnitude (from the UKIRT list of standard stars, or the compilation of IR observations by Gezari, Schmitz & Mead 1987).

To examine the accuracy of the flux calibration and the stability of the system, the measured signals at $2.2\,\mu$m from the flux standards (corrected to an airmass of 1.00 using an extinction–airmass relation derived either from multiple observations of standard stars, or assumed to be 0.05 mag/airmass, typical for Mauna Kea, for nights

Table A.1: Standard stars used for flux calibration.

Star	K mag	Star	K mag
BS 437	1.43	BS 4695	2.20
BS 458	2.85	BS 4737	1.90
BS 874	1.40	BS 5191	2.20
BS 1195	2.09	BS 6703	1.62
BS 1552	4.14	BS 7446	5.04
BS 2219	1.94	BS 7806	1.44
BS 2574	0.66	BS 8167	2.24
BS 3903	2.04	BS 8173	1.64
BS 4335	0.44	BS 8498	1.05
BS 4358	3.24*	SAO 129959	3.14*
BS 4550	4.39		

*Own flux calibration, extrapolated from measurements of other standard stars.

where it could not be calculated), are plotted against their quoted K magnitudes in Fig A.2. Various observing runs are represented by different symbols and the cross in the lower left corner illustrates 10% uncertainty in the measurement. The small internal scatter, within each symbol, implies that the uncertainty in the galaxian spectral measurements introduced by flux calibration is, at most, comparable with that due to photon noise and baseline uncertainty (typically 10%; see data tables in Chapters 4 and 5). The reason for the discrepancy in Fig. A.2 between the measured signal — magnitude relation for 1986 March and the other observations is not known, but it has no effect on the flux calibration since only standards observed close in time to the galaxian measurements were used. As with the corrections for wavelength–dependent effects, the caveat regarding observation of flux standards close in projection on the sky to the source should be noted.

A.3 Wavelength Calibration

Calibration of the wavelength scale may be performed by observation of a line (or lines) of known wavelength, either from a laboratory or astronomical source. In practice, the Brγ hydrogen recombination line (λ=2.166 μm) from planetary nebulae (PNe) was used due to its strength and the weakness of their 2-μm continuum. Measurement of the difference between the wavelength of the line centre and 2.166 μm provided the linear shift required to wavelength calibrate the spectrum. The shift was invariably small (<0.01 μm). The low spectral resolution of the instrument (see below) meant that the planetary nebulae could be regarded as being at rest with respect to the Earth, thus simplifying the wavelength calibration.

The observations of PNe also enabled the resolution of the spectrophotometer to be determined. As shown in Figure A.3, the instrumental line profile is well approximated by a Gaussian having full width at half maximum (FWHM) of 0.0192 μm (equivalently, a velocity resolution at 2.17 μm of about 2660 km s^{-1}).

Several planetary nebulae were measured during each observing run but no detectable differences in wavelength calibration within each session were seen. However, there were variations between runs comparable to the instrumental resolution.

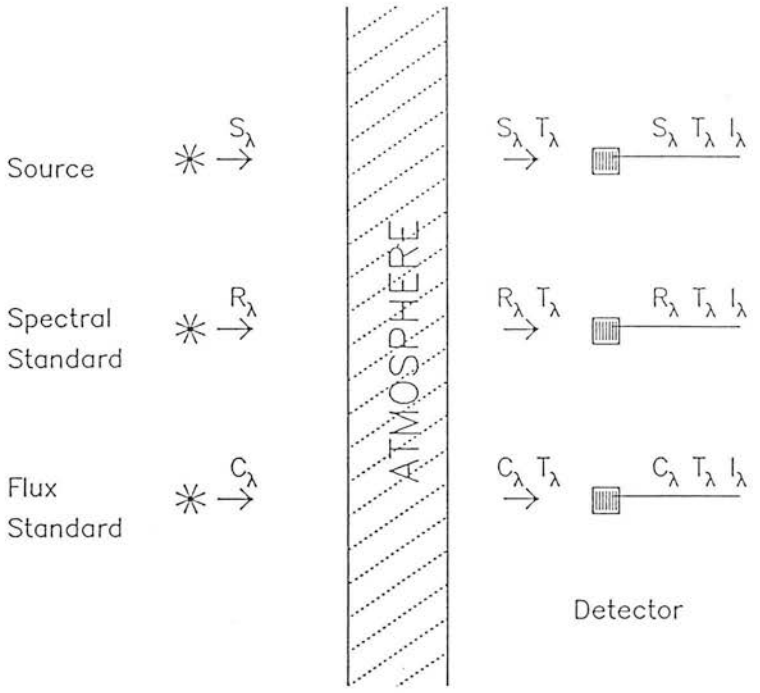

Figure A.1: Schematic of the propagation of radiation through the atmosphere and instrument.

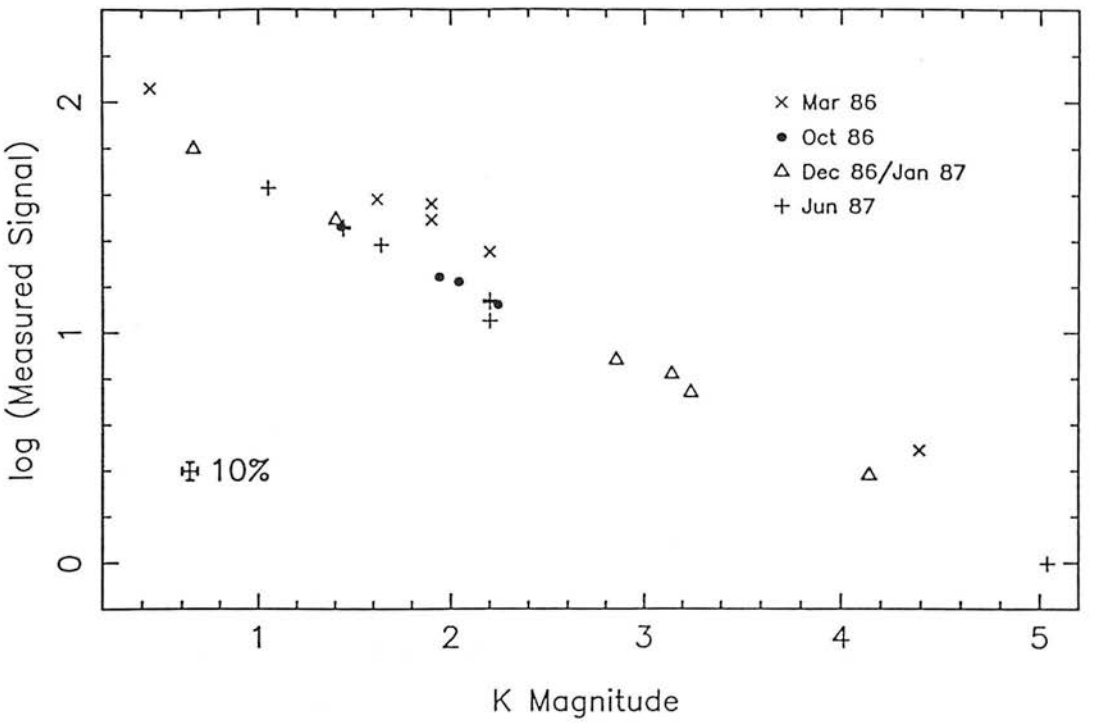

Figure A.2: Measured signal at 2.2 μm (in arbitrary units) as a function of the broad-band K magnitude for flux standard stars.

A.4 Determination of Line and Continuum Emission : an example

All of the steps involved in the reduction of the UKT 9 spectrophotometry were carried out using routines in a data reduction package called "SPAN" written by Gordon Thompson of the Royal Observatory, Edinburgh, and which correctly propagates the measurement uncertainties. The various stages in the reduction and analysis are illustrated in Figure A.4.

(a) The raw spectrum of NGC 1808, showing the measured signal (in arbitrary units) at each of 52 wavelength steps from 2.09 to 2.49 μm. The equally–spaced steps are separated by 0.008 μm, *i.e.* by 0.4 of the instrumental resolution, and therefore the spectrum is slightly oversampled. This spectrum is the co–addition of 5 individual scans (though, normally, 8 scans were taken) made with an integration time of 10 s per spectral point per scan. The "co–added" spectrum is formed by taking the mean of the scans at each point and the error assigned is the rms about this mean.

(b) The spectrum in Fig A.4a divided by the G9 III star BS 1195 which was used as both the flux and spectral standard. The abscissa is calibrated. This diagram illustrates one of the principal problems in low resolution spectrophotometry of galaxies : the emission lines have only a very small equivalent width. For example, the v=1–0 S(0) line (λ=2.223 μm) in this galaxy (which has a strength typical of the Brγ line in most of the other systems observed) is only about 1.5% of the continuum.

(c) As Fig A.4b but zero–suppressed. Several emission features can be seen and identified with transitions of atomic and molecular hydrogen on the basis of wavelength co–incidence. The spike at 2.28 μm and features between it and 2.38 μm do not correspond to expected transitions and are probably due to incomplete correction for wavelength–dependent effects, partly because of the redshift of the galaxy relative to the spectral standard. The difference between the continuum levels at about 2.2 and 2.45 μm is due to the photospheric CO feature (§1.1.1) which is clearly deeper in the galaxy than in the spectral standard.

(d) Fully–calibrated spectrum of NGC 1808 with the continuum subtracted.

Fig A.4 shows that despite the small equivalent widths of the lines, careful observational practice can reduce the measurement errors of the continuum to only a fraction of the line strength allowing the line fluxes to be determined. Continuum points, identified by eye, were fitted with a second order polynomial. The emission lines were fitted with Gaussians of fixed FWHM, there being no evidence that they were resolved at the low resolution employed. Both the central wavelength and peak flux density above the continuum were fitted, except for the blend of v=1–0 S(0) and v=2–1 S(1) (λ=2.223 and 2.248 μm, respectively) for which the redshifted central wavelengths were fixed. The integrated line flux was then found from

$$F = 1.064\, S_\lambda\, \Delta_\lambda \qquad \text{(A.5)}$$

where S_λ is the peak flux density and Δ_λ is the FWHM. The uncertainty in the integrated emission was evaluated from the error on the fitted peak flux added in quadrature to the estimated error of the fitted baseline, and taking the signal–to–noise at each spectral point into account.

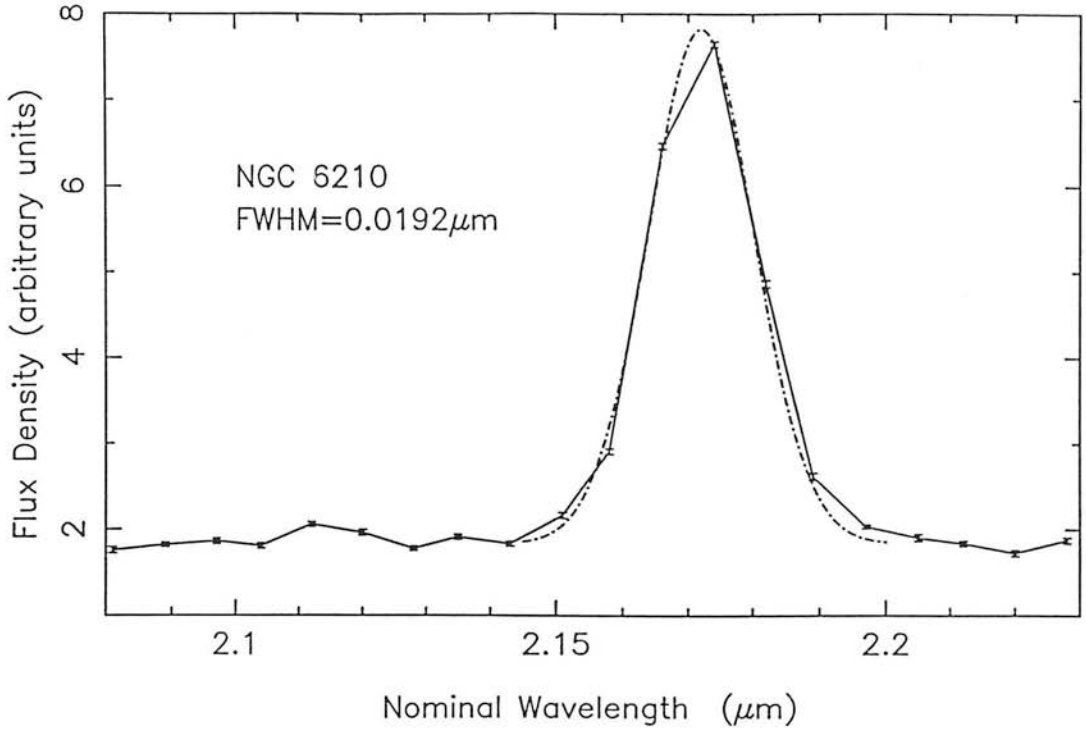

Figure A.3: The Brγ hydrogen recombination line in the planetary nebula NGC 6210, and a fitted Gaussian.

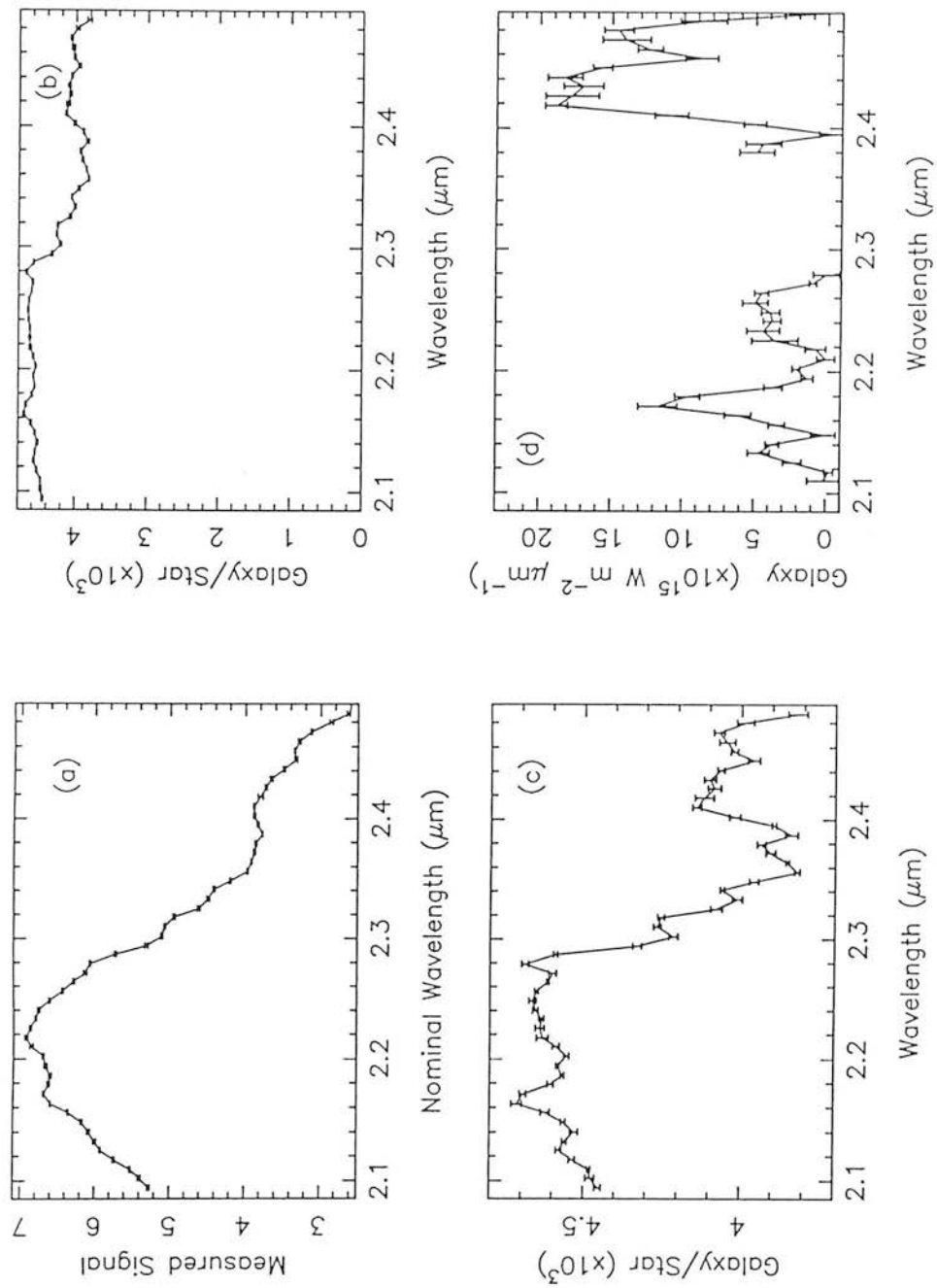

Figure A.4: Stages in the analysis of 2-μm spectrophotometry of the galaxy NGC 1808

References

Gezari, D.Y., Schmitz, M. & Mead, J.M., 1987. NASA RP–1196.

Hoffleit, D. & Jascheck, C., 1982. *The Bright Star Catalogue*, Yale University Observatory.

Mountain, C.M., Leggett, S.K., Selby, M.J., Blackwell, D.E. & Petford, A.D., 1985. *Astr. Astrophys.*, **151**, 399.

Appendix B

Extinction in Star–forming Complexes

Correction of the observed radiation for attenuation by dust is essential for investigating the true nature of the emitting source(s). This is particularly true for star–forming regions where the dust content, and thus the extinction, may be large. The purpose of this section is to describe modifications to the standard techniques which are necessary if the sources are distributed amongst dust. (This problem is analogous to that of dusty HII regions, considered by Mathis 1970).

Consider a star–forming region which consists of emitting sources (*e.g.* stars, HII regions) and absorbing dust, both of which are uniformly distributed. Let the dusty medium have an absorption coefficient κ_ν (per unit volume) and a volume emissivity ϵ_ν. This model is shown schematically in Figure B.1b. The propagation of radiation through this region is described by the radiative transfer equation :

$$\frac{dI_\nu}{d\tau_\nu} = -I_\nu + \frac{\epsilon_\nu}{\kappa_\nu} \tag{B.1}$$

where I_ν is the intensity at a frequency ν, and τ_ν is the optical depth. The latter is related to the radial variable by $d\tau_\nu = \kappa_\nu \, dL$. If there are no external sources (*i.e.* no radiation enters the region), and ϵ_ν and κ_ν are not functions of τ_ν (which is true for a homogeneous distribution), then Eqn. (B.1) may be integrated to give :

$$I_\nu(\tau_\nu) = \frac{\epsilon_\nu}{\kappa_\nu}\left(1 - \mathrm{e}^{-\tau_\nu}\right) \tag{B.2}$$

If $I_{\nu,0}$ is the intensity emitted by the source then since $\tau_\nu = \kappa_\nu \, L$:

$$I_\nu(\tau_\nu) = I_{\nu,0}\left(\frac{1 - \mathrm{e}^{-\tau_\nu}}{\tau_\nu}\right) \tag{B.3}$$

We can re–write Eqn. (B.3) for emission at two frequencies :

$$\frac{I_1}{I_2} = \frac{I_{1,0}}{I_{2,0}} \left(\frac{\tau_2}{\tau_1} \right) \left(\frac{1 - \mathrm{e}^{-\tau_1}}{1 - \mathrm{e}^{-\tau_2}} \right) \tag{B.4}$$

This form is useful since the emitted (intrinsic) ratio may be inferred, for example, from recombination theory in the case of hydrogen lines, or by assumption of the source temperatures for broad band fluxes.

Eqn. (B.4) differs from that usually employed to calculate the extinction, which only applies if the attenuation is purely foreground (see Figure B.1a) :

$$\frac{I_1}{I_2} = \frac{I_{1,0}}{I_{2,0}} \left(\frac{\mathrm{e}^{-\tau_1}}{\mathrm{e}^{-\tau_2}} \right) \tag{B.5}$$

and which is derived in similar fashion but assumes $\epsilon_\nu = 0$.

It is instructive to examine the effects of the two models described by Eqn. (B.4) and (B.5) on various recombination lines which are commonly used to determine the reddening. Figures (B.2a,b) show the observed $H\beta/H\alpha$ and $Br\gamma/Br\alpha$ line ratios for the two models as a function of the dust content; the latter being expressed in terms of the visual extinction (A_V). The dust optical depth for each line was calculated from the extinction at that wavelength :

$$\tau_\nu = 0.92\, A_\nu \tag{B.6}$$

using the Galactic reddening law by Rieke & Lebofsky (1985). Interpolated values of A_λ/A_V for several lines of interest are given in Table B.1. The intrinsic line ratios were taken from Hummer & Storey (1987) assuming an electron density and temperature of 10^4 cm^{-3} and 10^4 K, respectively. These are :

$$\frac{I(Br\gamma)}{I(Br\alpha)} = 0.354 \tag{B.7a}$$

and

$$\frac{I(H\beta)}{I(H\alpha)} = 0.351 \tag{B.7b}$$

Examination of Figure (B.2) shows that the observed line ratios diverge dramatically, even for the infrared Brackett lines, for only relatively modest values of the extinction.

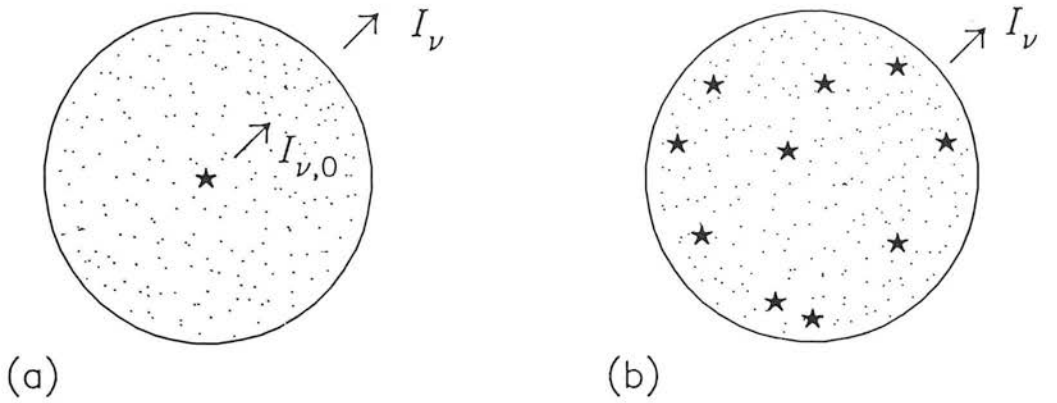

Figure B.1: The distribution of ionizing sources (stars) and obscuring dust (stippled) for (a) point source and (b) homogeneous models.

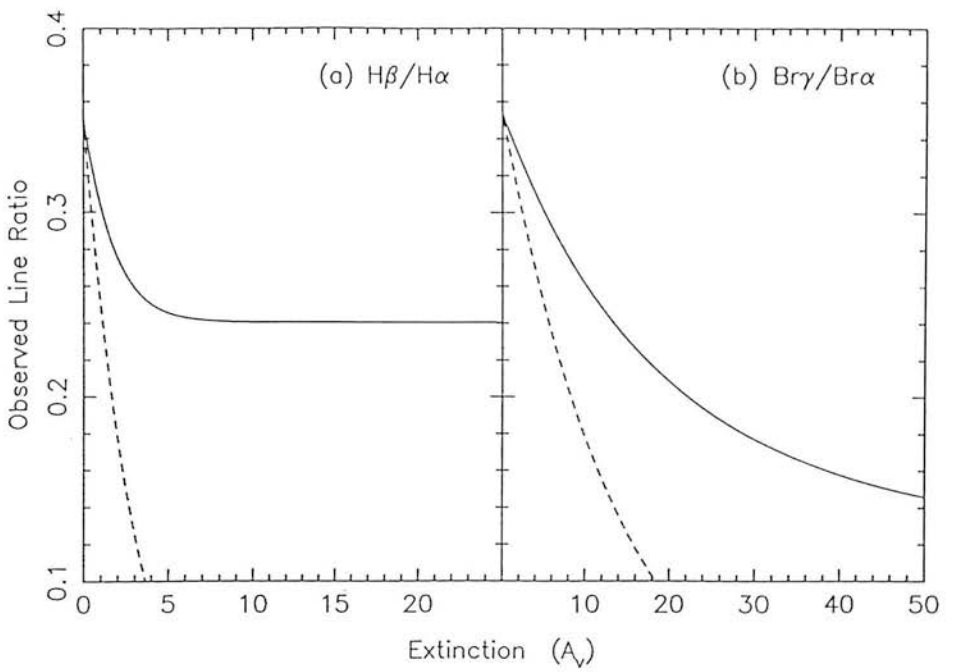

Figure B.2: Predicted (a) Hβ/Hα and (b) Brγ/Brα line ratios. The homogeneous and point-source models are represented by solid and dashed lines, respectively.

Table B.1: Relative extinction, in magnitudes, at the wavelengths of several hydrogen recombination lines.

Line	Wavelength (μm)	A_λ/A_V
Hβ	0.486	1.190
Hα	0.656	0.815
Paγ	1.094	0.345
Paβ	1.282	0.270
Brγ	2.166	0.115
Brα	4.052	0.040

Physically, this occurs because, in the homogeneous model, lines of longer wavelength (and thus smaller A_λ) probe further into the region and consequently sample more sources. The data are presented in another way in Figures (B.3) and (B.4) where the apparent visual extinction inferred from the observed line ratio is shown as a function of the real extinction. The apparent extinction is derived under the usual assumption of foreground dust. Obviously, for the point source (foreground extinction) model, the two agree. However, the loci representing the homogeneous model clearly demonstrate that the extinction may be severely under- or overestimated if incorrect assumptions concerning the source and dust distributions are made.

There are two solutions to this problem : (i) measurement of a very long wavelength line that suffers no attenuation (*e.g.* H53α; Chapter 6); and (ii) observation of several (≥ 3) lines. Figure (B.5) illustrates the latter technique. Loci representing the observed $Br\gamma/Br\alpha$ and $Pa\beta/Br\gamma$ line ratios as a function of the dust content (A_V) are plotted. These diverge due to the frequency dependence of the extinction. Also shown is the observed $Br\gamma/Br\alpha$ ratio for the nearby starburst galaxy NGC 253 (0.11; Beck & Beckwith 1984). This ratio indicates an extinction of $A_V \sim 17$ if the attenuation is purely foreground, but much larger values are implied if the dust is distributed amongst the sources of the line radiation. For this galaxy, measurement of an additional line (*e.g.* Paβ) would enable the foreground and intrinsic dust contents to be estimated, and the total extinction derived.

The distributed–sources model can therefore explain the discrepancy between values of the extinction derived from comparison of recombination line fluxes and those calculated by comparing the recombination line and thermal radio continuum fluxes; the latter always being the larger. This effect has been noted by several authors (*e.g.* Skillman & Israel 1988, and references therein).

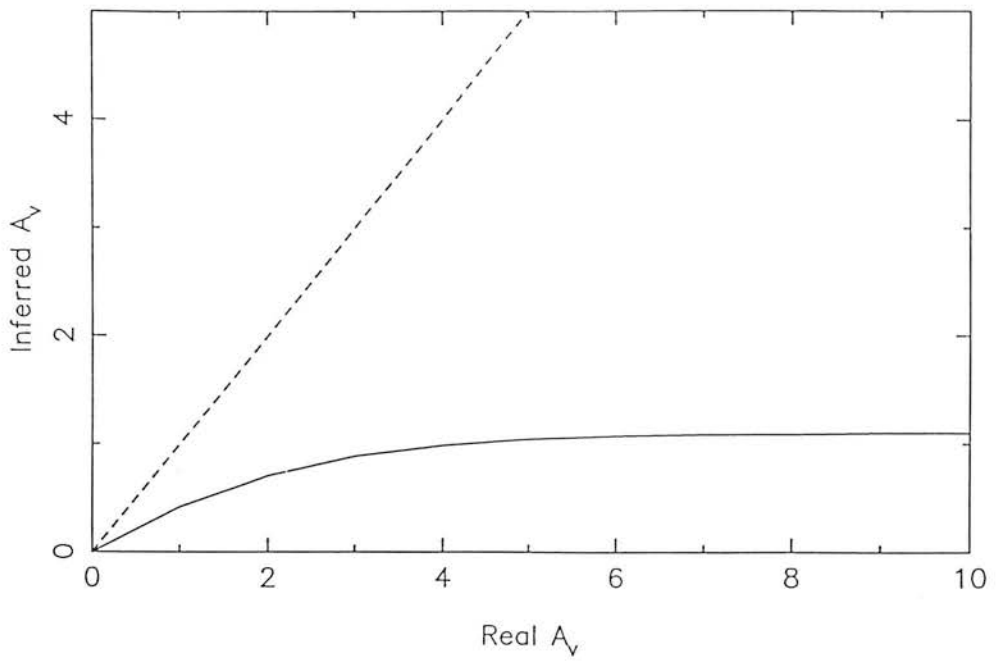

Figure B.3: Visual extinction (A_V) inferred from the predicted Hβ/Hα line ratios for the homogeneous (solid) and point–source (dashed line) models assuming foreground extinction.

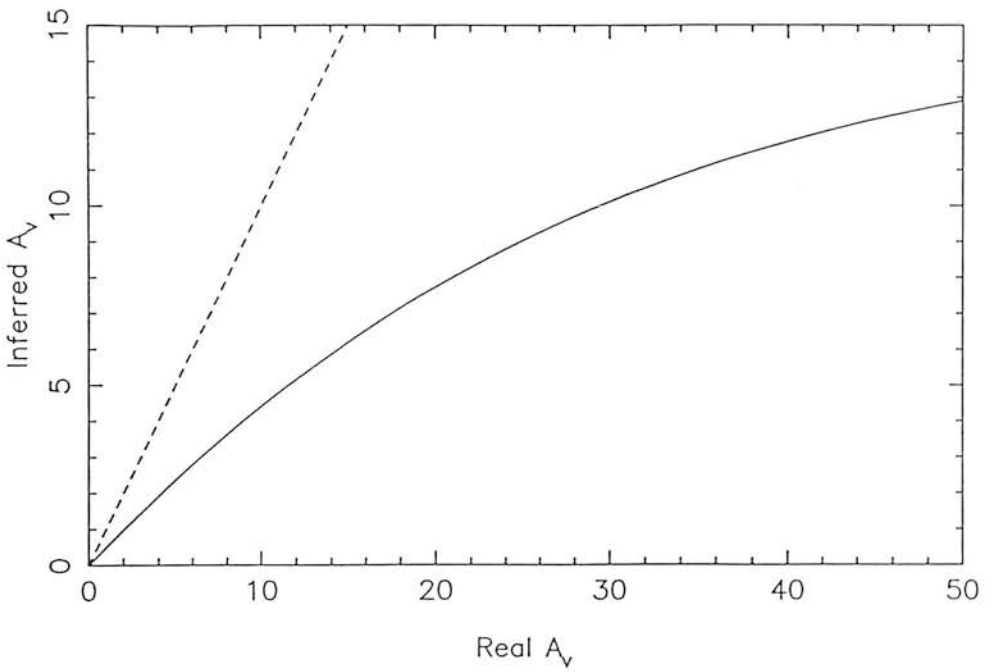

Figure B.4: As Figure (B.3) for Brγ/Brα lines.

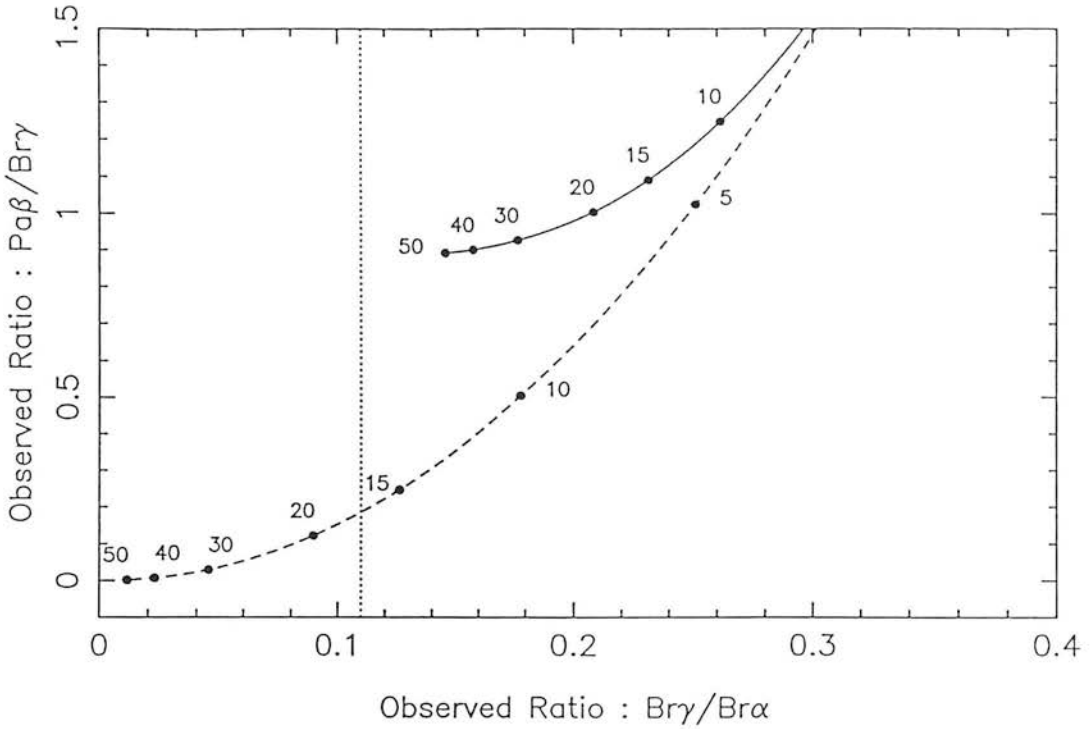

Figure B.5: Predicted $Br\gamma/Br\alpha$ and $Pa\beta/Br\gamma$ ratios as a function of visual extinction for the two models. Several values of A_V are marked. The vertical, dotted, line represents the measured $Br\gamma/Br\alpha$ ratio for NGC 253.

References

Beck, S.C. & Beckwith, S.V., 1984. *Mon. Not. R. astr. Soc.*, **207**, 671.

Hummer, D.G. & Storey, P.J., 1987. *Mon. Not. R. astr. Soc.*, **224**, 801.

Mathis, J.S., 1970. *Ap. J.*, **159**, 263.

Rieke, G.H. & Lebofsky, M.J., 1985. *Ap. J.*, **288**, 618.

Skillman, E.D. & Israel, F.P., 1988. *Astr. Astrophys.*, **203**, 226.

Appendix C

Line and Continuum Modelling of Starbursts

This appendix presents details of the model used to examine the line and continuum emission from regions of vigorous star formation. It is divided into two parts; the first describes the principles employed and derives the relevant equations. The second section gives the model parameters used.

C.1 Formulation of the Model

Following Gehrz, Sramek & Weedman (1983), the number of stars formed per year per unit mass interval in the starburst can be written :

$$dN = N_0 \, \psi(m) \, dm \tag{C.1}$$

where $\psi(m)$ is the initial mass function (the number distribution of stars with mass), and N_0 is a normalisation factor which sets the scale of the star formation rate. Note that Eqn. (C.1) is occasionally defined as the number of stars per unit *logarithmic* mass interval. The relationship between these two forms is :

$$m \, \psi(m) = \psi(\log m) \tag{C.2}$$

such that IMFs parameterised as power–law distributions :

$$\psi(m) \propto m^{\gamma} \tag{C.3a}$$

$$\psi(\log m) \propto m^{\Gamma} \tag{C.3b}$$

have slopes related by :

$$\gamma = \Gamma - 1 \tag{C.4}$$

It is not uncommon for the interval to be not specified, but it can usually identified if one of the standard IMFs is adopted; the Salpeter (1955) mass function has a slope of $\gamma = -2.35$.

Consider a starburst in which the stars are being formed at a constant rate, R. If the time since initiation of the current episode of star formation is t, then the total number of stars ever formed (per unit mass interval) is simply :

$$dN' = N_0 \, \psi(m) \, t \, dm \tag{C.5}$$

However, the lifetime of a star in a particular evolutionary stage, such as the main sequence, is a function of its mass. Let this be $\tau(m)$ for a star in the interval $m \rightarrow m + dm$, and define the mass of a star whose main sequence lifetime is $\tau = t$ to be $m = m_0$. There are two cases to consider. Stars with mass $m < m_0$, *i.e.* $\tau(m) > t$, have not yet reached the end of their main sequence lifetimes. Thus the number of stars in existence is simply :

$$dP_1 = N_0 \, \psi(m) \, t \, dm \tag{C.6}$$

Stars with mass $m > m_0$ have been 'dying', so that the fraction of all those ever formed which are still alive is $(R\,\tau(m)\,/R\,t)$. Thus the number still in existence is :

$$dP_2 = N_0 \, \psi(m) \, \tau(m) \, dm \tag{C.7}$$

Having found the number of stars present in the starburst at time t, the total emission in any waveband can be written :

$$F = \int_{m_l}^{m_0} f(m) \, dP_1 + \int_{m_0}^{m_u} f(m) \, dP_2 \tag{C.8}$$

where the mass–dependent emission, $f(m)$, is integrated between the lower (m_l) and upper (m_u) bounds of the IMF. This equation is completely general.

Equation (C.8) may be simplified if the radiation is dominated by massive stars whose lifetimes are less than the age of the starburst. For example, only stars with

masses $m \gtrsim 13\,\mathrm{M}_\odot$ contribute significantly to the number of ionizing photons. Letting the Lyman continuum emission from a star in the interval $m \rightarrow m + dm$ be n_{LyC}, gives the total number of such photons (equivalently, the ionization rate) as :

$$N_{LyC} = N_0 \int_{13}^{m_u} n_{LyC}(m)\, \psi(m)\, \tau(m)\, dm \tag{C.9}$$

provided that $\tau(13\,\mathrm{M}_\odot) < t$.

It is useful to define the star formation rate, R. Two definitions are in common use : the *mass* of stars formed per year, and the *number* of stars formed per year. The former is just the total mass of stars ever created divided by the starburst age :

$$\begin{aligned} R &= \frac{\int_{m_l}^{m_u} m\, dN'}{t} \\ &= N_0 \int_{m_l}^{m_u} m\, \psi(m)\, dm \end{aligned} \tag{C.10}$$

The latter form is obtained by integrating Eqn. (C.1) :

$$R = N_0 \int_{m_l}^{m_u} \psi(m)\, dm \tag{C.11}$$

The unknown normalisation parameter N_0 may be eliminated by substitution of Eqn. (C.8) (or C.9) into Eqn. (C.10) (or C.11). Thence the relationship between the star formation rate and an observable, *e.g.* the ionization rate :

$$R = N_{LyC}\, \frac{\int_{m_l}^{m_u} m\, \psi(m)\, dm}{\int_{m_l}^{m_u} n_{LyC}(m)\, \psi(m)\, \tau(m)\, dm} \tag{C.12}$$

reduces to a single constant for an assumed mass function. Similarly, the (type II) supernova rate, ν_{SN}, can be predicted from the ionization rate by replacing the lower limit of the IMF (m_l) in Eqn. (C.11) with the minimum mass for a supernova progenitor, m_{SN}. The normalisation parameter is more frequently eliminated by comparison of two observable properties, *e.g.* the ratio of ionization rate to infrared luminosity, which allows the uncertain properties of the IMF (m_l, m_u and slope) and starburst age, to be investigated.

If suitable data exists, *e.g.* observations in a number of wavebands which trace several different mass ranges, the time dependence of the star formation rate can be examined. Following Rieke *et al.* (1980), let the rate vary as e^{-t/τ_0}, where τ_0 is a constant scale factor. By analogy with Eqn. (C.5), the total number of stars ever formed is :

$$dN' = N_0\, \psi(m) \int_0^t e^{-t/\tau_0}\, dt\, dm \tag{C.13}$$

Here it has been assumed that the IMF is time–independent. (Note that this may not be true if it is related to the level of star formation activity). Again we consider two cases of star. For those having $m < m_0$, the number in existence is :

$$dP_1 = N_0\, \psi(m)\, \tau_0\, (1 - e^{-t/\tau_0})\, dm \tag{C.14}$$

For short–lived stars, only those born during the last $\tau(m)$ yr will still be alive. Thus, the fraction still existing is :

$$\frac{\int_{t-\tau(m)}^{t} e^{-t/\tau_0}\, dt}{\int_0^t e^{-t/\tau_0}\, dt} \tag{C.15}$$

and consequently, the number remaining is :

$$dP_2 = N_0\, \psi(m)\, \tau_0\, e^{-t/\tau_0}\, (e^{-\tau(m)/\tau_0} - 1)\, dm \tag{C.16}$$

The predicted emission can then be calculated using Eqn. (C.8), as before.

Due to computational reasons, two approaches were followed in the actual modelling. In the case of photo–ionized (H^+, O^{2+}, N^{2+}) gas (Chapter 6), the dependences of the observed emission, and main sequence lifetimes, on stellar mass were parameterised as segmented power–laws. In contrast, the total luminosity, and for consistency the ionization rate, in Chapter 6, and the photo–excited (H_2) gas (Chapter 5), were evaluated at each of the available stellar masses. There are negligible differences between the results obtained using these two models.

C.2 Details of the Model Parameters

C.2.1 Initial Mass Function

There are three uncertain parameters associated with the choice of IMF : slope, and lower and upper mass limits. The adopted gradient was taken from the analysis of the most recent data by Scalo (1986). For simplicity, a segmented power–law function was chosen and fitted to the data by eye, yielding :

$$\psi(m) = k\, m^{-1.25} \qquad 0.1 \leq M/\,\mathrm{M}_{\odot} < 0.7 \qquad \text{(C.17a)}$$

$$\psi(m) = 0.565k\, m^{-2.85} \qquad 0.7 \leq M/\,\mathrm{M}_{\odot} < 100 \qquad \text{(C.17b)}$$

where k is a scaling factor. The adopted IMF slope and original data are shown in Figure C.1.

The choices of lower and upper mass limits are somewhat arbitrary due to our ignorance concerning the processes determining the IMF (*e.g.* Silk 1987). The upper limit is thought to be set by the interaction of radiation from the protostellar core with accreting infalling matter; as an example Kahn (1974) gives :

$$\left(\frac{m_u}{\mathrm{M}_{\odot}}\right) = 60\left(\frac{\mathrm{Z}_{\odot}}{Z}\right)^{1/2} \qquad \text{(C.18)}$$

For the models of the atomic and molecular hydrogen emission (Chapters 4 & 5), various values between $m_u = 30$ and $100\,\mathrm{M}_{\odot}$ were employed. The absolute lower limit is believed to be set by the minimum mass for core ignition of hydrogen, $m_l \sim 0.1\,\mathrm{M}_{\odot}$, but may be substantially higher in starburst regions (see Scalo 1986 for a review). In any case, the observable properties examined in this thesis (*i.e.* photo–excited gas and bolometric luminosity) are dominated by more massive stars and are thus insensitive to the theoretical minimum stellar mass.

The rates of emission of ionizing (N_{LyC}) and non–ionizing (N_{NUV}) ultraviolet photons were calculated using the best available stellar atmosphere models, from Kurucz (1979). These models are tabulated as the photon energy flux emitted from unit surface area of a star of effective temperature, T_{eff}, at a range of wavelengths. The production rates (*i.e.* number s^{-1}) of photons capable of either ionizing atomic hydrogen or exciting molecular hydrogen were determined by integrating under the Kurucz model spectra over the ranges $\lambda \leq 91.2$nm and $91.2 < \lambda \leq 110.8$nm, respectively. Conversion from T_{eff} to the equivalent stellar mass was made using the compilation of stellar properties by Landolt–Börnstein (1982). Stellar radii taken from the same source were used to calculate the total photon production rates per star. Thus :

$$N_{LyC}(m) = 4\pi R(m)^2(\pi/h\,c)\int_0^{91.2} F(m,\lambda)\,\lambda\,d\lambda \qquad \text{(C.19a)}$$

$$N_{NUV}(m) = 4\pi R(m)^2(\pi/h\,c)\int_{91.2}^{110.8} F(m,\lambda)\,\lambda\,d\lambda \qquad \text{(C.19b)}$$

where $R(m)$ is the radius of a star of mass m and $F(m,\lambda)$ is the 'flux density' at a wavelength λ. (Note that the flux densities tabulated by Kurucz must be multiplied by π to obtain the usual definition). The results of the integration are given in Table C.1, and shown graphically in Figure C.2. The columns are : (1) effective temperature in K; (2) mass in $M_\odot$; (3) radius in $R_\odot$; (4) $\log_{10}$ ionizing photon flux in $\gamma\ s^{-1}$; (5) $\log_{10}$ non–ionizing photon flux in $\gamma\ s^{-1}$; and (6) $\log_{10}$ bolometric luminosity in $L_\odot$ (see §C.2.3). Details of the conversion from non–ionizing fluxes to molecular hydrogen line emission are given in Chapter 5.

For the far–infrared forbidden line modelling of M82, the recent models of photoionized regions by Rubin (1985) were adopted. One significant change made to these models was rejection of the assumption of constant N_{LyC} and the subsequent definition of an "effective stellar radius". Instead, the ionization rates given in Table C.1 were used to predict the hydrogen recombination line emission, and the fluxes in transitions of other species given by Rubin (1985) were scaled appropriately. The values employed are presented in Table C.2, for an electron density of $n_e = 100\ cm^{-3}$ and solar metal abundances, in units of the flux from an ionised region at a distance of 1 kpc (*c.f.* Table

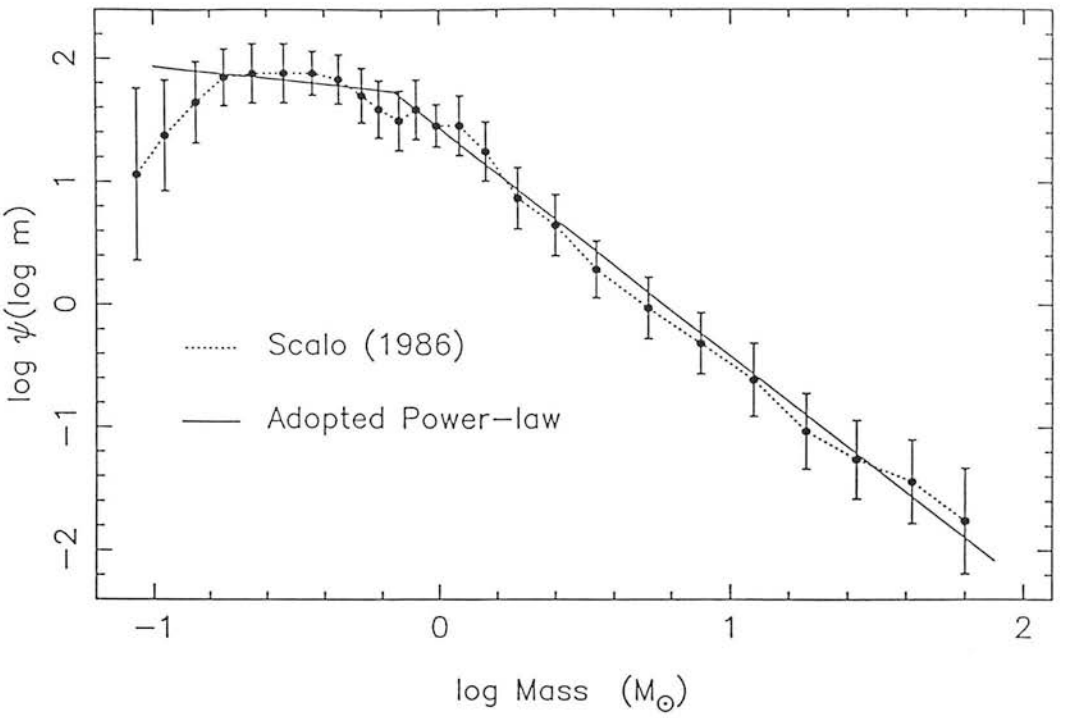

Figure C.1: The stellar initial mass function derived by Scalo (1986) and the adopted power–law parameterisation.

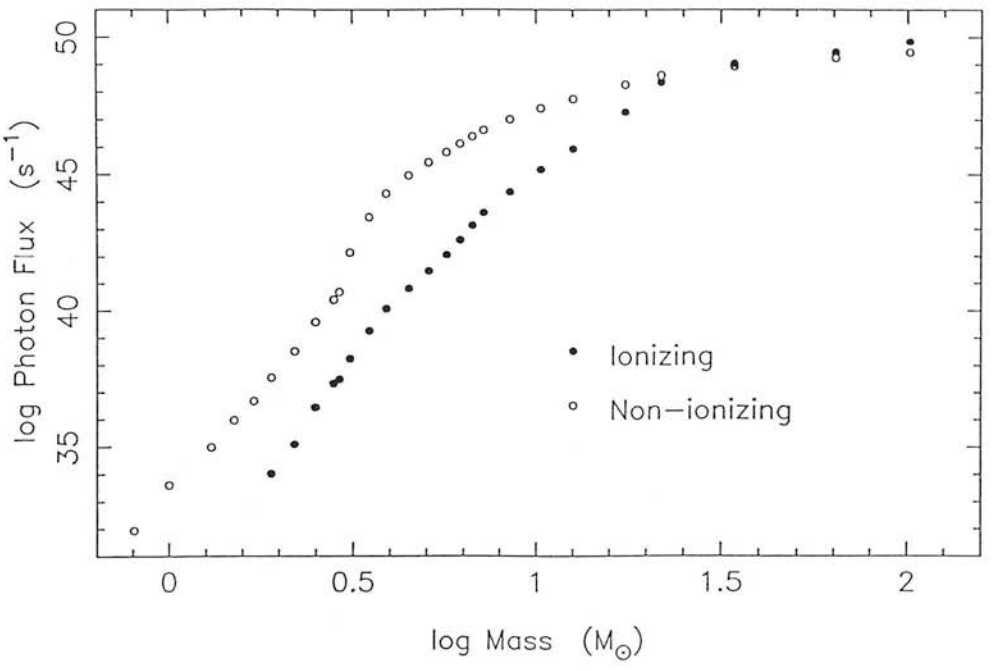

Figure C.2: The ionizing and non–ionizing UV photon fluxes as a function of stellar mass.

Table C.1: Mass dependences of stellar temperature and radius (Landolt–Börnstein 1982), and properties derived from Kurucz (1979) model atmospheres.

T_{eff}	Mass	Radius	Derived Properties		
			N_{LyC}	N_{NUV}	L_{BOL}
5500	0.8	0.88	–	31.95	–.24
6000	1.0	1.08	–	33.61	0.14
6500	1.3	1.32	–	34.99	0.45
7000	1.5	1.45	–	35.98	0.67
7500	1.7	1.56	–	36.68	0.84
8000	1.9	1.66	34.01	37.54	1.01
8500	2.2	1.86	35.08	38.50	1.21
9000	2.5	2.12	36.43	39.57	1.43
9400	2.8	2.34	37.31	40.38	1.59
9500	2.9	2.39	37.46	40.66	1.62
10000	3.1	2.52	38.22	42.10	1.76
11000	3.5	2.77	39.24	43.40	2.00
12000	3.9	3.03	40.05	44.27	2.24
13000	4.5	3.28	40.79	44.94	2.45
14000	5.1	3.54	41.43	45.42	2.64
15000	5.7	3.80	42.02	45.79	2.82
16000	6.2	4.06	42.57	46.10	2.98
17000	6.7	4.34	43.11	46.37	3.15
18000	7.2	4.61	43.58	46.60	3.30
20000	8.5	5.12	44.35	46.99	3.57
22500	10.3	5.72	45.17	47.39	3.87
25000	12.6	6.31	45.92	47.73	4.15
30000	17.5	7.40	47.26	48.26	4.59
35000	21.9	8.30	48.34	48.60	4.96
40000	34.3	10.19	49.03	48.92	5.37
45000	63.8	12.19	49.46	49.24	5.75
50000	101.3	14.06	49.84	49.45	6.05

4 of Rubin, which are, essentially, arbitrary units). The predicted line fluxes for the two–component density model discussed in Chapter 6 and for other metallicities were obtained in similar fashion.

C.2.3 Luminosity

The stellar luminosities were derived in a similar way to the UV photon rates (§C.2.2), but in this case the *energy* fluxes were integrated under the entire spectra. For consistency, the same stellar properties from Landolt–Börnstein (1982) were used. The mass–dependence of the luminosity is incorporated in Table C.1.

C.2.4 Main Sequence Lifetimes

For the purpose of simplifying the starburst modelling, it was assumed that all stars were on the main sequence. The effects of this assumption on the observed integrated properties are small, since massive main sequence stars dominate the gas ionization and excitation. Similarly, the input of post–main sequence stars to the total luminosity is relatively small (Telesco 1985). Scalo (1986) reviews observational and theoretical determinations of the main sequence lifetime–mass relationship. There are significant variations in the numerical models due to uncertainty in treating convection in the core. This occurs because convection can increase the effective core size, *i.e.* the amount of hydrogen available, and thus prolong the H–burning lifetimes. A power–law parameterisation was chosen since it was deemed that this gave the best fit to the observational data :

$$\tau(m) = 5.32 \times 10^{9} m^{-2.38} \ yr \qquad 0.1 \leq M/\,\mathrm{M}_{\odot} < 13 \qquad \text{(C.20a)}$$

$$\tau(m) = 5.39 \times 10^{7} m^{-0.59} \ yr \qquad 13 \leq M/\,\mathrm{M}_{\odot} < 100 \qquad \text{(C.20b)}$$

Detailed results of the molecular and atomic hydrogen modelling are given in Chapter 5. This section presents a brief analysis of the predicted ionization rate and luminosity. Taking data from Table C.1, the star formation rate was calculated using Eqns. (C.10) and (C.11) in terms of the ionization rate (*c.f.* Eqn. C.12) for several values of the lower and upper mass limits. These equations reduce to the simple relation :

$$R = c\, N_{LyC} \tag{C.21}$$

and values of the coefficient, c, are given in Table C.3 for both definitions of the star formation rate. The type II supernova rate can also be estimated from the final column of Table C.3, *e.g.* for a minimum progenitor mass between $m_l = m_{SN} = 5$ and $10\,\mathrm{M}_\odot$.

It is instructive to examine the distributions with mass of the total mass, ionization rate and luminosity for a starburst with an unevolved IMF (*e.g.* Telesco 1985). These functions are shown in Figure C.3 as $m\,\psi(m)$, $\psi(m)\,N_{LyC}$ and $\psi(m)\,L_{BOL}$ to illustrate the contributions from each stellar mass. As noted elsewhere, the integrated ionization rate is dominated by massive stars, whilst most of the mass is concentrated in the lower end of the IMF. The major contributors to the total luminosity are not the high–mass stars as might naively be expected, but those of intermediate mass due to their larger abundance. It is precisely this difference in the N_{LyC} and L_{BOL} distributions which allows them to be used as part of investigations into the star formation history.

In Figure C.4 the variation of the ratio N_{LyC}/L_{IR} as a function of starburst age is shown for several mass functions and assuming a constant rate of star formation (*c.f.* Telesco 1985). The ratio is constant for times less than the main sequence lifetime of the most massive star present, since no stars have died. In general, it decreases thereafter because the intermediate mass stars, which have low N_{LyC}/L_{IR} compared with those of higher mass, accumulate in the starburst due to their longer lifetimes. The decline is arrested when stars of the lowest mass start dying, *i.e.* when the birthrates and deathrates of all stars come into equilibrium. If the lower mass limit is large, there is negligible change in the ratio throughout the starburst lifetime.

Table C.2: Far–infrared line fluxes from photo–ionized regions surrounding stars of given effective temperature.

T_{eff}	Mass	Integrated Line Fluxes		
(K)	($M_\odot$)	H53α	[OIII]λ88 μm	[NIII]λ57 μm
31000	18.0	3.54×10^{-17}	1.41×10^{-12}	3.02×10^{-12}
33000	19.0	8.68×10^{-17}	2.88×10^{-11}	2.75×10^{-11}
36000	23.5	5.23×10^{-16}	7.41×10^{-9}	1.86×10^{-9}
37000	26.2	1.02×10^{-15}	3.24×10^{-8}	6.76×10^{-9}
40000	34.3	1.51×10^{-15}	1.18×10^{-7}	1.95×10^{-8}
45000	63.8	4.68×10^{-15}	4.91×10^{-7}	7.27×10^{-8}

Table C.3: Coefficients of the relation between star formation and ionization rates.

IMF Limits		log SFR coefficient	
m_l	m_u	$M_\odot$ yr^{-1}	yr^{-1}
0.1	30	–52.004	–51.678
0.1	60	–52.463	–52.140
0.1	100	–52.581	–52.261
1	30	–52.424	–52.736
1	60	–52.875	–53.198
1	100	–52.991	–53.319
5	30	–53.100	–54.046
5	60	–53.512	–54.497
5	100	–53.612	–54.615
10	30	–53.465	–54.647
10	60	–53.819	–55.066
10	100	–53.899	–55.177

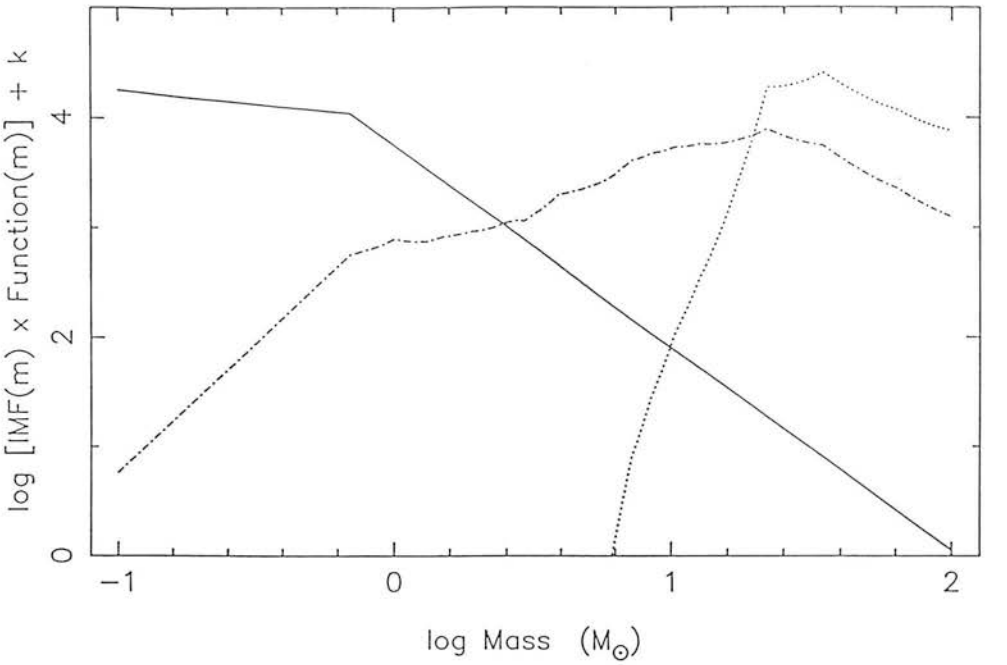

Figure C.3: Dependence on mass of the total mass (solid line), luminosity (dash–dot line) and ionization rate (dotted line) for an unevolved starburst. The ordinate scale has arbitrary units.

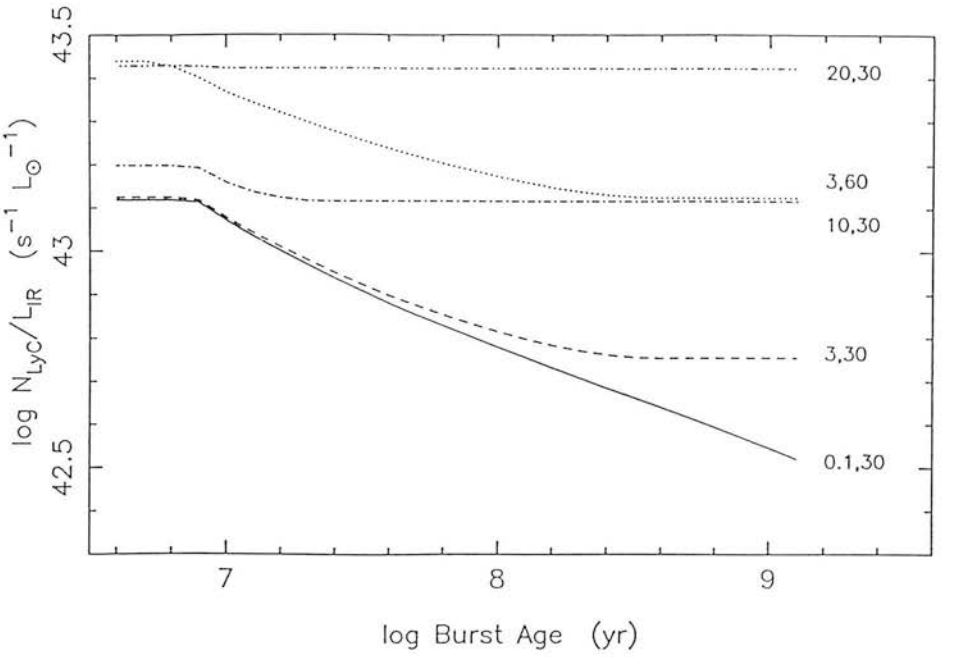

Figure C.4: Evolution of the N_{LyC}/L_{IR} ratio for a starburst with constant star formation rate. Tracks representing several mass functions (m_l, m_u) are shown.

In Figure C.5 the dependence of N_{LyC}/L_{IR} on the star formation rate is displayed. The loci indicate the ratio as a function of time for a specific IMF ($m_l = 3$, $m_u = 60$) and for various values of the time constant τ_0 (rate $\propto e^{-t/\tau_0}$; §C.1). For large τ_0, the behaviour is identical to that of a model with constant star formation rate, as expected. As τ_0 decreases, the variation in N_{LyC}/L_{IR} becomes much more rapid since few of the short–lived high–mass stars evolving off the main sequence get replaced.

Finally, it is worthwhile pointing out the dependence of N_{LyC}/L_{IR} on some of the adopted model parameters since this ratio is often used to determine properties of the starburst, such as age (*e.g.* Telesco & Gatley 1984). Unfortunately, the actual bounds of the particular IMF are rarely known and thus inference of the starburst age from N_{LyC}/L_{IR} is often meaningless since its value is very sensitive to the upper mass limit. Compare, for example, the curves of $m_l = 3$ and $m_u = 30$ and 60 $M_\odot$ in Figure C.4. Furthermore, Figure C.5 demonstrates that this ratio is also dependent on the star formation rate. By comparison, the effect of reasonable variations of the IMF slope is small. For example, a model with $m_l = 10$ and $m_u = 30$ and constant star formation rate has N_{LyC}/L_{IR} differing by only 0.05 dex between the adopted Scalo (1986) IMF and that by Salpeter (1955) : $\gamma = -2.85$ and -2.35, respectively.

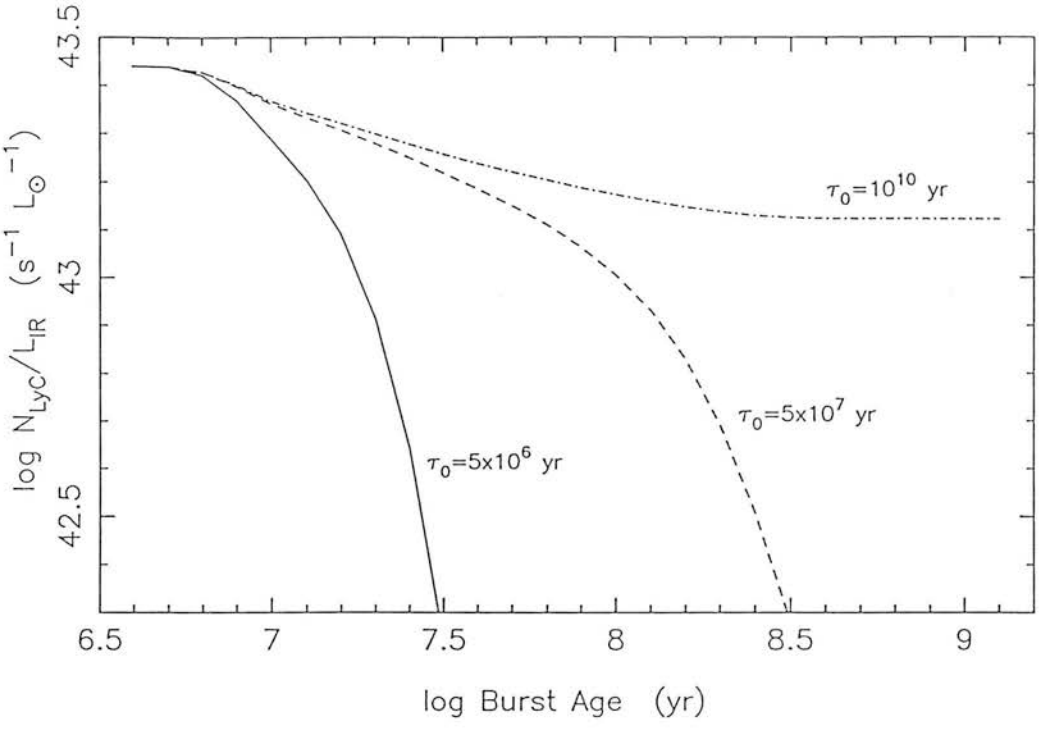

Figure C.5: Evolution of the N_{LyC}/L_{IR} ratio for a burst with exponentially decreasing star formation rate : $R \propto e^{-t/\tau_0}$.

References

Gehrz, R.D., Sramek, R.A. & Weedman, D.W., 1983. *Ap. J.*, **267**, 551.

Kahn, F.D., 1984. *Astr. Astrophys.*, **37**, 149.

Kurucz, R.L., 1979. *Ap. J. Suppl.*, **40**, 1.

Landolt–Börnstein 1982. *Astronomy & Astrophysics*, **2b**, Stars & Star Clusters. Eds. Schiaffers, K. & Voigt, H.H.

Rieke, G.H., Lebofsky, M.J., Thompson, R.I., Low, F.J. & Tokunaga, A.T., 1980. *Ap. J.*, **238**, 24.

Rubin, R.H., 1985. *Ap.J. Suppl.*, **57**, 349.

Telesco, C.M., 1985. In *Extragalactic Infrared Astronomy*, p87, Rutherford Appleton Laboratory. Ed. Gondhalekar, P.M.

Telesco, C.M. & Gatley, I., 1984. *Ap. J.*, **284**, 557.

Salpeter, E.E., 1955. *Ap. J.*, **121**, 161.

Scalo, J.M., 1986. *Fund. Cosm. Phys.*, **11**, 1.

Silk, J., 1987. In *Star Forming Regions (IAU 115)*, p.663 , eds. Peimbert, M. & Jugaku, J., Reidel.

Mon. Not. R. astr. Soc. (1988) **234,** *Short Communication,* 29P–40P

Fluorescent molecular hydrogen in galaxies

P. J. Puxley *Department of Astronomy, University of Edinburgh, Blackford Hill, Edinburgh EH9 3HJ*

T. G. Hawarden* and C. M. Mountain *Royal Observatory, Blackford Hill, Edinburgh EH9 3HJ*

Accepted 1988 June 3. Received 1988 June 1; in original form 1988 April 18

Summary. We present new near-infrared spectrophotometric observations of seven nearby spiral galaxies with vigorous central star-forming complexes. Emission from molecular hydrogen has been detected from near the nucleus of each of these galaxies and in every case it proves to be fluorescent, not shock excited. Comparison with the Brγ emission shows that excitation and ionization by ultraviolet radiation of power-law slope, as expected from an active nucleus, is not a viable mechanism. Instead, the observed molecular and atomic hydrogen line fluxes can be understood if the source of UV is an ensemble of stars having an initial mass function consistent with that of the solar neighbourhood. Our results contrast sharply with those so far available, for interacting, merging and some Seyfert galaxies, in which the excitation mechanism appears to be shocks. This difference may perhaps be due to beam size effects; if not, there appears to be a qualitative difference between the star-forming complexes in merging and interacting galaxies, on the one hand, and in barred spiral galaxies, on the other.

1 Introduction

Emission from molecular hydrogen in astronomical sources can be excited in two ways: by absorption of soft UV radiation in the Lyman and Werner bands (91.2–110.8 nm) followed by fluorescence down to the excited vibrational/rotational levels of the ground electronic state and subsequent radiative decay, or by collisional excitation with X-ray or shock-heated gas (Shull & Hollenbach 1978; Lepp & McCray 1983; Black & van Dishoeck 1987, 'BVD'). In both cases, the v=1–0 $S(1)$ line at 2.122 μm is generally the most easily detected transition. Discrimination between the two mechanisms is possible on the basis of the strength, relative to this line, of the v=1–0 $S(0)$ and v=2–1 $S(1)$ lines at 2.223 and 2.248 μm. These approach 50 per cent of the strength of v=1–0 $S(1)$ only in the case of fluorescence and are expected to be much weaker from shocked sources. [Note, however, that it is in principle possible for shock-like line ratios to arise

*Present address: Joint Astronomy Centre, 665 Komohana Street, Hilo, Hawaii 96720, USA.

from dense gas which is *radiatively* excited by an intense UV field; see Sternberg (1986) for details.]

The measured line ratios in most galactic sources (which include bipolar flows, planetary nebulae and supernova remnants) are consistent with the theoretical values for shock excitation (Shull & Beckwith 1982). It is therefore natural to associate the molecular hydrogen emission from other galaxies with shock heated gas; indeed, almost all systems observed thus far with sufficient spectral coverage and signal to noise to permit measurement of the strengths of the discriminant lines exhibit ratios appropriate to shock excitation, e.g. NGC 1068 (Thompson *et al.* 1978; Hall *et al.* 1981); NGC 6240 and Arp 220 (Joseph, Wright & Wade 1984; DePoy, Becklin & Wynn-Williams 1986). Although models of outflow sources in star-forming regions are only able to account for about 1 per cent of the observed H_2 emission (e.g. Kawara, Nishida & Gregory 1987, hereinafter KNG; see also Oliva & Moorwood 1986) supernovae, cloud–cloud collisions (*cf.* NGC 6240 and Arp 220), or the wind from an active nucleus (*cf.* NGC 1068) have been suggested, quite credibly, to make up the deficit.

In this paper we present observations of the v=1–0 $S(1)$, v=2–1 $S(1)$, v=1–0 $S(0)$ and v=1–0 Q-branch lines of molecular hydrogen, and the Brγ (7–4) line of atomic hydrogen for a number of galaxies. We report that in all but one of these systems, the line ratios do not indicate collisional excitation, but are, instead, very suggestive of *radiative pumping by the UV field from an ensemble of stars*. Fischer *et al.* (1987) have recently argued that molecular hydrogen emission from the Seyfert 1 galaxies NGC 3227 and 4151 is fluorescent, albeit with the excitation produced by the power-law UV continua of the Seyfert nuclei. Observations of fluorescent emission in a few other sources have also been made recently; in Orion's Bar (Hayashi *et al.* 1985), in the reflection nebulae NGC 2023 (Gatley *et al.* 1987) and Parasamyan 16 (Sellgren 1986), in the planetary nebula Hubble 12 (Dinerstein *et al.* 1988), in the extranuclear H II region NGC 604 in M33 (Israel *et al.* 1988), and possibly in the SMC H II region N88 (Israel & Koornneef 1988).

2 Observations of H_2 emission in nearby bright galaxies

The observations were obtained on the 3.8-m UK Infrared Telescope (UKIRT) with the facility single-channel photometer–spectrometer UKT9, using a Circularly Variable Filter (CVF) operated at a spectral resolution ($\lambda/\delta\lambda$) of 120. This cryostat is equipped with Fabry optics which make the spectral resolution of the system effectively independent of the size of the acceptance solid angle on the sky. All of these observations were carried out using a beam FWHM of 19.6 arcsec; the sensitivity variations within most of this beam are only a few per cent and there are no spectral variations across it. This permits photometry to be performed at consecutive CVF settings with very great internal precision and thus measurements can be made of lines which are a small fraction of the strong continuum against which they are observed: the practical limit is probably about 1 per cent.

Fig. 1(a–g) shows the K-window spectra of the nearby spiral galaxies NGC 1365, 1808, 3504, 4102, 4536, 5236 and 6946. Identifications for the emission features and their redshifted central wavelengths are shown. These galaxies represent a subset of the sample of spirals having *IRAS* 25-μm flux densities S_{25}>1.5 Jy which we are observing as part of a programme of large-beam near-IR spectrophotometry at UKIRT. A discussion of the recombination line emission and general properties of this sample will be presented elsewhere (Puxley *et al.*, in preparation). The spectra were divided by photometric standard stars oberved at a similar airmass and fitted continua have been subtracted. Late-type giant stars were used for the range 2.08–2.20 μm and earlier types, without stellar CO absorption features, for 2.20–2.50 μm. Emission line strengths were determined by fitting Gaussian functions to the lines, all of which were found to be unresolved at the resolution of the CVF. Table 1 lists the observed integrated line fluxes. The

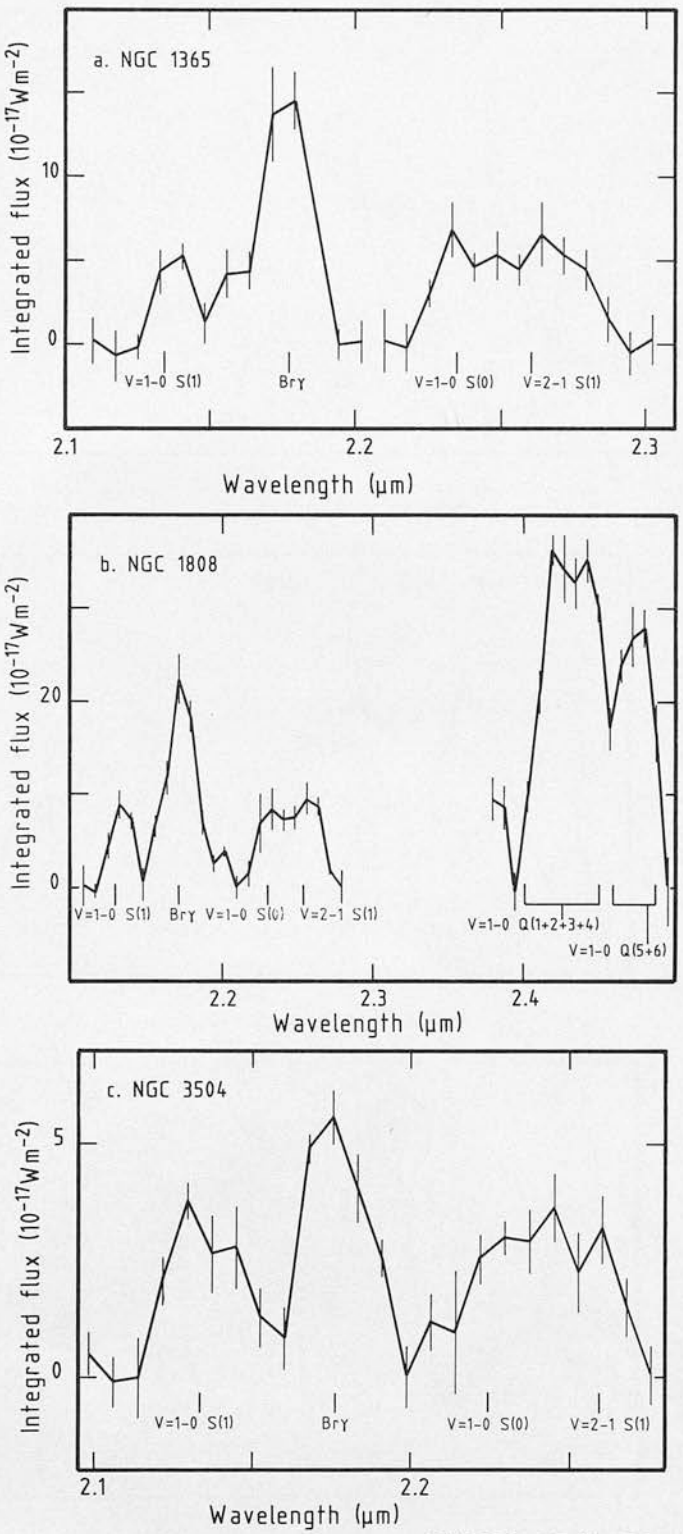

Figure 1. New 2-μm continuum-subtracted large-aperture spectra of (a) NGC 1365, (b) NGC 1808, (c) NGC 3504, (d) NGC 4102, (e) NGC 4536, (f) NGC 5236 and (g) NGC 6946.

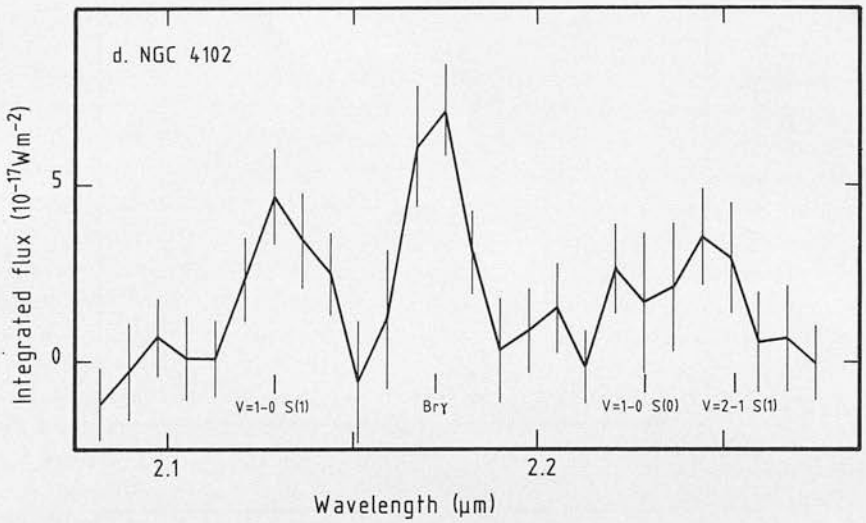

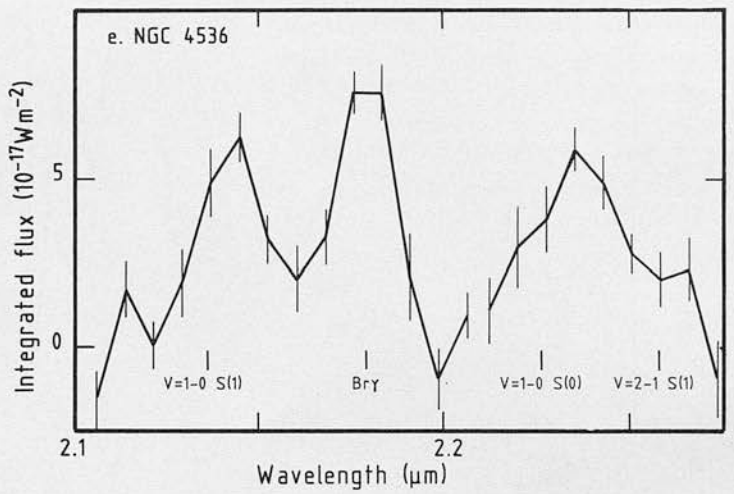

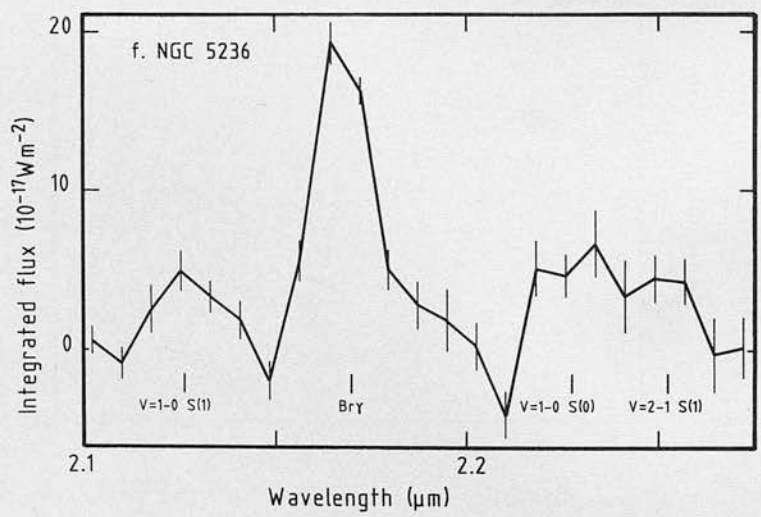

Figure 1 – *continued*

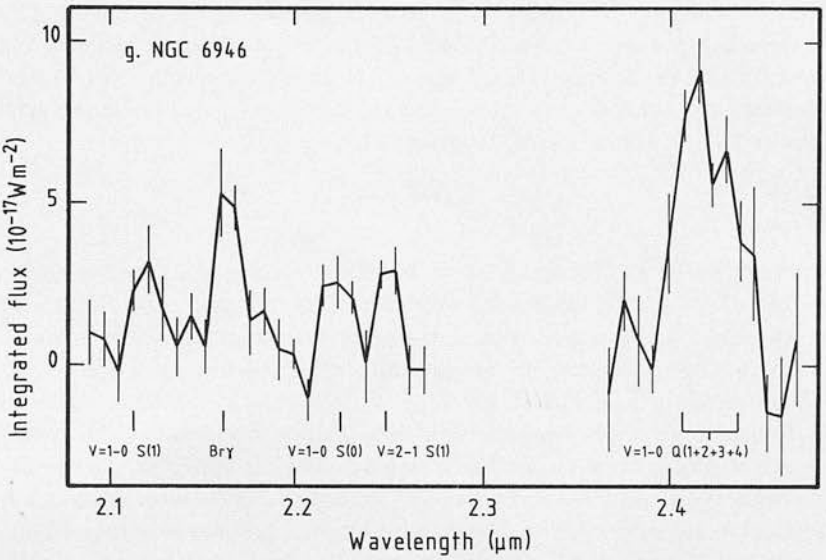

Figure 1 – *continued*

Table 1. Two micrometre spectrophotometric data for nearby spiral galaxies and theoretical line flux ratios.

Galaxy	Integrated Line Fluxes in 10^{-17} Wm^{-2}					
name	v=1–0 S(1)	Brγ	v=1–0 S(0)	v=2–1 S(1)	v=1–0 Q(1+2+3+4)	v=1–0 Q(5+6)
NGC 1365	7.5 ± 0.8	19.6 ± 1.1	5.7 ± 1.3	6.1 ± 1.3	–	–
NGC 1808	9.8 ± 0.8	22.3 ± 0.7	6.5 ± 1.2	8.9 ± 0.9	52 ± 7	28 ± 4
NGC 3504	4.8 ± 1.2	6.8 ± 1.2	3.9 ± 0.7	3.1 ± 0.7	–	–
NGC 4102	4.1 ± 0.6	5.9 ± 0.4	2.1 ± 0.7	2.1 ± 0.7	–	–
NGC 4536	6.4 ± 0.4	8.4 ± 0.5	5.4 ± 0.9	3.0 ± 0.8	–	–
NGC 5236	5.1 ± 0.7	19.6 ± 1.3	6.4 ± 1.4	4.6 ± 1.2	–	–
NGC 6946	3.2 ± 0.5	6.1 ± 1.2	2.6 ± 0.7	2.5 ± 0.7	16 ± 3	–
Fluorescent H_2 model	1.00	–	0.52 ± 0.06	0.54 ± 0.02	2.63 ± 0.14	0.43
Shocked H_2 model	1.00	–	0.23	0.08	1.97	0.53

indicated errors include a contribution from uncertainties in the level of the continuum fit. The final two rows in Table 1 give the expected theoretical values for the fluorescent and shock excited molecular hydrogen line ratios, relative to the v=1–0 $S(1)$ line (BVD; P. W. J. L. Brand, personal communication). In the former case, the errors reflect the ranges assumed for the model parameters, whilst the latter ratios are essentially constant (Brand *et al.* 1988).

There are no published measures of the fluxes of these lines in our galaxies with which we may

make direct comparisons, because of our large beam size. However, we note that the Brγ and v=1–0 S(1) fluxes listed here for NGC 1365 and 1808 are 4–5 times larger than those measured by KNG through a 7×4.5 arcsec aperture (*cf.* Kawara, Nishida & Taniguchi 1988). This is consistent with their inference from line observations that star formation extends over at least the central 1 kpc (see also Puxley, Hawarden & Mountain 1988).

3 Discussion

It is apparent, from Table 1, that the H_2 S-branch line ratios observed in all of these galaxies are not consistent with shock heating but are approximately those predicted by the UV pumping model. These ratios cannot be simulated by any reasonable amount of extinction applied to a shock excited source because of the small wavelength differences of the lines. The effect of reddening on the ratios is discussed in detail in Section 3.1, below. In Section 3.2 we argue that an ensemble of stars can produce sufficient ionizing and non-ionizing ultraviolet flux to excite both the atomic and molecular hydrogen line emission which we have observed. However, a power-law UV field with reasonable slope (β=1.2–1.6; Ferland & Osterbrock 1986) *cannot* produce enough non-ionizing radiation. In Section 3.3 we briefly address the implications of our results for models of central starbursts in galaxies. All of these issues will be examined in more detail elsewhere.

3.1 MOLECULAR LINE EMISSION AND REDDENING

Although the extinction in the near-infrared is much less than in the visible, the large amounts of dust observed towards the nuclei of IR-bright galaxies (DePoy 1987; Puxley *et al.*, in preparation) implies that there can be significant differential absorption even between the 2-μm lines of molecular hydrogen; thus, for example, between v=1–0 S(1) and Q-branch $A_{1\text{-}0\,S(1)}-A_Q \simeq 0.02\,A_V$.

To make some correction for this we have estimated the visual extinction (A_V) for each galaxy using the observed Brγ line strength (Table 1) together with values for the Hα or Hβ flux – taken from the literature – by assuming case B recombination theory (Baker & Menzel 1938) and simple foreground reddening. The extinction derived in this way is only a *lower* limit since the sources are probably spatially distributed amongst intervening dust. If so, and if there exists a significant amount of dust *between* the H II regions producing the recombination lines, then the reddening within these galaxies may have been severely underestimated (see also Mathis 1970; Puxley & Brand, in preparation). This is because the optical lines, which are the most affected, will tend to arise near the front surface of any such distributed region, whereas the longer-wavelength Brγ line will come from all sources to a greater physical, and far greater optical depth. For example, if the observed ratio of the Hβ/Brγ emission is 4 then an apparently low extinction $A_V \sim 2.2$ would be inferred from the conventional model of a point source and dust blanket, but a much higher value $A_V \sim 20$ is implied if the sources and dust are homogeneously mixed. Recognizing this, we proceed using the conventional technique and later investigate its viability.

The optical line fluxes were corrected to the 20 arcsec aperture of the CVF by assuming that the recombination line emission is co-extensive with the 10μm or radio continuum emission. References to the line strengths and source extents are given beneath Table 2. No correction has been made in the case of NGC 1365 due to uncertainty regarding the relative contributions of the active nucleus, for which case B is probably not applicable, and the inner star forming region. For NGC 5236 (M83) we adopt A_V=20 (Turner, Ho & Beck 1987). Table 2 shows the derived values for the visual extinction (column 2) together with the corrected line fluxes and ratios – using the reddening law of Rieke & Lebofsky (1985) – in columns 3–7. We note that Phillips, Aitken & Roche (1984) find that the reddening inferred from optical and infrared recombination lines in

Table 2. Extinction corrected line fluxes and ratios for nearby galaxies, together with results from the power-law and 'starburst' ionization/excitation modelling (see text).

Galaxy name	A_V [1]	Corrected Line Fluxes (in 10^{-17} Wm^{-2}) and Ratios					Power-law Model	'Starburst' Model		
		$1-0\,S(1)$	$Br\gamma$	$\frac{1-0\,S(0)}{1-0\,S(1)}$	$\frac{2-1\,S(1)}{1-0\,S(1)}$	$\frac{1-0\,Q(1+2+3+4)}{1-0\,S(1)}$	$R_{UV,\beta=1.6}$	$R_{UV}(100\,M_\odot)$	$R_{UV}(30\,M_\odot)$	$R_{UV}(3.5\times10^7 yr, 100\,M_\odot)$
NGC 1365	–	7.5 ± 0.8	19.6 ± 1.1	0.76 ± 0.19	0.81 ± 0.19	–	0.50	1.06	2.34	1.54
NGC 1808	5	17.1 ± 1.4	37.9 ± 1.2	0.64 ± 0.13	0.86 ± 0.11	4.8 ± 0.8	0.43	0.90	1.99	1.31
NGC 3504	4	7.5 ± 1.9	10.4 ± 1.8	0.78 ± 0.24	0.62 ± 0.21	–	0.27	0.56	1.24	0.82
NGC 4102	4	6.4 ± 0.9	9.0 ± 0.6	0.49 ± 0.20	0.49 ± 0.20	–	0.27	0.57	1.26	0.83
NGC 4536	6	12.5 ± 0.8	15.9 ± 0.9	0.80 ± 0.14	0.44 ± 0.12	–	0.24	0.52	1.18	0.75
NGC 5236	20	46.9 ± 6.4	164 ± 11	1.06 ± 0.27	0.74 ± 0.22	–	0.67	1.42	3.14	2.07
NGC 6946	6	6.2 ± 1.0	11.5 ± 2.3	0.78 ± 0.24	0.74 ± 0.24	4.4 ± 1.1	0.36	0.75	1.66	1.10

[1] References used for calculation of visual extinction (see text): NGC 1808 – Véron-Cetty & Véron 1986; Telesco *et al.* 1987; NGC 3504 – Stauffer 1982; Hummel, van der Hulst & Dickey 1984; NGC 4102 – Keel 1983a; Condon *et al.* 1982; NGC 4536 – Keel 1983b; Telesco *et al.* 1987; NGC 5236 – Turner, Ho & Beck 1987; NGC 6946 – Heckman, Balick & Crane 1980; Condon *et al.* 1982.

NGC 1808 and 6946 is considerably less than that implied by the depths of their 10 μm silicate features.

Although the observed H_2 S-branch line ratios are roughly those predicted by the UV pumping model, we note that relative to the v=1–0 $S(1)$ line, the blended Q-branch lines are stronger than expected in both NGC 1808 and 6946 – the only two objects observed at 2.3–2.5 μm. This is probably due to the sources being spatially distributed through the dust, and the reddening consequently underestimated, as outlined above. If we make the assumption that all of the molecular hydrogen emission in these galaxies is fluorescent, then we can derive a more accurate value of the reddening since the S- and Q-branch lines are relatively close to one another in wavelength and thus probe approximately the same depth of material. Using an intrinsic value for the ratio v=1–0 $Q(1+2+3+4)/v$=1–0 $S(1)$ of 2.63±0.14 (Black & van Dishoeck 1987), we estimate the visual extinction in NGC 1808 and 6946 to be A_V=33±11 and 30±15, respectively. These values are consistent with those inferred by Phillips, Aitken & Roche (1984) from the 10-μm optical depth, i.e. A_V=16±9 and 31±8 respectively. Adopting the values for A_V derived from the Q-branch and 1–0 $S(1)$ lines also brings the other ratios into closer agreement with the theoretical fluorescent model.

3.2 THE SOURCE OF THE UV

Recently, Fischer *et al.* (1987) have detected molecular and atomic hydrogen emission from the Seyfert galaxies NGC 1275, 4151 and 3227. In the latter they interpret the H_2 line ratios as indicating fluoresence. By assuming a power-law spectrum for the ultraviolet to X-ray continua of the Seyfert nuclei, they use the Brγ flux to calculate the number of UV photons in the range 91.2–110.8 nm that are available to excite the molecular hydrogen. This is then compared with the observed v=1–0 $S(1)$ flux by assuming that one $S(1)$ photon is emitted for every 50 UV photons absorbed, as predicted by the UV pumping model of BVD. Hence they derive a relationship:

$$R_{\mathrm{UV},\,\beta=1.6}=0.64f\,\frac{F(\mathrm{Br}\gamma)}{F[1\text{–}0\ S(1)]} \qquad (1)$$

where $(1-f)$ is the fraction of non-ionizing UV photons absorbed by dust before being able to excite the molecular gas, β=1.6 is the power-law slope ($f_\nu \propto \nu^{-\beta}$), and F(Brγ) and F[1–0 $S(1)$] are the measured fluxes. Essentially, R_{UV} is the number of ultraviolet photons available in the Lyman and Werner bands relative to the number required to produce the observed $S(1)$ emission. A value of $R_{UV}\geqslant 1$ means that there are sufficient photons available to excite the gas. Adopting $f\sim$0.3 (Sternberg 1986), Fischer *et al.* conclude that UV fluorescence is a viable mechanism in NGC 4151 (with R_{UV}=1.21) and, possibly, in NGC 3227 (R_{UV}=0.4), in which the diagnostic lines were actually detected. In column 8 of Table 2 we give the values of $R_{\mathrm{UV},\,\beta=1.6}$ calculated for the galaxies presented in this paper. No correction has been made for reddening since the differential extinction between 2.122 and 2.166 μm is negligible even for $A_V\sim$30. In each case the value of R_{UV} is much less than unity implying that excitation by a power-law UV field can probably be ruled out. Thus we must search for other sources of the UV – the most obvious being stars. [We note in passing, however, that of the galaxies with the largest values of R_{UV}, NGC 1365 and 1808 are known to possess active nuclei (Edmunds & Pagel 1982; Véron-Cetty & Véron 1985). It is possible that in these two cases there is a contribution to the fluorescent excitation by the nucleus itself, though given the small Brγ and 1–0 $S(1)$ fluxes measured by KNG it by no means dominates this process.]

We now give brief details from our modelling of UV excitation by an episode of star formation; fuller information will be presented in a future paper. In general, the value of some observable

property in a 'starburst' can be written (e.g. Gehrz, Sramek & Weedman 1983):

$$S_{\rm obs}=N_0\left[t\int_{m_l}^{m_0} S(m)\psi(m)\,dm+\int_{m_0}^{m_u} S(m)\psi(m)\tau(m)\,dm\right] \quad . \tag{2}$$

where $S(m)$ is the emission from a star of mass m, $\tau(m)$ is the main sequence lifetime of this star, $\psi(m)$ is the initial mass function (IMF) with upper and lower limits of m_u and m_l respectively, t is the time since star formation began and N_0 is a scaling factor. This equation is simply the sum of the emissions from stars whose main sequence lifetimes are larger than t [so that m_0 is the mass of a star having $\tau(m_0)=t$], and from those which have been dying. A constant star formation rate is assumed. By integrating under model stellar atmospheres (Kurucz 1979) we have calculated the ionizing ($\lambda\leqslant 91.2$ nm) and non-ionizing ($91.2<\lambda<110.8$ nm) photon production rates as a function of stellar mass. We also adopt the IMF given by Scalo (1986) and the lifetime–mass relation from Bahcall & Piran (1983). Assuming that 70 ionizing photons are required to produce each Brγ photon, as for Case B with $T=10^4$ K and $n_e=10^4$ cm^{-3} (Hummer & Storey 1987), and that 50 non-ionizing photons produce one 1–0 $S(1)$ photon (BVD), we can construct a relationship analogous to that in equation (1). For a 'zero-age' starburst [i.e. dropping the second term in equation (2) and setting $m_0=m_u=100\,M_\odot$, $m_l=0.8\,M_\odot$ and $t=1$] we find:

$$R_{\rm UV,\,s/burst}=1.35f\frac{F({\rm Br}\gamma)}{F[1-0\,S(1)]} \tag{3}$$

We have also calculated values for this parameter assuming $m_u=30\,M_\odot$ and for an episode of star formation with age $t=3.7\times10^7$ yr (and having $m_u=100\,M_\odot$). In these cases, the numerical factor in equation (3) becomes 2.99 or 1.97, respectively. The effect of decreasing the upper mass limit or increasing the age of the starburst (keeping a constant star formation rate) is just to increase the relative number of low-mass stars present, which in turn increases the relative fraction of non-ionizing UV photons. The effect on $R_{\rm UV,\,s/burst}$ of increasing the lower mass limit up to about $5\,M_\odot$ is negligible for a starburst of age 3.7×10^7 yr. In columns 9–11 of Table 2 we give the values of $R_{\rm UV,\,s/burst}$ for the galaxies taking $f\sim0.3$. It can be seen that, though dependent on the upper mass cut-off and the age of the starburst, the proposed mechanism of UV pumping by an ensemble of stars is viable.

Given higher signal-to-noise line observations and a better understanding of the factor f, it should be possible to use this technique to investigate the initial mass function and the age of the starburst in a more quantitative way. For the present, we can only say that the mass functions in the systems studied here are consistent with that in the solar neighbourhood.

3.3 H_2 EXCITATION AND THE PROPERTIES OF STARBURSTS

The galaxies in which the lines diagnostic of the H_2 excitation mechanism have previously been observed comprise the ultraluminous objects NGC 6240 and Arp 220, several Seyferts, including NGC 3227, hitherto the lone confirmed example of fluorescent molecular hydrogen emission, and about 10 galaxies selected as being IR-luminous interacting or post-merging systems, which are being studied by R. D. Joseph, G. S. Wright and collaborators (G. S. Wright, personal communication; see also Joseph *et al.* 1987). All except one, NGC 1068, are highly disturbed, with every indication that their gaseous components contain an abundance of kinetic energy. In contrast, the galaxies in the present study are morphologically quite normal spirals. Intuitively, therefore, it is perhaps not surprising that the H_2 emission from most of the former is shock excited, but from most of the latter it is not.

Unfortunately, except in that minority of interactors in which actual collisions of large masses of ISM are taking place (*cf.* NGC 6240), this comfortable intuition does not agree particularly well with our limited knowledge of the physical causes of vigorous star formation, or the

properties of star-forming complexes. In 'normal' galaxies, such star formation is effectively confined to barred systems (Hawarden *et al.* 1986) which strongly suggests that it owes its existence to the presence of the bar. In so far as we can claim to understand the causes of the more luminous starbursts in the interacting and merging galaxies, it would appear that the underlying mechanism is the same – the rotating non-axisymmetric potential produced by the bar or the companion galaxy drives an inflow of interstellar material which fuels, and perhaps even initiates, the star formation (Combes & Gerin 1985; Combes 1987). Thus there is no good reason to expect that the kinetic energy per unit mass of ISM in the starbursts in the two groups of galaxies is radically different, as the observational results appear to imply.

Perhaps more likely is that the difference between the spectroscopic properties of the two groups is the result of a selection effect. The disturbed systems are on average at a markedly larger distance than the normal galaxies, so that the spectrophotometry samples a larger spatial region around the nucleus. Observations of the former systems (covering 5 kpc, or more, in extent) may therefore be dominated by emission from shocked material being moved inwards, outside the central starburst, whilst our measurements (over ~1 kpc) may be dominated by the UV-rich central regions. Unpublished observations of the nearby system NGC 253 by G. S. Wright and collaborators (private communication) show a substantial increase in the strength of $v=1$–$0\,S(1)$ relative to Brγ at increasing radial distances from the nucleus. The situation is not simple, however, as these workers also find that their spectrum taken through a 20 arcsec aperture, in common with those of Rieke *et al.* (1988) using a 7.8 arcsec beam, and F. P. Israel (personal communication) in a 6 arcsec aperture, shows that the H_2 emission from the 'nuclear' regions of this galaxy is shock excited, not fluorescent.

The luminosities in the $v=1$–$0\,S(1)$ line of the galaxies studied here are between 1×10^{31} and 4×10^{32} W (for $H_0=75$ km s^{-1}), very much less than the $\sim10^{34}$ W emitted in this line by shocked H_2 in the ultraluminous *IRAS* galaxies such as Arp 220, NGC 6240 and *IRAS* 14348−1447 (Geballe 1988), but comparable to the 4×10^{32} W from shocked gas in NGC 1068. Sanders *et al.* (1988) have suggested that the ultraluminous *IRAS* galaxies are generically related to the most luminous AGNs and, perhaps, draw their power from a buried central quasar. It might therefore be speculated that in these and the other luminous (disturbed) systems the shocked H_2 emission is caused by a wind from an active nucleus, rather than by mass motions of the molecular material itself. This is certainly true of the nearby low-luminosity active spiral NGC 3079 (Hawarden *et al.*, in preparation) and is consistent with the observation by KNG that the AGNs in their sample have markedly higher luminosity in 1–$0\,S(1)$ than do the starburst systems. However, it should be noted that on their figure Arp 220, an excellent candidate for an ultraluminous galaxy containing a buried quasar, lies amongst the starburst systems, while NGC 6240, which may only contain a mere LINER nucleus, has an order of magnitude more luminosity in $S(1)$, for its total luminosity, than do the rest of the AGNs.

Our results clearly demonstrate the need for caution in using spectrophotometry of H_2 emission in one or a few galaxies to infer an evolutionary sequence for starbursts such as that by Rieke *et al.* (1988). While the general picture proposed by these workers may be correct, it now appears that the H_2 emission from NGC 253 which inspired it may be quite atypical in its excitation mechanism. Similar reservations apply to the use of the $v=1$–$0\,S(1)$ line strengths, alone, to examine the physics of galactic nuclei. At present it seems clear only that if meaningful progress is to be made in understanding these problems, an increase in the sample of *adequately* studied galaxies, and much more information on radial variations of the excitation mechanism, are essential.

Acknowledgments

Most of the data upon which this paper is based were obtained in observing time awarded by the

UK Panel for the Allocation of Telescope Time (PATT). The successful employment of this time is a tribute to the skill and efficiency of telescope operators Joel Aycock, Dolores Walther and Thor Wold. Certain important supplementary and confirming observations were obtained for us as part of the UKIRT Service Observing programme. We are particularly grateful to Gillian Wright and Bob Joseph for showing, discussing and allowing us to refer to their unpublished spectroscopy of interacting and merging starburst galaxies. Toby Moore, Peter Brand, Frank Israel and Tom Geballe all contributed help, advice and stimulus to this work, and its presentation was improved by the helpful comments of the referee. We thank Marjorie Fretwell for drawing the diagrams. PJP acknowledges an SERC studentship.

References

Bahcall, J. N. & Piran, T., 1983. *Astrophys. J.,* **267,** L77.
Baker, J. G. & Menzel, D. H., 1938. *Astrophys. J.,* **88,** 52.
Black, J. H. & van Dishoeck, E. F., 1987. *Astrophys. J.,* **322,** 412. (BVD).
Brand, P. W. J. L., Moorhouse, A., Burton, M. G., Geballe, T. R., Bird, M. & Wade, R., 1988. *Astrophys. J.,* submitted.
Combes, F., 1987. *Whistler Conference on Extragalactic Star Formation,* in press.
Combes, F. & Gerin, M., 1985. *Astr. Astrophys.,* **150,** 327.
Condon, J. J., Condon, M. A., Gisler, G. & Puschel, J. J., 1982. *Astrophys. J.,* **252,** 102.
DePoy, D. L., 1987. *PhD thesis,* University of Hawaii.
DePoy, D. L., Becklin, E. E. & Wynn-Williams, C. G., 1986. *Astrophys. J.,* **307,** 116.
Dinerstein, H. L., Lester, D. F., Carr, J. S. & Harvey, P. M., 1988. *Astrophys. J.,* **327,** L27.
Edmunds, M. G. & Pagel, B. E. J., 1982. *Mon. Not. R. astr. Soc.,* **198,** 1089.
Ferland, G. J. & Osterbrock, D. E., 1986. *Astrophys. J.,* **300,** 658.
Fischer, J., Geballe, T. R., Smith, H. A., Simon, M. & Storey, J. W. V., 1987. *Astrophys. J.,* **320,** 667.
Gatley, I., Hasegawa, T., Suzuki, H., Garden, R., Brand, P., Lightfoot, J., Glencross, W., Okuda, H. & Nagata, T., 1987. *Astrophys. J.,* **318,** L73.
Geballe, T. R., 1988. *Mon. Not. R. astr. Soc.,* in press.
Gehrz, R. D., Sramek, R. A. & Weedman, D. W., 1983. *Astrophys. J.,* **267,** 551.
Hall, D. N. B., Kleinmann, S. G., Scoville, N. A. & Ridgway, S. T., 1981. *Astrophys. J.,* **248,** 898.
Hawarden, T. G., Mountain, C. M., Leggett, S. K. & Puxley, P. J., 1986. *Mon. Not. R. astr. Soc.,* **221,** 41P.
Hayashi, M., Hasegawa, T., Gatley, I., Garden, R. & Kaifu, N., 1985. *Mon. Not. R. astr. Soc.,* **215,** 31P.
Heckman, T. M., Balick, B. & Crane, P. C., 1980. *Astr. Astrophys. Suppl.,* **40,** 295.
Hummel, E., van der Hulst, J. M. & Dickey, J. M., 1984. *Astr. Astrophys.,* **134,** 207.
Hummer, D. G. & Storey, P. J., 1987. *Mon. Not. R. astr. Soc.,* **224,** 801.
Israel, F. P. & Koornneef, J., 1988. *Astr. Astrophys.,* **190,** 21.
Israel, F. P., Hawarden, T. G., Wade, R., Geballe, T. R. & van Dishoeck, E. F., 1988. *Mon. Not. R. astr. Soc.,* submitted.
Joseph, R. D., Wright, G. S. & Wade, R., 1984. *Nature,* **311,** 132.
Joseph, R. D., Wright, G. S., Wade, R., Graham, J. R., Gatley, I. & Prestwich, A. H., 1987. In: *Second IRAS Conference: Star Formation in Galaxies,* p. 421, ed. Lonsdale-Persson, C. J.
Kawara, K., Nishida, M. & Gregory, B., 1987. *Astrophys. J.,* **321,** L35.
Kawara, K., Nishida, M. & Taniguchi, Y., 1988. *Astrophys. J.,* **328,** L4.
Keel, W. C., 1983a. *Astrophys. J.,* **269,** 466.
Keel, W. C., 1983b. *Astrophys. J. Suppl.,* **52,** 229.
Kurucz, R. L., 1979. *Astrophys. J. Suppl.,* **40,** 1.
Lepp, S. & McCray, R., 1983. *Astrophys. J.,* **269,** 560.
Mathis, J. S., 1970. *Astrophys. J.,* **159,** 263.
Oliva, X. & Moorwood, A. F. M., 1986. *Astr. Astrophys.,* **164,** 104.
Phillips, M. M., Aitken, D. K. & Roche, P. F., 1984. *Mon. Not. R. astr. Soc.,* **207,** 25.
Puxley, P. J., Hawarden, T. G. & Mountain, C. M., 1988. *Mon. Not. R. astr. Soc.,* **231,** 465.
Rieke, G. H. & Lebofsky, M. J., 1985. *Astrophys. J.,* **288,** 618.
Rieke, G. H., Lebofsky, M. J. & Walker, C. E., 1988. *Astrophys. J.,* **325,** 679.
Sanders, D. B., Soifer, B. T., Elias, J. M., Madore, B. F., Matthews, K., Neugebauer, G. & Scoville, N. Z., 1988. *Astrophys. J.,* **325,** 74.

Scalo, J. M., 1986. *Fundam. Cosmic Phys.,* **11,** 1.
Sellgren, K., 1986. *Astrophys. J.,* **305,** 399.
Shull, J. M. & Beckwith, S., 1982. *Ann. Rev. Astr. Astrophys.,* **20,** 163.
Shull, J. M. & Hollenbach, D. J., 1978. *Astrophys. J.,* **220,** 525.
Stauffer, J. R., 1982. *Astrophys. J. Suppl.,* **50,** 517.
Sternberg, A., 1986. *PhD thesis,* Columbia University.
Telesco, C. M., Decher, R., Ramsey, B. D., Wolstencroft, R. D. & Leggett, S. K., 1987. In: *Second IRAS Conference: Star Formation in Galaxies,* p. 497, ed. Lonsdale-Persson, C. J.
Thompson, R. I., Lebofsky, M. J. & Rieke, G. H., 1978. *Astrophys. J.,* **222,** L49.
Turner, J. L., Ho, P. T. P. & Beck, S. C., 1987. *Astrophys. J.,* **313,** 644.
Véron-Cetty, M.-P. & Véron, P., 1985. *Astr. Astrophys.,* **145,** 425.
Véron-Cetty, M.-P. & Véron, P., 1986. *Astr. Astrophys. Suppl.,* **66,** 335.

Mon. Not. R. astr. Soc. (1988) **231**, 465–478

Enhanced star formation in barred spiral galaxies – II. Radio continuum emission

P. J. Puxley *Department of Astronomy, University of Edinburgh, Royal Observatory, Blackford Hill, Edinburgh EH9 3HJ*

T. G. Hawarden and C. M. Mountain *Royal Observatory, Blackford Hill, Edinburgh EH9 3HJ*

Accepted 1987 October 1. Received 1987 September 24; in original form 1987 August 4

Summary. The radio properties of an *IRAS*-selected sample of nearby spiral galaxies have been investigated using new and published 20-cm continuum observations. Virtually all of the galaxies with steep 12–25 μm spectra are barred and possess a central radio source of linear extent less than 1–3 kpc. We argue that the activity in these systems is due to enhanced star formation rather than a compact nucleus. The central sources contribute, on average, 35 per cent to the total radio emission and their typical far-infrared luminosity is estimated to be a few $\times 10^9 L_\odot$. In contrast to the other *IRAS* wavebands, the 25 μm–radio correlation shows a marked dependence on the level of star-formation activity.

1 Introduction

During the last 15 years there has been a number of surveys investigating the dependence of radio continuum emission on morphological type for optical- or radio-selected samples of bright spiral galaxies. Low-resolution observations generally measure only the total flux and show no clear dependence of the radio emission on Hubble type or the existence of a bar (Cameron 1971; Dressel & Condon 1978; Dressel 1979). Surveys made with an angular resolution of better than about 20 arcsec are able to separate the central (<few kpc) and disc components in these nearby spirals (Condon & Dressel 1978; Hummel 1980, henceforth H80; Hummel 1981, henceforth H81). Several trends are apparent in the radio properties. The emission from the disc is indistinguishable for the de Vaucouleurs (1959) morphological families SA, SB and SX. This is consistent with the low-resolution results since the disc contributes, on average, 90 per cent to the total 1415-MHz flux. The central component, however, is typically twice as powerful in those systems possessing a bar (H81). There is also a strong correlation with Hubble type; the contribution of the central component to the total flux is significantly greater in early-type spirals.

Observations at even higher resolutions, typically 0.2 to 2 arcsec, probe the structure of the central regions and can suggest mechanisms for energy production in these sources (Condon 1980; van der Hulst, Crane & Keel 1981; Condon *et al.* 1982; Hummel, van der Hulst & Dickey

1984). Although the number of galaxies so far observed at high resolution is small, several interesting relations are emerging. Galaxies of type Sab or earlier generally have compact core sources with flat or inverted radio spectra and high brightness temperatures, whilst galaxies of type Sb and later preferentially have complex sources and steep, non-thermal spectra. These observations have been cited as evidence for the existence of two different energy sources in the central regions (e.g. Condon & Dressel 1978; Biermann 1980; Ulvestad 1982). Emission from an active nucleus may be responsible for the compact core sources, whereas numerous supernovae and H II regions produced in a burst of vigorous star formation are the most likely power source in those systems with a complex extended radio structure. Some galaxies show an intermediate class of central radio structure in which both mechanisms may be operating.

In many spiral galaxies, much of the luminosity is thermal emission from dust at wavelengths between 10 μm and 1 mm. Hence the all-sky survey provided by the *Infrared Astronomical Satellite* (*IRAS*) at 12, 25, 60 and 100 μm is a valuable database with which to examine the infrared properties of galaxies and their dependence on optical morphology. Of dominant importance appears to be the presence of an interacting companion galaxy or the existence of a stellar bar (e.g. Hawarden *et al.* 1986, hereafter Paper I; Joseph *et al.* 1984; see also the reviews by Wynn-Williams 1987 and Becklin 1987).

Galaxy–galaxy interactions and mergers have been identified as causing strong infrared emission in some systems both from ground-based 1–10 μm photometry (Joseph *et al.* 1984; Cutri & McAlary 1985; Joseph & Wright 1985) and from *IRAS* observations (e.g. Lonsdale, Persson & Matthews 1984). Indeed, some of these galaxies are amongst the most luminous known, having $L_{\rm IR} = 10^{11}$–$10^{13}\,L_{\odot}$ ($H_0 = 75\,{\rm km\,s^{-1}\,Mpc^{-1}}$); in contrast, the infrared luminosity of nearby spirals varies between 10^9 and $10^{11}\,L_{\odot}$ (de Jong *et al.* 1984; Fairclough 1985).

Hawarden *et al.* (1986) have analysed Shapley–Ames galaxies (Sandage & Tammann 1981, RSA) in the *IRAS Point Source Catalog* (1985) and find that the most luminous of the non-Seyfert normal spirals are invariably barred (see also Devereux 1987). They conclude that their extra luminosity and 'warm' 25–100 μm *IRAS* colours are best fitted by a burst of vigorous star formation, although a heavily obscured active nuclear source is not excluded in all cases; indeed it is possible that active nuclei and vigorous star formation coexist in a number of systems. For both interacting and barred galaxies it has been suggested that the non-axisymmetric perturbation in the gravitational potential induced by the companion or the bar causes an inflow of interstellar material towards the centre (e.g. Combes & Gerin 1985), capable both of feeding a compact nuclear source and of increasing the rate of star formation.

As a first step in testing this hypothesis for the barred spirals, it is necessary to identify the location of the source producing the excess infrared emission, since the resolution available with *IRAS* (typically 1–2 arcmin) is too poor to allow discrimination between central and disc infrared sources. Observation of continuum radio emission from the H II regions and supernova remnants associated with the starburst or compact nucleus is the simplest way of determining the source location.

In this paper we investigate the dependence of radio continuum emission on morphological type for an infrared-selected sample of nearby galaxies, with particular emphasis on the barred systems. The sample is defined in Section 2 and new 20-cm continuum observations are presented. These are analysed together with data taken from H80 in Section 3.

2 Sample, observations and results

Our infrared-selected sample comprises the 194 Shapley–Ames spiral galaxies (Sandage & Tammann 1981) with morphological types in the *Second Reference Catalogue of Bright Galaxies* (de Vaucouleurs, de Vaucouleurs & Corwin 1976, RC2) between S0/a and Scd which were

detected by *IRAS* in all four bands. The non-uniform *IRAS* limiting fluxes, particularly those at 12 and 25 μm, means that this sample is not flux-limited. Approximate limiting flux densities are 0.5 Jy at 12, 25 and 60 μm, and 1.5 Jy at 100 μm (*IRAS Explanatory Supplement* 1985). Version 2 of the *IRAS Point Source Catalog* (PSCII) was used since it contains a statistical correction for the overestimation of fluxes of weak sources in the first edition of the catalogue. The earlier version (PSCI) was used for Paper I, but the differences between the catalogued flux densities for galaxies in our sample are small; only 17 per cent have corrections greater than the quoted 1σ errors and all are less than 2σ. Seyfert and LINER galaxies in the catalogue by Véron-Cetty & Véron (1985) were excluded from the sample.

As in Paper I, galaxies with ratios of the *IRAS* 25 μm/12 μm point source flux density $S_{25}/S_{12} \geq 2.22$ are denoted by the prefix h and it is these which are believed to contain regions of enhanced star formation. Galaxies with $S_{25}/S_{12} < 2.22$ are denoted by the prefix l. The use of point source flux densities biases towards the central regions of galaxies, but there is no evidence of any distance-related selection effects in this sample. For example, the 25 μm/12 μm colour temperture shows no correlation with distance as might be expected due to an increasing contribution from the cooler disc for more distant objects. The lack of any such dependence is due to the major contribution of the central regions to the total infrared emission at these wavelengths.

H80 observed 280 optically bright spirals with the Westerbork Synthesis Radio Telescope (WSRT) at a resolution of about 20 arcsec. Of these, 97 are in common with our *IRAS* sample as are eight of the Sbc spirals observed at 1465 MHz with the VLA by Hummel *et al.* (1985); these latter observations have resolution about 14 arcsec. No corrections have been applied to convert between 1465- and 1415-MHz flux densities as such corrections would be smaller than the quoted errors. Both sets of observations have sufficient resolution to be able to separate disc and central emission.

To increase the overlap between the radio and *IRAS* samples, observations were made during 1986 February, using the WSRT at 1400 MHz, of a further 22 galaxies. Integration times were typically 10 min per object and the observations were performed, wherever possible, at an hour angle which maximized the ratio of projected optical major axis to resolution. The east–west linear array of telescopes resulted in a fan-shaped synthesized beam; to minimize confusion between sources close together in declination, most galaxies were therefore observed twice with an hour-angle separation of about 2 hr. The two observations were combined and 'CLEANed' maps were produced in the usual way (Högbom 1974; Clark 1980). Calibration was performed by regular observation of 3C 286, 3C 147 and 3C 48 which are unresolved at the longest baseline. We assume 20-cm flux densities for these sources of 14.30, 21.57 and 15.67 Jy respectively (Strom, van Someren Greve & Miley 1980).

Following Hummel (1980), we have subdivided the galaxies into four categories according to their radio structures:

(i) C – small-diameter ($\leq$20 arcsec) central source, unresolved in our observations, which is conspicuous above any extended emission;
(ii) E – extended disc emission;
(iii) CE – both disc and central components;
(iv) ND – non-detections.

An uncertain classification is indicated with a question mark. To facilitate classification, we produced slices through the galaxies in our maps at a position angle corresponding to maximum resolution. Due to the fan-shaped beam this was commonly close to 90°. Typical examples for each of the four categories (C, E, CE and ND) are illustrated in Fig. 1. Two methods were used to determine the 20-cm flux density: (i) the total flux density (S_{tot}) was calculated by summing over a box drawn around each source on the map; (ii) where appropriate, the flux density of the central

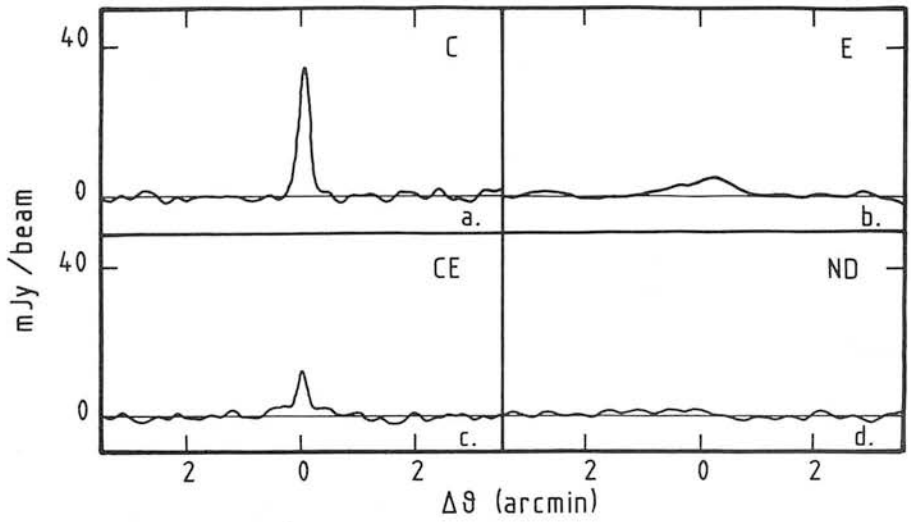

Figure 1. Examples of one-dimensional slices through galaxies illustrating the radio morphology classification scheme: (a) C: NGC4419, (b) E: NGC 1832, (c) CE: NGC3147 and (d) ND: NGC 1241.

component (S_{cen}) was determined by fitting the Gaussian 'CLEAN' beam to the map peak. To confirm it as unresolved, the value obtained in (ii) was compared with the peak flux estimated directly from the map. For many of the galaxies, lower-resolution maps were also made by editing out the data pertaining to the longest baselines. Total flux densities were estimated as above. Comparison between the low- and high-resolution results reveals no significant differences within our estimated error of 15 per cent. However, it should be noted that our estimates of the total flux density may be less than values derived from single-dish observations due to our low sensitivity to extended structure arising from missing short spacings.

Results for the 22 galaxies observed by us are given in Table 1. The columns are:

(1) galaxy name (NGC number),

(2) distance in Mpc, derived from the RC2 or RSA radial velocity. We adopt $H_0 = 75\,\mathrm{km\,s^{-1}\,Mpc^{-1}}$ throughout,

(3) flux density of central component (S_{cen}),

(4) total flux density (S_{tot}),

(5) radio structure classification,

(6) *IRAS* (h, l) and RC2 morphological family classification (SA: unbarred, SB: barred).

Notes concerning individual galaxies are indicated in column (7) and given beneath Table 1. For the non-detections we quote 3σ upper limits. There are three galaxies in common between our observations and those of H80 and Hummel *et al.* (1985). Estimates of the flux densities are consistent within the quoted errors.

3.1 ANALYSIS OF SAMPLE – RADIO STRUCTURE

By combining our observations with the published results referred to above, we have constructed a homogeneous data set for 124 of the 194 galaxies in the *IRAS*-selected sample. To investigate the dependence of radio continuum structure on optical structure (specifically the presence of a bar), we have tabulated (see Table 2) the incidence of central sources (classified either C or CE), extended sources and non-detections for the sub-classes (i) all h systems, (ii) lSB and l mixed-type

Table 1. New observations at 20 cm of 22 *IRAS*-selected bright spiral galaxies.

NGC name	Distance (Mpc)	S_{cen} (mJy)	S_{tot} (mJy)	Radio class.	*IRAS*/RC2 class.	Notes
(1)	(2)	(3)	(4)	(5)	(6)	(7)
922	40.0	<5 mJy beam^{-1}		ND	lSB	
1022	20.0	33	33	C	hSB	
1241	53.5	<3 mJy beam^{-1}		ND	lSB	
1309	27.6	<6 mJy beam^{-1}		ND	lSA	*
1832	23.7	<5	45	E	lSB	*
2280	22.1	<5	34	E	lSA	*
2748	22.1	<3 mJy beam^{-1}		ND	lSA	*
2967	27.3	<7	39	E	lSA	*
2985	19.1	<3 mJy beam^{-1}		ND	lSA	
3044	15.9	11	30	CE	hSB	
3147	38.4	12	130	CE	lSA	*
3177	16.1	20	34	CE	lSA	
3367	38.8	22	61	CE	hSB	
3611	19.6	13	30	CE	lSA	
3655	18.6	<8	55	E	lSA	
3885	20.9	32	64	CE?	hSA	
4419	13.7	33	33	C?	hSB	*
4900	11.7	<7 mJy beam^{-1}		ND	lSB	
5775	21.1	<6 mJy beam^{-1}		ND	lSB	
5792	26.3	15	30	CE	lSB	
5915	29.7	20	55	CE?	hSB	
5936	54.3	46	145	CE	hSB	*

Notes

NGC 1309: There is a 7-mJy source 3 arcmin north of the field centre.

NGC 1832: Hummel *et al.* (1985) find $S_{tot} = 58$ mJy and $S_{cen} = 2$ mJy from VLA observations at 1465 MHz.

NGC 2280: The source consists of two components separated by about 2 arcmin. The source located at the field centre has $S_{tot} = 18$ mJy.

NGC 2748: Hummel *et al.* (1985) find $S_{tot} = 55$ mJy and $S_{cen} < 5$ mJy.

NGC 2967: A second source in the field has $S_{tot} = 33$ mJy, but the separation is very uncertain due to the low declination. It is not included in the flux quoted in Table 1.

NGC 3147: Hummel (1980) finds $S_{tot} = 124$ mJy using the WSRT and $S_{cen} = 20$ mJy from VLA observations (Hummel *et al.* 1985).

NGC 4419: A second source 2 arcmin north-west of the galaxy is not included in the quoted flux density. If included, the total flux density becomes $S_{tot} = 55$ mJy.

NGC 5936: A second source 0.5 arcmin from the field centre is included in the total flux density. Otherwise, $S_{tot} = 46$ mJy and the radio classification becomes C.

Table 2. Incidence of central and extended radio sources and non-detections as a function of *IRAS*/RC2 galaxy type. Percentages of observed number of galaxies are given in parentheses.

IRAS/RC2 type	Number observed	Radio morphological classification		
		C or CE	E	ND
h	30	27 (90 per cent)	2 (7 per cent)	1 (3 per cent)
lSB+lSX	41	18 (44 per cent)	16 (39 per cent)	7 (17 per cent)
lSA	53	14 (26 per cent)	22 (42 per cent)	17 (32 per cent)

(lSX) spirals, and (iii) lSA galaxies. The relative fractions of galaxies in these sub-classes are shown in Fig. 2. There are several interesting results.

Virtually all the h galaxies, those believed to possess enhanced star formation, contain central radio continuum sources. Less than one half of the l barred galaxies and only a quarter of the

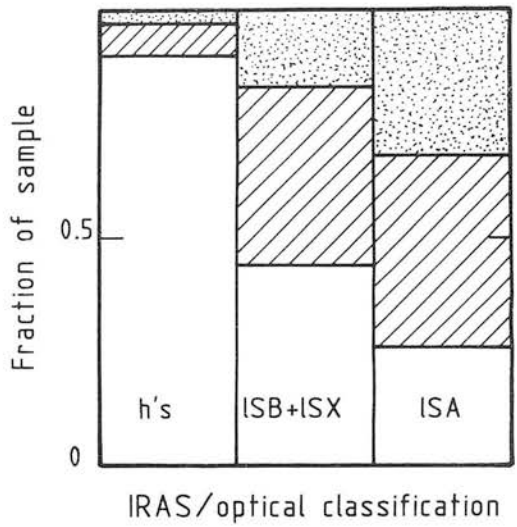

Figure 2. The relative fractions of central radio sources (blank), extended sources (hatched), and non-detections (stippled) for three sub-samples of spirals: all h galaxies (h's), l barred and mixed-type galaxies (lSB+lSX), and unbarred l galaxies (lSA).

unbarred systems exhibit this feature. This effect is much clearer than that recently reported by Kalloglyan & Kandalyan (1986). If our interpretation of the *IRAS* data is correct, then this result strongly suggests that *the enhanced star formation is contained within a region of angular diameter 15–20 arcsec located at the galactic nucleus*. This corresponds to a region of linear extent between 1 and 3 kpc for typical distances to our galaxies of 10–30 Mpc. The three h galaxies which are not classified as possessing central sources are NGC 3310, 4088 and 4369. NGC 3310 possesses a central star-forming complex which is known from 10-μm mapping (Telesco & Gatley 1984) to be 25 arcsec across; subsequent VLA observations show that the radio emission is coextensive and therefore resolved in our Westerbork survey. VLA images of NGC 4088 (Hummel *et al.* 1985) show a knotted radio structure over about 90 arcsec which is therefore also resolved. The unbarred spiral NGC 4369 has a 12-μm flux density of only moderate accuracy and is perhaps misclassified by us as an h system.

3.1.1. The l galaxies

In view of the excellent agreement between the *IRAS* h classification and the presence of a central radio source, there appears to be a surprisingly large number of spirals which possess central radio components but which are of *IRAS* type l. These sources are puzzling because we have excluded from our sample all known Seyferts, and because the l galaxies are not believed currently to have a high star-formation rate.

A number of possibilities may account for the presence of these central sources:

(i) A density-wave-driven inflow of material may generate a density enhancement of the interstellar medium in the central region accompanied by compression of the frozen-in magnetic field. This may suffice to produce a detectable radio source even if the density enhancement is too low to initiate vigorous star formation. Similar suggestions have been made by H81 to explain the strong central sources in early-type and barred galaxies, and by van der Kruit & Allen (1976) to explain the spiral arms of M51. To investigate the feasibility of this model we have utilized the flux densities of the central sources and the extent of the disc emission given by H80 to calculate the

rate of central-to-disc flux density per beam, and thereby estimate the relative enhancement of the radio emission in the central regions. We find a range of values for this ratio of between 4 and 200 for l galaxies possessing extended sources, and lower limits of between 100 and 200 for those systems without detectable disc emission. Since the synchrotron radio emissivity is proportional to $nB^{1-\alpha}$, where n is the number density of relativistic electrons and B is the magnetic field strength, then, for a gas density enhancement factor η and a magnetic field scaling as the square root of the gas density (Mouschovias, Shu & Woodward 1974), the emissivity of the compressed region will be $\eta^{(3-\alpha)/2}nB^{1-\alpha}$. The further assumptions of a typical synchrotron spectral index $\alpha=-0.75$ and that we are observing similar volumes of material give the expected enhancement of the radio emission, which varies as $\eta^{1.88}$. Using the observed ratios of central-to-disc radio emission given above, this implies values for the density enhancement factor of $\eta\sim2$–20. These are consistent with empirical estimates made by Struck-Marcell & Scalo (1987) for the critical value of the density enhancement factor ($\eta_{cr}\sim3$–100) below which, they suggest, vigorous star formation does not occur. Compression, alone, cannot account for the enhanced emission in the h systems since this mechanism is unlikely to heat the dust and thereby create the steep 12–25 μm spectra exhibited by these galaxies.

There is no detectable systematic deviation in the 20-cm – far-infrared relation for l galaxies containing central radio sources. The contribution of the central source to the total radio emission in these systems, typically 10–30 per cent (see Fig. 4), corresponds to an increase in the total radio power, relative to the galaxy before compression, of only about 25 per cent. This is much smaller than the scatter in the radio–far-infrared relationship (see Fig. 7c).

(ii) We are seeing the very end of a burst of vigorous star formation. The virtual absence of stars more massive than about 5 $M_\odot$, which would otherwise heat the dust, is necessary to explain the low values of the 25 μm/12 μm flux density ratio in these galaxies. Synchrotron emission from relativistic electrons produced by the death of the last high-mass stars could produce a detectable radio source.

Consider a subset of the *IRAS*-selected sample of Shapley–Ames galaxies, described in Section 2, which have all been observed at 1400 MHz. A suitable example is the SB and SAB systems having $\delta>+30°$ and $B_0<13.0$ mag. In this essentially complete sub-sample (only one galaxy has not been observed at 20 cm), there are similar numbers of l galaxies with central radio sources and h galaxies exhibiting active star formation; being 20 and 35 per cent respectively of the total number of spirals in the sub-sample. This suggests that the duration of these two phases must be approximately the same. The absence of stars with mass greater than 5 $M_\odot$ (lifetime $\sim10^8$ yr) and other estimates for the lifetime of bursts of star formation ($\sim10^7$–10^8 yr; e.g. Rieke *et al.* 1980; Telesco 1985) imply electron lifetimes against synchrotron losses also of about 10^8 yr. For GeV electrons this yields a reasonable upper limit on the magnetic field strength in the central regions of $\sim10^{-9}$ T. Only a small fraction of the total energy available from supernovae is required to produce the observed mean 1.4-GHz radio power in these systems of about 2×10^{21} W Hz^{-1} (Helou, Soifer & Rowan-Robinson 1985). Nevertheless, this model has difficulty in accounting for the central radio sources in unbarred spirals since few, if any, exhibit vigorous star formation.

(iii) The central-source l galaxies contain active nuclei, possibly obscured by a thick dust shroud. In Paper I (fig. 3) we showed that about one-quarter of the Seyferts detected by *IRAS* in all four wavebands have low 25 μm/12 μm flux density ratios which mimic those of normal 'disc' galaxies. Furthermore, the typical 20-cm radio power of the central sources in the l galaxies ($\sim2\times10^{21}$ W Hz^{-1}) is not greatly different from that seen in the very compact sources (>few$\times10^{21}$ W Hz^{-1}; van der Hulst *et al.* 1981) which are thought to be powered by accretion on to massive objects. One possible candidate for an active nucleus amongst the l galaxies is NGC 3079 which shows lobes and bridges of radio emission in the VLA maps by Duric *et al.* (1983). We note, however, that all strongly barred Seyfert galaxies (de Vaucouleurs type SB) in the aforemen-

tioned *IRAS* two-colour diagram have an h classification; that is, a high value of their *IRAS* 25 μm/12 μm ratio.

Since the strongly barred (SB) Seyfert galaxies are all classified by us as h, we suggest that the central radio sources in the lSB spirals are produced either by a simple density enhancement or during the last phases of a burst of star formation. The apparent absence of vigorous star formation amongst the unbarred (SA) galaxies suggests that the latter model is inapplicable in this case, and that the central sources are powered by either a density enhancement or an obscured active nucleus. The radio sources in l mixed-type (SX) galaxies may be explained by any of the three suggested models. High-resolution (~1 arcsec) radio continuum observations, which probe the nuclear radio structure, may be able to distinguish between these various possibilities.

3.1.2 The h galaxies

It has been suggested (Devereux 1987) that the h barred galaxies are morphologically of earlier type than the l spirals. This would be consistent with our observed high incidence of central radio components in the h systems, since it is known that early-type galaxies have stronger central radio emission than later types (Condon & Dressel 1978; H81). We have examined the distribution of optical morphological type (RC2 classification) for the three sub-classes: all h systems, lSB+lSX galaxies, and lSA spirals. These distributions are shown in Fig. 3. Note that although the h galaxy sample contains a significantly higher proportion of early-type spirals (Sb and earlier), it is *not* dominated by them; they comprise only 13 out of 30 h systems. Therefore this suggestion cannot fully account for the higher occurrence of central radio sources in the h spirals.

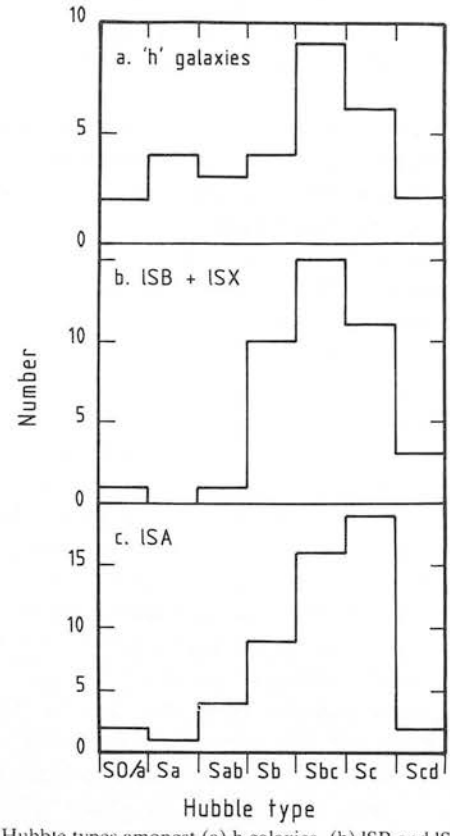

Figure 3. The distributions of Hubble types amongst (a) h galaxies, (b) lSB and lSX galaxies, and (c) lSA galaxies.

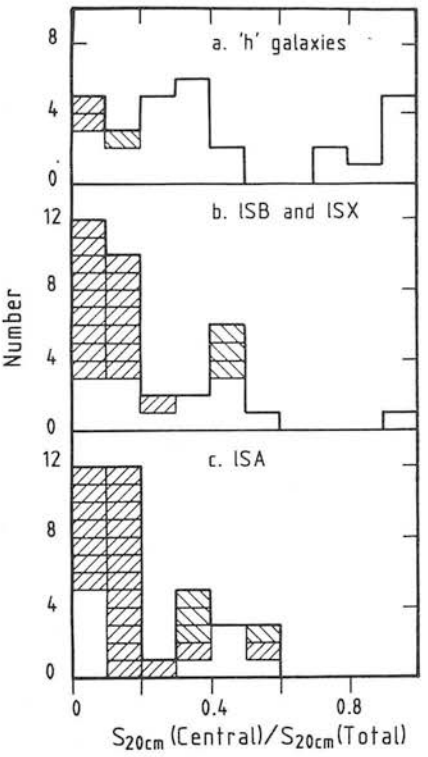

Figure 4. The ratio of central to total 20-cm continuum flux densities for (a) h galaxies, (b) ISB and ISX galaxies, and (c) ISA galaxies. Upper and lower limits are indicated by positively and negatively sloped hatching respectively.

We have also investigated the relative contribution of the central component to the total emission for the 99 detected galaxies. In Fig. 4 we show the ratio of central to total 20-cm continuum flux densities for the same three sub-classes. Of course, since our data set is based on that of H80, the distributions for both ISA and ISB+ISX systems reproduce his result that only about one tenth of the total emission arises from the central component. In the 'h' galaxies, however, the central component supplies a much larger fraction of the total emission – typically 30–40 per cent. As a consequence, there is a marked tendency for the total radio emission to increase with increasing central flux, as illustrated in Fig. 5.

One possibility not yet fully discussed is that both the radio continuum and *IRAS* emission are the result of a non-thermal active nucleus. Even though we have excluded known Seyfert galaxies from our sample, an active nucleus which is deeply embedded in a dust cocoon could conceivably account for the observations thus far described, since neither the data presented here, nor the *IRAS* observations, are useful for distinguishing between 'starburst' and Seyfert galaxies. High-resolution (~1 arcsec) observations are more useful, since they can probe the central regions of these systems and investigate the near-nuclear radio structure. Galaxies containing active nuclei are expected to have strong compact components, whilst spirals possessing regions of vigorous star formation are expected to contain extended complex components. About one-half of our h systems have been observed at high resolution and frequently (~80 per cent) show complex and/or extended central sources; for example NGC 2633 (Hummel *et al.* 1984), NGC 3556 and 4536 (van der Hulst *et al.* 1981). A few (~20 per cent) possess compact central components in addition to extended emission (e.g. NGC 2782 – van der Hulst *et al.* 1981). Nevertheless, in general, the published high-resolution continuum radio maps of the central components show structure consistent with, and indicative of, enhanced star formation.

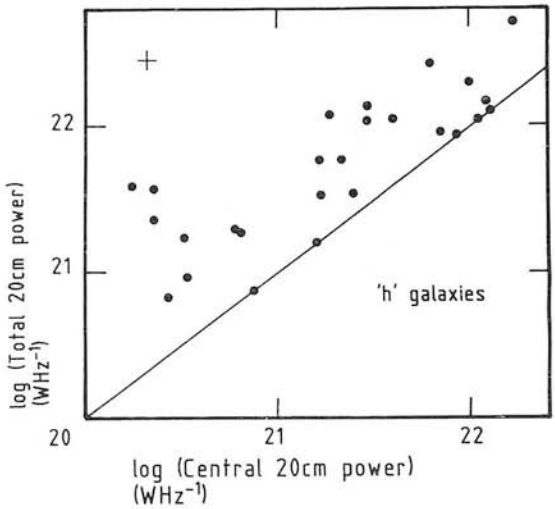

Figure 5. The total 20-cm radio power as a function of the power from the central source in h galaxies. The equality central=total power is indicated. Best estimates of the typical 1σ error are shown.

3.2 ANALYSIS OF SAMPLE – CORRELATIONS OF RADIO EMISSION WITH MID- AND FAR-INFRARED FLUXES

In this section we make use of the ability of the radio observations to distinguish between compact 'nuclear' and extended 'disc' sources to investigate the spatial origin of the mid- and far-infrared emission. This is one of the main objectives of this work, since the coarse-resolution *IRAS* data generally contain little spatial information on any but the nearest galaxies.

In Fig. 6 we present a comparison between the *IRAS* point-source 25-μm monochromatic power (defined as $4\pi(\text{dist})^2 \times$ *IRAS* point-source flux density) and the central and total 20-cm radio powers for the h galaxies. To maintain clarity, upper limits have not been included but they are consistent with the data shown. Best estimates of the typical 1σ errors are also illustrated. It is apparent that the point-source 25-μm power (and to a lesser extent the 12- and 60-μm powers, not shown here) correlate better with the central radio power (Spearman rank correlation coefficient, $\varrho=0.894$) than with the total emission ($\varrho=0.779$). This result is consistent with the enhanced star formation (which dominates the 25-μm emission – see Paper I) being located within the central 15–20 arcsec.

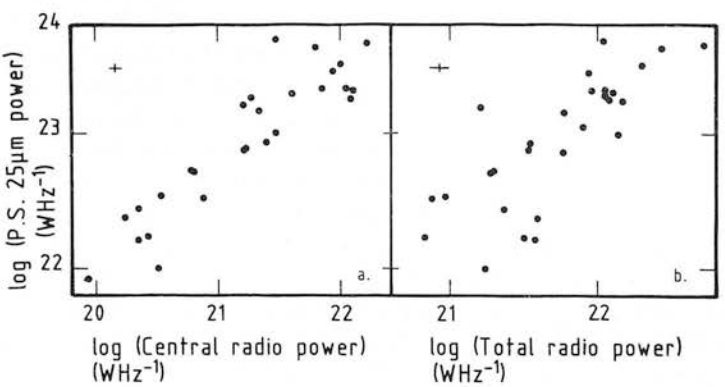

Figure 6. The dependences of (a) central and (b) total 20-cm continuum power on the *IRAS* point-source 25-μm monochromatic power for h galaxies. Best estimates of the typical 1σ error bars are shown.

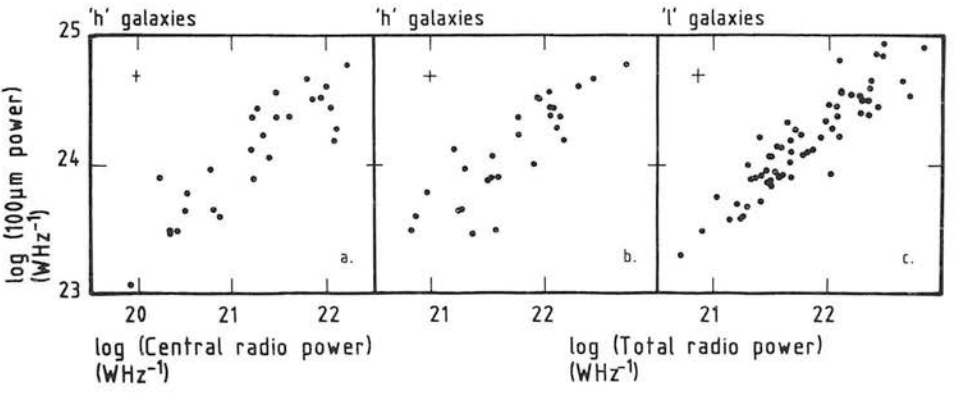

Figure 7. The variation of *IRAS* point-source 100-μm power with (a) central and (b) total radio power for the h galaxies, and (c) with total radio power for both barred and unbarred l galaxies. Best estimates of the typical 1σ error bars are shown.

The dependence of the *IRAS* point-source 100-μm power on (a) central and (b) total radio power, again for the h galaxies, is illustrated in Fig. 7, and best estimates of the typical 1σ error bars are shown. The correlation coefficients are 0.839 and 0.838 respectively. The relationship between point-source 100-μm power and total radio emission is also shown for the l galaxies and will be discussed later. Although we have previously identified a correlation between central and total radio emission for the h galaxies (Fig. 5), the comparable tightness of the 100 μm–radio relationships suggests that a significant fraction of the far-infrared flux must arise in the central active star-formation region. *The variable contribution of the central source to the total radio emission and the tightness of the 100 μm–total radio correlation (Fig. 7b) argue that the ratio of the far-infrared to radio flux is approximately constant over scales as small as 1 kpc.* If, on average, the central source contributes about 35 per cent to the total radio emission, *then it must also contribute a similar fraction to the total far-infrared flux of the galaxy.* The mean total luminosity of the h galaxies in this sample is $L_{\rm FIR}\sim10^{10}\,L_{\odot}$ (see Lonsdale *et al.* 1985 for the definition of FIR), implying that the luminosity of the central star-formation complex is a few$\times10^{9}\,L_{\odot}$. Approximately 10^{5} bright H II regions (mean luminosity ~few$\times10^{4}\,L_{\odot}$) are required to match this output. This is the same number of H II regions as determined in Paper I from consideration of the different luminosities and spectral shapes of the h and l galaxies.

There must, however, also be a major contribution (typically 65 per cent) to the total far-infrared flux from extended emission in the h galaxies. We speculate that this predominantly arises in disc star-formation regions (see also Haslam & Osborne 1987; Leggett, Brand & Mountain 1987). We can investigate this hypothesis a little further by examining the *IRAS Small Scale Structures Catalog* (Helou & Walker 1986) for galaxies in our sample which possess extended ($\geq$1 arcmin) source associations of good or moderate flux quality. Nearly one-half (43 per cent) of the galaxies exhibit extended 25-μm emission which may originate from warm dust in the galactic discs heated by young star-formation regions.

In Fig. 8 we show correlations between the extended 25-μm power (or the point-source 25-μm power if no extended emission was detected) and the total 20-cm radio power for both the h and l systems. Best estimates of the typical 1σ error bars are also indicated. The l galaxies which possess central radio sources are indicated, and the line log(total 25-μm power)=4.88+0.84 log (total radio power) is drawn in both plots as a guide for the eye. We note that there is a significant difference between the two relationships. *For a given total 20-cm radio power, the total 25-μm power is about a factor of 2 greater in the actively star-forming h galaxies than in the l spirals.* This dichotomy is also apparent when the point-source 25 μm–central radio powers are compared.

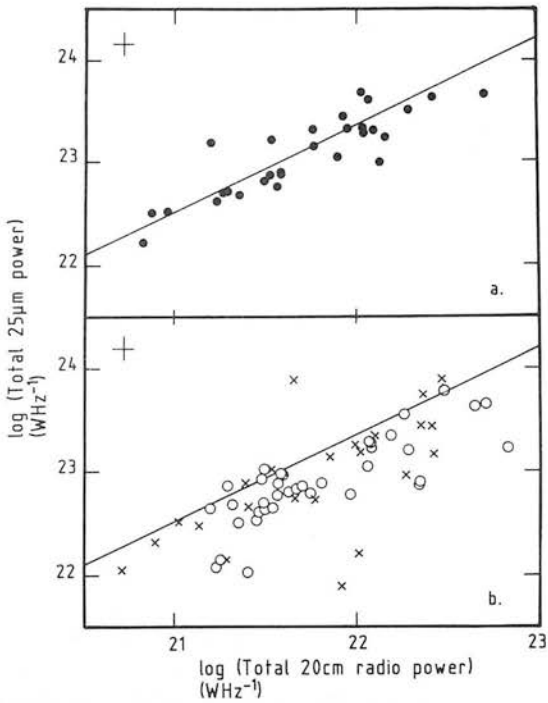

Figure 8. The correlations between total (point source or extended source, see text) *IRAS* 25-μm power and total 20-cm radio power for (a) h galaxies (filled circles) and (b) l galaxies (open circles and crosses). The crosses indicate l galaxies which possess central radio sources. The line log (total 25-μm power) = 4.88 + 0.84 log (total radio power) is shown in both plots as a guide for the eye. Best estimates of the typical 1σ error bars are shown.

Re-examination of Fig. 7, however, shows no difference in the correlation between point-source 100-μm and radio powers for h and l galaxies. The point-source 100-μm flux is sufficient for investigating this property, since the large beam size (3×5 arcmin^2) takes in virtually all of the emission from these galaxies; only one exhibits extended emission of good or moderate flux quality at 100 μm. The results in Fig. 7 are in concordance with the major fraction of the 100-μm emission arising in the disc and with the single tight correlation between far-infrared and radio luminosity found by Helou *et al.* (1985) which is independent of the level of galactic activity or Hubble type (Gavazzi, Cocito & Vettolani 1986).

We now consider two possible explanations for the apparent dependence of the (mid-) infrared-radio correlation on the level of star-formation activity.

(i) It may simply be another manifestation of the phenomenon noted in Section 3.1.1; namely that a surprisingly high fraction of the l galaxies possess significant radio emission but low 25-μm flux. Whilst it is true that the central source l galaxies tend to exhibit the greater scatter about the average 25 μm/total power ratio (see Fig. 8b), this cannot be the complete answer since the majority of the l systems are without central radio components but still exhibit a different 25 μm–radio relationship to that seen in the h galaxies.

(ii) If the radio emission is a direct measure of the level of star-formation activity (that is, the radio flux scales linearly with the supernova, and hence star-formation, rate), then it is apparent that the dependence of the (mid-) infrared–radio correlation on star-formation activity is most likely due to a variation in the amount of emission from warm dust per unit quantity of star formation. We speculate that the dust heated by massive young stars is warmer in the centrally located, very active star-formation regions found in the h galaxies than in the much less vigorous l

spirals. A similar suggestion has been made by Helou (1986) who models the *IRAS* colour of normal galaxies by 'cirrus' and variable temperature 'active' components. Note that, although the *IRAS* flux densities used in this paper have not been colour-corrected (Lonsdale *et al.* 1985), the correction factor at 25 μm varies by less than about 7 per cent, assuming dust temperatures of between 50 and 100 K, and does not significantly affect this result. Since the *IRAS* 25-μm band is close to the expected peak of the Planck function for warm dust heated by massive young stars (having a characteristic temperature of about 75 K), only a small variation in the dust temperature is necessary to increase the detected flux in this band by the required factor of 2.

4 Conclusions

We have examined the 1.4-GHz radio continuum properties of an *IRAS*-selected sample of nearby spiral galaxies. This analysis shows that virtually all the systems with *IRAS* 25 μm/12 μm flux density ratios $S_{25}/S_{12}>2.22$ (the h galaxies) have central radio sources of angular size less than about 15 arcsec. This strongly suggests that the enhanced star-formation activity believed to be occurring in these galaxies is contained within regions of linear extent less than 1–3 kpc and located near or at the galactic nuclei.

The ratio of the far-infrared to radio emission is found to be approximately constant over scales as small as 1 kpc. Given this tight correlation, which is independent of the level of contribution from the central source, we estimate that the typical far-infrared luminosity of the central star-forming complex is a few$\times 10^9 L_\odot$. This is consistent with other estimates of this parameter.

A significant fraction of galaxies believed not currently to have a high star-formation rate (l systems) also possess central radio sources. Having examined three plausible models we suggest that, amongst the strongly barred (SB) galaxies, the radio emission arises either from a simple density enhancement or from the embers of a burst of star formation. The central radio emission in the unbarred (SA) galaxies may be powered by a density enhancement or an obscured active nucleus, whilst that from the mixed-type (SX) galaxies may be due to any of the three suggested models.

We identify a correlation between the *IRAS* 25-μm and 20-cm radio emission which, in contrast to the far-infrared results, shows a marked dependence on the level of star-formation activity. We speculate that this effect is due to the presence of a warmer dust component in the actively star forming h galaxies than in the l systems.

Acknowledgments

We thank Thijs van der Hulst for assistance at Westerbork in the reduction of these observations, and STARLINK and IPMAF for providing the hardware and software used to compile and analyse the database. The Westerbork Synthesis Radio Telescope is operated by the Netherlands Foundation for Radio Astronomy with the financial support of the Organization for the Advancement of Pure Research. We are grateful to Marjorie Fretwell for production of the diagrams and also wish to thank Peter Brand, Charlie Telesco and the referee for valuable comments on this manuscript. PJP acknowledges an SERC studentship.

References

Becklin, E. E., 1987. *Second IRAS Conference: Star Formation in Galaxies,* p. 753, ed. Lonsdale Persson, C. J., Pasadena, California.

Biermann, P., 1980. *Highlts Astr.*, **5,** 209.

Cameron, M. J., 1971. *Mon. Not. R. astr. Soc.*, **152,** 403.

Clark, B. G., 1980. *Astr. Astrophys.*, **89,** 377.

Combes, F. & Gerin, M., 1985. *Astr. Astrophys.*, **150,** 327.
Condon, J. J., 1980. *Astrophys. J.*, **242,** 894.
Condon, J. J. & Dressel, L. L., 1978. *Astrophys. J.*, **221,** 456.
Condon, J. J., Condon, M. A., Gisler, G. & Puschell, J. J., 1982. *Astrophys. J.*, **252,** 102.
Cutri, R. M. & McAlary, C. W., 1985. *Astrophys. J.*, **296,** 90.
de Jong, T., Clegg, P. E., Soifer, B. T., Rowan-Robinson, M., Habing, H. J., Houck, J. R., Aumann, H. H. & Raimond, E., 1984. *Astrophys. J.*, **278,** L67.
de Vaucouleurs, G., 1959. *Handbuch der Physik,* **53,** 275.
de Vaucouleurs, G., de Vaucouleurs, A. & Corwin, H. C., 1976. *Second Reference Catalogue of Bright Galaxies,* University of Texas Press, Austin (RC2).
Devereux, N., 1987. *Second IRAS Conference: Star Formation in Galaxies,* p. 219, ed. Lonsdale Persson, C. J., Pasadena, California.
Dressel, L. L., 1979. *PhD thesis*, University of Virginia.
Dressel, L. L & Condon, J. J., 1978. *Astrophys. J. Suppl.*, **36,** 53.
Duric, N., Seaquist, E. R., Crane, P. C., Bignell, R. C. & Davis, L. E., 1983. *Astrophys. J.*, **273,** L11.
Fairclough, J. M., 1985. In: *Rutherford Appleton Laboratory Workshop on Extragalactic Infrared Astronomy,* p. 32, ed. Gondhalekar, P. M.
Gavazzi, G., Cocito, A. & Vettolani, G., 1986. *Astrophys. J.*, **305,** L15.
Haslam, C. G. T. & Osborne, J. L., 1987. *Nature,* **327,** 211.
Hawarden, T. G., Mountain, C. M., Leggett, S. K. & Puxley, P. J., 1986. *Mon. Not. R. astr. Soc.*, **221,** 41P (Paper I).
Helou, G., 1986. *Astrophys. J.*, **311,** L33.
Helou, G. & Walker, D. W., 1986. *IRAS Small Scale Structures Catalog,* 1986. US Government Printing Office, Washington, DC.
Helou, G., Soifer, B. T. & Rowan-Robinson, M., 1985. *Astrophys. J.*, **298,** L7.
Högbom, J. A., 1974. *Astr. Astrophys. Suppl.*, **15,** 417.
Hummel, E., 1980. *Astr. Astrophys. Suppl.*, **41,** 151 (H80).
Hummel, E., 1981. *Astr. Astrophys.*, **93,** 93 (H81).
Hummel, E., Pedlar, A., van der Hulst, J. M. & Davies, R. D., 1985. *Astrophys. J. Suppl.*, **60,** 293.
Hummel, E., van der Hulst, J. M. & Dickey, J. M., 1984. *Astr. Astrophys.*, **134,** 207.
IRAS Explanatory Supplement, 1985. Eds. Beichman, C. A., Neugebauer, G., Habing, H. J., Clegg, P. E. & Chester, T. J., US Government Printing office, Washington DC.
IRAS Point Source Catalog, 1985. Joint IRAS Science Working Group, US Government Printing Office, Washington DC.
Joseph, R. D. & Wright, G. S., 1985. *Mon. Not. R. astr. Soc.*, **214,** 87.
Joseph, R. D., Meikle, W. P. S., Robertson, N. A. & Wright, G. S., 1984. *Mon. Not. R. astr. Soc.*, **209,** 111.
Kalloglyan, A. T. & Kandalyan, R. A., 1986. *Astrofizika,* **24,** 47.
Leggett, S. K., Brand, P. W. J. L. & Mountain, C. M., 1987. *Mon. Not. R. astr. Soc.*, **228,** 11P.
Lonsdale, C. J., Helou, G., Good, J. C. & Rice, W., 1985. *Cataloged Galaxies and Quasars Observed in the* IRAS *Survey,* Jet Propulsion Laboratory, Pasadena, California.
Lonsdale, C. J., Persson, S. E. & Matthews, K., 1984. *Astrophys. J.*, **287,** 95.
Mouschovias, T. C., Shu, F. H. & Woodward, P. R., 1974. *Astr. Astrophys.*, **33,** 73.
Rieke, G. H., Lebofsky, M. J., Thompson, R. I., Low, F. J. & Tokunaga, A. T., 1980. *Astrophys. J.*, **238,** 24.
Sandage, A. & Tammann, G. A., 1981. *A Revised Shapley Ames Catalog of Bright Galaxies*, Carnegie Institution of Washington Publication No. 635 (RSA).
Strom, R. G., van Someren Greve, H. W. & Miley, G. K., 1980. *Westerbork Synthesis Radio Telescope Users Manual.*
Struck-Marcell, C. & Scalo, J. M., 1987. *Astrophys. J. Suppl.*, **64,** 39.
Telesco, C. M., 1985. In: *Rutherford Appleton Laboratory Conference on Extragalactic Infrared Astronomy*, p. 87, ed. Gondhalekar, P. M.
Telesco, C. M. & Gatley, I., 1984. *Astrophys. J.*, **284,** 557.
Ulvestad, J. S., 1982. *Astrophys. J.*, **259,** 96.
van der Hulst, J. M., Crane, P. C. & Keel, W. C., 1981. *Astr. J.*, **86,** 1175.
van der Kruit, P. C. & Allen, R. J., 1976. *Ann. Rev. Astr. Astrophys.*, **14,** 417.
Véron-Cetty,, M.-P. & Véron, P., 1985. *ESO Scientific Report No. 4.*
Wynn-Williams, C. G., 1987. *IAU Symp. No. 115, Star Forming Regions,* p. 125, eds Peimbert, M. & Jugaku, J., Reidel, Dordrecht, Holland.

Mon. Not. R. astr. Soc. (1986) **221**, *Short Communication*, 41P–45P

Enhanced star formation – the importance of bars in spiral galaxies

T. G. Hawarden and C. M. Mountain *Royal Observatory, Blackford Hill, Edinburgh EH9 3HJ*

S. K. Leggett and P. J. Puxley *Astronomy Department, University of Edinburgh, Blackford Hill, EH9 3HJ*

Accepted 1986 May 20. Received 1986 May 19

Summary. *IRAS* results demonstrate that, amongst intrinsically luminous spiral galaxies, more than one third of the barred systems have an excess of flux at 25 μm. The mean total infrared luminosity of these systems ($4.3\times10^{10}\,L_\odot$) is more than twice that of unbarred galaxies ($1.7\times10^{10}\,L_\odot$), few or none of which exhibit a 25 μm excess. We show that these properties are probably attributable to vigorous star formation in a 'circumnuclear' ring located near an inner resonance where material from a bar-driven inflow accumulates, and infer also that an active nucleus does not dominate this phenomenon.

1 Introduction

Two characteristic features of barred spiral galaxies of early to intermediate type are the dust lanes which trace the hydrodynamic shocks in the bar, and the associated rings of H II regions around the nucleus. Observations of H I by Sancisi, Allen & Sullivan (1979), and optical spectroscopy by Pence & Blackman (1984), for example, suggest that in such structures there is a bar-driven inflow of material. Theoretical models (e.g. Schwarz 1984; Combes & Gerin 1985) suggest that these 'circumnuclear' rings are situated near one of the inner resonances and that this is where material swept inwards would accumulate. At least two of these rings (in NGC 1097 and 3310) are unambiguously the location of enhanced star formation (Telesco & Gatley 1981, 1984).

As the radiation from star-forming regions is absorbed by dust and re-radiated in the mid- to far-infrared, we have used the unbiased all-sky survey provided by the *IRAS Point Source Catalog* (see the Explanatory Supplement, edited by Beichman *et al.* 1984) to study this process in spiral galaxies from the *Revised Shapley-Ames Catalog* (Sandage & Tammann 1981, 'RSA').

2 The sample of galaxies

The *IRAS* fluxes of star-forming regions rise steeply between band 1 and band 2 (12 and 25 μm), a consequence of the presence of a large component of 'warm' dust at temperatures around 100 K

(Adams & Shu 1985). To investigate their incidence in galaxies, we have constructed a two-colour diagram using the ratio of the fluxes in bands 1 and 2 and that between bands 4 (100 μm) and 2. This allows us to distinguish between this 'warm' component and the ubiquitous 'cool' dust (Cox, Krügel & Mezger 1986). Our sample comprises all objects in the RSA with morphological classifications in the *Second Reference Catalogue of Bright Galaxies* (de Vaucouleurs, de Vaucouleurs & Corwin 1976, 'RC2') between SO/a and Scd (inclusive) which have been detected by *IRAS* in all four bands. We have excluded those which are resolved by *IRAS* at 100 μm (as indicated by the point-source correlation coefficient) and those with serious cirrus contamination (cirrus 2 flag$\geq$4). We have also omitted those galaxies listed as Seyferts of types 1 or 2 or as LINERs by Véron-Cetty & Véron (1985, hereafter VCV). One hundred and eighty-six galaxies have been included.

3 Analysis of the *IRAS* results for the sample galaxies

Fig. 1(a), (b) and (c) show the distributions in the two-colour diagram for galaxies in our sample of type SB, SAB and SA, respectively. There is a dramatic difference between these distributions. A large fraction of the SB and many of the SAB galaxies have greatly enhanced 25 μm fluxes relative to their 12 μm and 100 μm fluxes. These galaxies include NGC 1097 and 3310, the positions of which are shown. We interpret this excess flux at 25 μm as arising in regions of active star formation and infer that high levels of this activity, sufficient to dominate the infrared colours of galaxies, *occur almost exclusively in the barred systems*.

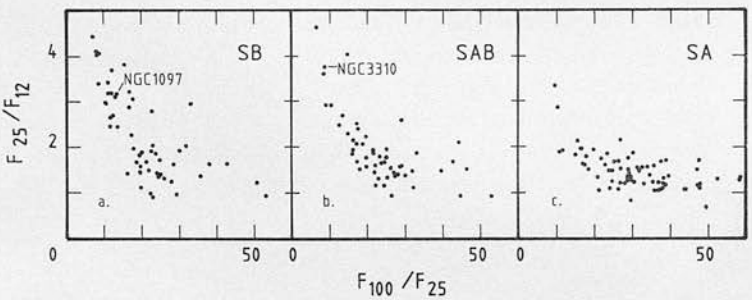

Figure 1. The distributions of SB, SAB and SA galaxies in the *IRAS* two-colour diagram, $f_\nu(25\,\mu\text{m})/f_\nu(12\,\mu\text{m})$ against $f_\nu(100\,\mu\text{m})/f_\nu(25\,\mu\text{m})$, are shown in (a), (b) and (c) respectively. The classification is from the RC2 and comprises a sub-set of all galaxies in the RSA detected by *IRAS* in all four bands. The two 'starburst' galaxies NGC 1097 and 3310 are marked.

Fig. 1 suggests that the galaxies with 'excess' star-forming activity are conveniently distinguished by values of the 2/1 ratio >2.2 because '*normal*' *galaxies evidently have flat spectra between 12 and 25 μm*. We have adopted the prefixes h and l for galaxies falling above and below this division.

Fig. 2 compares the distributions of (a) distance (corrected for group or cluster membership), (b) uncorrected total *B* magnitude, and (c) the distance-independent ratio [total far-infrared luminosity/total *B* luminosity] for *IRAS*-detected RSA spirals in our range of Hubble types with and without band 1 detections; the former comprise our sample in Fig. 1. The far-infrared flux parameter (FIR) is a linear combination of the 60 μm and 100 μm flux densities (Lonsdale *et al.* 1985). The detected galaxies are closer and optically brighter than the undetected objects but the difference is small. Conversely Fig. 2(c) shows that the sample in Fig. 1 is much more luminous in the far-infrared, relative to the blue, than the undetected systems.

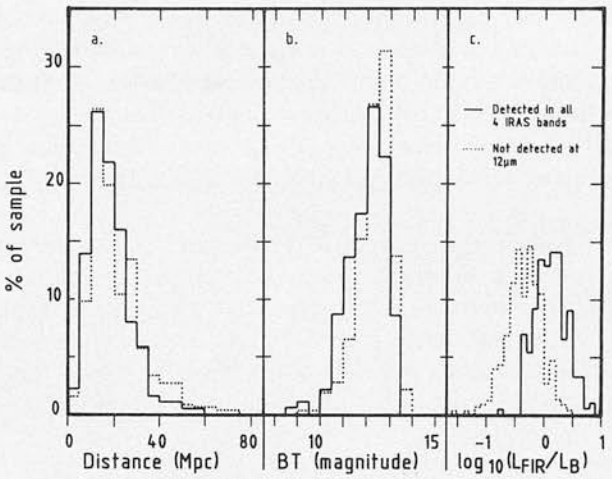

Figure 2. Comparisons between the samples of RSA galaxies detected in all *IRAS* bands (i.e. those in Fig. 1) (solid lines) and galaxies not detected at 12 μm (broken lines) showing the distributions of (a) distance, (b) uncorrected total B magnitude and (c) total FIR luminosity/B luminosity for each group.

The ratio of SA:SAB:SB galaxies in our sample (74:55:53) is similar to those not detected at 12 μm (98:103:110) and so our selection does not favour a particular morphology. As, surprisingly, bars are not over-represented in our intrinsically infrared-luminous sample, this suggests that the phenomena shown in Fig. 1 may only be important at high infrared luminosities, as remarked by Devereux, Becklin & Scoville (1986).

The hSB galaxies in Fig. 1 have a mean total infrared luminosity $\langle \mathrm{LIR} \rangle = 4.3 \times 10^{10} L_{\odot}$ ($H_0 = 75\,\mathrm{km\,s^{-1}\,Mpc^{-1}}$), markedly brighter than the lSB systems with $\langle \mathrm{LIR} \rangle = 2.8 \times 10^{10} L_{\odot}$. These are, in turn, more luminous than the SA galaxies with $\langle \mathrm{LIR} \rangle = 1.7 \times 10^{10} L_{\odot}$.

4 Discussion

To support our assertion that the galaxies exhibiting 25-μm excesses have greatly enhanced rates of star formation, we have constructed simple models using the averaged observed *IRAS* fluxes of a group of luminous, unresolved H II regions in a field in Cygnus. Addition of about 10^5 such objects to a model galaxy having the mean colours and total infrared luminosities of the SA systems in Fig. 1 reproduces quite accurately the *IRAS* colours and luminosities of a typical 'starburst' system such as NGC 1097. Only the 12-μm emission is underestimated. Wynn-Williams & Becklin (1985) showed that galactic H II regions are significantly redder than the integrated *IRAS* colours of extragalactic star-forming complexes and attributed this excess emission at 12 μm to fluorescent small grains. Our models so far omit the extended 12 μm emission seen by *IRAS* across the whole Cygnus complex (described in a future paper). In many respects these models resemble those of Rowan-Robinson & Crawford (1986) who also find enhanced star formation in barred galaxies.

Since star formation occurs in the discs of barred and unbarred galaxies alike, the discs are unlikely to be the source of the 25 μm excess amongst the 'h' galaxies. Hummel (1981) finds that at 21 cm unresolved (<20 arcsec) centrally concentrated continuum emission sources are significantly more luminous in barred than in unbarred galaxies, whereas the radio emission from the discs of barred and unbarred systems is indistinguishable. Hummel suggests that this continuum emission may trace the density of the ISM or the local star-formation rate. Helou,

Soifer & Rowan-Robinson (1985) also find a tight correlation between the radio continuum and the *IRAS* far-infrared flux. We have undertaken observations similar to those of Hummel which increase the overlap between the radio and infrared samples (Puxley *et al.*, in preparation). Initial results show that *all* the hSB and hSAB galaxies were detected at 21 cm and exhibit unresolved central sources, while only 20 per cent of the 'l' galaxies do so. These results strongly suggest that the star-forming regions which dominate the infrared colours are located within 20 arcsec of the galactic nuclei.

There remains the possibility that we are seeing phenomena causally associated with a compact nuclear source. We excluded from our initial sample all galaxies classified as Seyferts or LINER's in VCV. Fig. 3 shows the two-colour diagram for these galaxies, which exhibit a remarkably similar distribution to that of the spirals, even to the presence of the 'split' at 2/1 ~2. However, the accuracy with which the colours and luminosities of the 'h' galaxies are reproduced by the addition of H II regions to an 'l' system suggests that the nucleus does not have a significant effect on star formation in our sample.

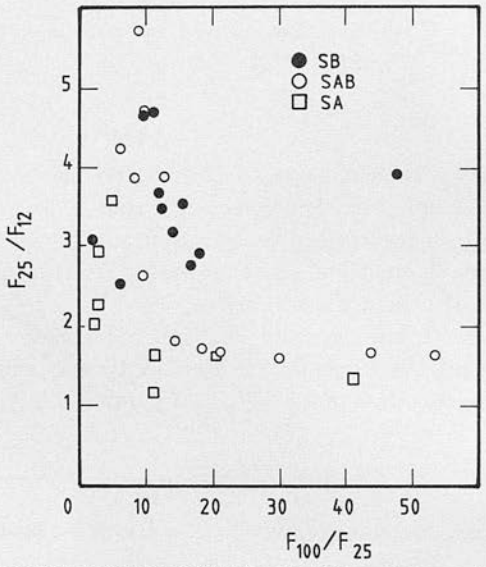

Figure 3. As for Fig. 1 but showing the galaxies excluded from that diagram because of the presence of Seyfert 1 or 2 or LINER features in their spectra.

5 Conclusions

In our sample, galaxies with *IRAS* flux ratios 2/1>2.2 are exclusively barred (with two exceptions) and have enhanced star formation which is probably concentrated within the central 20 arcsec, but not caused by nuclear activity. These hSB and hSAB systems have higher 60 μm and 100 μm luminosities than the 'l' galaxies of all families, but it is possible to account for all the extra luminosity in the 'h' systems by adding the 'average' spectrum and luminosity of $\sim 10^5$ galactic H II regions to an 'l' SA galaxy.

We conclude that, in the absence of violent interaction or an active nucleus, the circumnuclear rings in barred galaxies are the only locations in spirals earlier than Scd where vigorous star-forming activity occurs (see also Elmegreen 1986).

We speculate that NGC 3885 and 6810, the only two non-barred 'h' galaxies, may in fact be barred. On UK Schmidt IIIa-J plates NGC 6810, although dustier, resembles the 'starburst' SAB system NGC 253 and quite probably contains an obscured bar. NGC 3885 has strong dust lanes

characteristic of barred systems: Corwin (private communication) informs us that some have classified this galaxy SAB.

Acknowledgments

We are indebted to Jon Fairclough and IPMAF for providing *IRAS* software and we also thank Harold Corwin for classifications of NGC 6810 and 3885. We are grateful to Eric Becklin and Nick Devereux for stimulating debate and giving us access to unpublished data and to Bob Joseph for his advice and contributions to the early stages of this work. PJP acknowledges a SERC studentship, SKL a SERC fellowship.

References

Adams, F. C. & Shu, F. H., 1985. *Astrophys. J.*, **296,** 655.
Beichman, C. A., Neugebauer, G., Habing, H. J., Clegg, P. E. & Chester, T. J., 1984. *IRAS Explanatory Supplement,* Jet Propulsion Laboratory, Pasadena.
Combes, F. & Gerin, M., 1985. *Astr. Astrophys.*, **150,** 327.
Cox, P., Krügel, E. & Mezger, P. G., 1986. *Astr. Astrophys.*, **155,** 380.
de Vaucouleurs, G., de Vaucouleuers, A. & Corwin, H. C., 1976. *Second Reference Catalogue of Bright Galaxies*, University of Texas Press, Austin.
Devereux, N. A., Becklin, E. E. & Scoville, N., 1986. Preprint.
Elmegreen, B. G., 1986. *IAU Symp. No. 115, Star Forming Regions,* Tokyo, Japan.
Helou, G., Soifer, B. T. & Rowan-Robinson, M., 1985. *Astrophys. J.*, **298,** L7.
Hummel, E., 1981. *Astr. Astrophys.*, **93,** 93.
Lonsdale, C. J., Helou, G., Good, J. C. & Rice, W., 1985. *Cataloged Galaxies and Quasars Observed in the IRAS Survey*, Jet Propulsion Laboratory, Pasadena.
Pence, W. D. & Blackman, C. P., 1984. *Mon. Not. R. astr. Soc.*, **210,** 547.
Rowan-Robinson, M. & Crawford, J., 1986. *Light on Dark Matter,* p. 421, ed. Israel, P. P., Reidel, Dordrecht, Holland.
Sancisi, R., Allen, R. J. & Sullivan, W. T., 1979. *Astr. Astrophys.*, **78,** 217.
Sandage, A. & Tammann, G. A., 1981. *A Revised Shapley–Ames Catalog of Bright Galaxies*, Carnegie Institution of Washington Publication No. 635.
Schwarz, M. P., 1984. *Mon. Not. R. astr. Soc.*, **209,** 93.
Telesco, C. M. & Gatley, I., 1981. *Astrophys. J.*, **247,** L11.
Telesco, C. M. & Gatley, I., 1984. *Astrophys. J.*, **284,** 557.
Véron-Cetty, M.-P. & Véron, P., 1985. *ESO Scientific Report No. 4.*
Wynn-Williams, C. G. & Becklin, E. E., 1985. *Astrophys. J.*, **290,** 108.